STUDIES ON ELECTRICAL TRANSPORT AND ION KINEMATICS PHENOMENA IN SOME OXIDE GLASSY SYSTEMS

Thesis Submitted by

ASMITA PODDAR

DOCTOR OF PHILOSOPHY (ENGINEERING)

DEPARTMENT OF ELECTRICAL ENGINEERING

FACULTY COUNCIL OF ENGINEERING & TECHNOLOGY

JADAVPUR UNIVERSITY

KOLKATA, INDIA

2025

JADAVPUR UNIVERSITY

FACULTY OF ENGINEERING & TECHNOLOGY

Index No.-197/19/E

1. **Title of the Thesis:**

   STUDIES ON ELECTRICAL TRANSPORT AND ION KINEMATICS PHENOMENA IN SOME OXIDE GLASSY SYSTEMS.

2. **Name, Designation and Institution of the Supervisors:**

DR. MADHAB ROY
Associate Professor
Department of Electrical Engineering
Jadavpur University
Kolkata-700032,
West Bengal, India.

DR. SANJIB BHATTACHARYA
Associate Professor – Deputy Director
UGC-MMTTC (Physics)
University of North Bengal
Darjeeling-734013,
West Bengal, India.

3. List of Publications:

Journals:

I. **Asmita Poddar**, Shayeri Das, Madhab Roy, Koyel Bhattacharya, Sanjib Bhattacharya, "Transport properties of CdI_2-doped silver ion conducting system: validation with first-principle DFT estimations", Ionics, 28, 2285–2292 (2022). https://doi.org/10.1007/s11581-022-04462-1

II. **Asmita Poddar**, Madhab Roy, Mir Sahidul Ali, Dipankar Chattopadhyay, Prolay Halder, Sanjib Bhattacharya, "Mixed conduction in iodovanadate glass-nanocomposites: DC conductivity, hopping frequency, and frequency response curves", Ionics, 30, 3357–3373 (2024). https://doi.org/10.1007/s11581-024-05446-z

III. **Asmita Poddar**, Prolay Halder, Madhab Roy, Sanjib Bhattacharya, "Short and long range ordering on dielectric relaxation of AgI doped glass-ceramic", Physica B: Condensed Matter, 696, 416557 (2025). https://doi.org/10.1016/j.physb.2024.416557

Book Chapters:

I. **Asmita Poddar**, Madhab Roy, Sanjib Bhattacharya, **"Optical Properties of Some Li-Doped Glassy Systems"**, Lithium-Ion Glassy Electrolytes, Springer (2022). ISBN No. 978-981-19-3268-7. https://doi.org/10.1007/978-981-19-3269-4_9

II. **Asmita Poddar**, Madhab Roy, Sanjib Bhattacharya, **"Electrodes"**, Lithium-Ion Glassy Electrolytes, Springer (2022). ISBN No. 978-981-19-3268-7. https://doi.org/10.1007/978-981-19-3269-4_13

III. **Asmita Poddar,** Madhab Roy, Sanjib Bhattacharya, **"Conductivity Study on Silver doped Oxy-Salt Glass-Nanocomposite and Comparative Analysis"**, Recent trends in Materials Science and its Applications, Aryabhat Publication House (2023). ISBN No. 978-93-95463-02-7

IV. **Asmita Poddar**, Madhab Roy, Sanjib Bhattacharya, **"Light-Emitting Diode"**, Handbook of Semiconductors: Fundamentals to Emerging Applications, CRC Press (2024). ISBN No. 1040040926, 9781040040928.

Conferences:

I. **Asmita Poddar**, Madhab Roy, Sanjib Bhattacharya, "Dynamics of Ag^+ ions in CdI_2 doped electrolytes", Materials Today: Proceedings, 66, Part 7, Pages 3373-3376 (2022). https://doi.org/10.1016/j.matpr.2022.07.229

4. List of Patents:

None

5. List of Presentations in National/International/Conferences/ Workshops:

I. **Asmita Poddar**, Madhab Roy and Sanjib Bhattacharya, **"Dynamics of Ag^+ Ions in CdI_2 doped Electrolytes"**, 29th National (Virtual) Conference on Condensed Matter Physics, Condensed Matter Days-2021, Organized by Central University of Jharkhand, 10–12 December,2021.

II. **Asmita Poddar**, Madhab Roy and Sanjib Bhattacharya, **"Electrical Transport phenomena of Ag^+ ions in CdI_2 doped Electrolyte"**, 5^{th}Regional Science and Technology Congress, 2022-23, Organized by West Bengal State Science & Technology Congress, 4–5 January, 2023.

III. **Asmita Poddar**, Madhab Roy and Sanjib Bhattacharya, **"Conductivity Study on Silver doped Oxy-Salt Glass-Nanocomposite and Comparative Analysis"**, 2nd International Conference on Multidiscipline Academic Research and Innovation, Organized by Aryabhat Institute of Academics and Research, Lucknow, 28 -29 January, 2023.

IV. **Asmita Poddar**, Madhab Roy and Sanjib Bhattacharya, **"Study on dielectric relaxation behaviour of some AgI doped glass nano-composites"**, 7^{th} Regional Science and Technology Congress, 2022-23, Organized by West Bengal State Science & Technology Congress, 17–18 January, 2025.

STATEMENT OF ORIGINALITY

I, **ASMITA PODDAR**, registered on 01/07/2019 do hereby declare that this thesis entitled **"STUDIES ON ELECTRICAL TRANSPORT AND ION KINEMATICS PHENOMENA IN SOME OXIDE GLASSY SYSTEMS"** contains literature survey and original research work done by the undersigned candidate as part of Doctoral studies.

All information in this thesis have been obtained and presented in accordance with existing academic rules and ethical conduct. I declare that, as required by these rules and conduct, I have fully cited and referred all materials and results that are not original to this work.

I also declare that I have checked this thesis as per the "Policy on Anti Plagiarism, Jadavpur University, 2019", and the level of similarity as checked by iThenticate software is 7%.

Signature of Candidate: Asmita Poddar

Date: 03/04/2025

Certified by Supervisors:

Madhab Roy 03/4/25

DR. MADHAB ROY
Associate Professor
Department of Electrical Engineering
Jadavpur University
Kolkata-700032, West Bengal, India

Associate Professor
Electrical Engg. Dept.
Jadavpur University
Kolkata - 700 032

Sanjib Bhattacharya 03/4/25

DR. SANJIB BHATTACHARYA
Associate Professor – Deputy Director
UGC-MMTTC (Physics)
University of North Bengal
Darjeeling-734013, West Bengal, India

Dr. Sanjib Bhattacharya
Associate Professor - Deputy Director
UGC-MMTTC
University of North Bengal

CERTIFICATE FROM THE SUPERVISORS

This is to certify that the thesis entitled **"STUDIES ON ELECTRICAL TRANSPORT AND ION KINEMATICS PHENOMENA IN SOME OXIDE GLASSY SYSTEMS"** submitted by **Mrs. Asmita Poddar**, who got her name registered on **01.07.2019** for the award of **Ph.D.** (Engineering) degree of Jadavpur University is absolutely based upon her own work under the supervision of **Dr. Madhab Roy** and **Dr. Sanjib Bhattacharya** and that neither her thesis nor any part of the thesis has been submitted for any degree/diploma or any other academic award anywhere before.

Madhab Roy 03/04/25

DR. MADHAB ROY
Associate Professor
Department of Electrical Engineering
Jadavpur University
Kolkata-700032, West Bengal, India

Associate Professor
Electrical Engg. Dept.
Jadavpur University
Kolkata - 700 032

Sanjib Bhattacharya
03/4/25

DR. SANJIB BHATTACHARYA
Associate Professor – Deputy Director
UGC-MMTTC (Physics)
University of North Bengal
Darjeeling-734013, West Bengal, India

Dr. Sanjib Bhattacharya
Associate Professor - Deputy Director
UGC-MMTTC
University of North Bengal

ACKNOWLEDGEMENT

It is a matter of great honor for me to have an opportunity to extend my gratitude to those remarkable individuals who supported me in my pursuit of knowledge and contribution in this field of work.

Above all, I wish to express my gratitude to Dr. Madhab Roy and Dr. Sanjib Bhattacharya, who supervised my research. I am incredibly grateful to them for their guidance and unwavering support during my studies. For me, pursuing a doctorate under them was an opportunity to learn. My sincere gratitude goes out to Dr. Madhab Roy of Department of Electrical Engineering, Jadavpur University, Kolkata, for his constant encouragement. I am appreciative of Dr. Sanjib Bhattacharya of university of North Bengal for his motivational leadership in my scientific career as well as in other spheres of life. Throughout the course, his unwavering cooperation was really helpful.

The financial assistance for the work by the Science and Engineering Research Board, Govt. of India via Sanction No: CRG/2023/000046 is thankfully acknowledged (PI: Dr. Sanjib Bhattacharya).

I am extremely appreciative of the support I received from the HOD, faculty and staff members of Department of Electrical Engineering, Jadavpur University, throughout the course of my research to pursue my degree. Furthermore, I would like to acknowledge my thesis committee members for their support and enlightening feedback.

I would like to express my deep gratitude to all the faculty members, administrative and support staffs at University of North Bengal for allowing me to pursue my research and for providing all of the facilities I needed to do so. I consider myself extremely grateful to Siliguri Institute of Technology for providing me with experimental support at the Composite Materials Research Laboratory in the early phases of my study.

I am enormously grateful to Sophisticated Analytical Instrument Facility (SAIF), Gauhati

University, Guwahati, India and Department of Polymer Science and Technology, University of Calcutta, Kolkata, for providing me necessary experimental facilities.

I would like to thank Principal Sir, HOD, all my friends and colleagues and administrative staffs of Dream Institute of Technology for providing me a cordial working environment to carry out my research work.

I extend my gratitude to my fellow researcher Mr. Prolay Halder for his heartiest co-operation in any moment of need during the course. I am grateful to my senior fellow researchers, Mr. Amartya Acharya and Ms. Swarupa Ojha, for their guidance to carry out my research work. Last but not the least, I would like to express my thankfulness to my friend and colleague researcher, Mr. Anil Chamuah, for his constant assistance at any time of difficulties throughout the tenure.

In closing, I would like to appreciate especially one of my greatest supporters of all time, Mr. Sandip Bose, for staying with me as my valuable friend during the years and keeping faith in me. A special thanks to my friends, Mr. Sourish Chatterjee, Mr. Soham Mukherjee, Mr. Soumyadeep Dey and Mrs. Payel Bhattacharya in particular for their untiring support, patience and encouragement throughout this journey.

In my mind, there are no adequate words to show gratitude towards my beloved parents. They are the essence of my existence and without their unwavering support and encouragement; I could not have advanced far in my academic career. My father has always inspired me to achieve this milestone, and I owe him my accomplishment though he is not with me anymore. Finally, my sincere and heartfelt gratitude is towards my husband Mr. Deepanjan Das, for his continuous helps and support throughout the years.

And to conclude, nothing is conceivable without the light of knowledge that The Almighty has bestowed upon us. I am grateful that He gave me the perseverance and fortitude to finish this thesis.

Asmita Poddar

Asmita Poddar

This thesis is dedicated to my beloved parents.

Late Asim Kumar Poddar & Mita Poddar

Your unwavering support, endless sacrifices and boundless love have been my greatest source of strength and inspiration.
Thank you for believing in me, encouraging my dreams, and standing by me every step of the way.
I am forever grateful for your guidance, wisdom, and the values you have instilled in me.

This achievement is as much yours as it is mine.

PREFACE

The wide range of applications, compositional diversity, and adaptive properties of glassy nanocomposite systems have made them extremely important materials in recent years. These materials have improved mechanical strength, optical qualities, thermal stability, and electrical conductivity through the incorporation of nanoparticles (such as metals, metal oxides, or carbon-based nanostructures) into glass matrices. Because of their adaptability, they enhance performance and longevity in electronics, optoelectronics, and energy storage systems. Their stability and biocompatibility make them useful in biological applications like as tissue engineering, medication delivery, and bioimaging. Their versatility also makes it possible for them to be used in protective films, coatings, and sensors, providing enhanced chemical stability, scratch resistance, and UV protection. Glassy nanocomposites' adjustable characteristics, which are influenced by the distribution and selection of nanoparticles, make them indispensable in next generation technologies.

This study's specific goal is to investigate how charge carriers, such as ions or polarons, are transported in the context of different glassy systems. The intricate process of charge carrier transport in glassy materials is impacted by the matrix's amorphous form and structural disarray. The study's goal is to find out how ions and polarons — the quasiparticles that represent electrons or holes and are connected with local lattice distortions—move across the glass's disordered network. Finding the processes controlling charge mobility—such as hopping conduction, tunnelling effects, and diffusion pathways—will be the main goal of the study. These mechanisms are greatly impacted by the glass's composition, temperature, and local structural variations. By looking at these transport processes, the study aims to comprehend how elements like glass composition, doping concentration, and nanoparticle inclusion affect the system's electrical conductivity, ionic mobility, and relaxation dynamics. The development of sophisticated glassy materials with ideal electrical, thermal, and optical characteristics for use in solid-state batteries, sensors, and optoelectronic devices depends on this investigation.

CONTENTS

LIST OF FIGURES

LIST OF TABLES

LIST OF SYMBOLS

σ	Conductivity
T	Temperature
σ_{dc}	DC Conductivity
σ_{ac}	AC Conductivity
Z_e	charge of the carrier
n	Concentration of mobile carriers
μ	mobility
ΔG_c	Free energy required to impart a carrier population
ΔS_c	Entropy
ΔH	Enthalpy
k_B	Boltzmann Constant
N_e	Actual infinite temperature ion concentration
D	Diffusivity
ΔG_m	Free energy for ion migration
ΔS_m	Associated Entropy
γ	Geometrical factor for ion hopping
λ	Average hop distance
ν_e	Effective jump attempt frequency
ΔE_B	Electrostatic forces
G_D	Glass's shear modulus
r_d	interstitial window
r	mobile cation
r_0	non-bridging anion radii

Z	Number of charges on the mobile cation
Z_0	Number of charges on the mobile anion
e	Charge of the electron
V_M	Molar Volume
W	Weight of the Sample
W_a	Weight of the glassy system in air
W_b	Weight of the glassy system in buoyant liquid
ρ_b	Density of the buoyant liquid
M_i	Molecular weight of the sample
x_i	molar fraction
D	Average crystallite size
β	Full Width at Half Maxima of the peak
δ	Dislocation density
ε	Lattice strain
θ	Peak angle
ρ	Resistivity
L	Length of the sample between electrodes
A	Cross-sectional area of the sample
E_{dc}	Activation energy due to DC Conductivity
E_h	Activation energy due to Hopping Frequency
$N(E_F)$	localized states density near Fermi level
α^{-1}	Degree of localization
$G(\omega)$	Conductance

LIST OF ABBREVIATIONS

GNC	Glass Nano-Composite
CRT	Cathode Ray Tube
SOFC	Solid Oxide Fuel Cell
LCD	Liquid Crystal Display
CFL	Compact Fluorescent Lamp
LED	Light Emitting Diode
T_f	Fictive temperature
T_g	Glass transition temperature
GC	Glass Ceramic
BO	Bridging Oxygen
NBO	Non-Bridging Oxygen
VRH	Variable Range Hopping
XRD	X-Ray Diffraction
SEM	Scanning Electron Microscopy
FT-IR	Fourier Transform Infrared Spectroscopy
CVD	Chemical Vapor Deposition
CBD	Chemical Bath Deposition
CBH	Correlated Barrier Hopping
NSPT	Non-Symmetric Polarons and Tunneling

Chapter 1

Introduction

Outline

1.1 INTRODUCTION

Glass and glass Nano-Composite materials have drawn human interest for centuries. This is due to a number of notable and attractive features that make them materials of great interest to researchers [1-2]. Nanoscience and nanotechnology are among the most admired areas of contemporary research and development in practically all technical disciplines that deal with materials and structures that have dimensions as small as a billionth of a meter (nanometer). However, their application has always been limited because of its unfavorable qualities, which include low hardness, low tensile strength, and resistance to fracture. In recent years, scientists have been developing novel glass nano-composite systems that integrate metal nanoparticles into glass matrices, making them promising candidates for application in numerous fields [3–8].

These days, researchers are especially interested in the electrical, optical, and dielectric characteristics of glass nano-composite materials; the characterization process is being studied further. Through glass and glass nano-composite materials, the fields of physics, chemistry, biology, engineering, and technology are expanding into hitherto unachievable microscopic length scales. Now, at the nanoscale, one enters a world where physics and chemistry meet to give matter new properties. The remarkable variations in properties that these nano-composite exhibits depend on the number, size, and shape of the implanted nanoparticles [9–10]. Whitesides [11] has reportedly discussed about the elements that have contributed to the popularity and success of this inter/multidisciplinary study. According to several modern scientists and researchers, the number of research publications that use the prefix "Nano" has increased dramatically during the last 30 to 35 years [12]. It is a prelude to the quick growth of interest in and study of nanoscience and nanotechnology.

1.2 GLASSY SYSTEMS

Glass is one of the most often used materials, in addition to the materials used throughout human civilization. With the development of technology from the ancient to the mediaeval to the modern periods, glass has been used in a wide variety of applications, from mirrors to window glass to sophisticated solid electrolytes. The technological idea and literature around glass have progressively changed over time as science and technology have advanced. It is often recognized that the preparation of glass is not as difficult as the composition of the glass itself.

The glass family's hierarchical structure is illustrated in Fig. 1.1. To properly understand glass nano-

composite (GNC), one must be aware of the hierarchical relationships among the members of the glass family. The picture makes it abundantly evident that glass can be divided into two main categories — inorganic and organic — according to its chemical and structural composition. In general, inorganic glasses fall into one of two categories: natural or synthetic (made or artificial). All glassware that are used in daily life and may be found everywhere, including windows, mirrors, bottles, lights, glasses, tumblers, and more, are referred to as common glass.

This field's influence is growing not just in academia but also in industries, such as ceramics, chemical polishing agents, scratch-resistant coatings, stain-resistant clothing, cosmetics, sunscreens, etc. As a result, there is increased interest in creating new nanomaterials and gadgets through the synthesis of different nanoscale structures and particles. Clusters, nanomaterials, nanowires, long molecules like poly-nucleotides and nanotubes, and functional molecular nanostructures are a few examples of the materials that are now being explored as possible building blocks for nanotechnology and nano-electronic circuits and devices [13].

It indicates that the special qualities of glass nanocomposites—such as optical transparency, structural stiffness, compositional flexibility, property tailoring adaptability, and durability—are what draw us to them. Because of these special qualities, glass can be used for both conventional and cutting-edge technical applications. Table 1.1 shows a few instances of the numerous uses of glass and the products that go along with them.

1.2.1 Definition of Glass

"Glasses are supercooled liquids or supercooled as solids" is the conventional description of glass, as stated at the outset. Both recent articles [14] and earlier publications [15] by researchers use this conventional concept. Information regarding the Author and publication of this traditional definition of glass are still anonymous to us. But in the definition of glass given by Simon [16] in 1930, which states "In the physicochemical sense, glass is a frozen-in undercooled liquid", it can be significantly noted that for the preparation of glass the only method adopted so far is the cooling (quenching) of the molten glass (the liquid). But with the advancement of technology the revolution of glass has taken place and accordingly multiple definitions of glass have been put out in the literature by various authors at various points in time. Zachariasen, in 1932, has tried to give a new structural aspect and gave the definition [15] as "A glass has an extended three-dimensional network and its energy content is comparable to that of the corresponding crystal but without periodicity and symmetry". In 1933,

Tammann [17] illustrated "In the glassy state, there are solids, un-crystallized materials". Then Morey [18] tried to give an explicit definition of glass which describes as "A glass is an inorganic substance in a condition which is continuous with, and analogous to, the liquid state of that substance, but which, as the result of having been cooled from the fused condition, has attained so high a degree of viscosity as to be, for all practical purposes, rigid and cooled to a rigid condition without crystallizing".

Jones provided a different perspective on glass in his work [19]. It says, "A glass…is a material, formed by cooling from the normal liquid state, which has no discontinuous change … at any temperature, but has become more or less rigid through a progressive increase in its viscosity". Glass was defined by Mackenzie [20] as, "Any isotropic material, whether it is inorganic or organic, in which three-dimensional atomic periodicity is absent and the viscosity of which is greater than about 1014 poise, may be described as a glass. (By the three-dimensional atomic periodicity, we imply a long-range order, dependent on the material in question, of greater than, say, 20 Å units)". Further Doremus, in his work [21] demonstrated glass as, "Glass is an amorphous solid. A material is amorphous when it has no long-range order, that is, when there is no regularity in the arrangement of its molecular constituents on a scale larger than a few times the size of these groups". Elliott [22] and Shelby [23] also supported the concept of amorphous solid in their works. Varshneya and Mauro described glass in their work [24] "Glass is a solid having a non-crystalline structure, which continuously converts to a liquid upon heating".

1.2.2 Glass Transformation

The glass transition is a crucial feature of the glassy state that marks glasses unique among other amorphous materials. The smooth transition of a glass to its supercooled molten state during heating or the transformation of a very viscous supercooled melt into a solid (glass) while cooling is known as the "glass transition," which is an interesting thermal event. The transition temperature (T_g) signifies the phase transition in both the situations. For better understanding of the mechanism of glass creation [25–27] the proper knowledge of "glass transition" is required. The factor that commands the process of synthesization of glasses is speed.

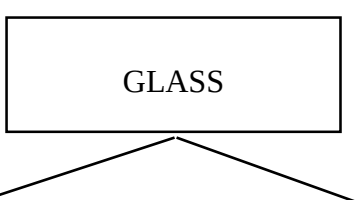

Fig.1.1: Hierarchical connections among glass family

As the liquid cools down further, its volume continuously lowers and it solidifies in two different ways that are illustrated in Fig. 1.2:

(1) Intermittently to a crystalline solid or
(2) Uninterruptedly to an amorphous solid (glass).

Different purpose	**Structural**	Windows, building glass, toughened glass, bullet proof glass, glass fiber reinforced plastics

	Electrical	Insulators of electric bulbs, CRT tubes, SOFC and other sealing glasses, X-ray generating tubes
	Electronic	Insulators and envelopes for electronic valves, glass plates with printed circuit boards, rockets
	Thermal	Thermometers, Thermo flasks, heat-absorbing window glasses, fire resistant glass walls
	Chemical	Containers, Tubes, Rods, Laboratory glass wares, Electrodes
	Mechanical	Bearings, Molds for rubber and plastic, Diffusion Vacuum Pumps, Torsion Fibres
	Optical	Lenses, Prisms, Mirrors, Spectacles, LCD glasses, Optical Fibres
	Lighting	Different lamps (Incandescent, Fluorescent, CFL, LED), Neon signs, Photoflash bulbs
	Nuclear	X-ray and γ-ray shields, dosimeter, glass for fixation of radio-active waste

Table 1.1: Miscellaneous sectors where glasses are used extensively [Ref.2].

Path 1 in the Fig. 1.2 elaborates the process of crystallization which vividly shows that it requires longer time to occur. In order to crystallize a molten substance into a solid form, the temperature is decreased to T_f in this procedure. When the temperature of the melted material lies between T_f and T_g the material is called super-cooled liquid. If material's temperature is abruptly decreased to T_g without giving any time to the material to get crystallized, the super-cooled liquid becomes glass and remain in that form forever. Therefore, the preparation of amorphous solid or glass is the process of avoiding crystallization which can be achieved by cooling the liquid material very speedy.

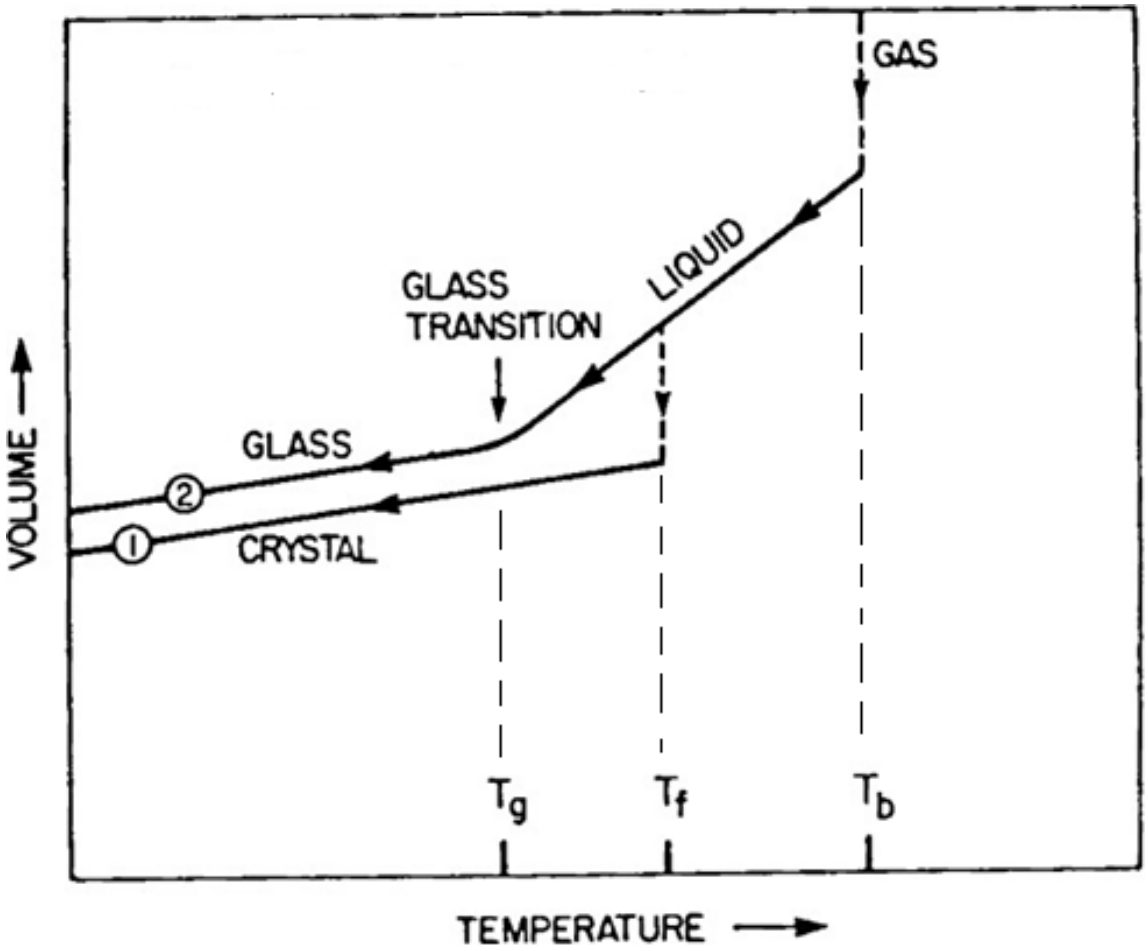

Fig.1.2: The two general cooling paths by which an assembly of atoms can condense (Ref.1)

1.2.3 Nano-Composites

Materials known as Nano-Composites are composed of many constituent parts, each of which must have at least one dimension in the range of 1 to 100 nm. Different kinds of Nano-Composites are depicted in Fig. 1.1.

There are three types of Nano scale materials:
(a) Nano Particles, which have three dimensions
(b) Nano Fibres, which have two dimensions
(c) Nano Clays, which have one dimension

The sample material, also referred to as the matrix, is combined with Nano-materials, also known

as fillers, to create a Nano-Composite in the macro scale regime [28-30]. The optical, thermal, mechanical, dielectric, and electrical conductivities of the matrix material are enhanced, along with many other properties, by the addition of Nano-materials or fillers. The potential of Nano-Composite materials to overcome the shortcomings of micro-composite materials is growing. Nano-Composites are regarded as the materials of the present and future centuries due to their special qualities that are not possible to find in a typical composite.

1.2.3.1 Classification of Nano-Composites

Depending on the materials used in the matrix the three classifications of Nano-Composites are:

(a) Metal matrix

(b) Ceramic matrix

(c) Polymer matrix

Due to their attractive characteristics, metal nanoparticle-containing Nano-Composites with insulating matrix, such as glass, ceramic, or polymer, have drawn attention from researchers. Metal glass Nano-Composites stand out among the others with intriguingly special qualities such improved electrical resistivity, mechanical strength, and refractive index. Glass matrices are combined with metal nanoparticles to create these Nano-Composites. Creating low power, high speed optical devices for communication systems is one of these materials' significant uses [31-32].

1.2.3.2 Glass Nano-Composites (GNC)

Glass ceramic (GC) materials are made by devitrifying glasses to form polycrystalline solids with nano to micro meter-sized crystals embedded in a residual glass matrix. To do this, one must first produce glass using traditional methods, which are followed by regulated crystallization [33-34]. Tiny crystals are formed as a result of this process, which separates a crystalline phase from the glassy parent phase. Appropriate heat treatment can regulate the quantity of crystals, their rate of growth, and their ultimate size [35].

Glass and ceramic materials are similar in many ways to GC materials. Along with the unique qualities of ceramics, they have the fabrication advantage of glass. The typical crystallinity of GCs ranges from 30% to 90%. They produce a wide range of materials with intriguing characteristics, such as low porosity, superior strength, durability, , rich chemical durability, biocompatibility, ion conductivity, superconductivity, low dielectric constant and loss, high resistivity, and break-down voltage, among other interesting attributes [36–41]. Controlling the composition of the base glass

and the base glass's-controlled heat treatment and crystallization can both be used to modify these characteristics [40-41].

GCs are typically made in two stages: A glass is first created through the glass making process. In a second process, the glass is reheated after cooling. This heat treatment causes some crystallization in the glass. Nucleation agents are typically added to the GC's base composition. The crystallization process is aided and controlled by these nucleation agents. GCs lack pores, in contrast to sintered ceramics, because there is typically no pressing or sintering involved.
Materials are classified as "Glass-Ceramic Nano-composites" (GCNC) if the crystals produced in them have sizes in the nano-meter or even micro range and were nucleated from some metal nanoparticles [42-43]. Due to their unique physical characteristics, including appearance, chemical durability, and mechanical stability, as well as their intriguing optical behaviour—particularly non-linear optical behaviour—metal nanoparticle-based Nano-composite materials containing Au, Ag, and Cu have potential applications [44-45].

1.2.4 Classification of Various Glasses

Amorphous semiconductors have electrical characteristics that differ from those of crystalline semiconductors now in use. Crystalline semiconductors include materials like germanium, silicon, gallium arsenide, and so forth. Materials with negative temperature coefficients of resistivity are known as amorphous semiconductors. These glasses fall into two categories based on their prevalence: (a) natural glasses and (b) artificial glasses. Depending on the components that make them up, artificial or man-made glasses are further divided into two classes: oxide and non-oxide. These kinds are explained in the sections that follow:

1.2.4.1 Oxide Glasses

Zachariasen made one of the first suggestions for the glass structure in his seminal paper [15]. His theories, known as random network theory, are still crucial to the study of glass structure till today. Zachariasen claims that identical interactions bind the atoms in a crystal and a glass, causing them to vibrate around their equilibrium positions. But the primary structural difference between the two exists because, unlike crystals, the structure of a glass lacks symmetry and periodicity. Zachariasen explained the details of the glass structure considering the instances of oxide glasses. Oxide glass is defined as glass that has oxygen as one of its basic elements. He analyzed the structure of vitreous silica. Zachariasen observed that the silicon atoms in the glass network are surrounded by oxygen tetrahedra. Each oxygen atom is linked to two silicon atoms by the corner sharing that holds the

tetrahedra together. Tetrahedra are shown as triangles in Figure 1.3 which is a two-dimensional representation of this structure. Zachariasen came to the conclusion that oxygen tetrahedra or oxygen triangles are the only shapes that can create a vitreous network.

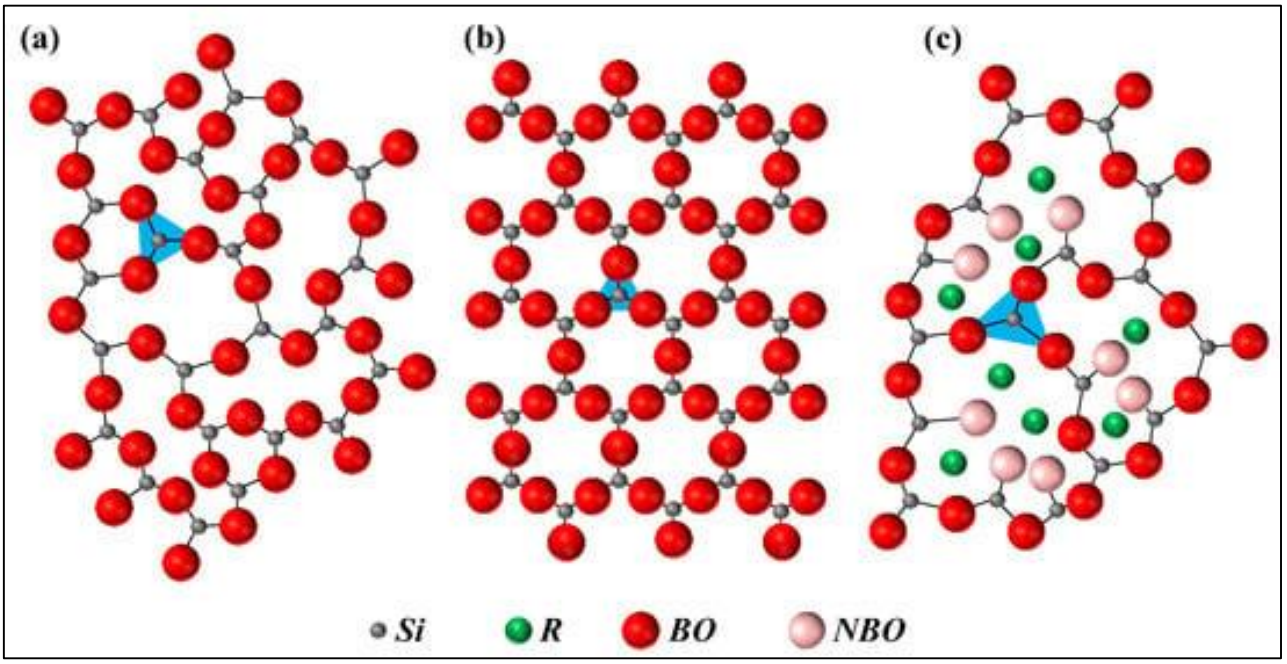

Fig.1.3: Two-dimensional representation of network structure of (a) vitreous and (b) crystalline silica; (c) vitreous silicate (R stands for a generic network modifier cation, while BO and NBO stand for bridging oxygen and non-bridging oxygen, respectively).

Zachariasen [15] observed few general guidelines that applies to vitreous oxides.

(1) There are only two cations bonded to each oxygen atom.
(2) The network cation's oxygen coordination number is low.
(3) Triangles or oxygen tetrahedra only share their corners—neither their edges nor their faces.
(4) To build a three-dimensional (3D) network, each oxygen polyhedron must share at least three of its corners.
(5)A significant portion of the sample is made up of cations, which are encircled by oxygen triangl es or tetrahedra.

Glass formation is generally governed by these broad guidelines. They do not, however, explain how glasses develop in non-oxide systems, and some of the rules—such as the existence of oxygen tri-

clusters—do not apply to oxide systems as well. Consequently, these guidelines shouldn't be used rigidly, yet they nonetheless serve as a foundation for the structural examination of glasses.
As seen in Figure 1.3 (c), by adding elements like alkali and alkaline earth oxides to the vitreous oxide networks, the excess oxygens no longer form bridges but rather free ends, which have a distinct structural purpose.

Therefore, the constituents of oxide glasses are categorised into three classes based on the type of structural function they perform:

Network formers: They are also known as network units or structural units, and are the parts that construct the glass network by creating oxygen triangles and tetrahedra. The key elements of the glass are the network formers because they can create three-dimensional structures. These sections are linked to one another through corner sharing, forming what random network theory refers to as bridging oxygens (BO), or oxygen bridges (shown in Figure 1.3 (a)). Typical instances include SiO_2, B_2O_3, and P_2O_5.

Network Modifiers: As seen in Figure 1.3 (c), network modifiers are the elements that disintegrate the glass network by generating terminal oxygens, also known as non-bridging oxygens (NBO). The alkali and alkaline earth oxides are typical examples.

Intermediate Oxides: Depending on the composition of the glass, intermediate oxides can act as either network formers or network modifiers.

The majority of glasses that are sold commercially are made of silica, or SiO_2. Sands are one of the many forms of silica that may be found in nature. Vitreous silica or silica glasses are defined as glasses composed entirely of silica. When quartz crystals melt in order to make these, they are occasionally referred to as fused quartz. Applications requiring low electrical conductance, strong thermal shock resistance, great chemical durability, and UV transparency are the principal ones where silica glasses are used. It has been discovered that soda lime silica glasses work best for making the majority of glass products used on a daily basis, such as flower vases, windows, bulbs, and glass containers, where the main needs are excellent durability and affordable pricing.

Generally speaking, oxides, sulfides, fluorides, and certain metallic salts are materials that can form glasses. They fall into two categories: "network modifiers" (Ag_2O, Na_2O, P_2O_5, BaO, etc.) and "glass

formers" (B_2O_3, P_2O_5, V_2O_5, MoO3, etc.). With these former and modifier combinations, studies have been conducted on metal oxide M_2O (M = Ag, Li, Na, and K) and a doping salt MX (X = I, Br, Cl, and F) [25–27]. An oxide that is easily able to make glass is called a glass former; on the other hand, an oxide that is not involved in the formation of the network structure is called a network modifier.

1.2.4.2 Non-Oxide Glasses

Non-oxide glasses are those that do not have oxygen as one of their basic constituents. The following categories apply to non-oxide glasses:

1.2.4.2.1 Heavy-Metal Fluoride Glasses (HMFGs):

These non-oxide glasses are typically composed of elements such as sodium, barium, lanthanum and aluminum. Due to their relatively low optical losses, these glasses are well suited for usage in telecommunication fibres. However, these glasses have a very difficult preparation process, and their chemical endurance is poor.

1.2.4.2.2 Glassy Metals:

These non-oxide glasses are made by fast quenching molten metals. These glasses, known as METGLAS in the commercial sector, are often made of iron, phosphorous, nickel, and boron. Power transformers and magnetic shielding are two areas where these glasses are used.

1.2.4.2.3 Chalcogenide Glasses:

These non-oxide glasses are amorphous semiconductors that include certain other appropriate elements from the periodic table along with chalcogens (sulfur, selenium, and/or tellurium). These glasses are semiconducting, which makes them useful in a variety of applications such as xerography and memory switching devices. Their potential for usage in photovoltaic applications, such as solar cells, has been established.

1.2.4.2.4 Glass Ceramics:

These are the glasses where there is a good chance of partially introducing crystallization in the normally chaotic atomic structures. Instead of occurring at the surface or in specific regions of the glasses, uniformly sized, high density, non-oriented crystals are achieved throughout bulk samples of the commercially available glass ceramics. These glasses are used in dental implants, cooking vessels, and other purposes.

1.2.4.2.5 Glass Composites:

To create useful glass goods, Glass composites are created by combining powders of metal, polymer, and ceramic materials. Products manufactured from these composites have special qualities that result from the interaction of all the component parts. These glasses find use as thick film conductors, resistors, dielectrics, and glass fiber reinforced polymer, among other applications where the electrical properties must be tailored for the field of microelectronics.

1.2.4.2.6 Natural Glasses:

These are the glasses that are found in the natural world. Tektites (made from terrestrial debris expelled by meteorite collisions), moldavites (produced from meteorite collisions typically found in central Europe), fulgarites (produced when lightning strikes the ground), obsidians or volcanic glass, and microtektites (generally found in Deep Ocean) are a few examples of these glasses. Microtektites are helpful in applications involving the control of hazardous waste because of their great chemical stability under water.

1.3 THEORY OF ELECTRIC TRANSPORT AND ION KINEMATICS IN GLASSY SYSTEMS

Glassy systems, because of their disordered atomic structure, have unique electrical transport features. Glassy materials lack long-range order, which results in distinctive transport methods, in contrast to crystalline materials, where ions and electrons travel in distinct lattice patterns. In glassy materials, electronic conduction and ionic conduction are the two main methods via which electric transport takes place.

1.3.1 Ionic Conduction:

Because glassy systems are random and disordered, the movement of ions inside them is characterized by complicated kinematic behaviors. In glassy systems, the flow of ions through amorphous, non-crystalline materials is referred to as ionic conduction [46–49]. Glassy materials have unique conduction pathways because they lack long-range order, in contrast to crystalline solids where ions flow through well-ordered lattice structures. Ionic transport is facilitated by a hopping mechanism in glassy systems that contain mobile ions, such as lithium, sodium, and silver. Ions travel via irregularly spaced energy minima due to the lack of a periodic lattice structure, frequently assisted by network flexibility and free volume. Thermal activation, the presence of modifying cations, and structural relaxation all affect ionic transport.

1.3.1.1 Mechanisms of Ionic Conduction in Glassy Systems:

Hopping Mechanism: Ions travel through the disordered matrix by hopping between available low-energy locations. Because there is no periodic lattice, ions can move along asymmetrical paths that are shaped by the local structural environment [46-47].

Percolation Pathways: Conduction takes place through percolation networks in certain glassy systems, where interconnected areas offer preferred ion movement pathways [47-48]. The structural flexibility of the glass matrix and the concentration of mobile ions both affect how these networks evolve.

Role of Network Formers and Modifiers: Network modifiers, such as alkali oxides like LiO and NaO, disrupt the network and introduce non-bridging oxygen, while network formers, such as SiO_2 and P_2O_5, produce the glass matrix in glassy systems. Ion mobility is facilitated by the paths that are created by these disruptions [47-49].

Temperature Dependence and Non-Arrhenius Behavior: The disordered structure's complicated energy landscape frequently causes non-Arrhenius behavior in ionic conductivity in glasses [48-49]. A temperature-dependent conductivity that deviates from a straightforward exponential relationship can result from variations in the activation energy for ion movement.

1.3.1.2 Factors Influencing Ionic Conductivity:

The structural and compositional properties of the material are the main factors influencing ionic conductivity in glassy systems. Ion transport in glass happens via complex pathways due to its lack of a periodic crystalline structure, and its effectiveness is influenced by a number of physical and chemical factors. The key factors affecting ionic conductivity include:

1. Composition of the Glass:

Ionic conductivity is greatly influenced by the kind and concentration of network formers (such as SiO_2, B_2O_3, and P_2O_5) and network modifiers (such as alkali oxides like Li_2O, Na_2O).

Network formers: These affect the availability of conduction channels and produce a stiff glass structure.
Network Modifiers: These increase ion mobility and weaken the glass network by introducing non-bridging oxygen atoms.
Alkali Oxides (Li_2O, Na_2O, K_2O): By supplying more mobile ions and breaking up the inflexible glass network, an increase in alkali oxide concentration usually results in improved ionic conductivity.

2. Nature and Concentration of Mobile Ions:

Ionic Size and Charge: Compared to larger ions (like Cs^+), smaller and less strongly charged ions (like Li^+) flow through the glass structure more readily.
Ionic Radius: Since they may fit into fewer conduction channels, smaller cations (e.g., $Li^+ < Na^+ < K^+ < Rb^+ < Cs^+$) typically have more mobility.
Ion Concentration: Conductivity rises with a greater concentration of mobile ions.

3. Glass Structure and Connectivity

The ease of ion migration depends on the level of connectedness within the glass network.
Open Network Structure: Ion mobility is increased by a more open shape because it offers greater free volume and conduction channels.

4. Non-Bridging Oxygen (NBOs)

Ion transit is facilitated and the structure is weakened by the presence of NBOs. Typically, ions in tetrahedral surroundings are more mobile than those in octahedral coordination.

5. Temperature Dependence

Ionic conductivity generally increases with temperature due to thermal activation of ion hopping. The temperature dependence often follows the Arrhenius equation relationship, indicating a complex interplay between thermal energy and structural relaxation.

6. Mixed Alkali Effect (MAE)

When two different alkali ions are present, ionic conductivity often decreases due to competition for conduction sites. This is attributed to ion trapping effects and structural rearrangement.

7. Mixed Glass Former Effect (MGFE)

Ionic conductivity can be increased by combining several network formers (e.g., B_2O_3 + P_2O_5) to create more conduction pathways. This impact varies depending on the type of glass and is very composition dependent.

8. Role of Dopants and Defects

By forming defect sites that either facilitate or impede ion flow, specific dopants can be added to change the conduction properties. Conduction efficiency can also be impacted by structural voids and point flaws.

9. Humidity and External Factors

Ionic mobility may be impacted by moisture absorption in certain glassy electrolytes because they are hygroscopic. Conduction pathways can be reoriented and ion mobility can be changed by applied electric fields.

1.3.2 Electronic Conduction:

In glassy systems, the flow of electrons through amorphous, non-crystalline materials is referred to as electronic conduction [50–52]. Glassy materials have distinct conduction pathways because they lack long-range order, in contrast to crystalline solids, where electrons flow through well-ordered lattice structures. Depending on temperature and applied electric fields, charge carriers (electrons or holes) travel via hopping between extended electronic states or defect states. Thermally activated behavior is a characteristic of this conduction mechanism, which is frequently non-metallic.

1.3.2.1 Mechanisms of Electronic Conduction in Glassy Systems:

Hopping Conduction:

Electrons do not go across extended band states in disordered systems; instead, they hop between localized states. In this process, electrons tunnel across sites; the likelihood of hopping depends on a number of variables, including temperature and the energy differential between sites. This mechanism's temperature dependency frequently adheres to Mott's variable-range hopping model, where conductivity (σ) varies with temperature (T).

Polaronic Conduction:

Polarons can develop in glassy systems as a result of interactions between electrons and the lattice. Through thermally triggered hopping, small polarons—where the electron is highly localized—move through the lattice. The degree of electron-lattice coupling and the disorder in the glassy matrix affect the activation energy for polaron hopping.

1.3.2.2 Polarons

A polaron is a quasi-particle composed of an electron (or hole) and a localized distortion of the surrounding lattice caused by interactions between electrons and phonons. A polaron's creation modifies a material's electrical characteristics, especially in amorphous and disordered systems like glassy materials.

1.3.2.2.1 Types of Polarons

In general, polarons are categorized according to how strongly they interact with the lattice:

Small Polarons:

The electron becomes highly localised within a single atomic site or a small region when there is a strong electron-phonon interaction. Thermal activation causes small polarons to hop from one localized location to another. Small polaron mobility has a temperature dependency of the Arrhenius kind.

Large Polarons:

The electron is able to stay delocalized across several lattice sites due to weak electron-phonon interaction. Instead of hopping, large polarons show band-like conduction.

1.3.2.2.2 Polaron Hopping in Glassy Systems

The disordered structure of glassy materials prevents the creation of extended electronic bands, making small polarons the dominating carriers. The following mechanisms are responsible for polaron hopping:

Thermally Activated Hopping:

The polaron can move to a nearby location and cross the energy barrier at higher temperatures because phonons supply a sufficient amount of energy. The observed rise in conductivity with temperature is explained by this mechanism, which predominates in non-crystalline materials.

Variable Range Hopping (VRH):

At lower temperatures, instead of hopping to the next neighbour, electrons hop across a varied range between localized states. This adheres to Mott's VRH concept.

1.3.2.3 Factors Affecting Electronic Conductivity

Temperature: The thermal energy accessible to electrons rises with temperature, increasing the hopping rate and, consequently, the conductivity.

Glass Composition: Polaron production is influenced by the presence of transition metal ions (e.g., Fe^{3+}, V^{4+}). These components have the ability to create localised electronic states that promote hopping conduction.

Structural Disorder: Hoping distances and activation energies are influenced by the density and distribution of localised states, which are influenced by the degree of disorder.

Carrier Concentration: Higher polaron densities may cause conductivity to change due to interaction effects.

1.4 STUDIES OF ELECTRIC TRANSPORT AND ION KINEMATICS IN GLASSY SYSTEMS

In order to comprehend ion kinematics and electric transport in glassy systems, scientists need to perform computational, theoretical, and experimental investigations. The essential studies that are needed are as follows:

1.4.1 Structural and Compositional Analysis

It is necessary to characterize the glass's composition and structure before examining its transport properties.

X-ray Diffraction (XRD) Characterization: It validates the material's glassy (amorphous) properties.

Electron Microscopy (SEM/TEM) Characterization: It displays microstructural elements that could influence transport, such as pores or phase separation.

Study of Infrared Spectroscopy: It examines the bond structures and vibrational modes that affect

the energy environment.

1.4.2 Ionic Conductivity and Transport Measurements

Studying ionic conduction aids in comprehending how ions flow across the glassy network.

AC Impedance Spectroscopy: By measuring frequency-dependent conductivity, it is possible to differentiate between electronic and ionic contributions (e.g., long-range diffusion at low frequencies and hopping conduction at high frequencies). It is employed to compute ion mobility and activation energy.

DC Conductivity Measurements: Bulk conductivity and its temperature dependence are determined by it. It is employed to realise the whole charge-transporting capacity of the material. It determines the conduction mechanism and shows whether the system behaves in an Arrhenius-type manner or if there are variations that point to variable-range hopping.

Dielectric Spectroscopy: Dielectric relaxation research aids in the examination of polarisation mechanisms and how they relate to charge transfer. Dielectric studies are used to measure the complex dielectric permittivity and analyse the relaxation time. It facilitates the correlation between conduction processes and dielectric relaxation peaks.

1.5 ION CONDUCTION IN GLASSES: DIFFERENT MODELS

For more than half a century ionic transport processes in glasses and glass nano-composites have piqued the interest of scientists worldwide. Numerous glass-forming systems have been studied across a broad range of compositions.

The early 1970s energy crisis and the finding of fast-ion-conduction in oxide glass [53] sparked a lot of interest in the use of glasses to serve as solid state electrolytes in advanced battery storage devices. The challenge of independently establishing the carrier concentration and mobility, however, has left the microscopic mechanics underlying ionic conduction in glasses poorly understood. For conventional glass formers such as SiO_2 [53], B_2O_3 [54], P_2O_5 [55], GeO_2 [56] etc, the dc and ac conductivity of the ionically conducting glasses have been thoroughly investigated.

The dc conductivity for materials with single type of carrier is specified by

$$\sigma_{dc} = (Ze)n\mu \tag{1.1}$$

where Ze is carrier charge, n represents the mobile carriers concentration and μ is mobility. It is possible for the concentration of mobile ions to be thermally activated and expressed as-

$$\begin{aligned} n &= N_0 \exp\left(\frac{-\Delta G_c}{k_B T}\right) \\ &= N_0 \exp\left(-\frac{\Delta S_c}{k_B}\right) \exp\left(\frac{-\Delta H_c}{k_B T}\right) \\ &= N_0 \exp\left(\frac{-\Delta H_c}{k_B T}\right) \end{aligned} \tag{1.2}$$

The Nernst – Einstein relation gives the idea about mobility –

$$\begin{aligned} \mu &= \frac{ZeD}{k_B T} = \frac{Ze\gamma\lambda^2 v_H}{k_B T} \\ &= \left(\frac{Ze\gamma\lambda^2 v_0}{k_B T}\right) \exp\left(\frac{-\Delta G_m}{k_B T}\right) \\ &= \left(\frac{Ze\gamma\lambda^2 v_0}{k_B T}\right) \exp\left(\frac{-\Delta S_m}{k_B}\right) \exp\left(\frac{-\Delta H_m}{k_B T}\right) \\ &= \left(\frac{Ze\gamma\lambda^2 v_e}{k_B T}\right) \exp\left(\frac{-\Delta H_m}{k_B T}\right) \end{aligned} \tag{1.3}$$

where free energy required for ion migration is represented by ΔG_m, ΔS_m is the linked entropy, enthalpy is denoted by ΔH_m, the geometrical factor designed for ion hopping is represented by γ, the average hop distance between the mobile ion sites is given by λ, ν_H signifies hopping frequency, ν_0 indicates ion's jump attempt frequency and ν_e represents the actual jump attempt frequency together with the entropy.

The enthalpy and energy state functions under constant specimen volume and temperature are e qual, according to the first law of thermodynamics. Thus ΔH can be replaced by ΔE and thus substituting Eqn. (1.19) and (1.18) to (1.17) yields

$$\sigma_{dc} = \left(\frac{N_e(Ze)^2\gamma\lambda^2 v_e}{k_B T}\right) exp\left\{\frac{-(\Delta E_c+\Delta E_m)}{k_B T}\right\} \quad (1.4)$$

Two themes need to be the main focus of the ion transport mechanism in glasses.

- Anderson – Stuart model (Strong – Electrolyte theory)
- Ravaine – Souquet model (Weak – Electrolyte theory)

1.5.1 Anderson –Stuart Model

According to the structural model Anderson-Stuart [57], activation energy is defined as -

$$\Delta E_{act} = \Delta E_B + \Delta E_S \quad (1.5)$$

where the binding energy term is given as,

$$\Delta E_B = \frac{ZZ_0e^2}{\varepsilon_\infty}\left[\frac{1}{r+r_0} - \frac{2}{\lambda}\right] \quad (1.6)$$

and the strain energy term is given as

$$\Delta E_s = \frac{\pi G_D \lambda (r-r_D)^2}{2} \quad (1.7)$$

These formulas use the following notation: G_D stands for the glass's shear modulus, the interstitial window is denoted by r_d, mobile cation by r and non-bridging anion radii by r_0, respectively. λ is the average jump distance. Z and Z_0 are the number of charges on the mobile cation and the anion and e is the charge of the electron.

McElfresh and Howitt [58] have suggested a few small modifications to the strain term in order to make the Anderson-Stuart model more realistic. Elliott [59] has highlighted that the Anderson-Stuart model incorporates these components into the overall coulomb potential but ignores some polarization and repulsion terms. Although there have been several models proposed to describe the activation energy, almost all of them adhere to the general ideas of the Anderson-Stuart model.

The physical and structural parameters essential to authenticate the legitimacy of the Anderson Stuart model and experimental methods for measuring these parameters are:

- ΔE_{act} : determined from wide temperature range ionic conductivity measurements.
- λ : approximated from NMR static line width measurements, or density measurements.
- G: determined from acoustic measurements
- r_D : the interstitial window radius determined from inert gas diffusion studies

To examine the validity of the Nerst-Einstein derivation for pre-exponent term, the following added parameters are needed:

- σ_0 : determined from wide temperature range ionic conductivity measurements
- ν_0 : determined from the Far-IR ion vibrational frequency
- γ : usually taken as approximately equal to $\frac{1}{6}$

1.5.2 Ravaine – Souquet Model

The Weak-Electrolyte or Ravaine-Souquet model derives its foundation from the relationship between ionic conductivity and thermodynamic activity [59]. When M_2O or M_2S are introduced to glasses, the added anions usually covalently link to the glass forming cations, becoming a part of the glass structure. A tiny percentage of the alkali cations may separate from these sites to create ionized or dissociated "mobile" cations, but the majority of them are unionized and immobile. It is believed that these ions aid in ionic conduction. The dissociation of modifying salt given to a glass is thought to be equivalent to the generation of mobile cations M^+ from related oxide complexes in glasses [60].

$$M_2O = M^+ + OM^- \tag{1.8}$$

and the concentration independent dissociation constant is given by

$$K = [M^+]\,[OM^-]/\,[M_2O] \tag{1.9}$$

The dissociated ion's concentration is given by

$$[M^+] = K^{1/2}\,[M_2O]^{1/2}$$
$$= K^{1/2}\,[a_{M2O}]^{1/2} \tag{1.10}$$

where a_{M2O} is the thermodynamic activity equated to the M_2O concentration.

The equality is valid for very dilute solutions (Henry's law). The ionic conductivity is proportional to the concentration of mobile ions, so that

$$\sigma \propto [M^{+}] = K^{1/2}[a_{M2O}]^{1/2} \quad (1.11)$$

For a range of sodium and potassium silicate glasses, Ravaine and Souquet measured the ionic conductivity and concentration cell emf. Plotting the conductivity ratio against the activity ratio for different pairs of glasses, they demonstrated that the log plot's slope was ½.

In addition to these two models, numerous alternative models that can be categorized as follows and have been put up to explain the transport properties:

1.5.3 Cluster – bypass Model

In accordance with this approach [61-62], vitrification is defined as the congelation of organized micro domains or clusters into a network filled with spaces. The main idea of this model is that the connective tissues are the preferred ion migration paths. A residual liquid occupies the interstitial space between the clusters at and below T_g, and upon cooling, it solidifies to form a residual phase, or connective tissue.

1.5.4 Dynamic Structure Model

Bunde et al. presented this model of the mixed cation/alkali impact [63-64]. According to the results of extended Xray absorption fine structure (EXAFS) measurements of mixed alkali glasses, each type of cation in a mixed alkali glass forms a unique environment. This fact clearly indicates that alkali B is less likely to visit a location that alkali A previously occupied, and vice versa. Elastic energy typically coexists with lattice distortion. While not precisely the same, the transfer mechanism of ion A into site $B^{-}$with substantial lattice distortion is comparable to modest polaron motion in solid state electron physics [65-66]. For transfer to an unoccupied site to occur in small polaron transport, the occupied site must deform by thermal energy (multi-phonon transition). Thermal activation, which derives its activation energy from the lattice deformation, determines the transfer rate.

1.6 SOME PREVIOUS WORKS ON OXIDE GLASS NANO-COMPOSITES

Zwanziger et al. [67] claim that doping silver phosphate with silver iodide can result in glasses with abnormally high ionic conductivity at particular compositions. Ionic conductors of this general kind,

comprising a glass forming, a network modifier, and a doping salt (P_2O_5, Ag_2O, and AgI, respectively in their study), have promising electrical properties and are easily manufactured. The dynamics of the temperature- and frequency-dependent silver iodide-silver phosphate system have been studied using a variety of methods.

Research has been done on the structure of the glass matrix as well as the interaction of the salt with the glass [68-69]. These investigations have shown that the network is composed of a variety of unique phosphates and that the glass structure of the network is not markedly changed by the addition of silver iodide. In an effort to accurately define the interactions between the mobile silver cations and the phosphate glass and silver iodide, they have studied the microstructure of the phosphate sites using a developed NMR technique [70]. The iodide glass system ($AgI–Ag_2O–MoO_3$), first reported by Minami [71-72], falls under this group of materials. Many studies have been conducted on its glass-forming regions, electrical properties, glass-transition temperatures, and local structures [71-76].

Studies on different AgI doped glasses [77-78] has shown that the ionic conductivity considerably increases with the addition of AgI as metal halide. However, AgI doped silver molybdate glasses and their nanocomposites show unique features and increasing evidence of structural anomalies when compared to silver borate and silver phosphate glasses [79-80]. The relationship between the microscopic structure in glasses and glass-nanocomposites and the fast ion conductivity has been the subject of extensive experimental investigation.

Kariper's [81] study states that cadmium iodide has a hexagonal unit cell and typically di-halides as MX_2 [82]. The layer of cadmium ions is compressed and encased by the iodine layers. There is an ionic connection between iodine and cadmium. Conversely, iodine ions are bound via van der Waals bonds. Some researchers were able to synthesize amorphous cadmium iodide by examining the optical properties of the metal halide. The optical band gap of cadmium iodide is 3.8 eV [83-84].

Till date, Tiyagi and Vedeshwar's [85] study is the most exhaustive on CdI_2 thin films. They noted hexagonal structural indexing and XRD peaks at (001), (101), and (111). A parabolic curve was found on the plot of CdI_2 particle size vs film thickness in their investigation. They discovered that when layer thickness and grain size increased, the optical band gap decreased.

Significant number of studies [86-88] have taken place where presence of CdI_2 has pronounced effect on the conductivity of the glass nano-composites. The study shows that the DC and AC conductivity increases with increase in concentration of CdI_2. Ionic conductivity is mainly due to Ag^+ ions. The studies have suggested that amalgamation of alkali halide modifiers in the Silver mixed glassy matrix augments the ionic conductivity to a huge extent. The super ionic conductors are formed like this. The glass transition temperature, T_g, decreases more sharply in the CdI_2 doped systems in comparison to AgI based silver vanadate system.

K.P. Padmasree et al have shown in a study [89] on the system $Ag_2O–V_2O_5–B_2O3$ with CdI_2 dopant that highest electrical conductivity is achieved for the composition with 30 mol% of CdI_2. At room temperatures, Silver oxy-salt complexes form the glasses which are the finest conductors as per the study. S. Kabi eta al have prepared samples of compositions xCdI2 – (1−x) (yAg_2O – (1−y) P2O5), for different values of y in their study [90]. It can be seen that conductivity rises for the metaphosphate (y=0.5) and polyphosphate (y=0.6) glasses but declines for ultra-phosphate (y=0.3, 0.4) glasses with the increase in CdI_2 content. Conductivity increases with the increase of the Ag_2O/P_2O_5 ratio for fixed CdI_2 contents.

Studies [91-92] have also been done by the researchers to investigate the mixed former effect on the glass nano-composites. The introduction of mixed formers has assisted to have developed T_g, consequently increases thermal stability. This in turn enhances electrical conductivity.

1.7 CONCLUSION

The present work aims to synthesize some novel semiconducting glassy nano-composite materials and studying their structural, dielectric and electrical characteristics. In the present work Ag^+, Cd^{+2} ion-conducting glass nano-composites have been formed from different non-conventional glass formers like V_2O_5, P_2O_5, MoO_3, TeO_2 etc. The study's main area of interest is the role that ions and polarons play in the conductivity analysis of the systems as prepared and to gather knowledge about the probable migration pathways. The effort has been given to find out their properties and change in ion dynamics due to incorporation of different modifiers. The possible technological applications of these materials in industry as well as in academic purposes is a great area of interest of this thesis.

The main objectives of the PhD work:

- Development of some novel (ionic and semiconducting) glass nanocomposite systems using conventional Melt – Quenching method.
- Identification of different nano phases and estimation of the average crystallite size of as prepared Glassy systems.
- Identification of the micro structure and nature of bonds of the as prepared Glassy systems.
- Exploration of Transport properties and the factors which influence the charge transport mechanism of as prepared glass nanocomposite systems.
- Identification of the appropriate theoretical model for frequency dependent conduction mechanism and to check whether the experimental data of dc conductivity and ac relaxation mechanism agree with that or not.
- Determination of the mobile carrier ion concentration and its relation with the conductivity and how it varies with temperature and composition.
- Identification of the suitable device applications.

References

[1] Elliott, S. R. (1990). Physics of amorphous materials. (No Title).
[2] Karmakar, B., Rademann, K., & Stepanov, A. (Eds.). (2016). Glass nanocomposites: synthesis, properties and applications. William Andrew.
[3] Kreijig, U., & Vollmer, M. (1995). Optical Properties of Metal Cluster.
[4] Dan, A., Satpati, B., Satyam, P. V., & Chakravorty, D. (2003). Diodelike behavior in glass–metal nanocomposites. Journal of applied physics, 93(8), 4794-4800.
[5] Fleming, L. A., Wackerow, S., Hourd, A. C., Gillespie, W. A., Seifert, G., & Abdolvand, A. (2012). Diffractive optical element embedded in silver-doped nanocomposite glass. Optics Express, 20(20), 22579-22584.
[6] Bhattacharya, S. (2020). Metal oxide glass nanocomposites. In Metal Oxide Glass Nanocomposites (pp. 27-35). Elsevier.
[7] Stepanov, A. L. (2016). Nonlinear optical properties of metal nanoparticles in silicate glass. In Glass Nanocomposites (pp. 165-179). William Andrew Publishing.
[8] Stalmashonak, A., Abdolvand, A., & Seifert, G. (2011). Metal-glass nanocomposite for optical storage of information. Applied Physics Letters, 99(20).
[9] Thomas, S., Nair, S. K., Jamal, E. M. A., Al-Harthi, S. H., Varma, M. R., & Anantharaman, M. R. (2008). Size-dependent surface plasmon resonance in silver silica nanocomposites. Nanotechnology, 19(7), 075710.
[10] Kreibig, U., Gartz, M., Hilger, A., Hovel, H., & Duncan, M. A. (1998). Advances in metal and semiconductor clusters. Adv Met Semicond Clusters, 4, p345.
[11] Whitesides, G. M. (2006). The origins and the future of microfluidics. nature, 442(7101), 368-373.
[12] Braun, T., Schubert, A., & Zsindely, S. (1997). Nanoscience and nanotecnology on the balance. Scientometrics, 38, 321-325.
[13] Contado, C. (2015). Nanomaterials in consumer products: a challenging analytical problem. Frontiers in chemistry, 3, 48.
[14] Debenedetti, P. G., & Stillinger, F. H. (2001). Supercooled liquids and the glass transition. Nature, 410(6825), 259-267.
[15] Zachariasen, W. H. (1932). The atomic arrangement in glass. Journal of the American Chemical Society, 54(10), 3841-3851.
[16] Simon, F. (1930). Ergebnisse der exakten naturwissenschaften. Ergebn Exakt Naturwiss, 9, 222-274.
[17] G. Tammann, Der Glaszustand, “The Glassy State”, (Voss, Leipzig, 1933).
[18] Morey, G. W. (1954). The properties of glass.
[19] G.O. Jones, “Glass”, (Methuen & Co, London, UK, 1956).
[20] Mackenzie, J. D. (1960). General aspects of the vitreous state. Modern aspects of the vitreous state, 1-9.
[21] Doremus, R. H., & Frieser, R. G. (1975). Glass Science. Journal of The Electrochemical Society, 122(2), 36Ca.

[22] Shelby, J. E. (2020). Introduction to glass science and technology. Royal society of chemistry.

[23] Chen, H. S., & Miller, C. E. (1970). A rapid quenching technique for the preparation of thin uniform films of amorphous solids. Review of Scientific Instruments, 41(8), 1237-1238.

[24] Varshneya, A. K., & Mauro, J. C. (2010). Comment on misconceived ASTM definition of" Glass" by AC wright. Glass Technology: European Journal of Glass Science and Technology Part A, 51(1), 28-30.

[25] Van Gool, W. (1973). Fast ion transport in solids, solid state batteries and devices. (Proceedings of the NATO-sponsored advanced study institute of fast ion transport in solids, solid state batteries and devices, Belgirate, Italy 5-15 September 1972).

[26] Shelby, J. E., & Ortolano, R. L. (1990). Properties and structure of NaF-Na2O-B2O3 glasses. Physics and chemistry of glasses, 31(1), 25-29.

[27] Fusco, F. A., Tuller, H. L., & Button, D. P. (1992). Lithium, sodium and potassium transport in fast ion conducting glasses: trends and models. Materials Science and Engineering: B, 13(2), 157-164.

[28] Ajayan, P. M., Schadler, L. S., & Braun, P. V. (2006). Nanocomposite science and technology. John Wiley & Sons.

[29] Davim, J. P. (Ed.). (2013). Tribology of nanocomposites. Springer Berlin Heidelberg.

[30] Manocha, L. M., Valand, J., Patel, N., Warrier, A., & Manocha, S. (2006). Nanocomposites for structural applications.

[31] Camargo, P. H. C., Satyanarayana, K. G., & Wypych, F. (2009). Nanocomposites: synthesis, structure, properties and new application opportunities. Materials Research, 12, 1-39.

[32] Camargo, P. H. C., Satyanarayana, K. G., & Wypych, F. (2009). Nanocomposites: synthesis, structure, properties and new application opportunities. Materials Research, 12, 1-39.

[33] Angell, C. A., Ngai, K. L., McKenna, G. B., McMillan, P. F., & Martin, S. W. (2000). Relaxation in glassforming liquids and amorphous solids. Journal of applied physics, 88(6), 3113-3157.

[34] Ediger, M. D., Angell, C. A., & Nagel, S. R. (1996). Supercooled liquids and glasses. The journal of physical chemistry, 100(31), 13200-13212.

[35] H. Vogel, Phys. Zeit., 22, 645 (1921).

[36] Yin, A. J., Li, J., Jian, W., Bennett, A. J., & Xu, J. M. (2001). Fabrication of highly ordered metallic nanowire arrays by electrodeposition. Applied Physics Letters, 79(7), 1039-1041.

[37] Le, J. D., Pinto, Y., Seeman, N. C., Musier-Forsyth, K., Taton, T. A., & Kiehl, R. A. (2004). DNA-templated self-assembly of metallic nanocomponent arrays on a surface. Nano Letters, 4(12), 2343-2347.

[38] Varshneya, A. K. (2013). Fundamentals of inorganic glasses. Elsevier.

[39] Santen, L., & Krauth, W. (2000). Absence of thermodynamic phase transition in a model

glass former. Nature, 405(6786), 550-551.

[40] Chakraborty, N., Banerjee, J., Chakraborty, P., Banerjee, A., Chanda, S., Ray, K., ... & Sarkar, J. (2022). Green synthesis of copper/copper oxide nanoparticles and their applications: a review. Green Chemistry Letters and Reviews, 15(1), 187-215.

[41] Kang, J., Yang, X., Hu, Q., Cai, Z., Liu, L. M., & Guo, L. (2023). Recent progress of amorphous nanomaterials. Chemical Reviews, 123(13), 8859-8941.

[42] Stanworth, J. E. (1971). Oxide glass formation from the melt. Journal of the American Ceramic Society, 54(1), 61-63.

[43] Poulain, M. (1981). Glass formation in ionic systems. Nature, 293(5830), 279-280.

[44] Chicot, D., Mercier, D., Roudet, F., Silva, K., Staia, M. H., & Lesage, J. (2007). Comparison of instrumented Knoop and Vickers hardness measurements on various soft materials and hard ceramics. Journal of the European Ceramic Society, 27(4), 1905-1911.

[45] James A. Schwarz, Christian I. Contescu, Karol Putyera, "Dekker Encyclopedia of Nanoscience and Nanotechnology", (Vol 10.1, Marcel Dekker, ISBN: 08247-5055-1, 2004).

[46] Hona, R.K., Guinn, M., Phuyal, U.S., Sanchez, S., & Dhaliwal, G.S. (2023). Journal of Materials Science and Chemical Engineering, 11, 31-72.

[47] Bosi, M., Fischer, J., & Maass, P. (2021). Network-forming units, energy landscapes, and conductivity activation energies in alkali borophosphate glasses: analytical approaches. The Journal of Physical Chemistry C, 125(11), 6260-6268.

[48] Bosi, M., & Maass, P. (2022). Theory for ion diffusion and conduction in glasses based on site energy distributions derived from network former unit concentrations. Diffusion Fundamentals, 35.

[49] Schulz, A., Lunkenheimer, P., & Loidl, A. (2021). Lithium-salt-based deep eutectic solvents: Importance of glass formation and rotation-translation coupling for the ionic charge transport. The Journal of Chemical Physics, 155(4).

[50] Pietrzak, T. K., Wasiucionek, M., & Garbarczyk, J. E. (2021). Towards higher electric conductivity and wider phase stability range via nanostructured glass-ceramics processing. Nanomaterials, 11(5), 1321.

[51] Kurnosov, A., & Lubchenko, V. (2025). The mechanism of electrical conduction in glassy semiconductors. Proceedings of the National Academy of Sciences, 122(10), e2414650122.

[52] Boolchand, P., Georgiev, D. G., & Goodman, B. (2001). Discovery of the intermediate phase in chalcogenide glasses. Journal of Optoelectronics and Advanced Materials, 3(3), 703-720.

[53] Otto, K. (1966). Electrical conductivity of SiO_2-B_2O3 glasses containing lithium or sodium. Physics and Chemistry of Glasses, 7(1), 29.

[54] A. Schtchukarev, W. R. Muller, J. Phys. Chem. Abst. A, 150, 489 (1930).

[55] Martin, S. W., & Angell, C. A. (1986). Dc and ac conductivity in wide composition range Li_2O- P_2O_5 glasses. Journal of Non-Crystalline Solids, 83(1-2), 185-207.W O. Anderson, D. Stuart, J. Amer. Soc. 37, 573 (1954).

[56] Martin, S. W. (2016). Glass and glass-ceramic sulfide and oxy-sulfide solid

electrolytes. In Handbook of Solid State Batteries (pp. 433-501).

[57] Elliott, S. R. (1993). Calculation of the activation energy for ionic conduction in glasses. Journal of non-crystalline solids, 160(1-2), 29-41.C. D. Ravaine, J. L. Souquet, Phys. Chem. Glasses, 18, 27 (1977).

[58] Isard, J. O., Jagla, M., & Mallick, K. (1982). Simple Models for The Ionic Conduction Mechanism In Glasses. Le Journal de Physique Colloques, 43(C9), C9-387.

[59] Ingram, M. D., Mackenzie, M. A., Müller, W., & Torge, M. (1988). Cluster and pathways: a new approach to ion migration in glass. Solid State Ionics, 28, 677-680.

[60] Ingram, M. D. (1989). Ionic conductivity and glass structure. Philosophical Magazine B, 60(6), 729-740.

[61] Bunde, A., Ingram, M. D., & Maass, P. (1994). The dynamic structure model for ion transport in glasses. Journal of non-crystalline solids, 172, 1222-1236.

[62] Bunde, A., Ingram, M. D., Maass, P., & Ngai, K. L. (1991). Mixed alkali effects in ionic conductors: a new model and computer simulations. Journal of non-crystalline solids, 131, 1109-1112.

[63] Mustarelli, P., Tomasi, C., Quartarone, E., & Magistris, A. (2003). Linear-superposition method for the multiple-scattering problem in low-energy-photoelectron diffraction. Phys. Rev. B, 58, 9054-9057.

[64] Sanson, A., Rocca, F., Fornasini, P., Dalba, G., Grisenti, R., & Mandanici, A. (2007). Thermal behaviour of the local environment around iodine in fast-ion-conducting AgI-doped glasses. Philosophical Magazine, 87(3-5), 769-777.

[65] Zwanziger, J. W., Olsen, K. K., & Tagg, S. L. (1993). Structure and disorder of phosphates in Ag 2 O-AgI-P 2 O 5 glasses. Physical Review B, 47(21), 14618.

[66] Minami, T., Katsuda, T., & Tanaka, M. (1979). Structural study with infrared spectroscopy and thin-layer chromatography of superionic conducting glasses in the system silver iodide-silver oxide-phosphorus pentoxide. Journal of Physical Chemistry, 83(10), 1306-1309.

[67] Hayashi, S., & Hayamizu, K. (1989). High-resolution solid-state 31P NMR study of network structure in AgI- Ag2O- P2O5 glass. Journal of Solid State Chemistry, 80(2), 195-200.

[68] Frydman, L., Chingas, G. C., Lee, Y. K., Grandinetti, P. J., Eastman, M. A., Barrall, G. A., & Pines, A. (1992). Variable-angle correlation spectroscopy in solid-state nuclear magnetic resonancea. The Journal of chemical physics, 97(7), 4800-4808.

[69] Minami, T., & Tanaka, M. (1980). Structure and ionic transport of superionic conducting glasses in the system AgI-Ag/sub2/O-MoO/sub 3. J. Non-Cryst.

Solids;(Netherlands), 38(39).

[70] Minami, T., Katsuda, T., & Tanaka, M. (1978). Infrared spectra and structure of superionic conducting glasses in the system AgI- Ag2O- MoO3. Journal of Non-Crystalline Solids, 29(3), 389-395.

[71] Sanson, A., Rocca, F., Dalba, G., Fornasini, P., & Grisenti, R. (2007). Influence of temperature on the local structure around iodine in fast-ion-conducting AgI: Ag2MoO4 glasses. New Journal of Physics, 9(4), 88.

[72] Mustarelli, P., Linati, L., Tartara, V., Tomasi, C., & Magistris, A. (2005). Structure/transport relationships in silver-based oxide glasses: 1-D and 2-D NMR information. Solid State Nuclear Magnetic Resonance, 27(1-2), 112-121.

[73] Sanson, A., Rocca, F., Fornasini, P., Dalba, G., Grisenti, R., & Mandanici, A. (2007). Thermal behaviour of the local environment around iodine in fast-ion-conducting AgI-doped glasses. Philosophical Magazine, 87(3-5), 769-777.

[74] Ghigna, P., Di Muri, M., Mustarelli, P., Tomasi, C., & Magistris, A. (2000). Local order of Ag in AgI–Ag2MoO4 glasses: an EXAFS study. Solid state ionics, 136, 479-481.

[75] Adhwaryu, V. A., & Kanchan, D. K. (2021). Ag+ ion conduction in AgI-Ag2O-B2O3-P2O5 glass electrolyte. Materials Science and Engineering: B, 263, 114857.

[76] Alrifai, B., Kassem, M., Toufaily, J., Bokova, M., & Bychkov, E. (2022). Pb2+ potentiometric chemical sensors based on lead and silver doped thioaresenate glasses. Solid State Sciences, 131, 106955.

[77] Sidebottom, D. L. (2000). Influence of cation constriction on the ac conductivity dispersion in metaphosphate glasses. Physical Review B, 61(21), 14507.

[78] Swenson, J., & Börjesson, L. (1996). Correlation between free volume and ionic conductivity in fast ion conducting glasses. Physical review letters, 77(17), 3569.

[79] Kariper, I. A. (2017). Optical and Structural Properties of Natural MnSeO 4 Mineral Thin Film. Materials Research, 20, 613-618.

[80] Levy, F. (1976). Structural chemistry of layer-type phases.

[81] S. Kondo, S. Kagawa, T. Saito. Jpn J Appl Phys. 32:5, 596 (1993).

[82] Rehwald, W., & Harbeke, G. (1965). On the conduction mechanism in single crystal β-indium sulfide In2S3. Journal of Physics and Chemistry of Solids, 26(8), 1309-1324.

[83] Verma, R. S., & Choudhary, S. (2022). Electronic and optical properties of TMDs/Hg0. 33Cd0. 66Te. Journal of Materials Science: Materials in Electronics, 33(14), 11542-11554.

[84] Kabi, S., & Ghosh, A. (2012). Microstructure and optical properties of CdI2 doped silver

vanadate glass-nanocomposites. Materials Research Bulletin, 47(11), 3195-3200.

[85] Rao, P. N., Ramesh Kumar, E., & Appa Rao, B. (2018). Structural and transport studies of CdI 2-doped silver borotellurite fast ion-conducting system. Journal of Solid State Electrochemistry, 22, 3863-3871.

[86] Ghosh, A., Dutta, D., Kabi, S., & Ghosh, A. (2009). Electrical relaxation in CdI2 doped silver vanadate superionic glasses. Journal of Applied Physics, 105(6).

[87] Padmasree, K. P., & Kanchan, D. K. (2005). Dielectric studies on CdI2 doped Ag2O–V2O5–B2O3 system. Materials chemistry and physics, 91(2-3), 551-557.

[88] Kabi, S., & Ghosh, A. (2011). Dynamics of Ag+ ions and immobile salt effect in CdI2 doped silver phosphate glasses. Solid State Ionics, 187(1), 39-42.

[89] Satyanarayana, N., Patcheammalle, R., Muralidharan, P., Venkateswarlu, M., & Rambabu, B. (2000). Preparation, characterization and impedance studies of the superionic conducting AgI–Ag2O–CrO3–V2O5 glassy system. Solid state ionics, 136, 1097-1100.

[90] Padmasree, K. P., Kanchan, D. K., Panchal, H. R., Awasthi, A. M., & Bharadwaj, S. (2005). Structural and transport properties of CdI_2 doped silver ion conducting system. Solid state communications, 136(2), 102-107.

Chapter 2

Experimental Methodology

Outline

2.1 INTRODUCTION

The methods utilized for producing oxide glassy systems with various compositions and the various characterization techniques that may be applied to analyze the systems' structural and electrical characteristics are the primary matters of this chapter. The first section discusses about the various methods of preparation of glassy systems using a range of techniques which includes mechanical milling, the sol-gel process, chemical vapor deposition (CVD), chemical bath deposition (CBD), melt-quenching, and more, along with their benefits and drawbacks [1–10]. The very popular melt quenching technique has been adopted to produce the oxide glassy systems in our work. After synthesization, the as-prepared samples have undergone several structural characterizations and the electrical conductivity and relaxation studies for investigation on their electrical transport phenomena. In the next section, the details of all the studies are discussed.

The structural and physical characteristics of the glassy systems' can be described using a variety of methods, such as XRD, FT-IR, SEM and density and molar volume measurements. Density is a key characteristic that determines the structure of any glassy system. For example, a glassy system with a higher density value reveals that the existing particles are closely packed together in its internal structure. The value of density has a direct effect on a system's molar volume, suggesting a shift in the network's structure [11]. X-ray diffraction (XRD) is a vital concept of structural characterization that identifies the glassy nature of the as-prepared samples. The detection of the nano-phases and their [h, k, l] values, calculation of the crystallite size, dislocation density and strain are the primary outcomes of the XRD analysis [12-15]. In order to identify unknown materials, ascertain the number of components in a combination, assess the quality and dependability of materials, and obtain other valuable system information, Fourier Transform Infrared spectroscopy (FT-IR) is an essential structural characterization approach [17–18]. Through the study of Scanning Electron Microscopy (SEM), information regarding the surface morphology of the as-prepared systems have been acquired.

Following the structural characterization investigation, the charge carrier transport phenomena of the system have been investigated by the examination of electrical conductivity data. Several analytical models, including Mott's model [19] and Greaves' model [20], are used to analyse DC conductivity data. From these, the density of states in the system can be computed for lower and higher temperature regions, respectively. AC conductivity data are analyzed using a variety of methods, including the Power law [21], Almond West formalism [22], Cole-Cole plot etc. With the use of

appropriate models like CBH, NSPT, etc., the conduction mechanism of a system can be determined. Permittivity and electric modulus studies are carried out to examine the dielectric characteristics of a system.

2.2 PREPARATION OF GLASSY SYSTEMS

There are numerous methods for creating glassy systems or materials that are in an amorphous state. Mechanical milling, the sol-gel method, chemical bath deposition (CBD), chemical vapor deposition (CVD), and metal dielectric co-sputtering deposition are a few of these approaches. The employment of these procedures has several serious drawbacks, including expensive cost, unsuitability for low melting or low softening glass preparations, the risk of sample damage from high intensity radiation exposure, possibility to create only thin glass plates, etc. Because of its efficiency, simplicity, and ability to make glass quickly, the melt quenching process is frequently utilized to overcome these drawbacks and form a glassy system.

The sections below provide specifics on a few methods for preparing glassy systems:

2.2.1 Mechanical Milling Technique

High purity elemental powders are needed for this approach, and they are weighted according to their stoichiometric proportion of atomic mass. To ensure homogeneity, the powders are blended, crushed, and constantly stirred using a mortar. To obtain a very homogenous solid solution of the system, the mixture is then put in an electric mill and ball-milled for at least 12 hours at 400 rpm using a stainless-steel ball. This ball typically has a diameter of 10 mm and a steel ball to mixture ratio of 5:1. This is among the simplest and least expensive ways to prepare glassy systems. However, it is a laborious procedure that needs safety precautions to avoid contamination from the milling medium. According to A.S. Hassanien et al. [1], the $Cd_{50}S_{50-x}Se_x$ glassy system was prepared by mechanically milling it.

2.2.2 Sol-Gel Process

A further technique for creating glassy systems, such as SiO_2, involves converting monomers into a colloidal solution known as "sol." The sol serves as a forerunner to the "gel," an integrated network that consists of both liquid and solid phases. Metal alkoxides or metal chlorides are common precursors. To generate a colloid, which is a mixture of solid and liquid particles dispersed in a liquid

medium, the precursor is subjected to hydrolysis and poly- condensation processes.
This process is thought to be promising for the creation of some non-oxide glassy systems and ultra-thin metallic oxide. The following are a few benefits of this method: versatile—allowing for the incorporation of organic materials and nanoparticles into systems created using this method; better homogeneity—as mixing occurs at the molecular level, which leads to better homogeneity; low energy consumption; and affordable—as expensive equipment is not needed. Nevertheless, there are a few disadvantages to this approach, such as the need for precursors, the potential for gel to shrink during drying, residual porosity, and the difficulty of avoiding OH groups. Tetraethyl orthosilicate was used as precursor in the sol-gel technique to generate the CdSe doped Silica glassy system, as reported by P. V. Jyothy et al. [2].

2.2.3 Chemical Vapour Deposition Technique

This method of vapour deposition involves the breakdown of chemical precursors in a vapour phase on the surface of a heated substrate. High-quality, high-performing solid materials are produced using this technology. This method involves exposing a substrate to a volatile precursor, which causes a chemical reaction that results in the deposition of a thin coating on the substrate's surface. This approach has several benefits, including high purity, low cost, and high throughput. It does, however, have several drawbacks, such as the need for high deposition temperatures for certain precursors that are inappropriate for substrates and the fact that precursors are frequently poisonous or hazardous. Therefore, further actions must be performed to address precursors. D. B. Potter et al. have reported on the use of CVD method to create Si-doped ZnO thin films [3].

2.2.4 Chemical Bath Deposition Technique

It's a technique for coating substrates with thin films. There are two processes in this technique: particle growth and nucleation. Simply this method forms a solid state from a solution. The substrate is submerged in bath (a precursor-containing solution) during this process. This method's ability to deposit thin films on a substrate depends on a number of variables, including time, temperature of the bath, pH level of the solution, and substrate composition. This technique cannot result in any physical harm to the substrate. The main advantage of this method is that it only needs solutions containers and substrate mounting mechanisms. This method can be used to create films that are stable, adhering, rigid, and uniform. The primary disadvantage of this method is the solution waste that occurs after every deposition. There are numerous studies on the fabrication of glassy system

thin films using this method [4-5].

2.2.5 Melt Quenching Method

In this study, bulk samples of oxide glassy systems with a range of compositions were prepared using a well-known technique called melt-quenching. By rapidly cooling the molten materials to prevent crystal formation in the solids, this approach creates amorphous solids from the molten states of materials. There are numerous studies [6–10] on the creation of glassy systems using this technique. The melt-quenching process produces the great majority of glasses in practical cases. The batch (combination of raw materials) is melted in this method for a set amount of time in the electric furnace. Then the molten liquid is rapidly quenched to obtain the "as-prepared glass." Glass samples that need to be prepared for various characterisation processes are sawed, ground and polished.

The process of melt quenching comprises of the following steps –

A. The right raw material selection is the first step in preparing the batch.
B. Measurement of Reagent Grade Precursors in appropriate Stoichiometry using a high accuracy mechanical balance (Maker: Dhona, Model no.: 200D), Fig. 2.1 (a)
C. Appropriate mixing of the precursors and proper grounding of the reagents to form a fine powder, Fig. 2.1 (b)
D. Heating the mixtures in high temperature furnace up to melting point or glass transition temperature usually between 700 and 1200 degrees Celsius, Fig. 2.1 (c)
E. Sudden cool down to room temperature by quickly pressing the melt between Two Aluminum Plates, Fig. 2.1 (d)
F. A Plate is formed which is the required Glass Nano-composite of thickness of around one millimeter. The compositions' nature determines the color of the glass samples, Fig. 2.1 (e)

Fig. 2.1 (a) Measurement of Reagent Grade Precursors

Fig. 2.1 (b) Mixing of the Precursors

Fig. 2.1 (c) Heating the Mixtures in High Temperature Furnace

Fig. 2.1 (d) Quick pressing of the Melt

Fig. 2.1 (e) Different as-prepared glasses

2.3 COMPOSITION DETAILS OF AS-PREPARED GLASS NANO-COMPOSITE SYSTEMS

The following oxide glassy system compositions have been synthesized in the current study using the melt quench method. The details are listed in Table 2.1.

Sl. No.	Compositions	Varying molar concentration
1.	x AgI - (1-x) {0.1CdO – 0.3V_2O_5 – 0.4P_2O_5 – 0.2ZnO}	x = 0, 0.05, 0.1, 0.2, 0.3, 0.4
2.	0.2 AgI – 0.8 {0.1CdO –y V_2O_5 – z P_2O_5 – 0.2 ZnO}	y = 0.1, z = 0.6 y = 0.2, z = 0.5 y = 0.3, z = 0.4
3.	x CdI_2 – (1-x) {0.3Ag_2O – 0.3 V_2O_5 – 0.3 P_2O_5 – 0.1 ZnO}	x = 0.1, 0.2
4.	0.3 CdI_2 – 0.7 {yAg_2O – 0.3 TeO_2 – z P_2O_5 – 0.1 ZnO}	y = 0.1, z = 0.5 y = 0.3, z = 0.3
5.	0.3 CdI_2 – 0.7 {yAg_2O – 0.3 MoO_3 – z P_2O_5 – 0.1 ZnO}	y = 0.1, z = 0.5 y = 0.3, z = 0.3

Table 2.1: Composition of the as-prepared samples

A. AgI - CdO – V_2O_5 – P_2O_5 – ZnO system:

The oxide glassy system x AgI - (1-x) {0.1CdO – 0.3 V_2O_5 – 0.4 P_2O_5 – 0.2 ZnO} has been prepared. The value of x has been taken as 0, 0.05, 0.1, 0.2, 0.3 and 0.4. The as-prepared sample has been synthesized using different reagent-grade chemicals (Maker: Aldrich 99%) maintaining their proper stoichiometry. After thoroughly mixing, the mixture is taken in an alumina crucible and then is melted in an electric furnace. Table 2.2 contains information about the samples, including the melting temperature history for the 5 grams batch.

Sample Designation (x)	Silver Iodide (AgI) (g)	Cadmium Oxide (CdO) (g)	Vanadium Pentoxide (V_2O_5) (g)	Phosphorus Pentoxide (P_2O_5) (g)	Zinc Oxide (ZnO) (g)	Melting Temperature (^oC)
0	0	0.4571	1.9424	2.0211	0.5793	850
0.05	0.4043	0.4202	1.7853	1.8577	0.5325	850
0.1	0.7832	0.3855	1.6381	1.7046	0.4886	800
0.2	1.4736	0.3224	1.3699	1.4255	0.4086	750
0.3	2.0863	0.2663	1.1317	1.7776	0.3376	800
0.4	2.6352	0.2162	0.9187	0.9559	0.2740	800

Table 2.2 Molecular Weight of the as-prepared sample A

B. AgI - CdO – V_2O_5 – P_2O_5 – ZnO system:

Samples of AgI doped CdO - V_2O_5 - P_2O_5 - ZnO system with constant quantities of AgI – CdO – ZnO and with varied proportion of V_2O_5 and P_2O_5 are made. The new Glass Nano-Composite holds the empirical formula 0.2 AgI – 0.8 {0.1CdO –y V_2O_5 – z P_2O_5 – 0.2 ZnO}, where y varies as 0.1, 0.2 and 0.3, and z as 0.6, 0.5 and 0.4. All are made from the reagent-grade chemicals. The necessary amounts of all the reagents (Maker: Aldrich 99%) are mixed well and heated in an electric furnace. Details about the samples are provided in Table 2.3, which also includes the melting temperature history for the batch of 5 grams.

Sample Designation (y, z)	Silver Iodide (AgI) (g)	Cadmium Oxide (CdO) (g)	Vanadium Pentoxide (V_2O_5) (g)	Phosphorus Pentoxide (P_2O_5) (g)	Zinc Oxide (ZnO) (g)	Melting Temperature (ºC)
0.1, 0.6	1.5351	0.3359	0.4757	2.2276	0.4257	800
0.2, 0.5	1.5037	0.3289	0.9319	1.8183	0.4169	800
0.3, 0.4	1.4736	0.3224	1.3699	1.4255	0.4086	750

Table 2.3 Molecular Weight of the as-prepared sample B

C. CdI_2 - Ag_2O - V_2O_5 - P_2O_5 - ZnO System:

Glass Nano-Composites with empirical formula x CdI_2 – (1-x) {0.3Ag_2O – 0.3 V_2O_5 – 0.3 P_2O_5 – 0.1 ZnO}, where x varies as 0.1 and 0.2, are made from the reagent-grade chemicals. The necessary amounts of CdI_2, Ag_2O, V_2O_5, P_2O_5 and ZnO powders (Maker: Aldrich 99%) are mixed well and heated before the mixtures are melted in an electric furnace. Details about the samples are provided in Table 2.4, which also includes the melting temperature history for the batch of 5 grams.

Sample Designation (x)	Cadmium Iodide (CdI_2) (g)	Silver Oxide (Ag_2O) (g)	Vanadium Pentoxide (V_2O_5) (g)	Phosphorus Pentoxide (P_2O_5) (g)	Zinc Oxide (ZnO) (g)	Melting Temperature (ºC)
0.1	0.8203	2.0547	1.1000	0.8585	0.1641	800
0.2	1.5322	1.7057	0.9132	0.7126	0.1362	850

Table 2.4 Molecular Weight of the as-prepared sample C

D. CdI_2 - Ag_2O – TeO_2 - P_2O_5 - ZnO System:

Two samples of CdI_2 doped Ag_2O – TeO_2 - P_2O_5 - ZnO system with constant quantities of CdI_2 – TeO_2 – ZnO and with varied proportion of Ag_2O and P_2O_5 are made. The new Glass Nano-Composite holds the empirical formula 0.3 CdI_2 – 0.7 {y Ag_2O – 0.3 TeO_2 – z P_2O_5 – 0.1 ZnO},

where y varies as 0.1 and 0.3, and z as 0.5 and 0.3 and are made from the reagent-grade chemicals. The necessary amounts of the powders (Maker: Aldrich 99%) are mixed well and heated before the mixtures are melted in an electric furnace. Details about the samples are provided in Table 2.5, which also includes the melting temperature history for the batch of 5 grams.

Sample Designation (y, z)	Cadmium Iodide (CdI_2) (g)	Silver Oxide (Ag_2O) (g)	Tellurium Dioxide (TeO_2) (g)	Phosphorus Pentoxide (P_2O_5) (g)	Zinc Oxide (ZnO) (g)	Melting Temperature (°C)
0.1, 0.5	2.4685	0.5343	0.7530	1.1162	0.1279	900
0.3, 0.3	2.1953	1.4256	0.6697	0.5956	0.1138	900

Table 2.5 Molecular Weight of the as-prepared sample D

E. CdI_2 - Ag_2O - MoO_3 - P_2O_5 - ZnO System:

Two samples of CdI_2 doped Ag_2O - MoO_3 - P_2O_5 - ZnO system with constant quantities of CdI_2 – MoO_3 – ZnO and with varied proportion of Ag_2O and P_2O_5 are made. The new Glass Nano-Composite holds the empirical formula 0.3 CdI_2 – 0.7 {y Ag_2O – 0.3 MoO_3 – z P_2O_5 – 0.1 ZnO}, where y varies as 0.1 and 0.3, and z as 0.5 and 0.3 and are made from the reagent-grade chemicals. The necessary amounts of the powders (Maker: Aldrich 99%) are mixed well and heated before the mixtures are melted in an electric furnace. Details about the samples are provided in Table 2.6, which also includes the melting temperature history for the batch of 5 grams.

Sample Designation (y, z)	Cadmium Iodide (CdI_2) (g)	Silver Oxide (Ag_2O) (g)	Molybdenum Trioxide (MoO_3) (g)	Phosphorus Pentoxide (P_2O_5) (g)	Zinc Oxide (ZnO) (g)	Melting Temperature (°C)
0.1, 0.5	2.5055	0.5423	0.6893	1.1329	0.1299	1000
0.3, 0.3	2.2245	1.4446	0.6120	0.6035	0.1153	1000

Table 2.6 Molecular Weight of the as-prepared sample E

2.4 PHYSICAL AND STRUCTURAL CHARACTERIZATIONS

The structural and physical properties of the as-prepared samples are examined by studying various techniques such as density (ρ) and Molar Volume (V_M) measurement, X-ray diffraction (XRD), Fourier Transform Infrared (FT-IR) Spectroscopy and Scanning Electron Microscopy (SEM).

2.4.1 Measurement of Density and Molar Volume

One important characteristic of a glassy system that determines its structure is its density. The notion that the composition of a glass influences its density has been the subject of numerous investigations. [11, 23]. The density (ρ) of the as-prepared systems is typically measured using the Archimedes principle, which states that [23].

$$\rho = \frac{W\,\rho_b}{W_a - W_b} \tag{2.1}$$

Here, W represents sample weight. W_a represents sample weight in air and W_b represents sample weight in buoyant liquid, respectively. ρ_b is the density of the buoyant liquid. In our work, acetone has been taken as the buoyant liquid whose density is given as 0.7845 g/cm^3. Each measurement has been made using an electro-mechanical balance (Dhona 200D). The set up is shown in Fig. 2.2.

When the composition of the system is changed, the molar volume changes, which indicates a change in the structure of the glass network [23]. Molar volumes (V_M) of as-prepared glassy samples can be calculated using the following expression [24]:

$$V_M = \sum \frac{x_i\ M_i}{\rho} \tag{2.2}$$

where, M_i is the molecular weight of the sample, ρ is the density and x_i is the molar fraction.

A glassy sample's density indicates the degree of compactness of the sample. The combination of its elemental oxides makes up the current systems. The type, quantity, and mode of entry of ions and molecules into the glass network can all affect density. As our as-prepared samples exhibit glassy nature, it is expected that large amount of non-bridging oxygen (NBO) is present in the system which affects the molar volume of the sample.

Measurement of weight of the sample, W; Measurement of weight of the sample in air, W_a

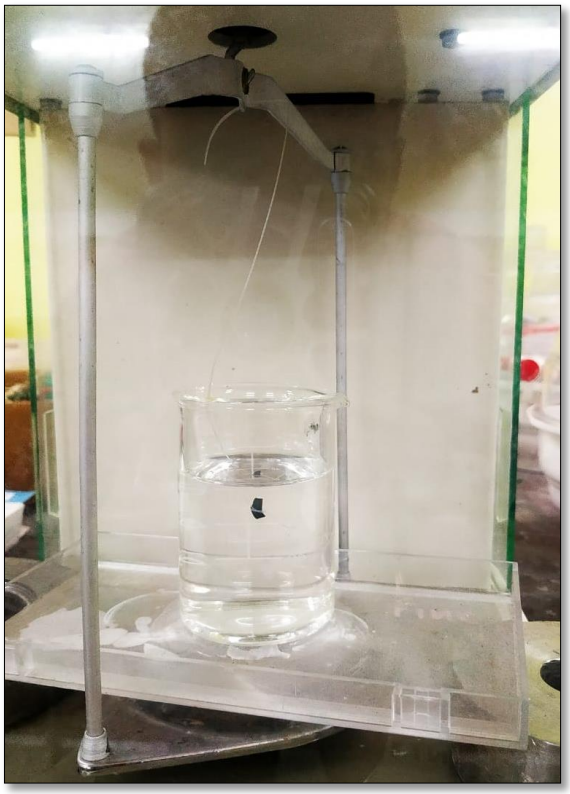

Measurement of weight of the sample immersed in acetone, W_b

Fig. 2.2 Density and Molar Volume measurement set-up

2.4.2 X-Ray Diffraction (XRD)

The XRD technique is widely used in the fields of material science and engineering for characterization purposes. This method can be used to analyze the crystal structure. It can be applied to ascertain the micro strain and crystallite size. It also aids in identifying the various nano-phases of the compositions that are contained within the system. It is appropriate for the analysis of both amorphous and crystalline materials.

For generation of x-rays, three things are needed.

a) *Source of electrons.*
b) *Means of accelerating the electrons at high speeds.*
c) *Target material to receive the impact of the electrons and interact with them.*

The as-prepared glassy systems are finely grained to make powder and then the powder is placed in the path of a monochromatic X-ray beam. The powder could be made up of several crystallites, which are tiny crystals that have been finely ground. They are randomly oriented to one another. The planes of the crystallites that are orientated at the proper angle to satisfy Bragg's condition will experience diffraction.
Bragg's Law states that when X-rays hit a crystal at certain angles, they reflect back at the same angle.

Bragg's condition is given as –

$$n\lambda = 2DSin\theta \tag{2.3}$$

where, the parameters have their usual meaning.

When an X-ray beam strikes a crystalline material, diffraction can occur in many directions since the X-ray wavelength and the interatomic spacing of the material are almost equal, typically falling within the Armstrong order. The diffraction patterns can provide information about the material's structure. The arrangement of atoms in the material's structure can be determined by measuring the intensities and angles of the diffracted beams.

The constructive interference is a result of the summation of all the diffracted beams and results in a

sharp peak which indicates the presence of crystallinity. In very small crystallites, there are not enough planes to produce complete interference, so a broadened peak is observed. The absence of any sharp peak represents amorphous nature of the sample.

The Crystallite Size or grain size of nanoparticles is estimated from Scherrer relation [12], which is given by:

$$D = \frac{K\lambda}{\beta \cos\theta} \tag{2.4}$$

Where, D is the Average crystallite size, K denotes the Scherrer Constant, (0.89). λ represents the wavelength of the X-ray source, (1.54 Å). The peak angle is given by θ and β is the Full Width at Half Maxima of the peak (broadening of the peak).

The dislocation density δ can be calculated using the X-Ray diffraction method and the equation holds good for that is [14]:

$$\delta = \frac{1}{D^2} \tag{2.5}$$

where, D represents the size of the crystallite, δ is the dislocation density.

The formula, that can be used to compute lattice strain (ε), which is related to the crystal defect that results in the diffraction line's broadening is given by [15, 16]:

$$\varepsilon = \frac{\beta}{4\tan\theta} \tag{2.6}$$

where, θ is the peak angle, β is the Full Width at Half Maxima of the peak (broadening of the peak).

2.4.3 Fourier-Transform Infrared Spectroscopy (FT-IR)

FT-IR is an infrared spectroscopy technique which identifies organic, inorganic, and polymeric materials and recognizes chemical bonds present in a molecule. It gathers knowledge about the presence or absence of certain functional groups. The study involves projecting infrared light onto a system's surface. The substance transmits some of the radiation while absorbing some of it. The device that is used to detect transmitted radiations and turn them into a spectrum is a Spectrometer. This spectrum illustrates how the material absorbs and transmits radiation, creating the molecular fingerprint of the substance. An identical infrared spectrum cannot be produced by two distinct materials. Because of this, FT-IR has developed into a potent method for characterizing the structural properties of materials.

Infrared spectrum represents absorbance or transmittance of IR light is represented in the y axis. The wavelength is represented in the x axis. In the infrared spectrum, wave number, or cm^{-1}, is used to represent frequency, and micrometres, or μm, to represent wavelength. When a molecule's vibration frequency matches that of the electromagnetic radiation, the molecule absorbs the radiation. This is how infrared spectroscopy operates. If any bond in the sample has a vibrational frequency that matches the infrared light's frequency, the sample will absorb light when it is exposed to an infrared light beam. The transmitted light can be used to determine the amount of light that is absorbed at each frequency. The number of components in a mixture, the quality and dependability of the material, the identification of unknown materials, and other vital information can all be obtained using FT-IR. That's why it is an essential structural characterization approach [17–18].

Within the electromagnetic spectrum, the infrared spectrum spans from 12500 cm^{-1} to 10cm^{-1}. The near-infrared (range: 12500 cm^{-1} – 4000 cm^{-1}), mid-infrared (range: 4000 cm^{-1} – 400 cm^{-1}), and far-infrared (range: 400 cm^{-1} – 10 cm^{-1}) regions make up this spectrum. Because the majority of fundamental molecule vibrations occur in the mid-infrared range, this region is rich in chemical information. Fundamental vibration mixes involving mostly hydrogen atoms occur in the near-infrared range, while vibrations involving heavier atoms occur in the far-infrared region.

2.4.4 Scanning Electron Microscopy (SEM)

Scanning electron micrographs (SEM) of the polished surfaces of the samples were obtained using a scanning electron microscope in order to investigate the microstructure and surface morphology of

as-prepared glasses and glass nanocomposites. Using a vacuum evaporation process, a thin layer of conducting platinum (~150 Å) was applied to the samples' polished surfaces. The EDS analysis of the related SEM picture was used to do the quantitative analysis of the finished compositions.

2.5 ELECTRICAL CONDUCTIVITY AND DIELECTRIC RELAXATION STUDY

The two-probe method has been opted for the purpose of carrying out the electrical conductivity and dielectric relaxation studies. One specific sample of the as-prepared glassy systems is taken and silver paste is applied on the both sides of the samples. Then the sample is placed in a spring-loaded sample holder and two copper electrodes (manufactured by Joy-Crucible) that have been polished, cleaned, and spring-loaded have been in contact with the sample inside the sample container. The sample holder has been kept in a furnace and the furnace is connected to a temperature controller. The set up is shown in Fig. 2.3.

Fig. 2.3 Two-probe method set up

2.5.1 DC Conductivity Studies

The "MetraviTM Digital Multimeter" (model no. 450 DMM) was utilised in the two-probe method to test the DC conductivity of all glassy systems developed in this investigation. Fig. 2.4 depicts the

experimental setup for determining the DC conductivities of each produced glassy system.

The conductivity σ can be calculated from the measured resistance R using:

$$\sigma = \frac{1}{\rho} = \frac{L}{R.A} \tag{2.7}$$

Where, the paremeters carry their usual meanings.

The temperature dependence of DC conductivity often follows the Arrhenius equation:

$$\sigma_{dc} = \sigma_0 \exp\left(\frac{-E_{dc}}{K_B T}\right) \tag{2.8}$$

Where, the paremeters carry their usual meanings.

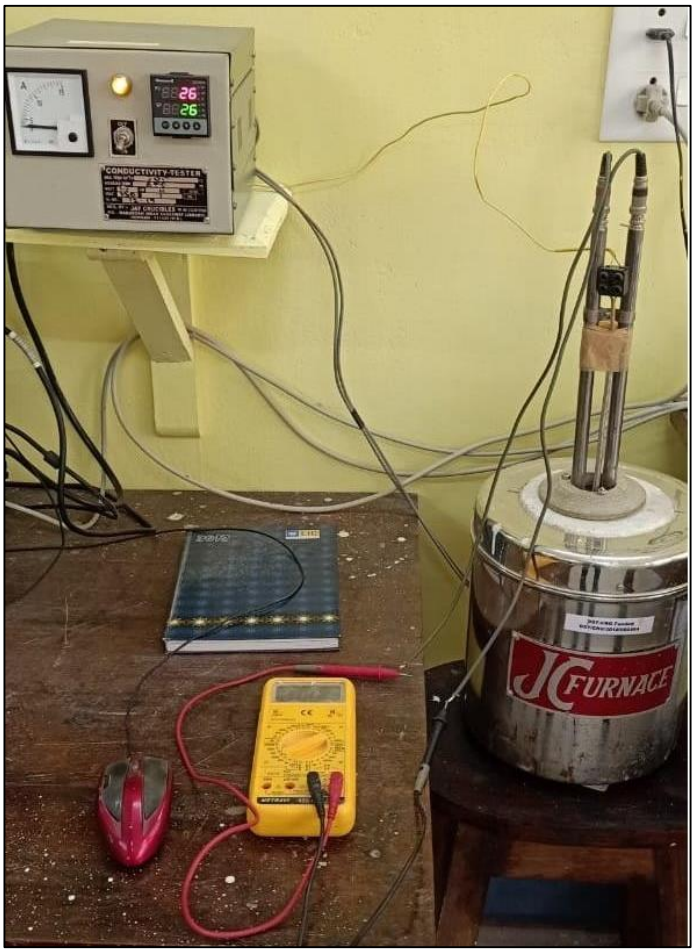

Fig. 2.4 DC measurement set up

By plotting $\log(\sigma_{dc})$ versus $\frac{1}{T}$, a linear relationship is expected, with the slope giving the activation energy E_{dc} as:

$$E_{dc} = -K_B.\text{slope} \quad (2.9)$$

The typical DC conductivity plot is found to follow Arrhenius equation and give a linear nature. Deviations from the linearity can reveal presence of other conduction processes, like the impact of localized states within the band gap or variable range hopping (VRH).

For those cases, various models, such as the Mott's and Greaves' models, are available for evaluating the DC conductivity of oxide glassy systems. The collected DC conductivity data at various temperatures can be examined at lower temperatures (below the Debye temperature) utilising Mott's model [19]. It claims that hopping of polarons in localised states near the Fermi level is the mechanism that causes conduction.

As stated by Mott's model [19]

$$\sigma = A\exp\left[-\frac{T_0}{T}\right]^{0.25} \quad (2.10)$$

Where, both A and T_0 are constant.

T_0 can be expressed as,

$$T_0 = \frac{16\,\alpha^3}{K_B\,N\,(E_F)} \quad (2.11)$$

Where, $N(E_F)$ represents localized states density near Fermi level, α^{-1} is degree of localization (value of a^{-1} = 10Å) and K_B denotes Boltzmann constant.

The Greaves model [20] can be employed to analyse the DC conductivity of a system at elevated temperatures, surpassing the Debye temperature. According to this hypothesis, in prolonged states of these systems, conduction occurs due to thermally assisted tunnelling of polarons.

The following formula [20] can be used to express this model:

$$\sigma_{DC} T^{\frac{1}{2}} = A^{/} \exp\left[-\left(\frac{T_0^{/}}{T}\right)^{\frac{1}{4}}\right] \quad (2.12)$$

Here, $A^{/}$ as well as $T_0{}^{/}$ are constant. $T_0^{/}$ is expressed as –

$$T_0^{/} = \frac{19.4\ \alpha^3}{K_B\ N\ (E_F)} \quad (2.13)$$

2.5.2 AC Conductivity Studies

The conductivity information of the amorphous glassy systems with respect to frequency at various temperatures is obtained using AC conductivity measurement. Power Law, Almond-West formalism was utilised to analyse AC conductivity data for these systems. For the purpose of measurement, the furnace is connected to a LCR meter. The Hioki LCR tester (Model No. 3532-50) was used to do the complex impedance measurements at different temperatures and in the frequency spectrum of 42 Hz to 5 MHz. The LCR meter is connected to a dedicated PC and the data has been collected from the computer. The AC conductivity and relaxation studies have been carried out on this data.

Fig. 2.5 AC conductivity measurement set up

In an amorphous glassy system, the total conductivity is expressed as [25]:

$$\sigma_{total} = \sigma_{dc} + \sigma_{ac} \quad (2.14)$$

Here, the conductivities of DC and AC are denoted as σ_{DC} and σ_{AC}, respectively. The frequency dependent AC conductivity, of the as-prepared samples have been estimated using the measured values of

conductance (G) –

$$\sigma_{ac} = G(\omega)\ \frac{t}{A} \tag{2.15}$$

Where, parameters carry their usual meanings.

The analysis of AC conductivity spectra can be done using the Almond West formalism [22], which is given by:

$$\sigma(\omega) = \sigma_{dc}\left[1 + \left(\frac{\omega}{\omega_H}\right)\right]^n \tag{2.16}$$

where ω_H stands for the hopping frequency of polarons', σ_{dc} corresponds to dc conductivity, n is the fractional power law exponent, and ω is the applied electric field frequency.

The temperature dependence of AC conductivity often follows the Arrhenius equation:

$$\sigma_{ac} = \sigma_0\ \exp\left(\frac{-E_h}{K_B T}\right) \tag{2.17}$$

Where, σ_0 is a pre-exponential factor, E_h is the activation energy due to hopping frequency, K_B is the Boltzmann constant, T is the absolute temperature. By plotting $\log(\sigma_{ac})$ versus $\frac{1}{T}$, a linear relationship is expected, with the slope giving the activation energy E_h as:

$$E_h = -K_B.\text{slope} \tag{2.18}$$

Almond-West formalism is mainly used for assessing the systems where ionic conduction is pre-dominant. The electronic/polaronic conduction is often explained by Jonscher's universal power law which can be expressed as [21]:

$$\sigma(\omega) = \sigma_0 + A\omega^S \tag{2.19}$$

Here, S stands for the frequency exponent, while A is a constant. S values are obtained from the values of slopes, which are obtained by linearly fitting AC conductivity graphs at various temperatures in the higher frequency range.

For these semiconducting glassy systems, a variety of theoretical models, including QMT, NSPT, CBH, OLPT, and others, have been utilised to explain AC conductivity based on S dependence on frequency and temperature. S is temperature independent and frequency dependent in the quantum mechanical tunnelling model, or QMT [26]. S must be dependent on both temperature and frequency

in order for the overlapping large polaron tunnelling model, or OLPT, [27] to be used. When S rises with temperature, the non-overlapping small polaron tunnelling model (NSPT) [26] can be used. CBH or the correlated barrier hopping model may be used for systems when it is discovered that S decreases as temperature rises [28].

Depending on the nature of the slopes, CBH or NSPT model has to be applied to interpret the nature of polaronic conduction in our systems.

Correlated Barrier Hopping model gives slope as –

$$S = 1 - \frac{6\,K_B\,T}{W_m + K_B(T - T_0) * \ln\left(\omega\,\tau_0\right)} \tag{2.20}$$

Where, W_m is the maximum barrier height, T_0 is the temperature at which S becomes unity, K_B is the Boltzmann constant, τ_0 is the relaxation period, T is the absolute temperature.

The expression of S using Non-Symmetric Polarons and Tunneling (NSPT) model is given as –

$$S = 1 - \frac{4}{\ln\left(\frac{1}{\omega\,\tau_H}\right) - \left(\frac{W_H}{K_B\,(T - T_0)}\right)} \tag{2.21}$$

Where, W_H is the highest barrier height, T_0 is the temperature at which S becomes unity, K_B is the Boltzmann constant, τ_H is the relaxation period, T is the absolute temperature

The charge carrier density in the as-prepared samples is calculated using Nernst-Einstein relation. It is given as –

$$\sigma_{dc} = \frac{N_c q^2 d^2 \omega_H}{12\,\pi k_B T} \tag{2.22}$$

Where, dc conductivity is indicated by σ_{dc}, N_c denotes the mobile charge-carrier concentration, charge is symbolized by q, the average jump distance between mobile charge-carriers by d, ω_H is the hopping frequency, K_B is the Boltzmann constant, T is the absolute temperature.

2.5.3 Study of Dielectric Relaxation Properties

2.5.3.1 Permittivity Study

The investigation of the dielectric relaxation process is essential in determining the electrical transport of the charge carriers. Dielectric relaxation spectroscopy includes study of Complex Permittivity and Electric Modulus. Permittivity study provides critical insights into the material's ability to store and transfer electrical energy under an applied electric field and reflects their polarizability, which is influenced by the structure, composition, and interaction of the glass matrix and embedded nanoparticles.

The following polarisations are likely in dielectric materials: Electronic polarisation, which results from the application of an electric field and causes the electron cloud of a negative atom to shift with respect to the nucleus; Ionic polarisation: a process wherein an electric field induces positive and negative ions to move out of their equilibrium locations and create a dipole moment; Orientation polarisation, which results from molecular dipoles orientated in the direction of the applied electric field; Space charge polarisation, which mostly happens at the electrode-material or grain boundary, often restricts the mobility of charges. It causes charge dipoles to align when an electric field is applied.

Analysing the structure of a solid is made easier by understanding the origin and nature of dielectric losses through the study of dielectric relaxation. The concept of a dielectric material's maximal energy storage capacity is revealed by its dielectric permittivity. Additionally, it provides information on the material's energy loss. A material's dielectric constant, also known as permittivity, ε, can be written as follows:

$$\varepsilon = \varepsilon^{/} - j\varepsilon^{//} \tag{2.23}$$

Where $\varepsilon^{/}$ represents the real component of ε and $\varepsilon^{//}$ denotes the imaginary part of ε [29].

Eq. 2.24 & 2.25 can be used to calculate $\varepsilon^{/}$ and $\varepsilon^{//}$.

$$\varepsilon^{/} = \frac{C_p t}{\varepsilon_0 A} \tag{2.24}$$

where ε_0 is the free space permittivity ($8.854*10^{-12}$ F/m), t is the sample's thickness, A is the area of the sample and C_p is the sample's capacitance.

The following equation can be used to get $\varepsilon^{//}$

$$\varepsilon^{//} = \varepsilon^{/}\tan\delta \tag{2.25}$$

where tanδ is the dielectric loss tangent and is a function of the sample's energy loss, which is expressed as heat. A characteristic of charged carrier systems is that both $\varepsilon^{/}$ and $j\varepsilon^{//}$ appear to be strongly scattered at low frequencies as the temperature rises [30].

A high ε′ value means the material is highly polarizable and can store a significant amount of electrical energy. At low frequencies, all polarization mechanisms (electronic, ionic, dipolar, and interfacial) contribute to ε′ [30], resulting in a high value. As frequency increases, slower polarization mechanisms (e.g., ionic and interfacial) cannot keep up with the rapid fluctuation of the field and that causes ε′ to decrease.

ε″ is associated with the conversion of electrical energy into heat due to resistive losses, relaxation processes, or conduction. Dielectric loss can arise from: (a) Relaxation losses (delayed dipole reorientation with respect to the applied field), (b) Conduction losses (movement of free charge carriers or ions in the material) and (c) Interfacial losses (charge accumulation at interfaces due to conductivity mismatches). High ε″ means the material loses significant energy during polarization.

Hunt's model can be utilised to examine the dielectric relaxation process in these oxide glassy systems. Numerous researchers have reported using this model for relaxation analysis in a variety of oxide glassy systems [31-33]. This model states that the conductivity of these glasses can be classified into two different zones based on two frequency domains. The relaxation process occurs due to carrier hopping in pairs between the sites in the frequency domain where $\omega > \omega_m$. Particle movement across macroscopic distances in clusters is the cause behind the relaxation process in the opposite frequency domain, that is, when $\omega < \omega_m$ [31-33].

According to Hunt, these glassy systems' frequency-dependent conductivity in the two areas is as follows [31-33]:

$$\sigma_t(\omega) = \sigma_{DC} + \left(1 + A\left(\frac{\omega}{\omega_m}\right)^s\right) \quad \text{for } s < 1,\ \omega > \omega_m \tag{2.26}$$

$$\sigma_t(\omega) = \sigma_{DC} + \left(1 + K(d)\left(\frac{\omega}{\omega_m}\right)^r\right) \quad \text{for } r > 1,\ \omega < \omega_m \tag{2.27}$$

where, r is given by $(1 + d - d_f)$.

d represents the dimensionality of the space comprising relevant clusters, the peak frequency is ω_m, A and K(d) are constants and the functional dimensionality of the clusters is represented by d_f. Therefore, the dielectric relaxation investigations are a great way to learn about the glassy system's conduction mechanism.

2.5.3.2 Electrical Modulus Study

Electrical modulus research can be used to examine a material's complicated electrical response and counteract the effects of electrode polarisation [34]. The reciprocal of complex permittivity is the definition of the complex electrical modulus [34], that is,

$$M^* = \frac{1}{\varepsilon^*} = M^{/} + jM^{//} = \frac{\varepsilon^{/}}{(\varepsilon^{/})^2 + (\varepsilon^{//})^2} + j\frac{\varepsilon^{//}}{(\varepsilon^{/})^2 + (\varepsilon^{//})^2} \tag{2.28}$$

where ε* denotes complex dielectric permittivity and M* is the complex modulus.

Mathematically, M* can alternatively be shown as follows using the Fourier Transform of the relaxation function θ(t):

$$M^* = M_\infty\left[1 - \int_0^\infty \exp(-\omega t)\left(\left(\frac{d\varphi}{dt}\right)dt\right)\right] \tag{2.29}$$

where θ(t) is the Kohlrausch-Williams-Watts, or KWW, function [35-37] that expresses the time evolution function of the electric field inside the material and is described as follows:

$$\varphi(t) = \exp\left[-\left(\frac{t}{\tau_m}\right)^\beta\right] \tag{2.30}$$

where τ_m and β stand for the KWW stretched coefficient and conductivity relaxation time,

respectively, and $0 < \beta < 1$.

The activation energy (E_τ) and relaxation time τ_m can be interpreted using the relation shown below [35-37]:

$$\tau_m = \tau_0 \exp\left(-\frac{E_\tau}{K_B T}\right) \quad (2.31)$$

where a pre-exponential factor, denoted by τ_0.

An improved understanding about the charge carriers' conductivity effects can be obtained by examining the electric modulus formalism on the dielectric data. When no clearly defined can be seen in dielectric loss plots, the dielectric modulus, given by Eqn. (2.28), is used to obtain information regarding the relaxation mechanism. The dielectric modulus loss $M^{//}$ vs frequency graphs can be used to determine relaxation maxima, which show how much the system's conductivity effects contribute.

2.6 CONCLUSION

This chapter largely addresses the following concerns:

- Various methods for creating oxide glassy systems, with a prime focus on the melt-quenching method in particular has been discussed.
- The empirical formula for diverse metal halide doped glassy systems with varying compositions has been created.
- Techniques for calculating molar volume and density has been described.
- The procedure to determine strain in glassy systems, dislocation density, and crystallite sizes of different nano-phases from the most important structural characterization, X-Ray Diffraction (XRD), has been explained.
- The Fourier Transform Infrared (FT-IR) method, which can be used to determine which molecules and functional groups are present in a glassy system has been discussed.
- The process of calculation of density of states at higher and lower temperature ranges by analyzing DC conductivity data using different models, such as the Greaves model and Mott's model, respectively has been explained.
- Application of multiple techniques, like Power law, Almond West formalism, etc., to analyze

the data on AC conductivity and determination of the conduction mechanism by applying appropriate models, like CBH, NSPT, OLPT, etc., have been discussed.

- Dielectric relaxation studies have been discussed to provide insight into the maximum energy storage capacity and degree of energy loss of a dielectric substance. Understanding the effect of conductivity on a glassy system is made easier by combining the electric modulus formalism with the dielectric data.

Thus, this chapter overall discusses about the process of synthesization of the oxide glassy systems and their characterization and electrical conductivity techniques. This analysis greatly aids in understanding the link between structural and electrical properties, which is essential for understanding the true conduction mechanism in a glassy system.

References

[1] Hassanien, A. S., & Akl, A. A. (2015). Estimation of some physical characteristics of chalcogenide bulk Cd50S50− xSex glassy systems. Journal of Non-Crystalline Solids, 428, 112-120.

[2] Jyothy, P. V., Kumar, K. A., Karthika, S., Rajesh, R., & Unnikrishnan, N. V. (2010). Dielectric and AC conductivity studies of CdSe nanocrystals doped sol–gel silica matrices. Journal of alloys and compounds, 493(1-2), 223-226.

[3] Potter, D. B., Powell, M. J., Darr, J. A., Parkin, I. P., & Carmalt, C. J. (2017). Transparent conducting oxide thin films of Si-doped ZnO prepared by aerosol assisted CVD. RSC advances, 7(18), 10806-10814.

[4] Suryanarayana, V., Sekhar, A. V., Bafti, A., Pavić, L., Reddy, A. S. S., Reddy, G. N. K., ... & Veeraiah, N. (2023). Dynamical behavior of Ag ions on structural and dielectric features of As2O3 glass ceramics containing chalcogenide oxides. Journal of non-crystalline solids, 610, 122299.

[5] Osuwa, J., & Oriaku, C. (2010). Laser induced changes on band gap and optoelectronic properties of chalcogenide Glassy Cu0. 11Cd0. 40S0. 49 thin films. J. Non-Oxide Glasses, 2, 1-5.

[6] Kumari, V., Kaswan, A., Patidar, D., Sharma, K., & Saxena, N. S. (2016). Electrical conduction mechanism in GeSeSb chalcogenide glasses. Bulletin of Materials Science, 39, 255-262.

[7] Fernandes, B. J., Ramesh, K., & Udayashankar, N. K. (2019). Crystallization kinetics of Si20Te80− xBix ($0 \leq x \leq 3$) chalcogenide glasses. Materials Science and Engineering: B, 246, 34-41.

[8] Pal, S. K., Kumar, A., & Mehta, N. (2019). Signature of rigidity percolation effect in dielectric behavior of germanium containing multi-component chalcogenide glasses (ChGs). Ceramics International, 45(13), 16279-16287.

[9] Ravagli, A., Naftaly, M., Craig, C., Weatherby, E., & Hewak, D. W. (2017). Dielectric and structural characterisation of chalcogenide glasses via terahertz time-domain spectroscopy. Optical Materials, 69, 339-343.

[10] Zhu, E., Liu, Y., Sun, X., Yin, G., Jiao, Q., Dai, S., & Lin, C. (2019). Correlation between thermo-mechanical properties and network structure in GexS100–x chalcogenide glasses. Journal of Non-Crystalline Solids: X, 1, 100015.

[11] Chanshetti, U. B., Shelke, V. A., Jadhav, S. M., Shankarwar, S. G., Chondhekar, T. K., Shankarwar, A. G., ... & Jogad, M. S. (2011). Density and molar volume studies of phosphate glasses. Facta universitatis-series: Physics, Chemistry and Technology, 9(1), 29-36.

[12] Singhal, S., Kaur, J., Namgyal, T., & Sharma, R. (2012). Cu-doped ZnO nanoparticles: synthesis, structural and electrical properties. Physica B: Condensed Matter, 407(8), 1223-1226.

[13] Mathew, X., Enriquez, J. P., Sebastian, P. J., Pattabi, M., Sanchez-Juarez, A., Campos, J., ... & Singh, V. P. (2000). Charge transport mechanism in a typical Au/CdTe Schottky diode. Solar energy materials and solar cells, 63(4), 355-365.

[14] Harrington, G. F., Cavallaro, A., McComb, D. W., Skinner, S. J., & Kilner, J. A. (2017). The effects of lattice strain, dislocations, and microstructure on the transport properties of YSZ films. Physical Chemistry Chemical Physics, 19(22), 14319-14336.

[15] Janosi, A. (1964). La structure du sulfure cuivreux quadratique. Acta Crystallographica, 17(3), 311-312.

[16] Van Ingen, R. P., Fastenau, R. H. J., & Mittemeijer, E. J. (1994). Laser ablation deposition of Cu-Ni and Ag-Ni films: Nonconservation of alloy composition and film microstructure. Journal of applied physics, 76(3), 1871-1883.

[17] Kishore, N., Kundu, R. S., & Dhankhar, S. (2015, February). FTIR and optical properties of various Se-S-Zn chalcogenide glasses. In IOP Conference Series: Materials Science and Engineering (Vol. 73, No. 1, p. 012150). IOP Publishing.

[18] Singh, A. K., Mehta, N., & Singh, K. (2009). Optical and FTIR properties of Se93−XZn2Te5InX chalcogenide glasses. Physica B: Condensed Matter, 404(20), 3470-3474.

[19] Mott, N. F. (1971). Conduction in non-crystalline systems: VII. Non-ohmic behaviour and switching. Philosophical Magazine, 24(190), 911-934.

[20] Greaves, G. N. (1973). Small polaron conduction in V2O5□ P2O5 glasses. Journal of Non-Crystalline Solids, 11(5), 427-446.

[21] Elliott, S. R. (1987). Ac conduction in amorphous chalcogenide and pnictide

semiconductors. Advances in physics, 36(2), 135-217.

[22] Almond, D. P., Duncan, G. K., & West, A. R. (1983). The determination of hopping rates and carrier concentrations in ionic conductors by a new analysis of ac conductivity. Solid State Ionics, 8(2), 159-164.

[23] Januszka, A., & Nowosielski, R. (2012). Structure and density of Fe 36 Co 36 B 19.2 Si 4.8 Nb 4 bulk glassy alloy. Journal of Achievements in Materials and Manufacturing Engineering, 52(2).

[24] Xiong, H. M., Zhao, X., & Chen, J. S. (2001). New polymer− inorganic nanocomposites: PEO− ZnO and PEO− ZnO− LiClO4 films. The Journal of Physical Chemistry B, 105(42), 10169-10174.

[25] Karmakar, S., Raviteja, B., Mistari, C. D., Parey, V., Thapa, R., More, M. A., & Behera, D. (2020). Superior field emission and alternating current conduction mechanisms for grains and grain boundaries in an NiO-[CdO] 2 nanocomposite. Journal of Physics and Chemistry of Solids, 142, 109462.

[26] Ghosh, A. (1990). Frequency-dependent conductivity in bismuth-vanadate glassy semiconductors. Physical review B, 41(3), 1479.

[27] Long, A. R. (1982). Frequency-dependent loss in amorphous semiconductors. Advances in physics, 31(5), 553-637.

[28] Murawski, L., & Barczyński, R. J. (1995). Dielectric properties of transition metal oxide glasses. Journal of non-crystalline solids, 185(1-2), 84-93.

[29] Camargo, P. H. C., Satyanarayana, K. G., & Wypych, F. (2009). Nanocomposites: synthesis, structure, properties and new application opportunities. Materials Research, 12, 1-39.

[30] Ahmad-Bitar, R., & Arafah, D. E. (1998). Processing effects on the structure of CdTe, CdS and SnO2 thin films. Solar energy materials and solar cells, 51(1), 83-93.

[31] Hunt, A. (1992). Some universalities in the relaxation of glasses. Journal of non-crystalline solids, 144, 21-31.

[32] Hunt, A. (1993). Non-Debye relaxation and the glass transition. Journal of non-crystalline solids, 160(3), 183-227.

[33] Murawski, L., & Barczyński, R. J. (1996). Dielectric relaxation in semiconducting oxide glasses. Journal of non-crystalline solids, 196, 275-279.

[34] Dult, M., Kundu, R. S., Hooda, J., Murugavel, S., Punia, R., & Kishore, N. (2015). Temperature and frequency dependent conductivity and electric modulus formulation of manganese modified bismuth silicate glasses. Journal of Non-Crystalline Solids, 423, 1-8.

[35] Karmakar, B., Rademann, K., & Stepanov, A. (Eds.). (2016). Glass nanocomposites: synthesis, properties and applications. William Andrew.

[36] Ojha, S., Roy, M., Chamuah, A., Bhattacharya, K., & Bhattacharya, S. (2020). AC conductivity and dielectric behavior of Cu-S-Te chalcogenide glassy system. Materials Letters, 258, 126792.

[37] Bhattacharya, S., & Ghosh, A. (2008). Relaxation dynamics in superionic glass nanocomposites. Journal of the American Ceramic Society, 91(3), 753-759.

Chapter 3

Study of Electrical Transport Phenomena in AgI Doped $CdO - V_2O_5 - P_2O_5 - ZnO$ System

Outline

The results presented in this chapter have been published in:

Ionics, 30, 3357–3373 (2024);

Physica B: Condensed Matter, 696, 416557 (2025).

3.1 INTRODUCTION

In recent times, the research community has given solid electrolytes a lot of attention because of their notable electrical conductivity at room temperature as well as their scholarly interest in studying conduction mechanisms [1–4]. AgI-doped superionic glassy conductors have been found to be largely prevalent in this area but only a limited number of investigations [5–7] has been carried out to investigate their conduction mechanisms. The literature survey suggests that, the presence of transition metal ions, like vanadium, in silver ion conducting glassy systems has been found to enhance conductivity by the means of contributing electrons and polarons [8-9]. In such amorphous semiconductors, this polaron ought to be in charge of the variable range hopping mechanisms [10]. It is further anticipated that a healthy contrast between Ag^+ ion conduction and polaron hopping in the same system would be a great area of academic interest in the field of solid-state electrolytes.

The current work aims to create a novel oxide glassy system with silver iodide (AgI) salts and vanadium as transition metal ions (TMI) in a system encompassed of CdO - P_2O_5 - ZnO. The effect of gradual addition of AgI salt to these V_2O_5 doped amorphous semiconductors on the electrical transport of these as-prepared systems is the prime focus of this work. With the purpose of having perception about the conduction process, ion transport and polaron hopping mechanisms in a glassy conductor at different temperatures and frequencies have been investigated. Additionally, it has been noted that different methods for examining the conductivity spectra and dielectric relaxation could provide insight into the microscopic details of these glassy materials. The research community may find the discussion between the two types of conduction in the current system to be highly interesting, both for their mixed conduction mechanisms and for establishing a relationship between microstructure and conduction processes.

3.2 PREPARATION OF GLASSY SYSTEMS

The extremely pure (Aldrich 99.9%) reagent grade chemicals were used to produce xAgI - (1-x) (0.1CdO - 0.3 V_2O_5 - 0.4 P_2O_5 - 0.2ZnO) with x = 0, 0.05, 0.1, 0.2, 0.3, 0.4 via melt quenching method [11-15]. Every necessary chemical was meticulously weighed in accordance with its determined stoichiometric proportion, discussed in section 2.3, in an

electromechanical analytical balance (Dhona 200D). The substances were then properly mixed and ground in a mortar and a powder was formed. Prior to use, the mortar was thoroughly cleaned and rinsed. Depending on their composition, the combinations were subsequently melted in an electric furnace at temperatures ranging from 750 to 850 °C. The compound P_2O_5 is considered a precursor and may contribute as a modifier. Because elemental phosphorus is unstable at higher temperatures, it has not been used here. Additionally, evidence is also present [16] that higher P_2O_5 concentrations enhance both the crystallization temperature and glass stability. As the melts were prepared, they were quenched between two aluminum plates after being equilibrated for 30 minutes. This method has produced glassy composites that were partially transparent and around 1 mm thick. Using the two-probe technique, measurements were made on samples for the electrical conductivity analysis. Two polished, cleaned, and spring-loaded copper electrodes (manufactured by Joy-Crucible) were placed in contact with the sample inside the sample holder. The Hioki LCR tester (Model No. 3532-50) was then used to perform complex impedance measurements. It is done in the frequency spectrum of 42 Hz to 5 MHz. The measurements were taken at regular intervals of 20 °C in the temperature range of 300–793 K. Here, the DC limit up to room temperature has been approximated. The LCR meter would not respond as the temperature dropped to room temperature because the current passing through the sample at that temperature was approximately 10^{-12} A. This suggests that ion motion and polaron hopping should be collapsed below room temperature because of the charge carriers' extremely low mobility.

3.3 RESULTS AND ANALYSIS

3.3.1 Structural Characterization

In order to learn about the structure of the glass-nanocomposite doped with silver iodide that contains different concentrations of CdO, V_2O_5, ZnO, and P_2O_5, this chapter has examined its structural characterizations using a variety of spectrographic and microscopic measurements [17]. The several methods of structural characterizations that are exploited in our study includes, measurement of density (ρ) and molar volume (V_M), X-ray Diffraction (XRD) characterization, Fourier Transform Infrared (FT-IR) spectroscopy and Scanning Electron Microscopy (SEM).

3.3.1.1 Measurement of Density and Molar Volume

The density and molar volume of the as-prepared samples are measured using the Archimedes principle, which is described in section 2.4.1. Eqs. 2.1 and 2.2 have been used in the computations. Acetone with density, ρ_b = 0.7845 gm/cm^3 has been utilized as the buoyant liquid in our study. The weights of the as prepared samples (W_a and W_b) were recorded in an electro-mechanical balance (Dhona, Model: 200D) with precession of 0.0001 gm and all the measurements were performed at room temperature. The calculated values of ρ and V_M of these AgI doped oxide glassy systems is given in Table 3.1 and Fig. 3.1 shows the variation of density and molar volume with the increase in concentration of AgI in the system.

The higher density of a glass means that its particles are packed closely together. Fig. 3.1 makes it clear that density increases with composition. A slow rise in density could be a clear sign of the existing system's growing compactness as the composition's AgI concentration steadily increases. This outcome might suggest that the current system is less porous in nature. In contrast, Fig. 3.1 shows that the molar volume of the current system decreases with composition. The reason behind this fall may rely on the increasing number of non-bridging oxygen (NBO) with the enhancement in the concentration of the dopant salt.

Composition (x)	**Density, ρ (g/ cc) (± 0.1)**	**Molar volume, V_M (cc/ mol) (± 0.1)**
0	2.574	54.577
0.05	2.811	51.651
0.1	2.927	51.217
0.2	3.419	46.591
0.3	3.847	43.869
0.4	4.505	39.549

Table 3.1: ρ and V_M of of the as-prepared systems for different values of x

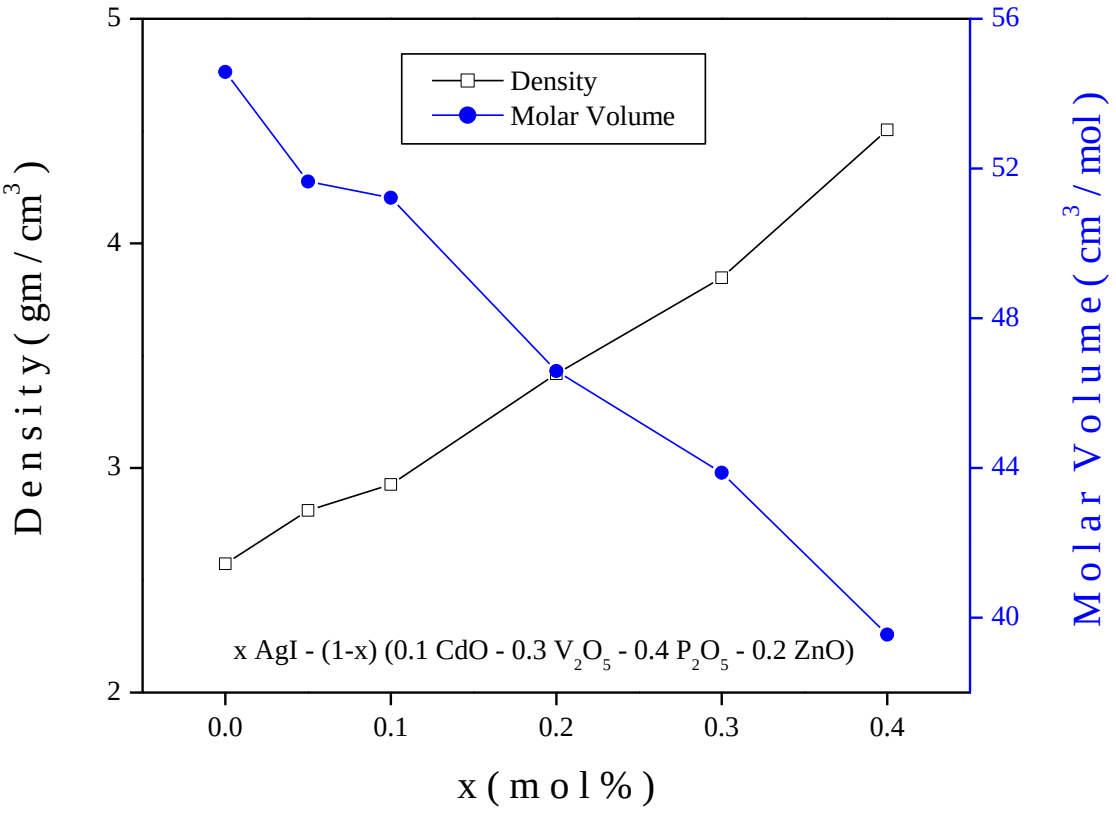

Fig. 3.1 Variation of density and molar volume at different values of x

3.3.1.2 X-ray Diffraction (XRD)

The X-ray diffraction study, explained in section 2.4.2, has been done on the different as-prepared samples to find out the nature of the samples. The presence of multiple peaks shows that the samples with x = 0, 0.05, and 0.1, are polycrystalline [18] in nature. The different peaks have been identified and is presented in Fig. 3.2. The as-developed nano-phases in the Fig. 3.2 have been recognized as $Zn_2V_2O_7$ (JCPDS no. 00–025-1031), VO_2 (JCPDS No. 00–031-1438), , V_6O_{13} (JCPDS no. 00–025-1251), ZnV_3O_8 (JCPDS no. 00–024-1481), and V_2O_5 (JCPDS card no. 00–041–1426). No peaks can be seen in the diffractograms for x = 0.2, 0.3, and 0.4. The presence of broad hump implies the amorphous character of the concerned samples. Thus, it is evident that there exists a distinct phase change with the advancement in the concentration of AgI. From the diffraction result, the crystallite size (d), dislocation density (δ) and lattice strain (ε) can be calculated using Eq. 2.4, 2.5 and 2.6. The results of X-ray diffraction, different phases with their Miller indices formed are given in Table 3.2. The most prevalent phase in this case is the $Zn_2V_2O_7$ nanophase. It is possible that the development of defect states is connected to these variations in crystallite sizes.

x	Nano-Phases	**Crystallite Size** (nm)	h k l	**Average Crystallite Size** (nm)	**Dislocation Density** (cm^{-2})	**Lattice** Strain
0	VO_2	45.57	1 1 0	34.33	4.81507838	0.347585167
	$Zn_2V_2O_7$	24.93	1 1 5		16.08523591	0.562732127
	V_6O_{13}	32.49	0 0 5		9.473028777	0.274126945
0.05	VO_2	41.12	1 1 0	48.97	5.911795272	0.385140551
	$Zn_2V_2O_7$	33.07	1 1 5		9.140254446	0.424196554
	ZnV_3O_8	48.98	1 1 3		4.167844123	0.27515093
	V_6O_{13}	72.71	0 0 5		1.891038983	0.122477846
0.1	P	40.91	0 2 1	38.55	5.972589439	0.3706082
	$Zn_2V_2O_7$	37.01	1 1 5		7.300143917	0.37909993
	ZnV_3O_8	24.54	1 1 3		16.5991735	0.549108901
	V_6O_{13}	51.72	0 0 5		3.737299319	0.172181402

Table 3.2: Crystallite Size, Dislocation Density and Lattice Strain of the system

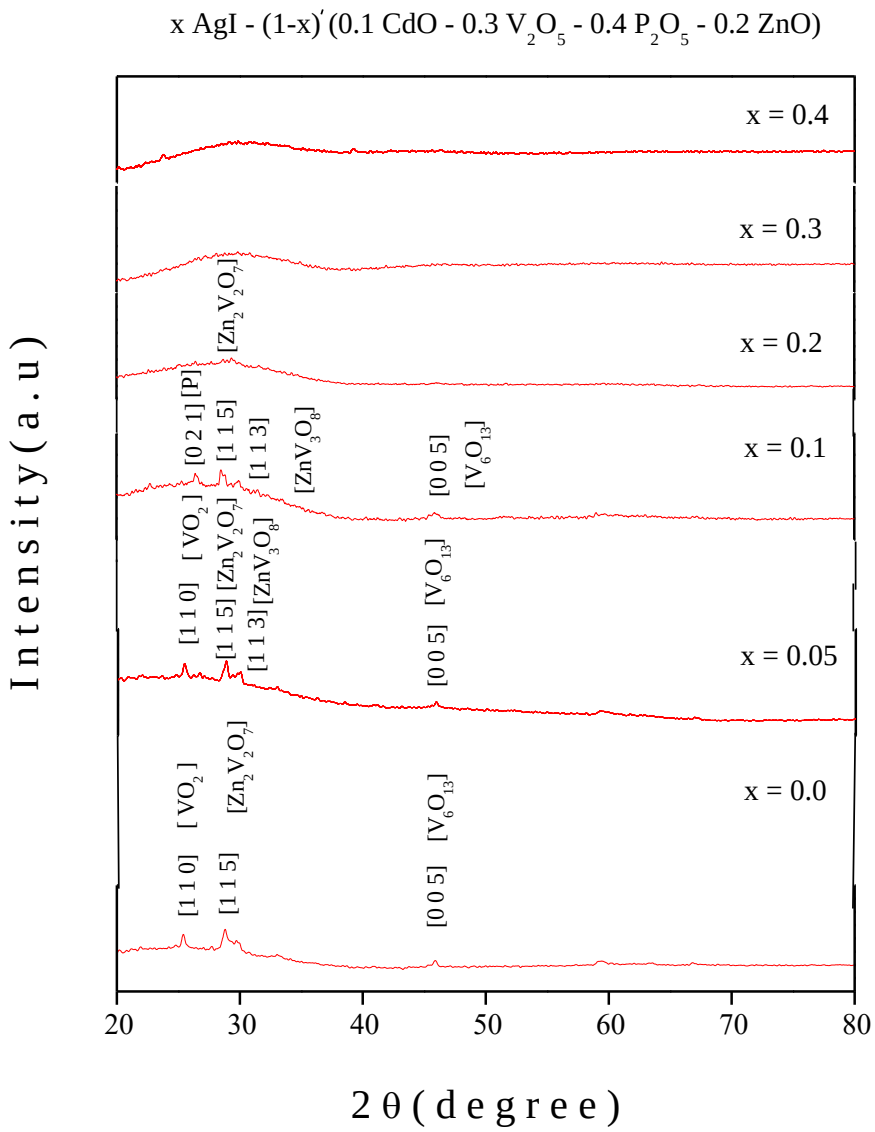

Fig. 3.2 X-ray diffractograms of the glass nanocomposites with different values of x

As the current system's AgI content begins to grow, it is anticipated that Ag^{+} will be surrounded by electrons released from vanadium (electrostatic force) and I^{-2} (covalent bonding), with a mechanism that involves less bridging oxygen and more non-bridging oxygen. It is predicted that substantial crystallinity will form due to the higher non-bridging oxygen content. But the present system with higher AgI content should have higher bridging oxygen as it develops more and more amorphous nature with the increase in AgI content. It can also be predicted that a strong covalent bond between Ag^{+} and O^{-2} exists, which may be the dominant factor in Ag^{+} transport over polaron hopping. However, the current glassy matrices should also have oxygen vacancies in the form of non-bridging oxygen (NBO) and other vacancy defects (like Frenkel defect), which must involve Ag^{+}

migration [19]. These features of the migration process and structure suggest strong electrochemical behaviors and characteristics of the current system being studied.

3.3.1.3 Fourier Transform Infrared Spectroscopy (FT-IR)

Figure 3.3 displays the current glassy system's FT-IR transmittance spectra in the mid-infrared region (spectral range $4000cm^{-1}$ – $400cm^{-1}$). Vibrational bands linked to the system's fundamental chemical bonds were not detectable since they were below the 400 cm^{-1} wave number. O-H symmetric vibrational modes has been found at 3600 cm^{-1} and 1600 cm^{-1} [20-21], indicating that they are hygroscopic in nature. For x = 0, 0.05, and 0.1, respectively, a doubly coordinated V-O-V band was observed at 1088 cm^{-1} [22]. However, this V-O-V band has been moved into a somewhat higher wavelength region as x rises from 0.2 forward, as shown in Fig. 3.3. An increase in wavelength for this specific V-O-V vibration at high x values could cause this vibration to require less energy. The covalent bond may be weakened by this type of V–O–V vibration at lower energies. The vanadium ion may therefore be liberated to provide extra electrons or polarons when it undergoes oxidation state changes [23]. The symmetric stretching mode of V = O has also been found for all compositions at 924 cm^{-1} [20]. A Zn–O vibration is detected at 552 cm^{-1}, demonstrating the stability of the current glass structures [24]. The fundamental vibration frequencies of the tetrahedral PO_4^{3-} ion are 515 cm^{-1} [19].

3.3.1.4 Field Emission Scanning Electron Microscope (FE SEM)

The FE-SEM images of the samples with x =0, 0.3 of xAgI - (1-x) (0.1CdO - 0.3 V_2O_5 - 0.4 P_2O_5 - 0.2ZnO) glass nano-composites are given in Fig. 3.4 (a) and (b) respectively. The figures show the presence of $Zn_2V_2O_7$ nanoflake-like structures [25] as XRD spectra has exposed $Zn_2V_2O_7$ nanophase as the most dominating phase. A flake-like structure might have tiny pores that allow nucleation to occur directly and randomly on the ZnO structure [26]. This could lead to an increase in the size of the flake-like structure, which also can be clearly seen in Fig 3.4 (b). Since these as-developed phases are functioning as localized states, it is anticipated that the increase in flake-like structure size for larger values of x will be advantageous for charge carrier conduction [27].

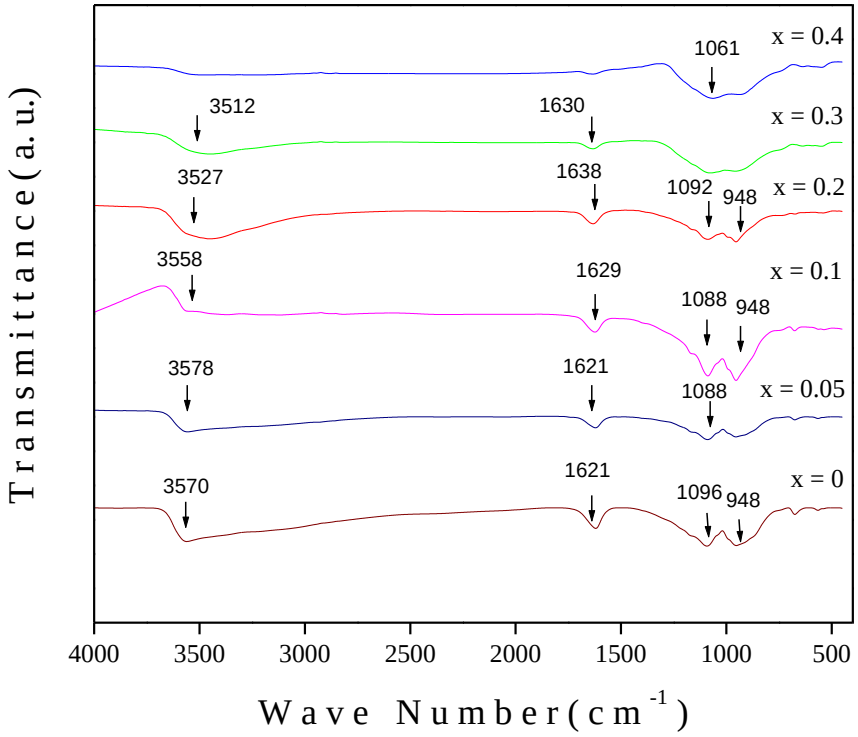

Fig. 3.3 FT-IR spectra of the glass nano-composite for different values of x

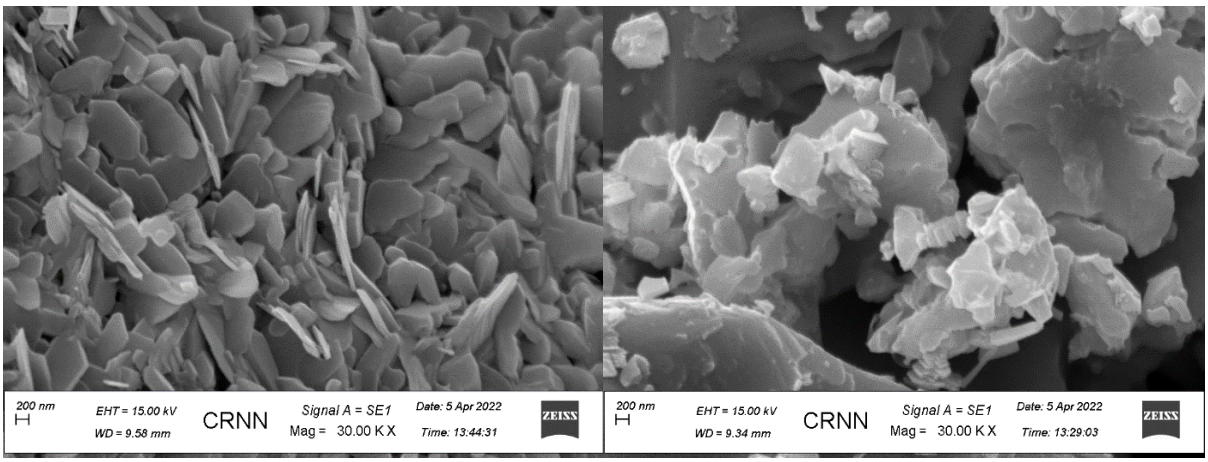

(a) **(b)**

Fig. 3.4 FE-SEM of the sample with (a) x = 0 (b) x = 0.3

3.3.2 Electrical Conductivity Study

Researchers across numerous fields continue to be very interested in the ion transport process in glasses and their nano-composites [28–30]. Theoretical understanding of the problem has advanced and many issues have been clarified by experimental data and computer simulations

on structure and dynamics. Nonetheless, a lot remains to be discovered because of the intricate structure of numerous crystals [28], glasses, and melts, in which the ions reside and diffuse [28, 30]. Electrical conductivity study explains many such unanswered questions.

Electrical conduction in semiconducting glass nano-composites is primarily caused by transition metal ions [31]. One of the factors contributing to electrical conductivity is the hopping of an electron between ions of the same transition metal across various valence states [32-33]. Numerous other parameters, such as the concentration of transition metal oxides [33], the spacing between the transition metal ions [34], the glass's melting and annealing temperatures [32-33,35], and others, also affect the electronic conductivity of oxide glasses.

3.3.2.1 DC Conductivity Study

The complex impedance plots [36] for all the as-prepared samples are shown in Fig. 3.5 (a) – (f) and from there the dc electrical conductivity (σ_{dc}) has been computed. As can be seen, all of the curves are semicircular in shape and the diameter of each curve corresponds to bulk resistance (R) of the material. As the temperature increases, the decrease in the diameter of the semi-circular arcs corresponds to increase in conductivity of the system and implies that all the systems show thermally activated nature. Furthermore, it is clear from Fig. 3.5 that none of the plots contain an additional spur, suggesting that the existing system is not affected by grain boundaries [36].

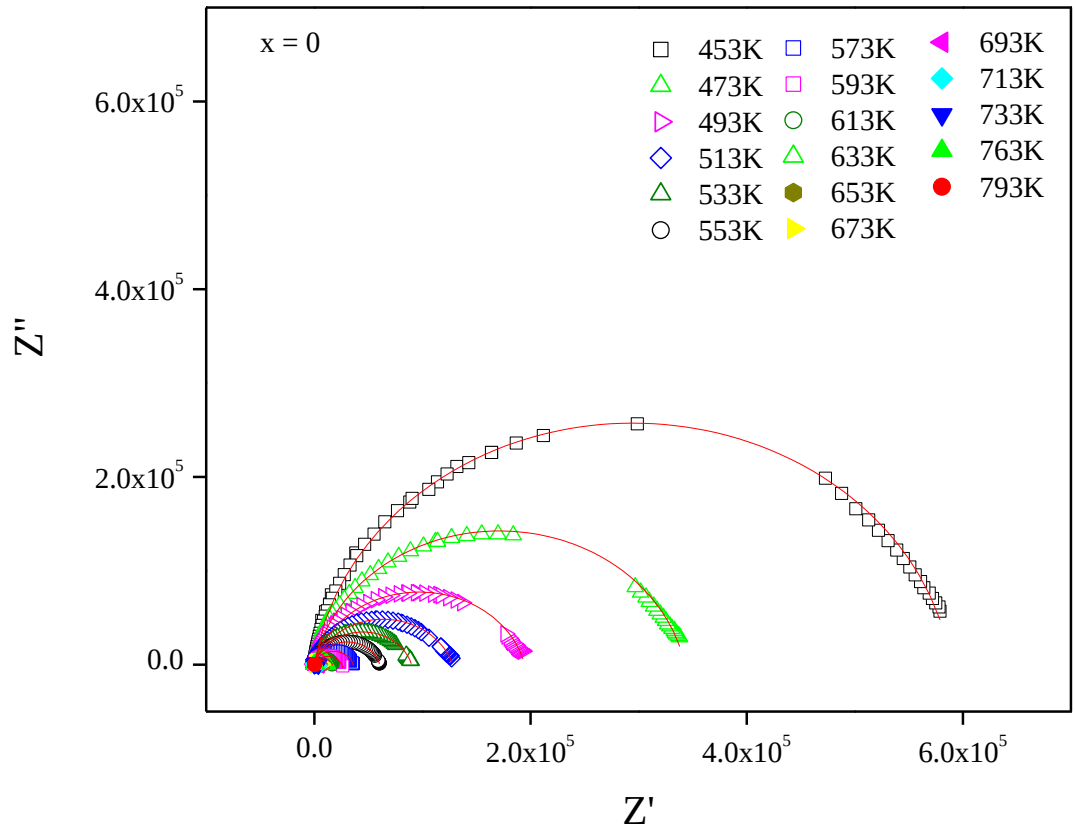

Fig. 3.5 (a) Complex impedance plot for x = 0 at various temperatures

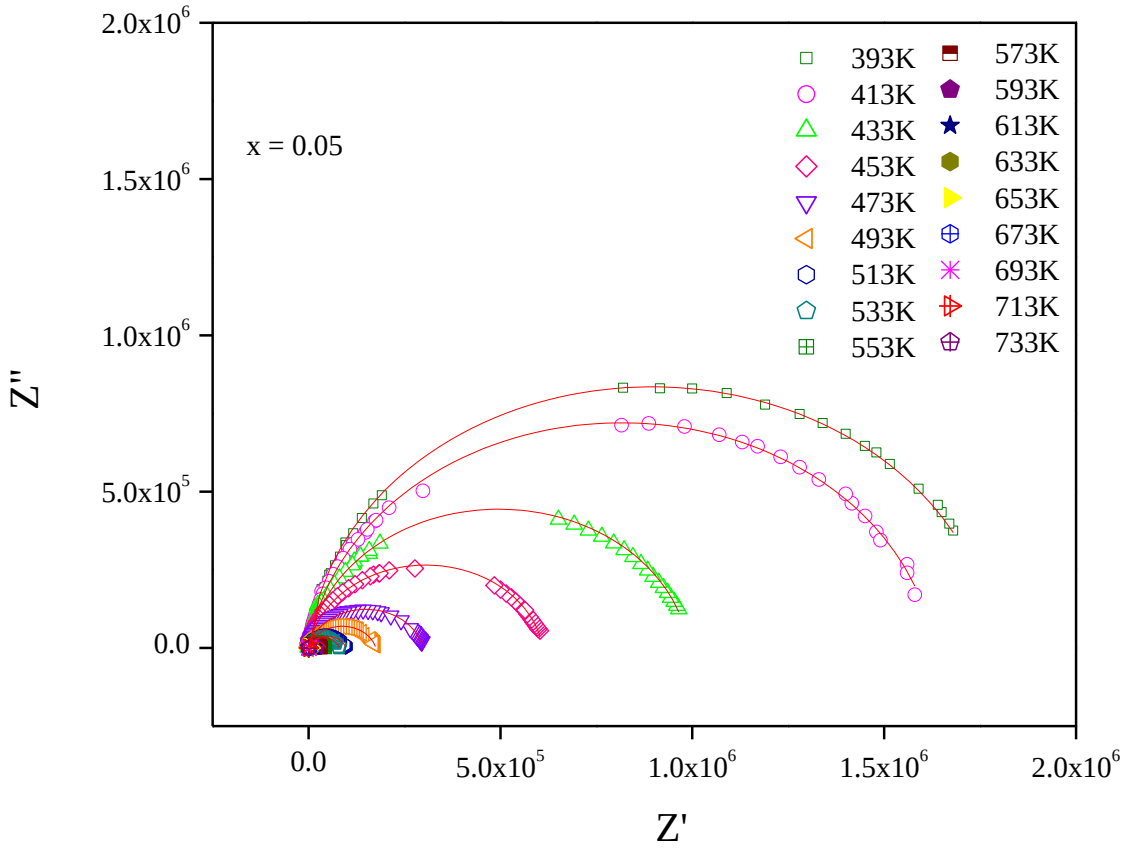

Fig. 3.5 (b) Complex impedance plot for x = 0.05 at various temperatures

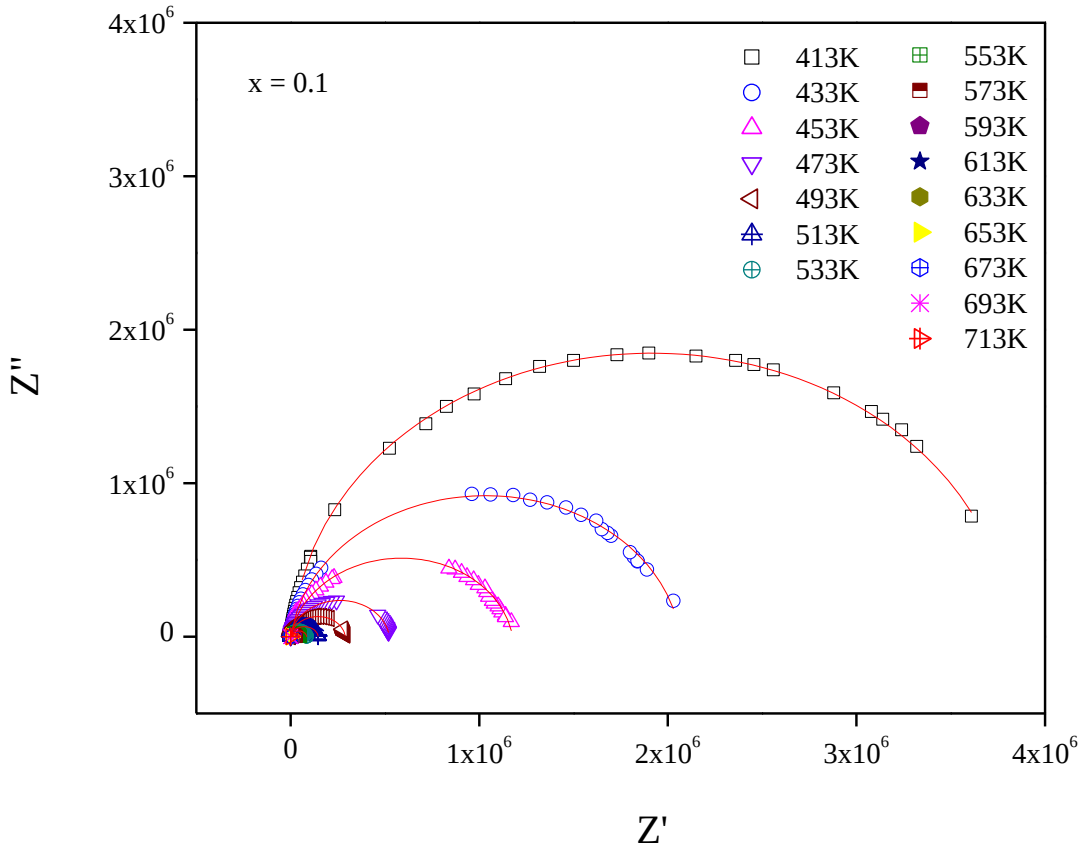

Fig. 3.5 (c) Complex impedance plot for x = 0.1 at various temperatures

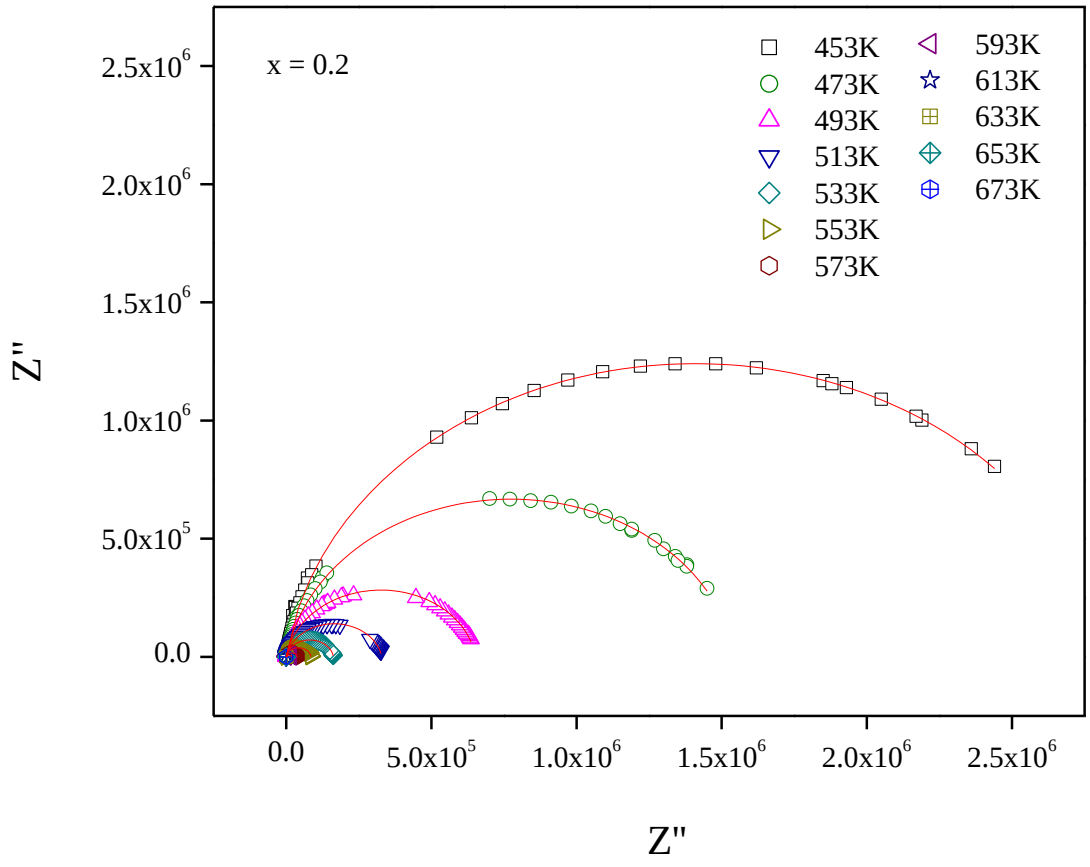

Fig. 3.5 (d) Complex impedance plot for x = 0.2 at various temperatures

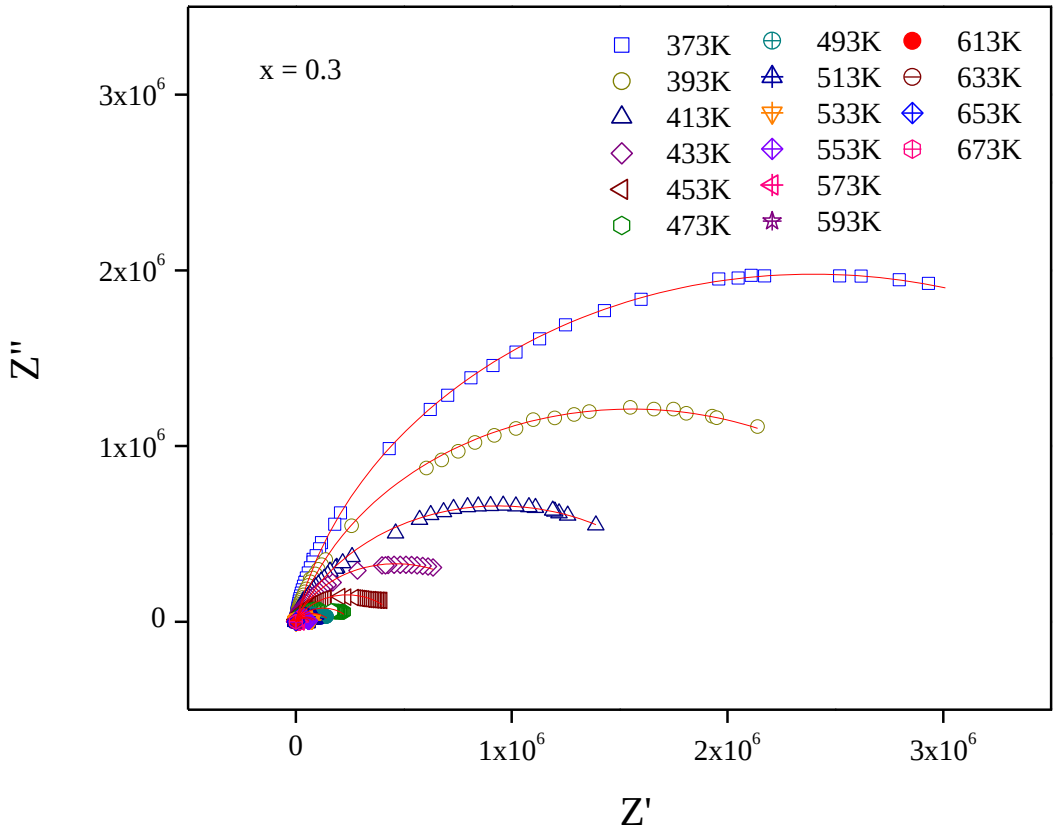

Fig. 3.5 (e) Complex impedance plot for x = 0.3 at various temperatures

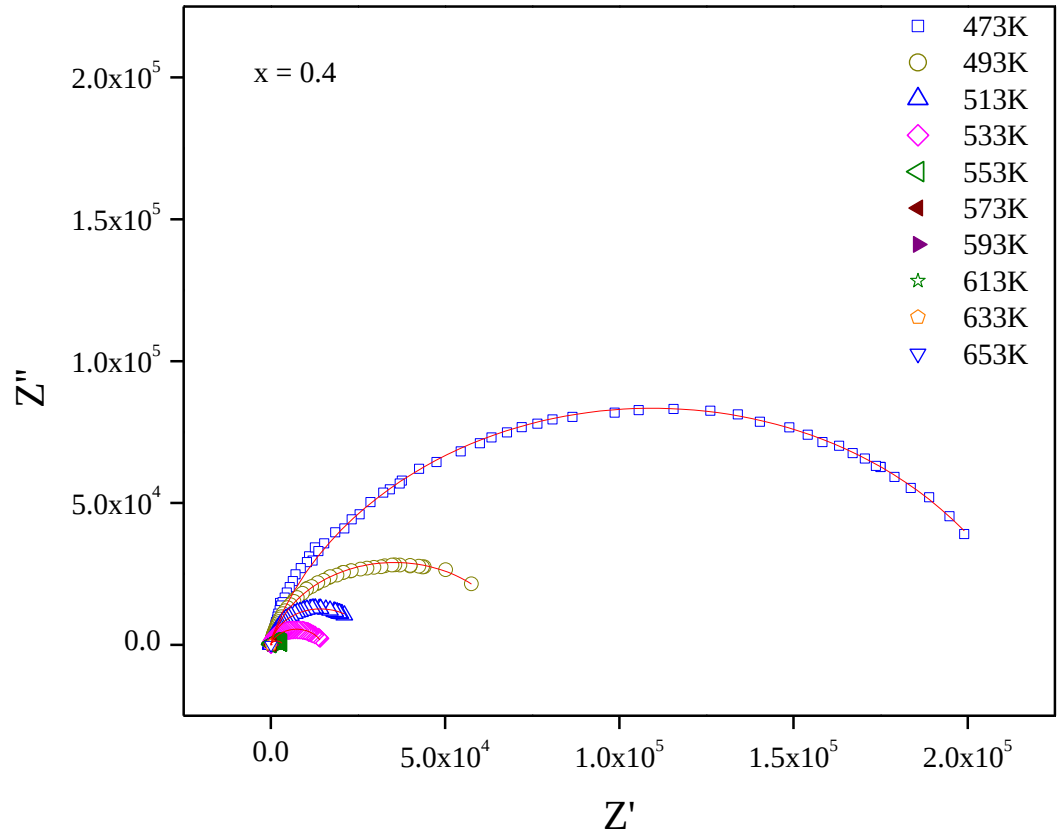

Fig. 3.5 (f) Complex impedance plot for x = 0.4 at various temperatures

To learn more about how the addition of AgI affects the electrical conductivity of the systems as prepared, Fig. 3.6 shows complex impedance graphs for all as-prepared samples at a certain temperature. As the concentration of AgI increases, it is found that the resistance falls and the conductivity rises, making it clear that doping of AgI augments the electrical conductivity in the as-prepared systems.

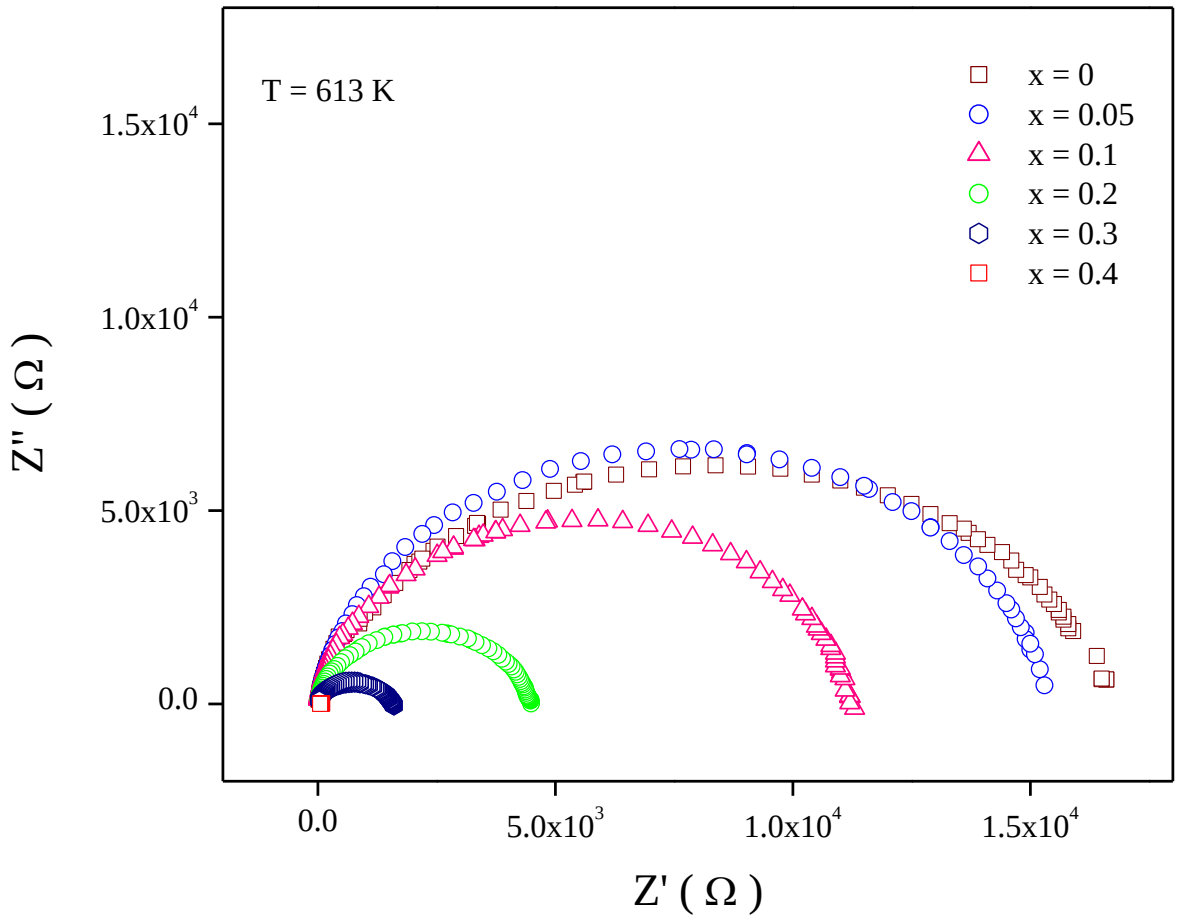

Fig. 3.6 Complex impedance plot for all x at a fixed temperature

DC conductivity [36-37] has been calculated from the complex impedance plots of all the samples using Eq. 2.7. The temperature dependence of the estimated DC conductivity has been plotted in Fig. 3.7 and it shows non-linear nature. It can be clearly seen that the current glassy system's DC conductivity gradually drops until x = 0.2, after which it escalates. This composition-dependent change in pattern of the DC conductivity ought to be related to their structure. Two different temperature zones have been taken into consideration while analyzing the experimental results due to the presence of non-linearity as shown in Fig. 3.7. The

Arrhenius relation, given by Eq. 2.8, has been found the most effective method for fitting this data in two separate temperature zones. The calculated values of activation energy are given in Table 3.3.

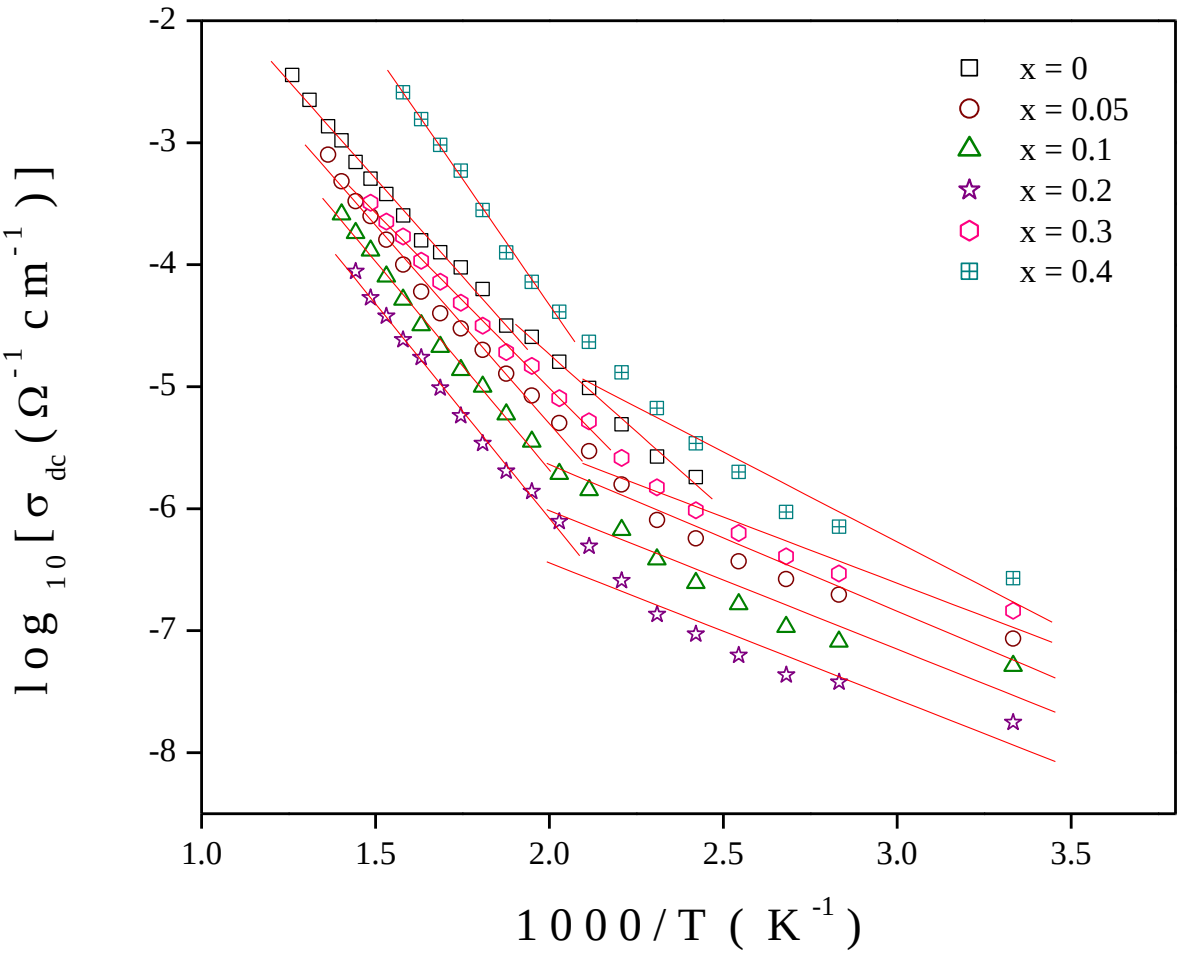

Fig. 3.7 Linear fit of temperature dependence plot of DC conductivity segregating Low and high temperature zone

The presence of two-fold activation energy has given a new insight in our studies. Scientific research on the nature of the charge carriers in light of our discoveries has been a major area of interest for our study as the current system is anticipated to be a mixed conductor with different proportions of electronic/polaronic and ionic contribution.

x	High Temperature Act. Energy E_{dc} (eV)	Low Temperature Act. Energy E_{dc} (eV)	High Temperature Act. Energy E_h (eV)	Low Temperature Act. Energy E_h (eV)
0	0.63	0.50	0.62	0.48
0.05	0.64	0.24	0.64	0.25
0.1	0.68	0.22	0.67	0.24
0.2	0.70	0.22	0.69	0.23
0.3	0.57	0.21	0.58	0.22
0.4	0.82	0.30	0.53	0.27

Table 3.3: Low & high temperature activation energy corresponding to DC conductivity (E_{dc}) and hopping frequency (E_h)

3.3.2.2 AC Conductivity Study

The current glassy system's AC conductivity change with frequency (42 Hz to 5 MHz) at different temperatures for all the x are shown in Fig. 3.8 (a) - (f). It has been observed that AC conductivity rises with temperature and is frequency independent in the lower frequency range. The frequency independent AC conductivity in the glasses could be due to polaron hopping [38-39], and may correspond to DC conductivity. The conductivity is dispersed over a large area as the frequency increases. It came to light that AC conductivity began to increase with frequency at higher frequency regions, above crossover or hopping frequency, which is a sign of correlated motion of polarons [38-39].

Long-time dynamics in the low-frequency realm can be characterised through random walks in terms of diffusive long-range charge carrier transport [37, 40]. As the frequency increases, sub-diffusive motion should be the outcome of the short-term dynamics of charge carriers in terms of back-and-forth motion over limited ranges [37, 40]. Accordingly, the crossover frequency distinguishes between the high-frequency dispersive region (short-time dynamics) and the low-frequency plateau region (long-range transport) [37,40]. The significance of this crossover frequency is that, according to Almond and West [36], hopping of charge carriers begins at that specific frequency when estimating the hopping rate of charge carriers. To obtain enough information related to the conduction in the system, AC conductivity spectra were fitted using the Almond West formalism [38], given by Eq. 2.16. The solid lines in Figure 3.8 (a) - (f) show the linear fitting of AC conductivity data. The calculated parameters $\square_{dc}$, $\square_H$ and n are tabulated in Table 3.4 – 3.9.

x	T(K)	σdc ($W^{-1}cm^{-1}$)	ω_H (rad s^{-1})	n
0	413	$2.43x10^{-07}$	9786.364	0.979
	433	$6.36\ x10^{-07}$	24470.626	0.971
	453	$1.49\ x10^{-06}$	57601.003	0.975
	473	$3.49\ x10^{-06}$	130078.948	1.017
	493	$5.07\ x10^{-06}$	186958.49	1.023
	513	$8.11\ x10^{-06}$	246598.222	0.986
	533	$1.00\ x10^{-05}$	330796.913	0.967
	553	$2.00\ x10^{-05}$	435041.189	0.934
	573	0.00003	769765.051	0.948
	593	0.00004	1252926.61	0.935
	613	0.00005	1607117.493	0.938
	633	0.00008	2791494.767	0.994
	653	0.00012	5032119.429	1.122
	673	0.00016	6553554.874	1.161
	693	0.00022	8807191.138	1.256
	713	0.00033	9047706.459	1.283
	733	0.00043	8603972.549	1.18
	763	0.00071	17934947.36	1.247
	793	0.00302	31421411.08	1.009

Table 3.4: Parameters obtained from Almond West fitting of x = 0

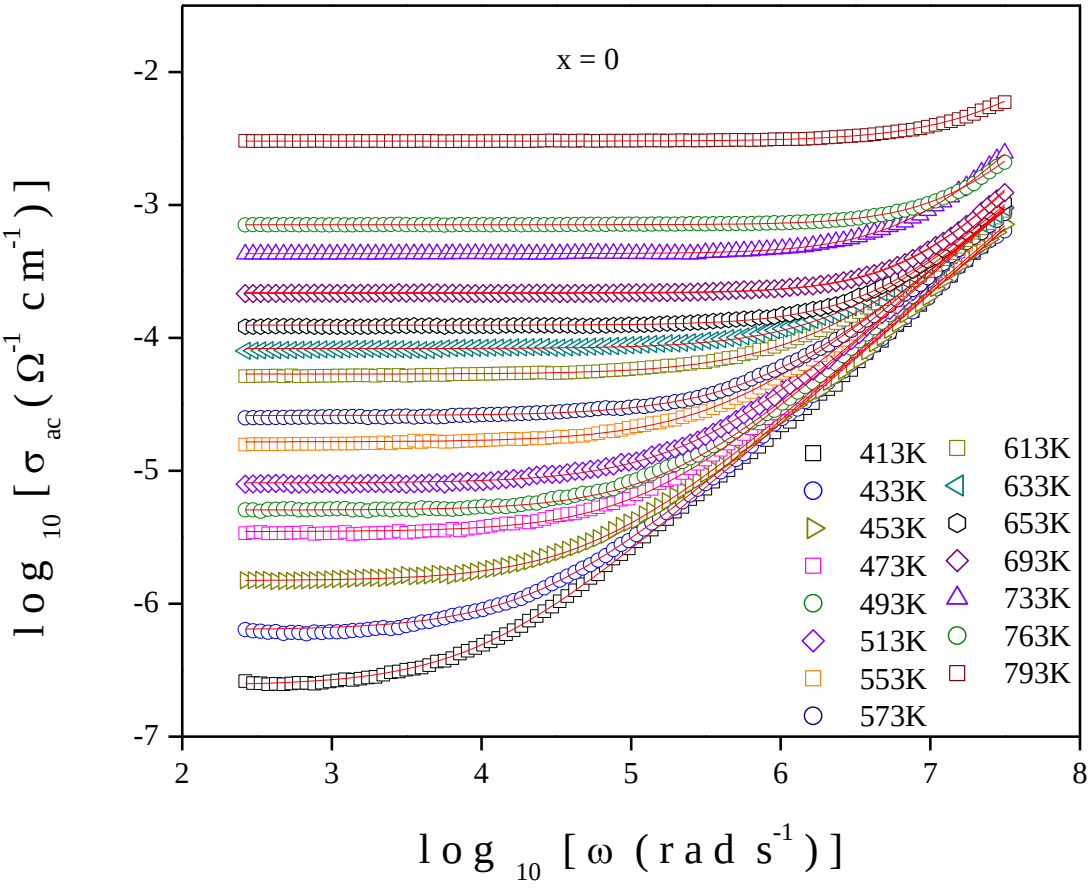

Fig. 3.8 (a) AC conductivity plot for x = 0 at various temperatures

x	T(K)	σdc ($W^{-1}cm^{-1}$)	ω_H (rad s^{-1})	n
0.05	300	9.51×10^{-08}	3221.186	0.944
	353	4.11×10^{-07}	11859.786	0.916
	373	4.12×10^{-07}	14338.517	0.944
	393	4.97×10^{-07}	18000.285	0.953
	413	6.00×10^{-07}	22025.792	0.955
	433	8.08×10^{-07}	30198.193	0.958
	453	1.74×10^{-07}	67313.237	0.963
	473	2.96×10^{-06}	109393.785	0.957
	493	6.12×10^{-06}	219794.547	0.973
	513	9.36×10^{-06}	348483.757	1.014
	533	1.00×10^{-05}	459100.432	1.061
	553	2.00×10^{-05}	721149.334	1.038
	573	0.00003	1034484.461	1.036
	593	0.00004	1480344.186	1.02
	613	0.00006	2240765.111	1.055
	633	0.0001	3332947.08	1.080
	653	0.00016	5467671.206	1.151
	673	0.00025	8032376.407	1.145
	693	0.00054	14500857.78	1.365
	713	0.00075	17587702.85	1.381
	733	0.0013	22415400.75	1.462

Table 3.5: Parameters obtained from Almond West fitting of x = 0.05

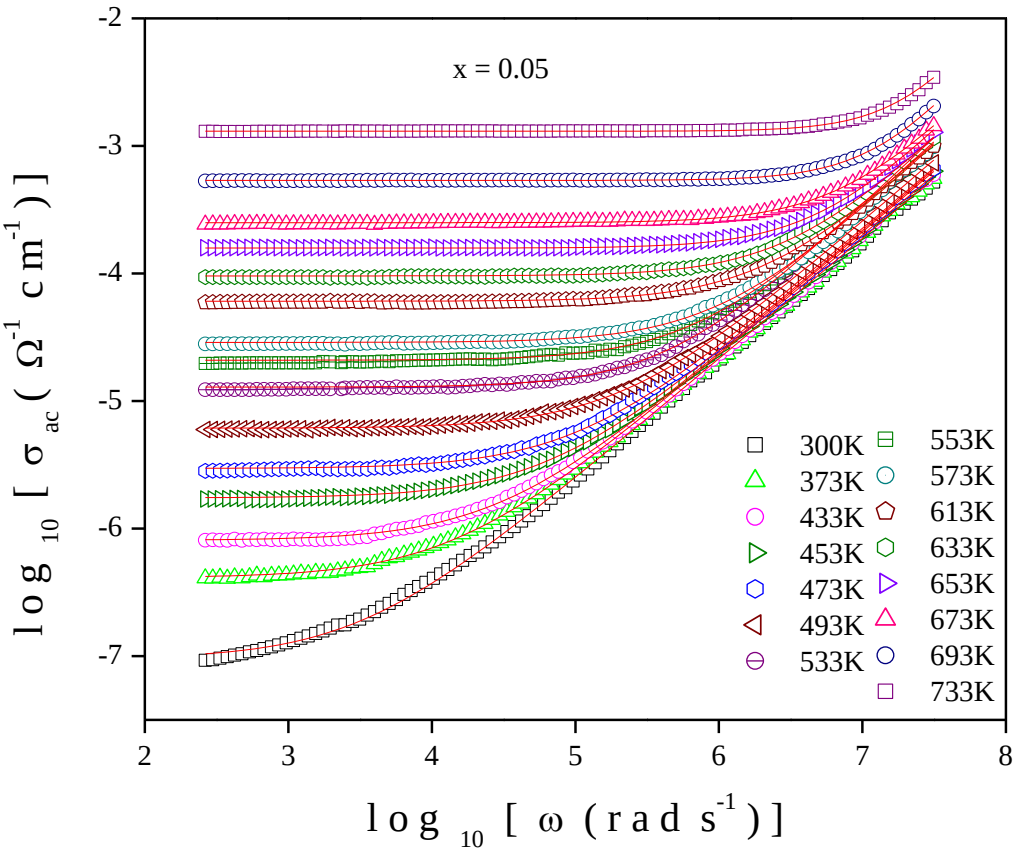

Fig. 3.8 (b) AC conductivity plot for x = 0.05 at various temperatures

x	T(K)	σdc ($W^{-1}cm^{-1}$)	ω_H (rad s^{-1})	n
0.1	300	8.03×10^{-08}	3141.593	0.929
	353	1.09×10^{-07}	5541.412	0.958
	373	1.31×10^{-07}	5043.760	0.976
	393	1.57×10^{-07}	6889.660	0.981
	413	2.02×10^{-07}	12892.875	0.993
	433	3.49×10^{-07}	21502.623	0.989
	453	8.16×10^{-07}	48803.469	0.985
	473	1.42×10^{-06}	82504.422	0.978
	493	2.86×10^{-06}	167955.495	0.99
	513	5.25×10^{-06}	304505.571	1.005
	533	9.21×10^{-06}	551261.356	1.033
	553	1.00×10^{-05}	814271.190	1.026
	573	0.00003	1662635.109	1.05
	593	0.00004	2667422.328	1.073
	613	0.00007	4316274.44	1.104
	633	0.00016	8609369.613	1.173
	653	0.0003	12893510.61	1.165
	673	0.0008	21199022.43	1.235
	693	0.00096	24784085.86	1.402
	713	0.0013	27943308.96	1.433

Table 3.6: Parameters obtained from Almond West fitting of x = 0.1

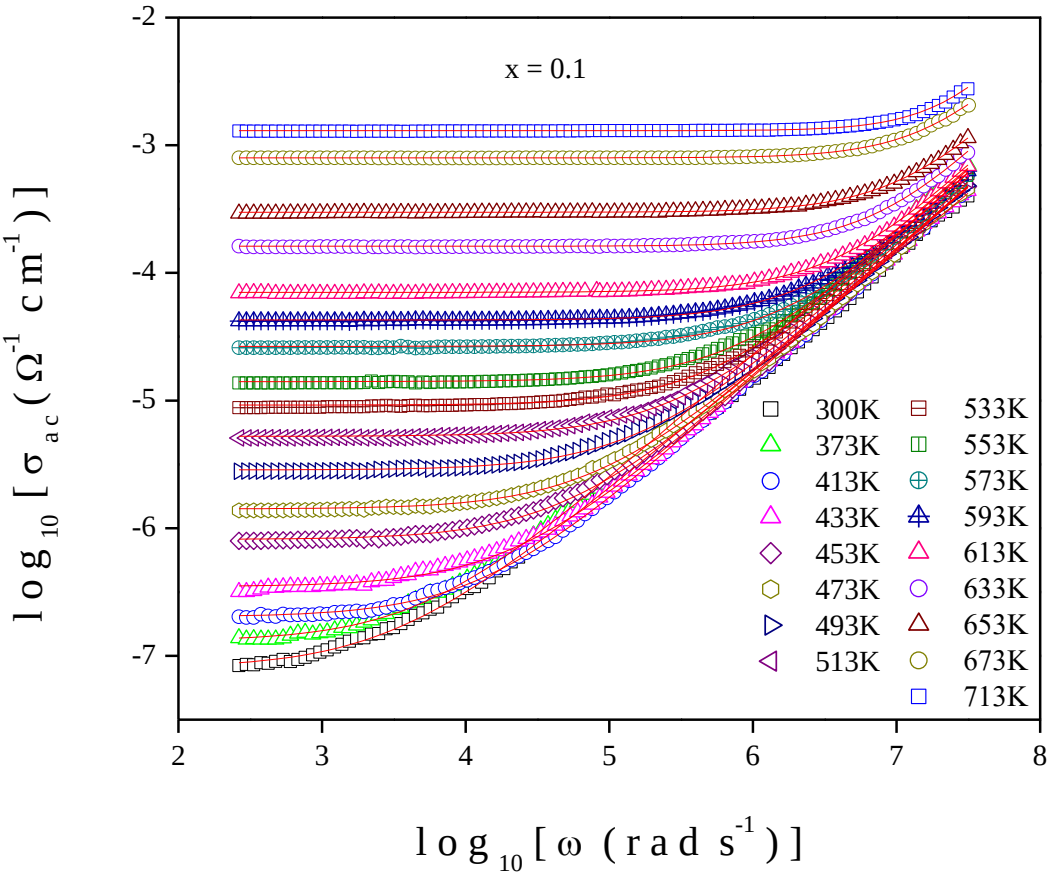

Fig. 3.8 (c) AC conductivity plot for x = 0.1 at various temperatures

x	T(K)	σdc ($W^{-1}cm^{-1}$)	ω_H (rad s^{-1})	n
0.2	300	1.66 x10^{-08}	1068.189	0.997
	353	3.79 x10^{-08}	1879.395	0.964
	373	4.33 x10^{-08}	1806.302	0.943
	393	6.30 x10^{-08}	2357.98	0.929
	413	9.39 x10^{-08}	3085.897	0.911
	433	1.36 x10^{-07}	3933.353	0.898
	453	2.57 x10^{-07}	7438.411	0.892
	473	4.93 x10^{-07}	13965.514	0.883
	493	1.09 x10^{-06}	31626.285	0.877
	513	2.50 x10^{-06}	76771.907	0.878
	533	4.46 x10^{-06}	156283.703	0.902
	553	9.77 x10^{-06}	486426.611	0.99
	573	0.00002	996688.481	1.088
	593	0.00005	2512586.097	1.117
	613	0.00015	6608043.094	1.097
	633	0.00049	14916476.96	1.192
	653	0.00138	20727124.56	1.140
	673	0.00289	27966258.22	1.355
	693	0.00802	69930976.93	0.835

Table 3.7: Parameters obtained from Almond West fitting of x = 0.2

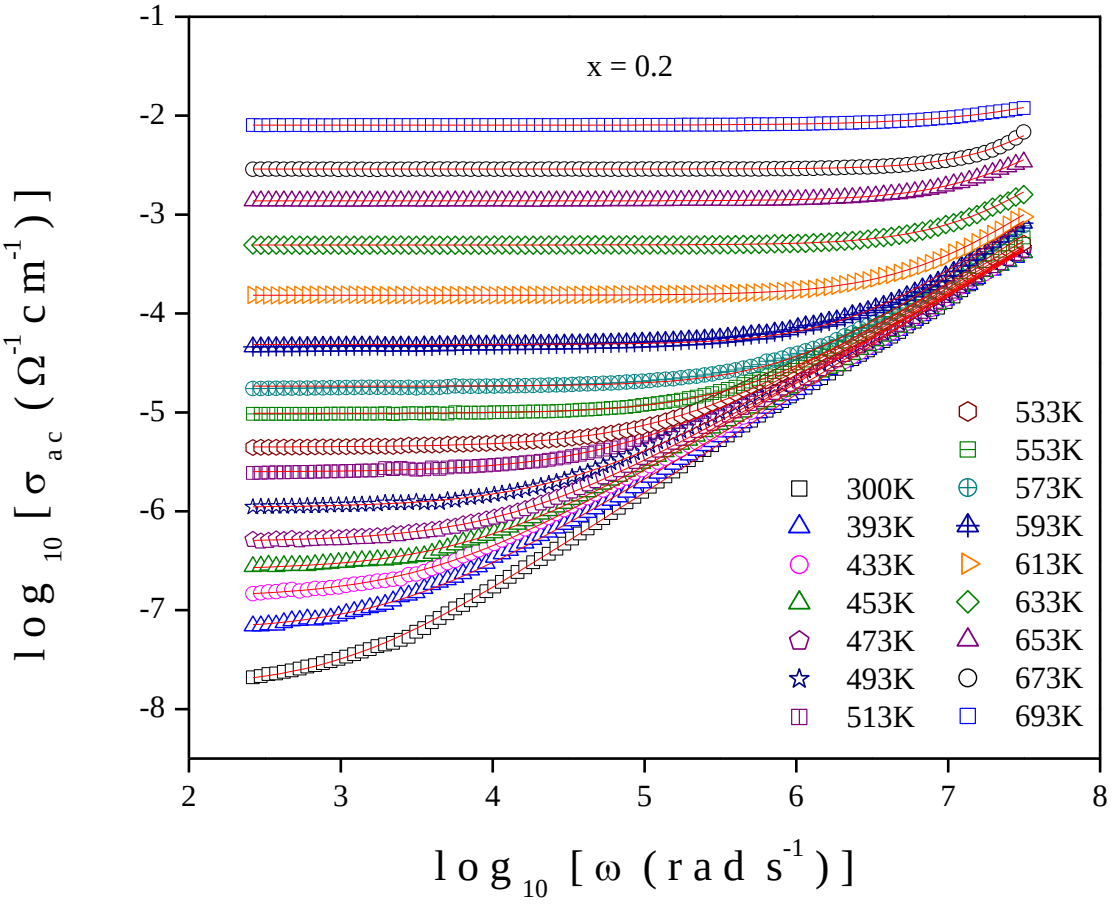

Fig. 3.8 (d) AC conductivity plot for x = 0.2 at various temperatures

x	T(K)	σdc ($W^{-1}cm^{-1}$)	ω_H (rad s^{-1})	n
0.3	300	3.47 x10^{-08}	1733.737	0.978
	353	1.18 x10^{-07}	4945.259	0.951
	373	2.11 x10^{-07}	7674.411	0.927
	393	3.51 x10^{-07}	9535.568	0.88
	413	5.76 x10^{-07}	10441.198	0.824
	433	1.15 x10^{-06}	21130.149	0.811
	453	2.15 x10^{-06}	36691.312	0.79
	473	4.27 x10^{-06}	66411.784	0.759
	493	6.19 x10^{-06}	74187.585	0.716
	513	1.00 x10^{-05}	93700.123	0.67
	533	0.00001	60792.065	0.621
	553	0.00002	126135.389	0.687
	573	0.00004	779115.111	0.781
	593	0.00022	7102292.551	0.993
	613	0.00059	9958273.619	0.863
	633	0.00218	21761719.45	1.312
	653	0.00457	28595465.4	1.386
	673	0.00697	37381747.41	1.196

Table 3.8: Parameters obtained from Almond West fitting of x = 0.3

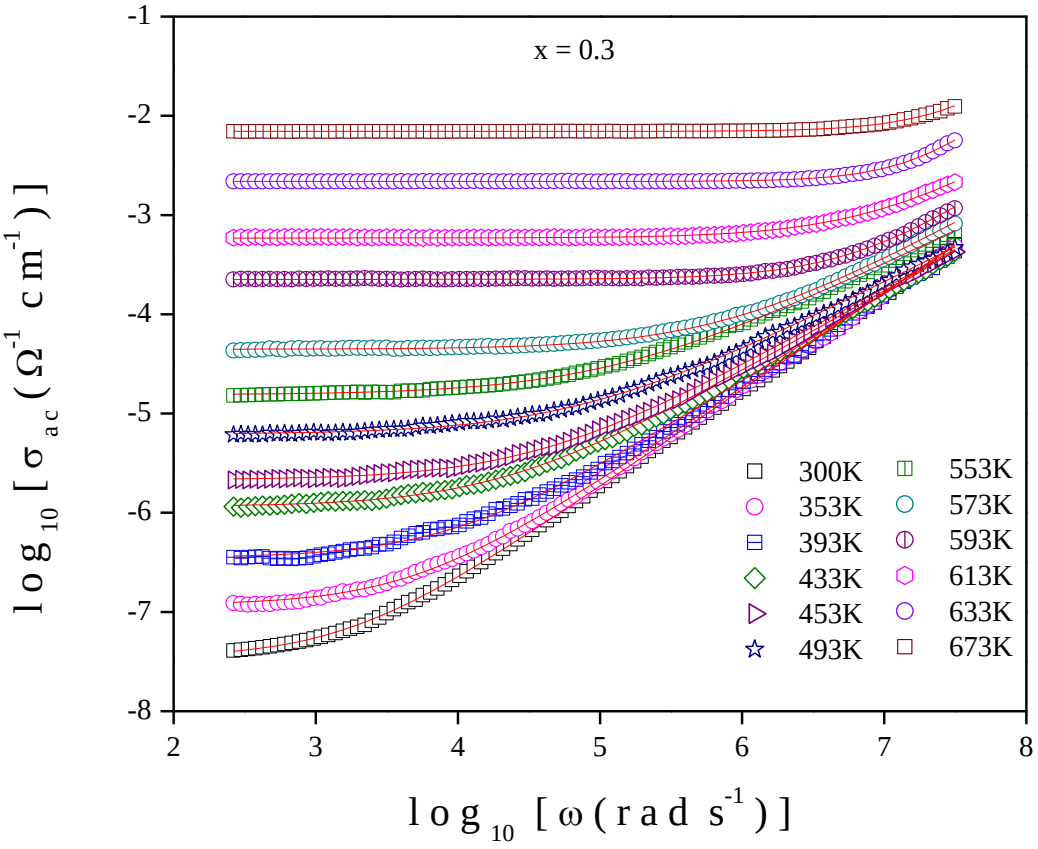

Fig. 3.8 (e) AC conductivity plot for x = 0.3 at various temperatures

x	T(K)	σdc ($W^{-1}cm^{-1}$)	ω_H (rad s^{-1})	n
0.3	300	2.87 x10^{-07}	4877.964	0.88
	353	7.12 x10^{-07}	11419.228	0.891
	373	7.72 x10^{-07}	4606.013	0.775
	393	2.00 x10^{-06}	10943.191	0.755
	413	3.00 x10^{-06}	8924.507	0.806
	433	5.15 x10^{-06}	12554.126	0.856
	453	7.77 x10^{-06}	79286.113	0.879
	473	8.72 x10^{-06}	119431.911	1.024
	493	2.00 x10^{-05}	236124.794	1.062
	513	4.00 x10^{-05}	519850.059	1.084
	533	7.00 x10^{-05}	1122719.331	1.118
	553	2.80 x10^{-04}	4720164.087	1.194
	573	0.00322	15838500.29	1.194
	593	0.00638	1745177.945	0.215
	613	0.01036	23017977.75	0.449
	633	0.01164	29794472.71	0.954

Table 3.9: Parameters obtained from Almond West fitting of x = 0.4

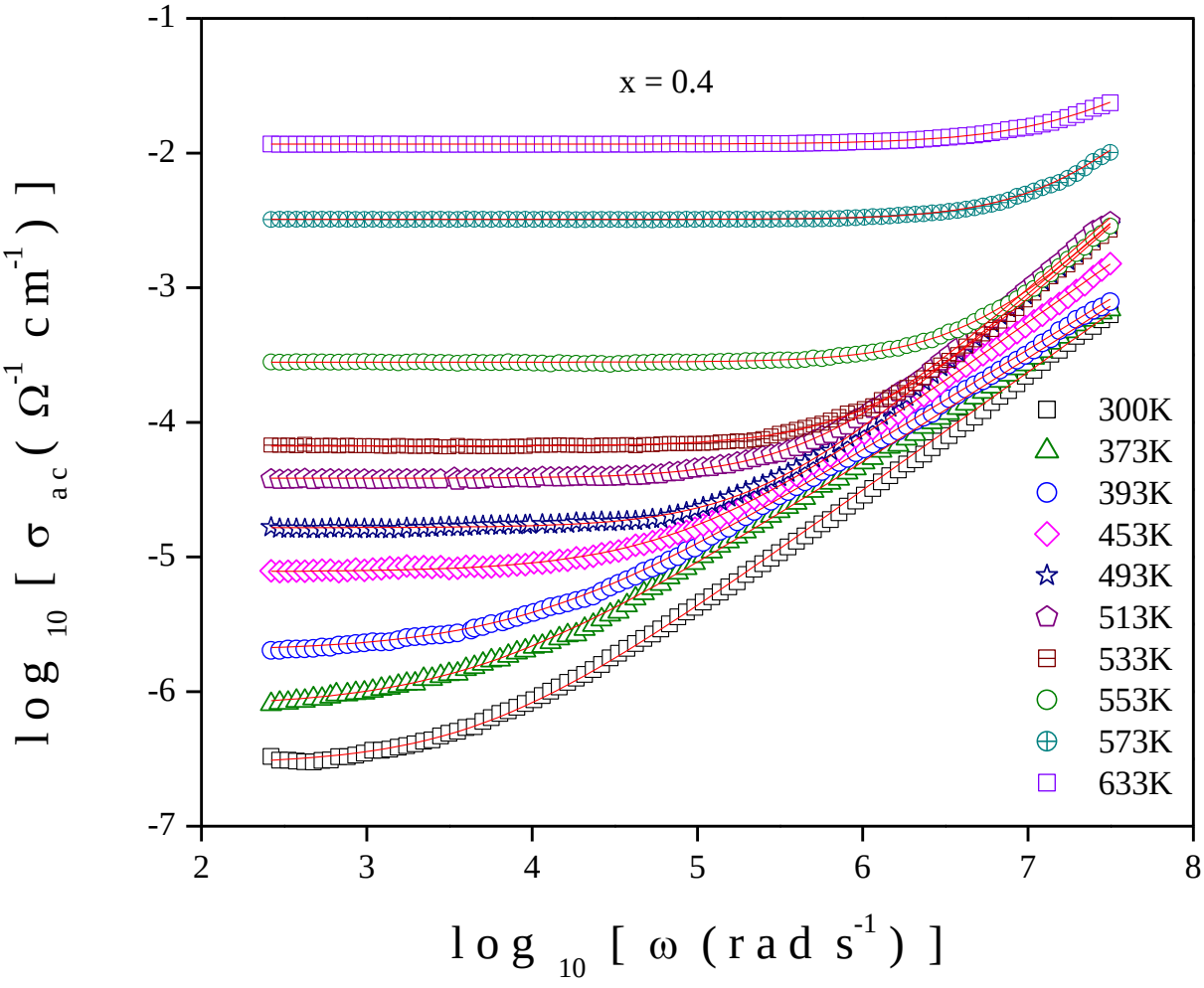

Fig. 3.8 (f) AC conductivity plot for x = 0.4 at various temperatures

Fig. 3.9 displays the ac conductivity spectra for each composition at a particular temperature of 613K. This indicates unequivocally that conductivity rises significantly from x = 0.2. An increase in ionic conduction in the system is correlated with an increase in the frequency independent region as the AgI content rises. This makes it abundantly evident that ionic conduction overtakes electronic conduction after x = 0.2.

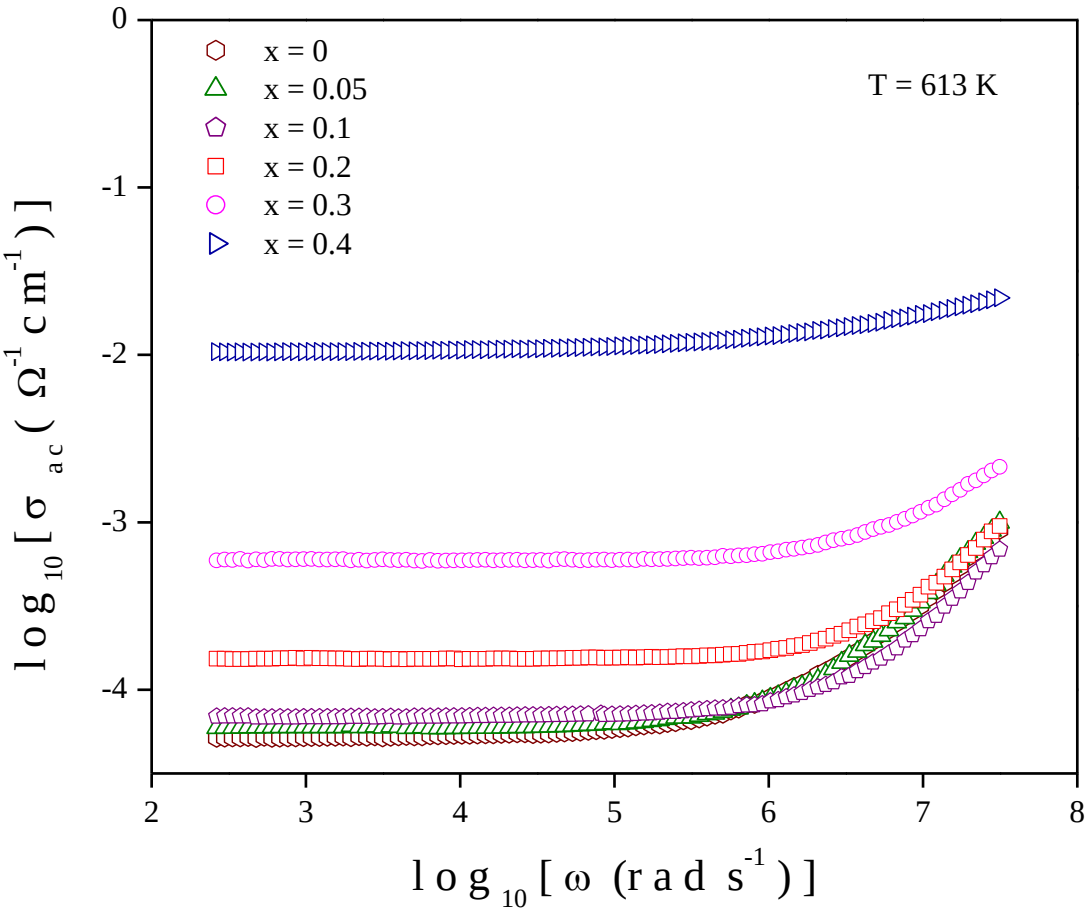

Fig. 3.9 AC conductivity spectra of all the samples at a fixed temperature

The estimated values of hopping frequency□□□$_H$) have been plotted against reciprocal of temperature in Fig. 3.10 (a) and it has been found to follow Arrhenius plot in two separate temperature zones. Table 3.3 displays the estimated activation energies (E_h) corresponding to crossover frequencies for low and high temperatures based on the best fits. It is noteworthy that E_h is very close to E_σ.

□$_H$ has been plotted against composition at a specific temperature, 473K in Fig. 3.10 (b). It has been found that hopping frequency increases after x= 0.2, indicating dominance of ionic conduction in the system.

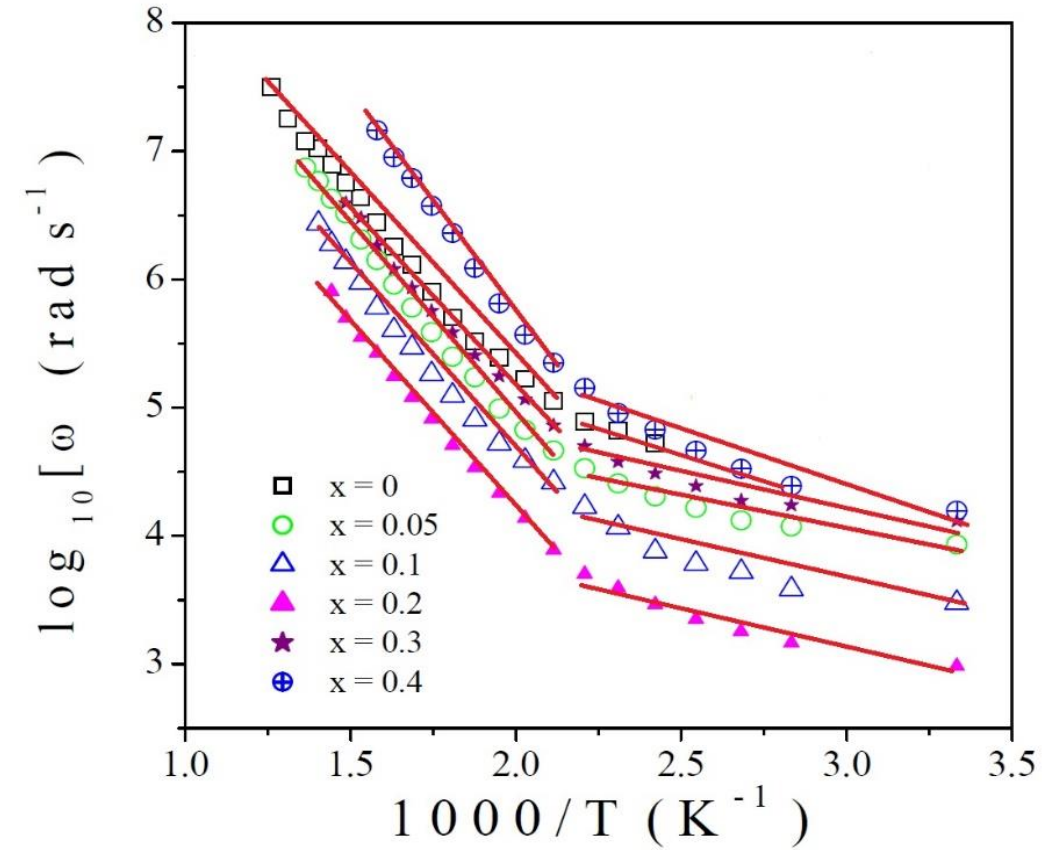

Fig. 3.10 (a) Linear fit of hopping frequency plot for all x at various temperatures

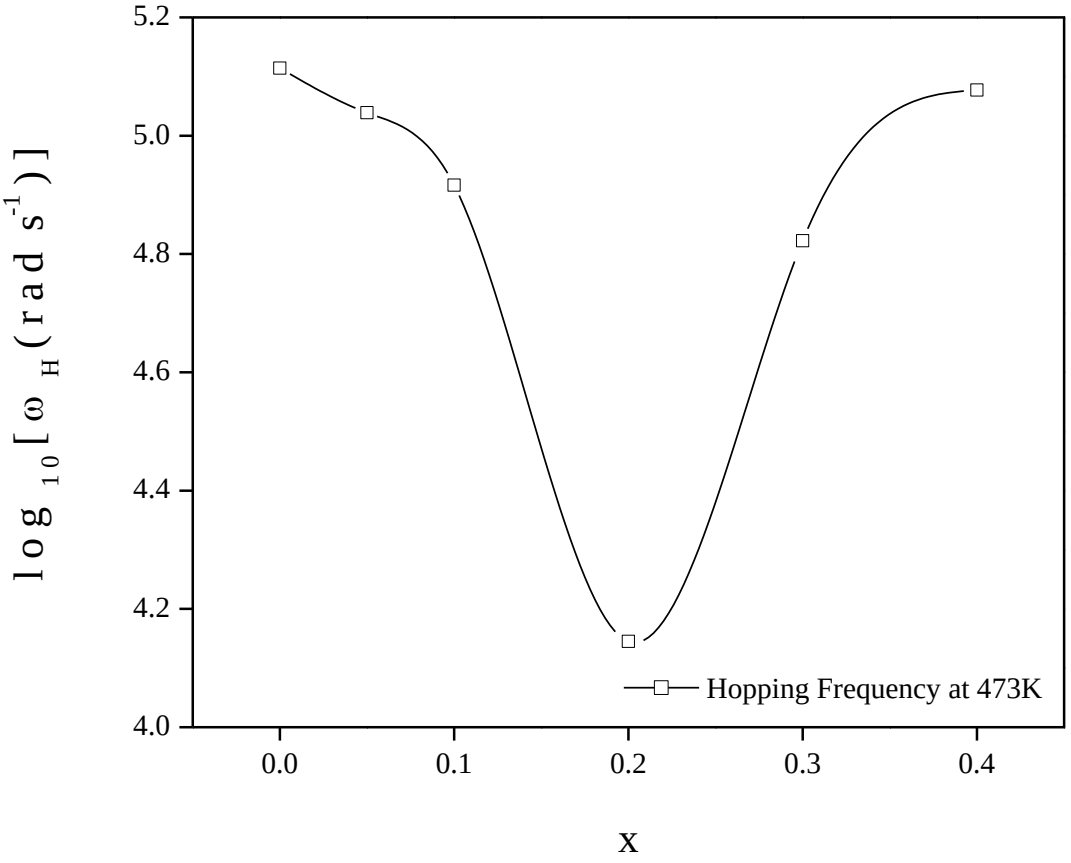

Fig. 3.10 (b) Hopping or Crossover frequency plot for all x at a fixed temperature

The present system exhibits presence of both electronic/ polaronic conduction as well as ionic conduction process [41-47]. Ionic conduction refers to the transport of electrical charge through the motion of ions in a material. This mechanism occurs in materials where ions can move through the lattice or amorphous structure under an applied electric field. Ions hop or migrate from one site to another within the material and the mobility is influenced by temperature, material structure, and defect density. On the other hand, polaronic conduction refers to the transport of electrical charge via polarons that distorts the crystal lattice around it due to its interaction with the ions in the lattice. The conduction occurs via hopping of the polaron from one lattice site to another.

Jonscher's universal power law [40], given in Eq. 2.19 has been considered to explore polaron conduction phenomena in the present system. As can be seen in Fig. 3.11 (a), high frequency conductivity spectra of the sample x = 0.2 at various temperatures have been examined. They demonstrate a progressive increase in conductivity with temperature, suggesting a thermal activation nature. Experimental data are well-fitted linearly to get the values of slopes. The values of S of Eq. 2.19 at various temperatures are estimated from the slopes.

Depending on the nature of the slopes, CBH model [48-50], given by Eq. 2.10 has been found to be the most suitable theoretical approach to interpret the nature of polaronic conduction. The corresponding S-T plot has been shown in Fig. 3.11 (b) and the calculated data are recorded in Table 3.10. Gradual decrease in W_m indicates increased charge carrier mobility, higher electrical conductivity, reduced temperature dependence of conductivity. The gradual decrease in relaxation time implies lower energy barriers which results in a higher AC conductivity.

x	W_m (eV)	τ_0 (s)
0.0	1.78785	2.39E-13
0.05	5.76426	9.33E-13
0.1	5.76371	3.57E-19
0.2	4.04157	2.63E-21
0.3	4.03508	3.31E-22
0.4	4.0339	3.78E-23

Table 3.10: Parameters obtained form S-T plot fitted by CBH model

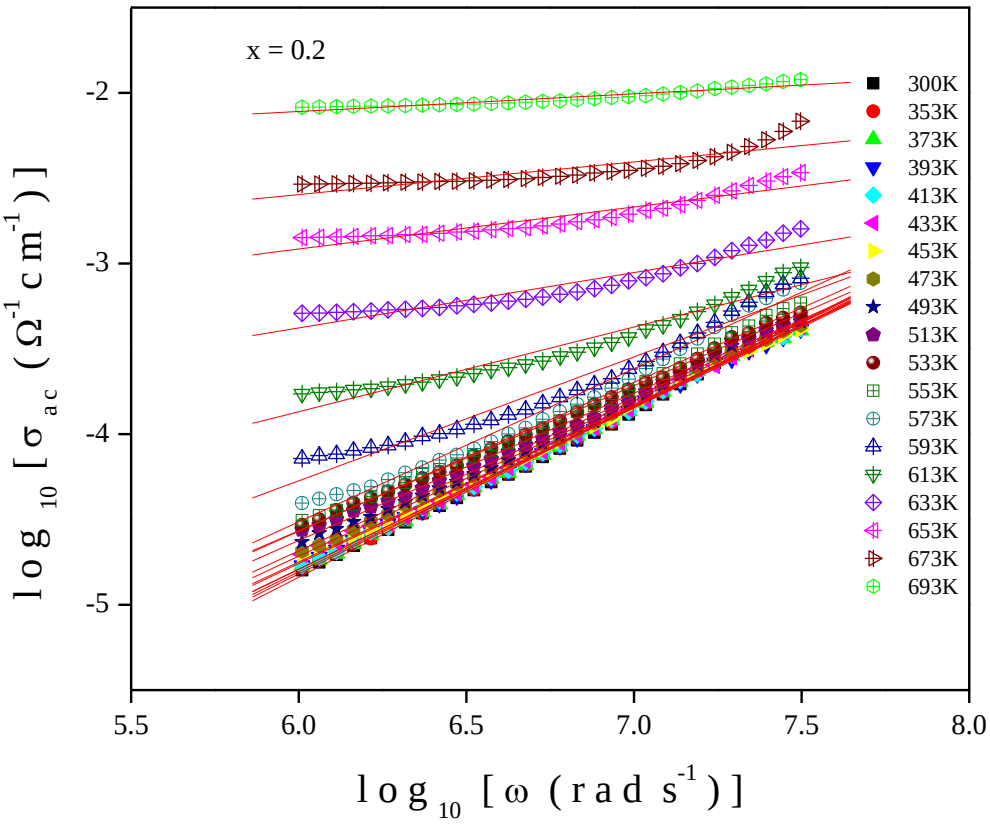

Fig. 3.11(a) Linearly fitted high frequency conductivity spectra for x = 0.2 at various temperatures

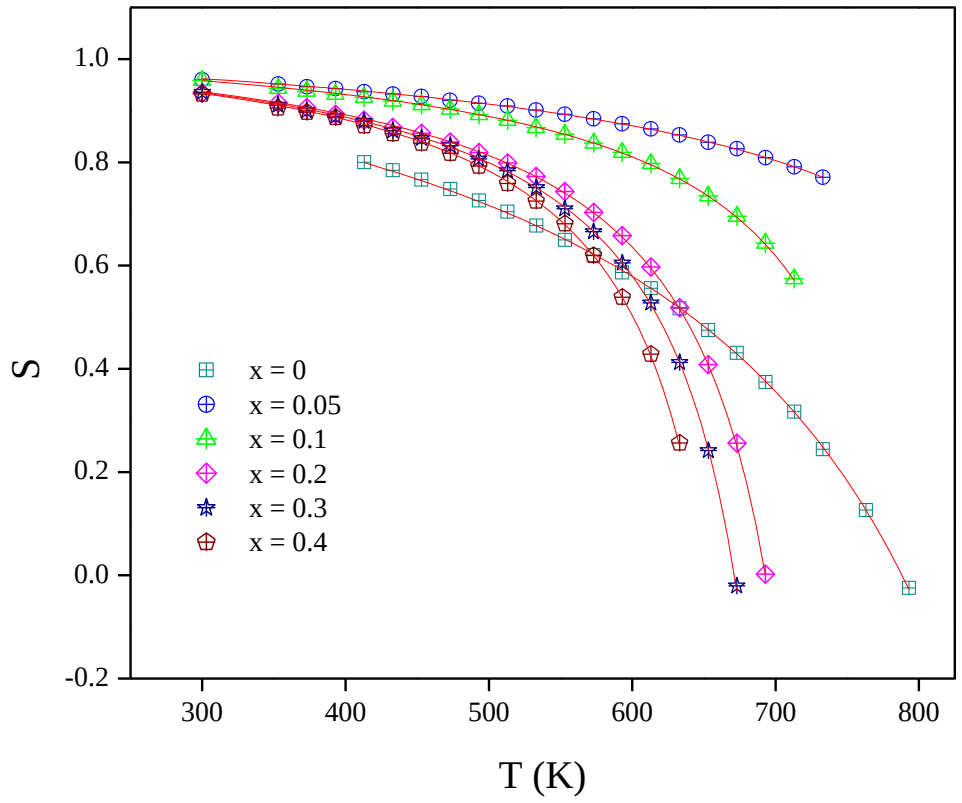

Fig. 3.11 (b) S-T plot for all the compositions

The calculation of carrier ion concentration is an important study to carry out on these kinds of samples. Nernst-Einstein relation [19,37], given by Eq. 2.22 has been exploited to calculate the charge carrier density in the as-prepared samples. Fig. 3.12 shows that N_c is virtually unaffected by composition and temperature. It is possible to draw the conclusion that charge carrier mobility is essential to the conduction process.

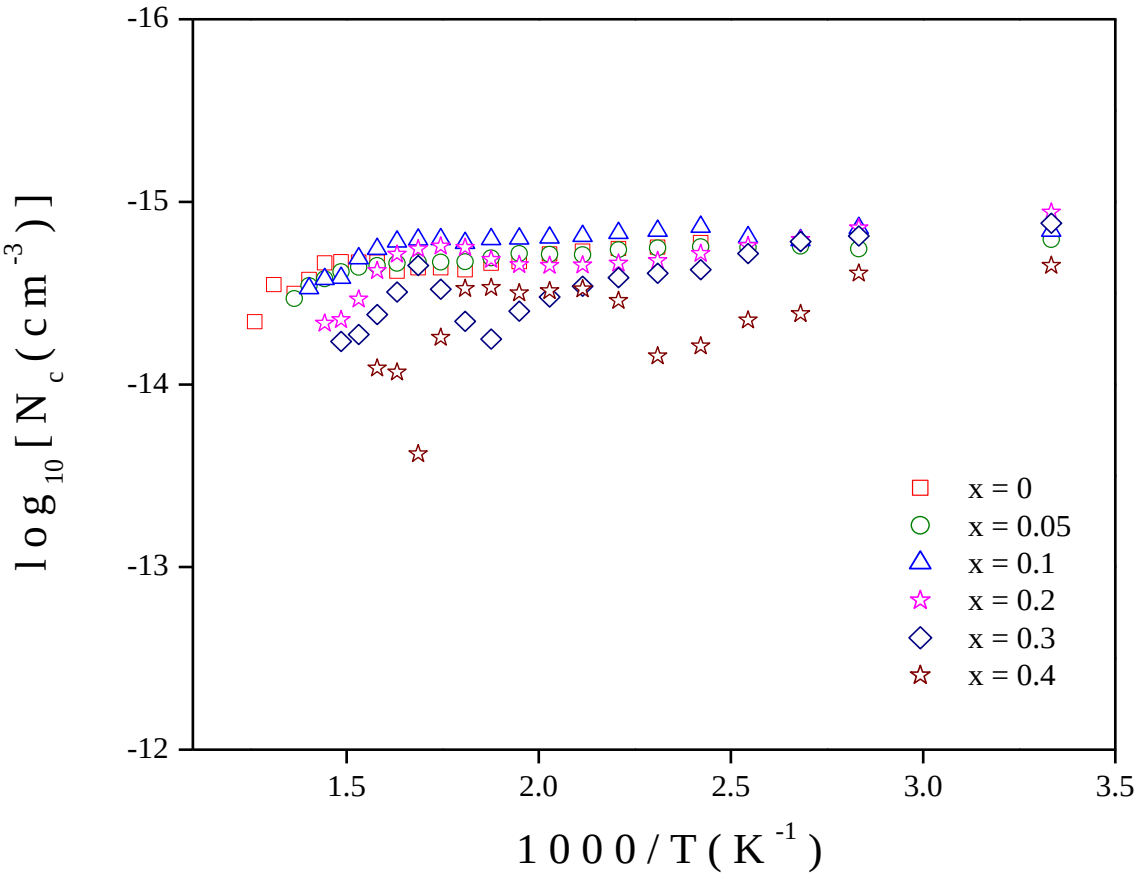

Fig. 3.12 Charge carrier concentration with respect to temperature plot for all the compositions

The frequency exponent (n) has been plotted against composition in Fig. 3.12. It shows that up to x = 0.2, n is fairly close to unity and then displays a diminishing tendency for x = 0.3 and beyond. Mixed carrier conduction in the current system may be the cause of this type of n values [51]. For lower values of AgI content ($0 < x < 0.2$), electron/polaron may be the most dominant factor over the motion of Ag^+. It is anticipated that Ag^+ conduction will predominate and that fewer electrons and polarons will be released in the composition with a greater AgI component ($x > 0.2$). This expectation may be confirmed by the plots in Figure 3.7, which

clearly show the change in slopes associated with the fluctuation of E_{DC}. In the lower concentration of AgI i.e. for $0 < x < 0.2$, presence of more and more non-bridging oxygen [19, 37] are expected. As the amount of non-bridging oxygen increases, more electrons will be released from the vanadium ions, forming the link between Ag^{+} and I^{-2}. Since, Ag^{+} has a strong connection with I^{-2}, compositions with lower AgI ($0 < x < 0.2$) should have an increasing number of electrons and polarons acting as mobile charge carriers through hopping. However, when the composition's AgI level rises, the scenario reverses. Higher bridging oxygen should be present in these compositions, which would cause Ag^{+}---I^{-2} covalent bonding to contribute an increasing amount of Ag^{+}.

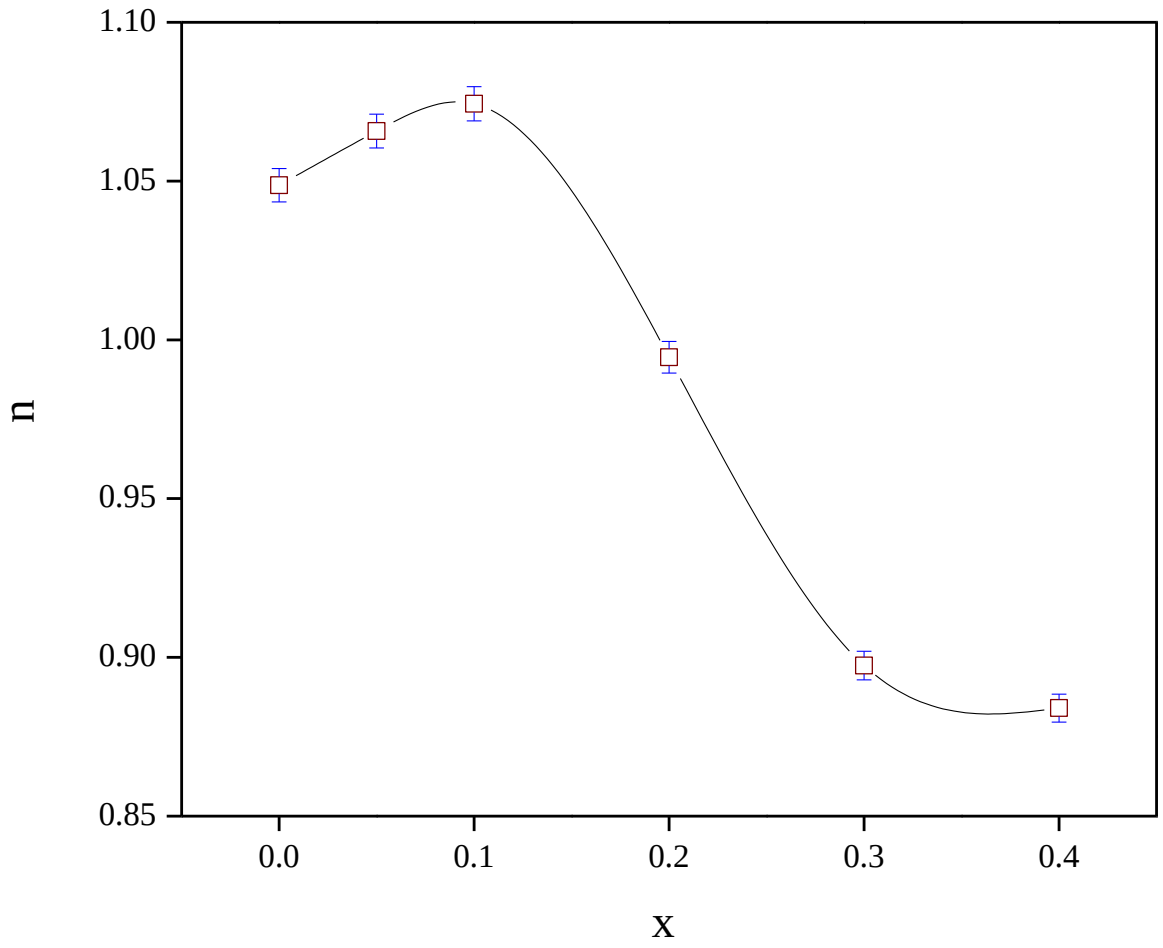

Fig. 3.13 Frequency exponent (n) with compositions

3.3.3 Dielectric Property study

Due to its employment in a wide range of device applications, glassy nano-composites' dielectric properties are currently attracting increasing attention from both industry and academia [52–54]. In complex systems, such as glassy nano-composites, dielectric relaxation spectroscopy has been frequently employed to realise the microscopic dynamical relaxation process [55–56]. An in-depth examination of electric modulus spectra, dielectric loss, and the relationship between composition and relaxation time is highly desirable [52–59]. Numerous research has focused on ionic conductivity and the ionic relaxation process in alkali oxide glasses [57–59] and their nano-composites [59–65]. Research is still being conducted, though, and no clear explanation for these processes has emerged.

3.3.3.1 Study of electrical permittivity

Permittivity study provides critical insights into the material's ability to store and transfer electrical energy under an applied electric field and reflects their polarizability, which is influenced by the structure, composition, and interaction of the glass matrix and embedded nanoparticles. In the frequency range of 42 Hz to 5 MHz, the dielectric constant $\varepsilon^{/}$ and dielectric loss $\varepsilon^{//}$ of the system has been investigated using Eqs. 2.24 – 2.25. Fig. 3.14 (a) – (f) present the variation of dielectric constant of the sample against frequency for all x and it shows an exponential drop as the frequency increases at varying temperatures. A high ε' value means the material is highly polarizable and can store a significant amount of electrical energy.

At low frequencies, all polarization mechanisms (electronic, ionic, dipolar, and interfacial) contribute to ε' [66], resulting in a high value. As frequency increases, slower polarization mechanisms (e.g., ionic and interfacial) cannot keep up with the rapid fluctuation of the field and that causes ε' to decrease. Dielectric Constant ($\varepsilon^{/}$) for all the samples show same kind of spectra. Gradual decrease in the value of $\varepsilon^{/}$ has been found with increasing x which implies poor polarization as the dopant salt concentration increases. This suggests that most charge carriers contribute to conduction rather than polarization which in turn implies that higher conductivity can be achieved with the increase in x.

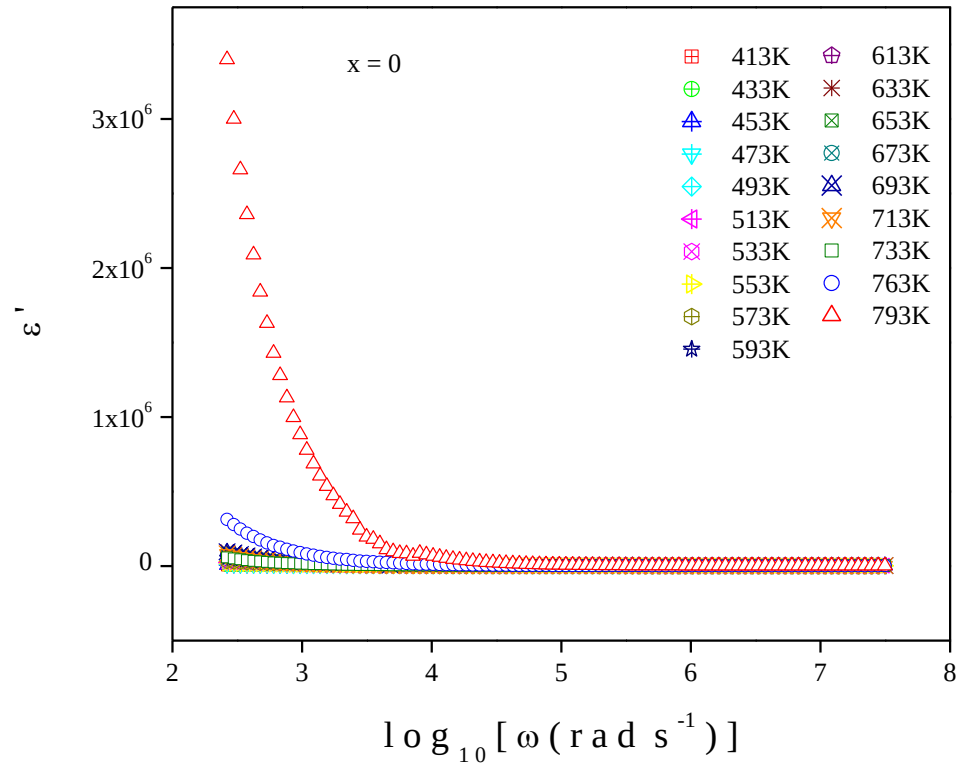

Fig. 3.14 (a) Spectra of dielectric constant ε' for x = 0

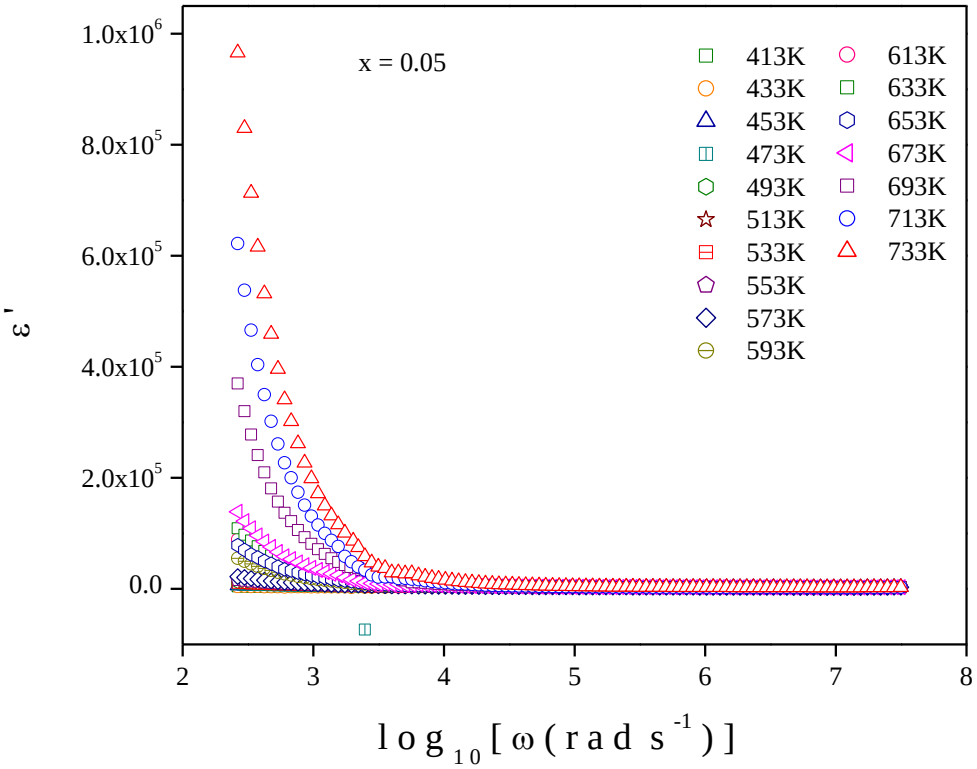

Fig. 3.14 (b) Spectra of dielectric constant ε' for x = 0.05

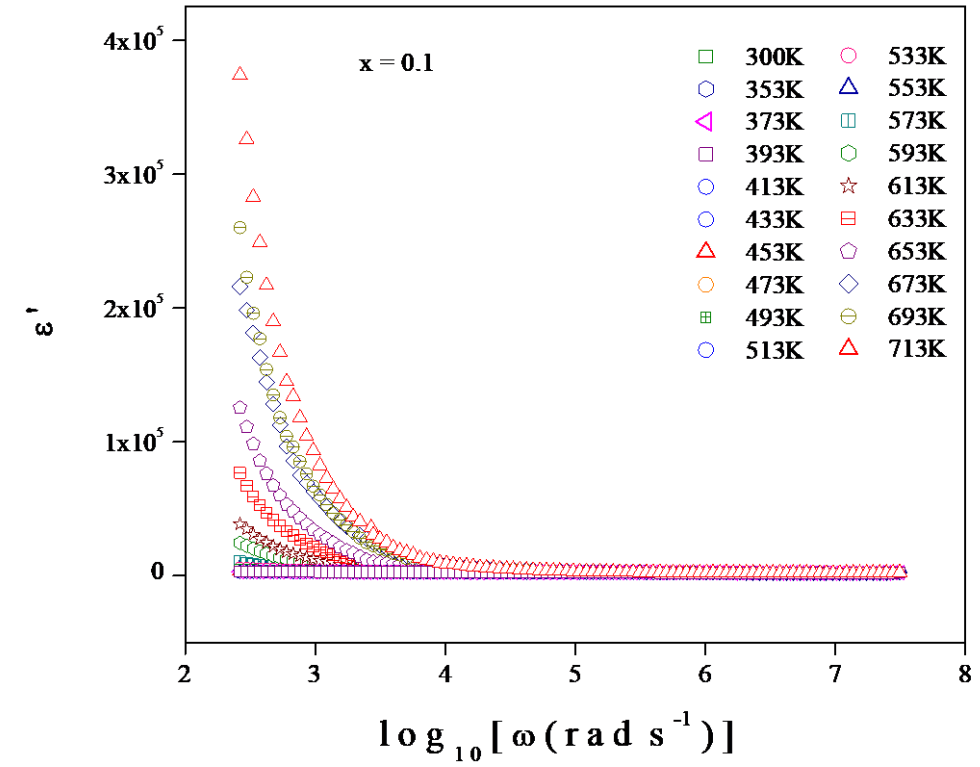

Fig. 3.14 (c) Spectra of dielectric constant ε/ for x = 0.1

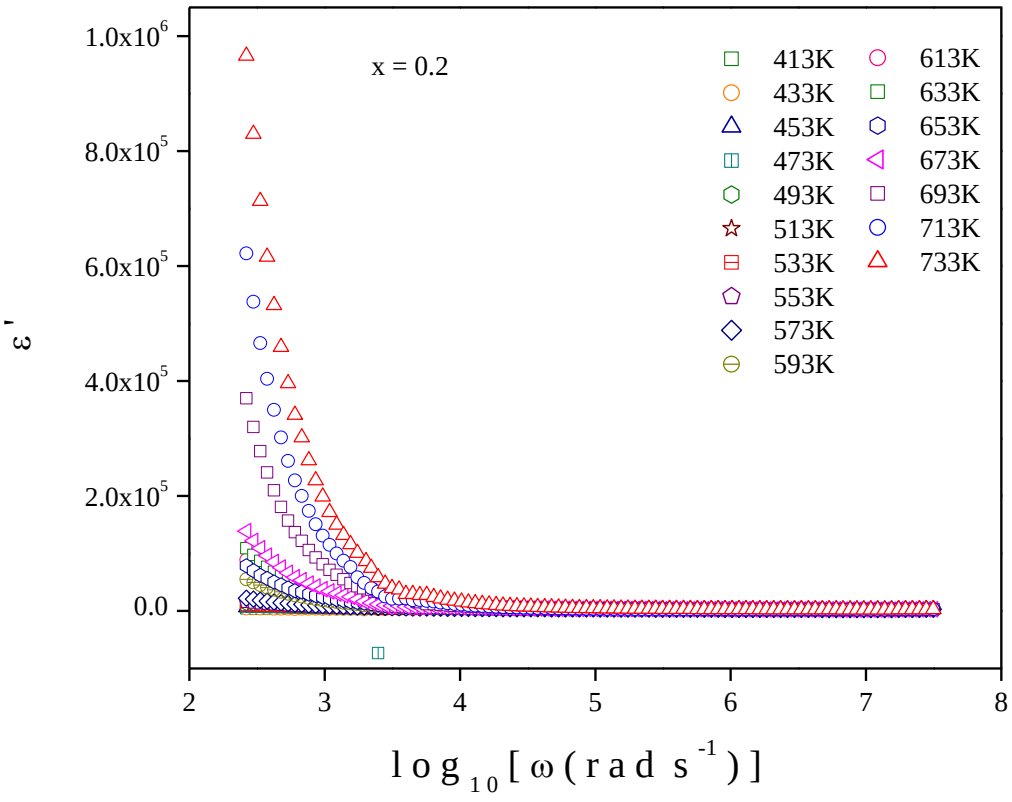

Fig. 3.14 (d) Spectra of dielectric constant ε/ for x = 0.2

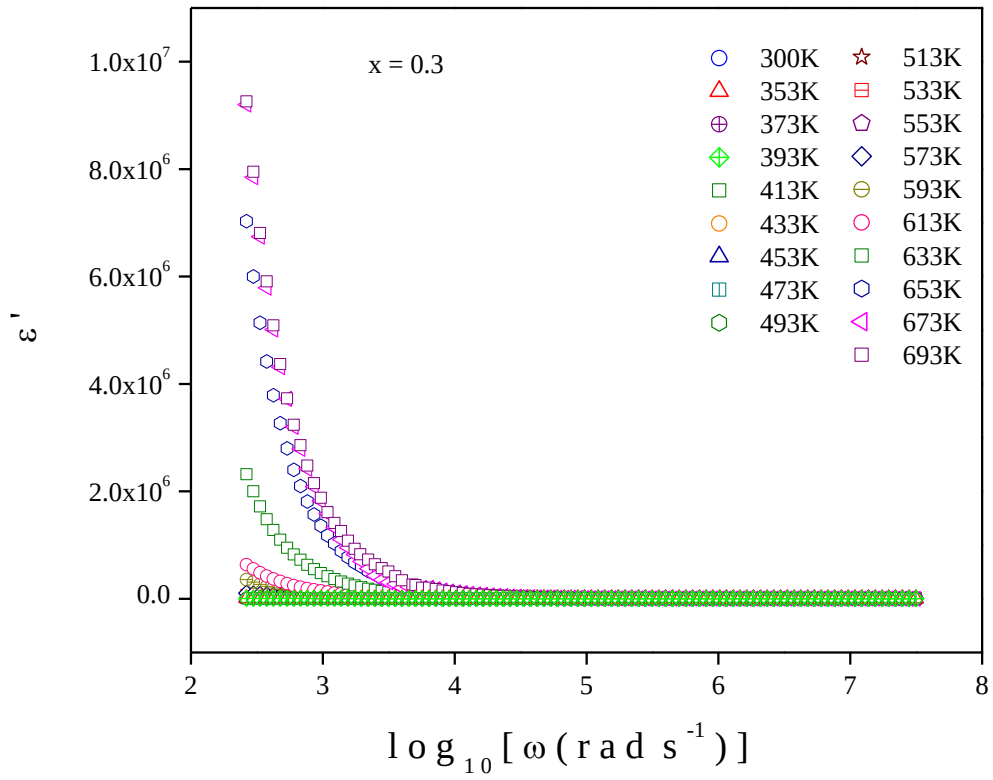

Fig. 3.14 (e) Spectra of dielectric constant ε/ for x = 0.3

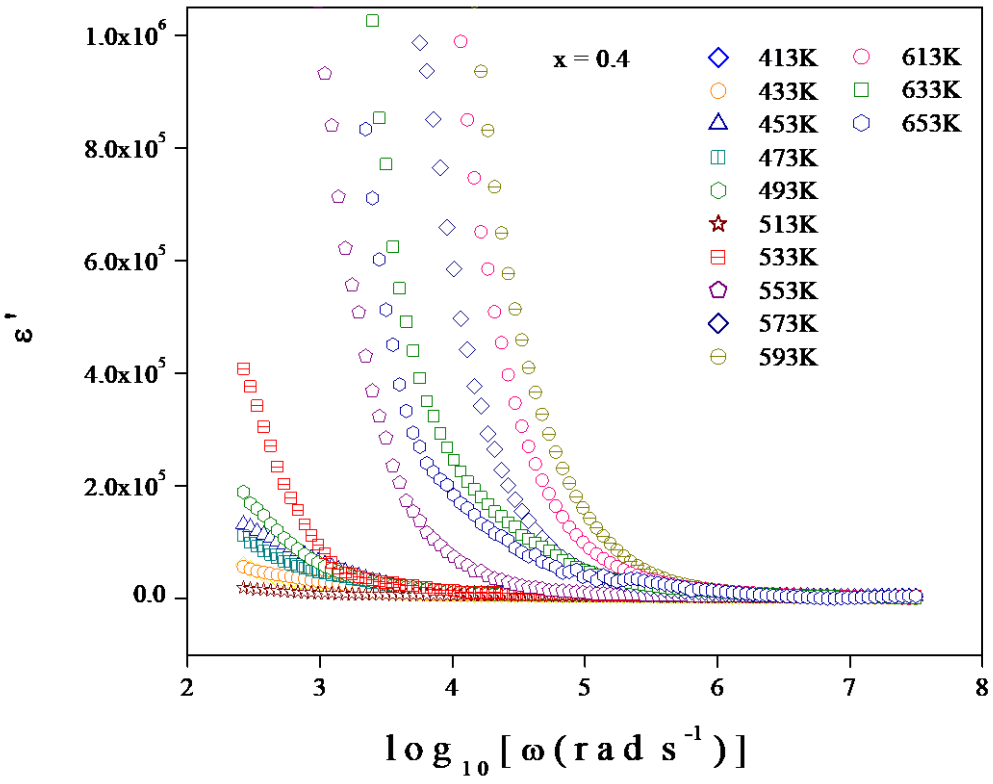

Fig. 3.14 (f) Spectra of dielectric constant ε/ for x = 0.4

Likewise, Fig. 3.15 (a) – (f) present the plots of ε'' of the sample against frequency for all x at various temperatures. Dielectric loss also shows the similar type of spectra as dielectric constant. ε'' is associated with the conversion of electrical energy into heat due to resistive losses, relaxation processes, or conduction. Dielectric loss can arise from: (a) Relaxation losses (delayed dipole reorientation with respect to the applied field), (b) Conduction losses (movement of free charge carriers or ions in the material) and (c) Interfacial losses (charge accumulation at interfaces due to conductivity mismatches). High ε'' means the material loses significant energy during polarization. Gradual decrease in the value of ε'' has been found with increasing x which indicates lowering of energy dissipation with the increase in AgI concentration.

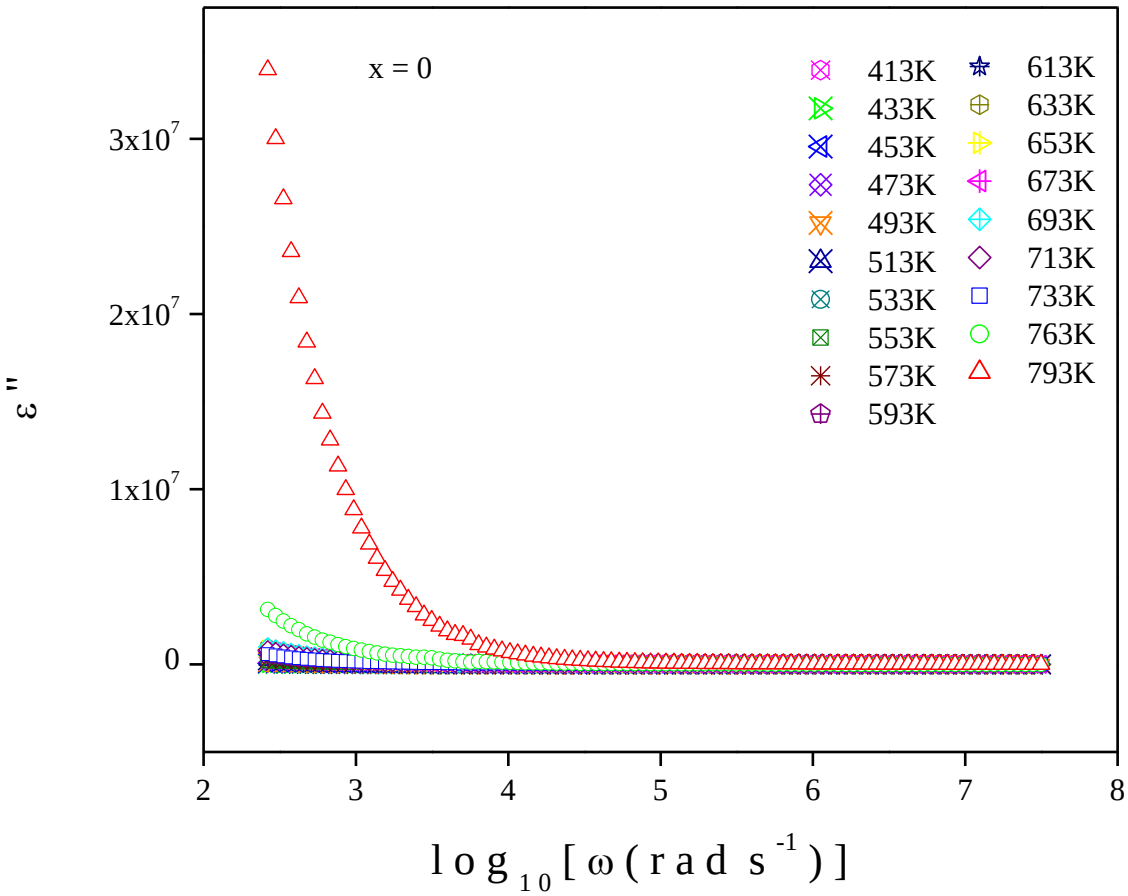

Fig. 3.15 (a) Spectra of dielectric loss ε'' for x = 0

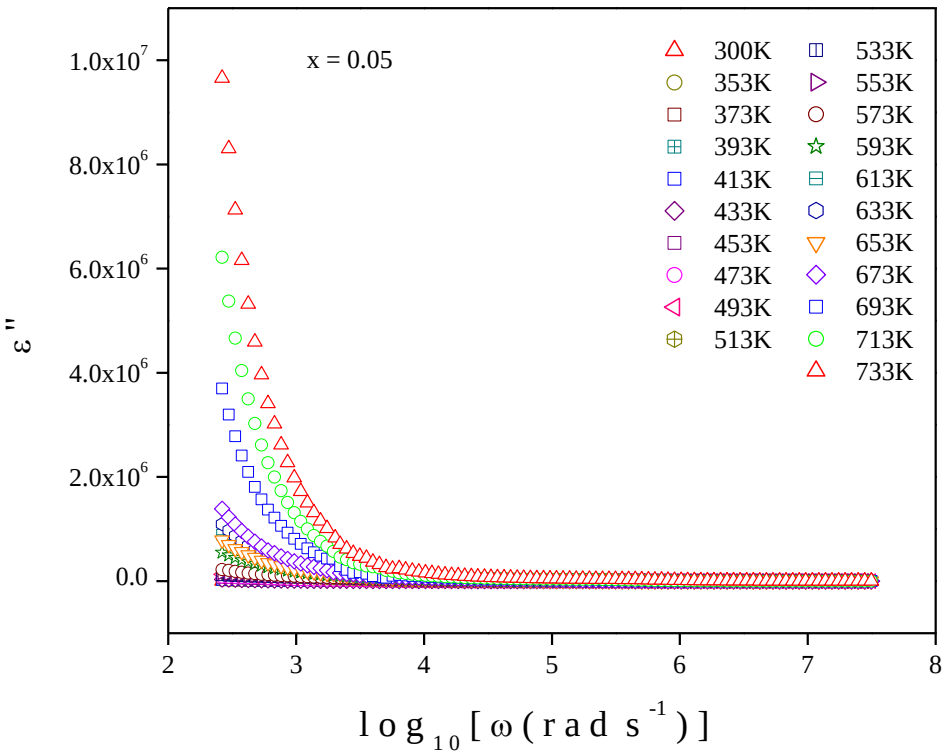

Fig. 3.15 (b) Spectra of dielectric loss $\varepsilon^{//}$ for x = 0.05

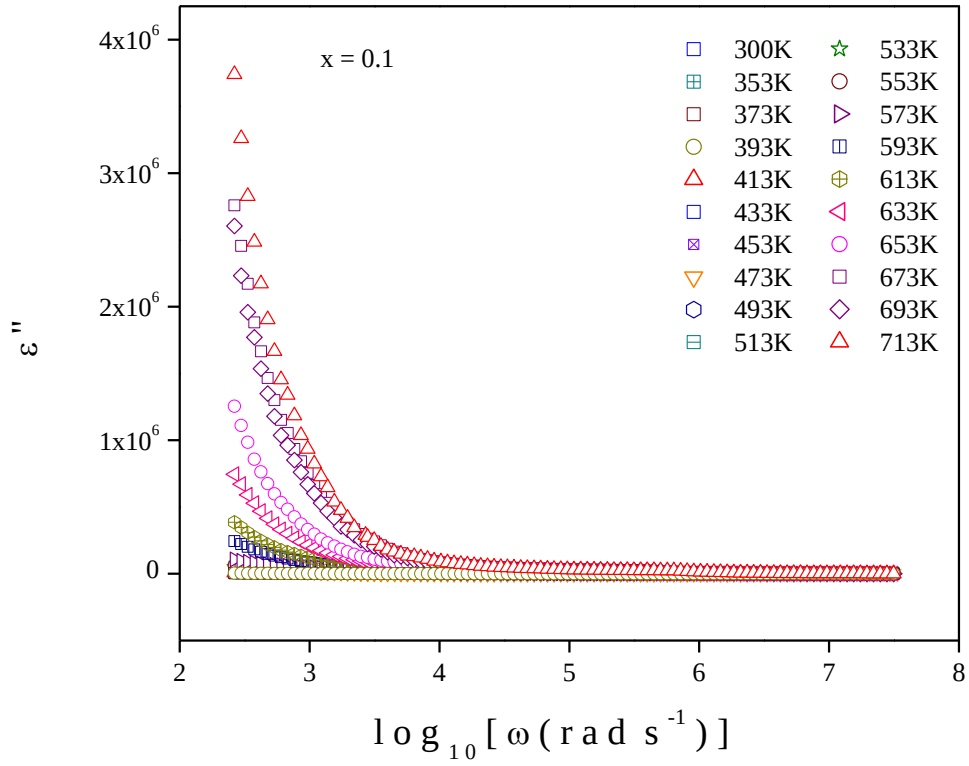

Fig. 3.15 (c) Spectra of dielectric loss $\varepsilon^{//}$ for x = 0.1

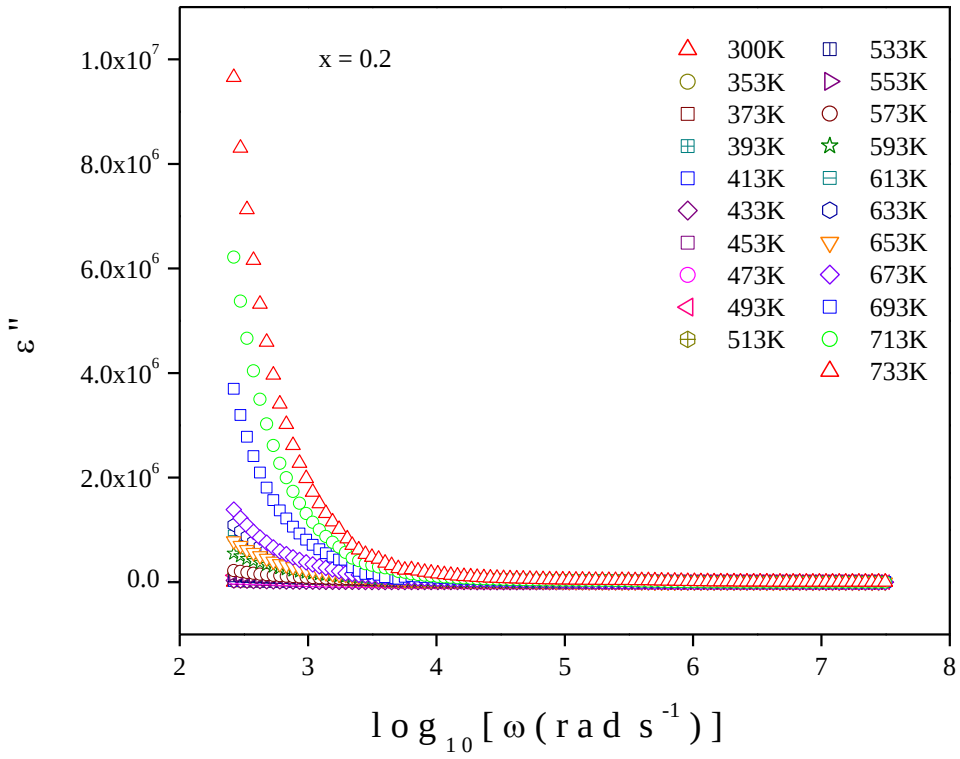

Fig. 3.15 (d) Spectra of dielectric loss ε'' for x = 0.2

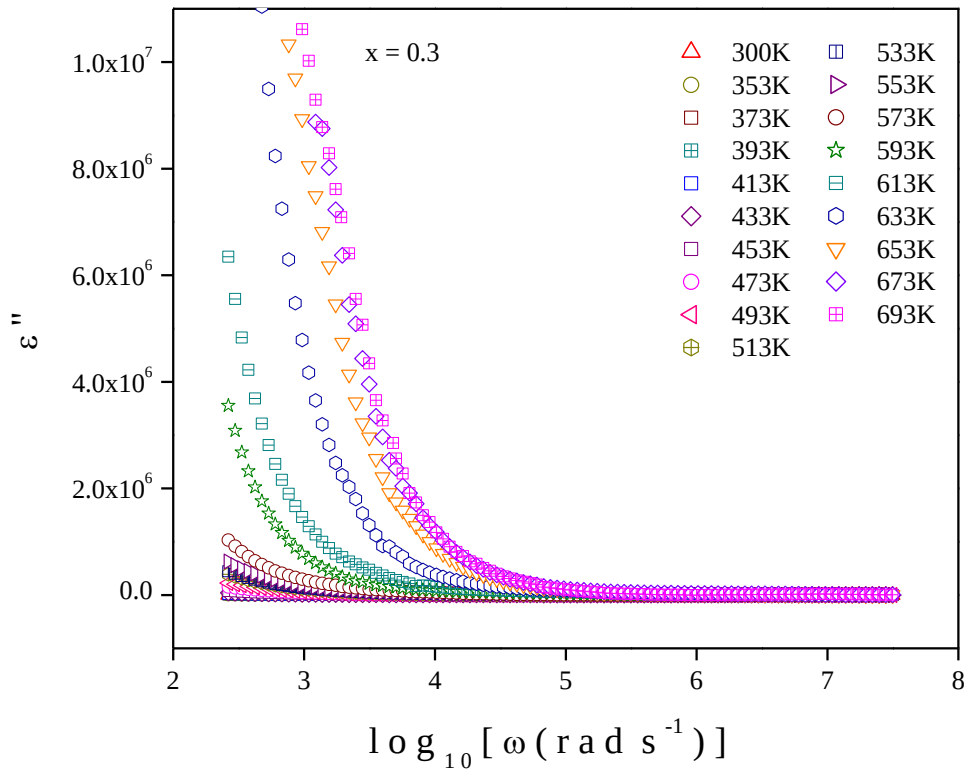

Fig. 3.15 (e) Spectra of dielectric loss ε'' for x = 0.3

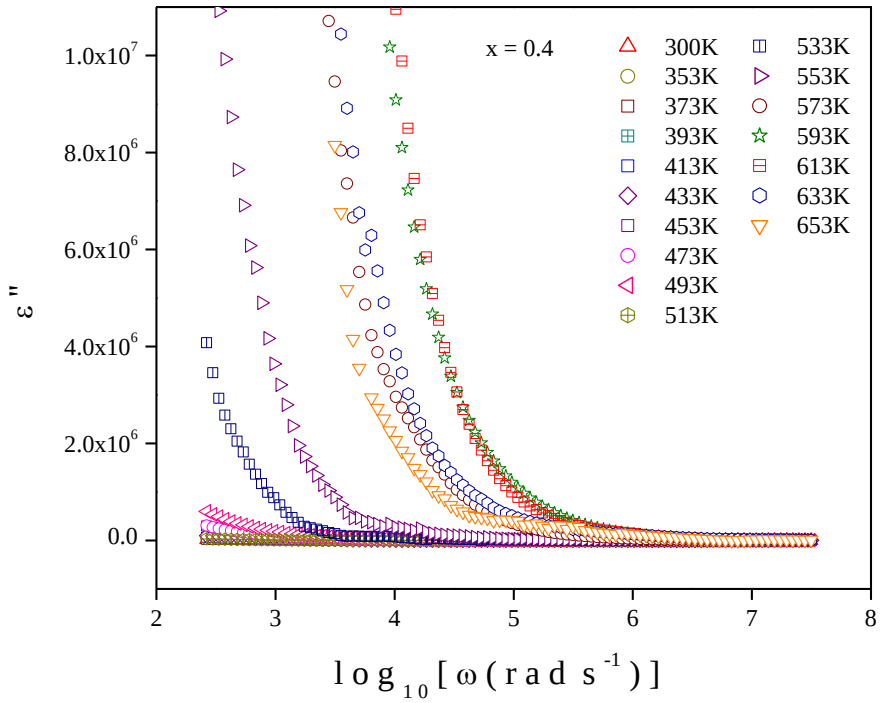

Fig. 3.15 (f) Spectra of dielectric loss $\varepsilon^{//}$ for x = 0.4

Both $\varepsilon^{/}$ and $\varepsilon^{//}$ increase with temperature rise, as shown in Figs. 3.14 and 3.15. This happens primarily because of the escalation in system's polarization effect due to a decrease in bond energies. It happens so as the intermolecular interactions weakens with rise in temperature. This also enhances orientational vibrations. It can also be noted that both $\varepsilon^{/}$ and $\varepsilon^{//}$ grow as x decreases in the current system's composition, as seen in Figs. 3.14 and 3.15. This is a clear indication of higher conductivity.

3.3.3.2 Study of electric modulus

The electric modulus provides a complementary way of analyzing dielectric properties by emphasizing the relaxation processes in materials rather than their polarization. It highlights the conduction or relaxation behavior of ions and dipoles within the material. At a glass's electrode-electrolyte interface, a complex electric modulus reduces the effects of polarization [67-68]. For the current glassy system, graphs of the real $M^{/}$ component of the electric modulus against frequency are displayed in Fig. 3.16 (a) - (f). In the low frequency zone, $M^{/}$ approaches zero at all the temperatures shown in Fig. 3.16. This is mostly due to the suppression of electrode polarization caused by the lack of restoring forces of charge carriers (polarons) [67-68]. However, dispersion in $M^{/}$ has been discovered at higher frequencies, and due to the electrical relaxation of polaron, $M^{/}$ exhibits a maximum value, which is $(M) = (\varepsilon)^{-1}$ [67-68].

Fig. 3.16 shows a progressive drop in M/ as the temperature rises, which may indicate that the system's conduction mechanism involves the mobility of polaron in a limited range.

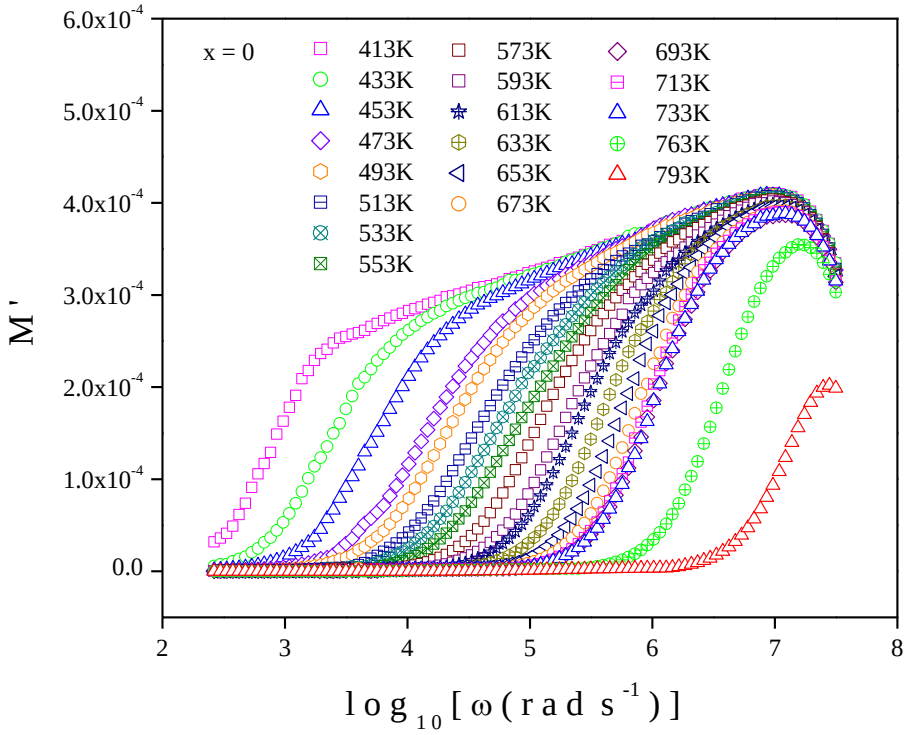

Fig. 3.16 (a) Spectra of M/ for x = 0

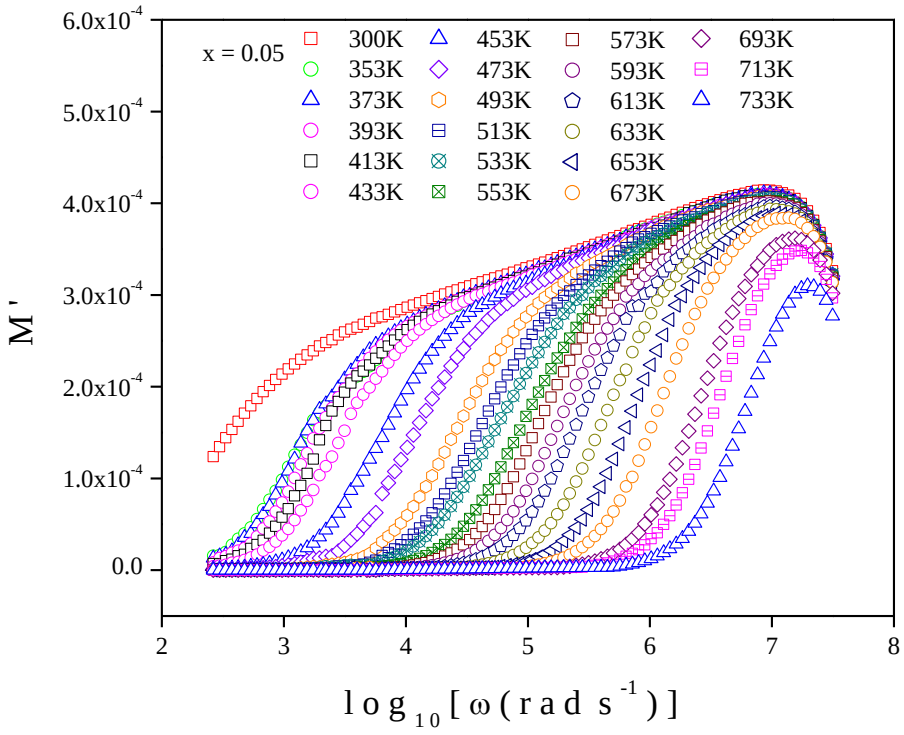

Fig. 3.16 (b) Spectra of M/ for x = 0.05

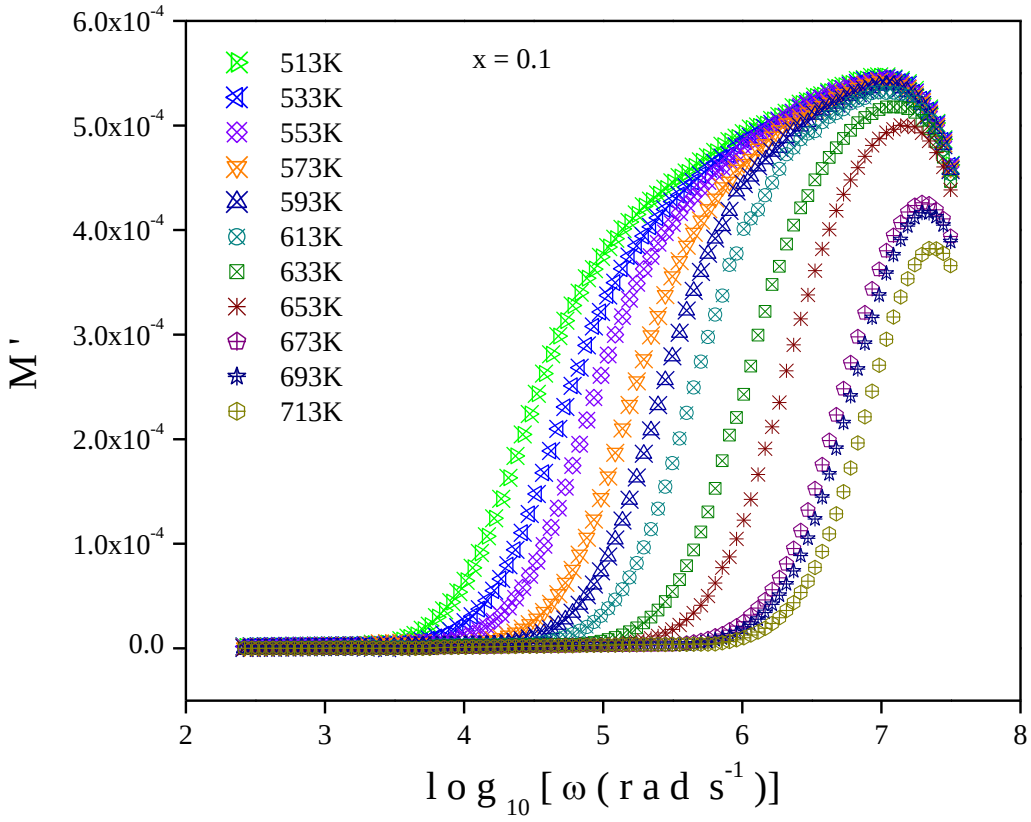

Fig. 3.16 (c) Spectra of M/ for x = 0.1

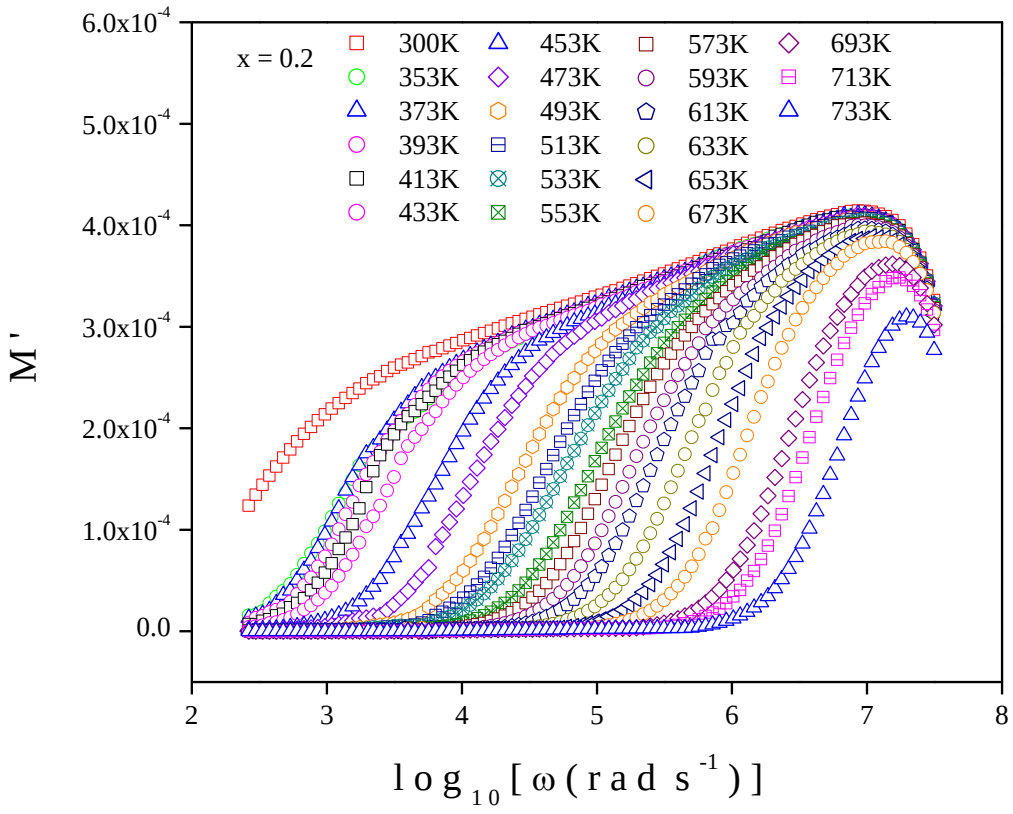

Fig. 3.16 (d) Spectra of M/ for x = 0.2

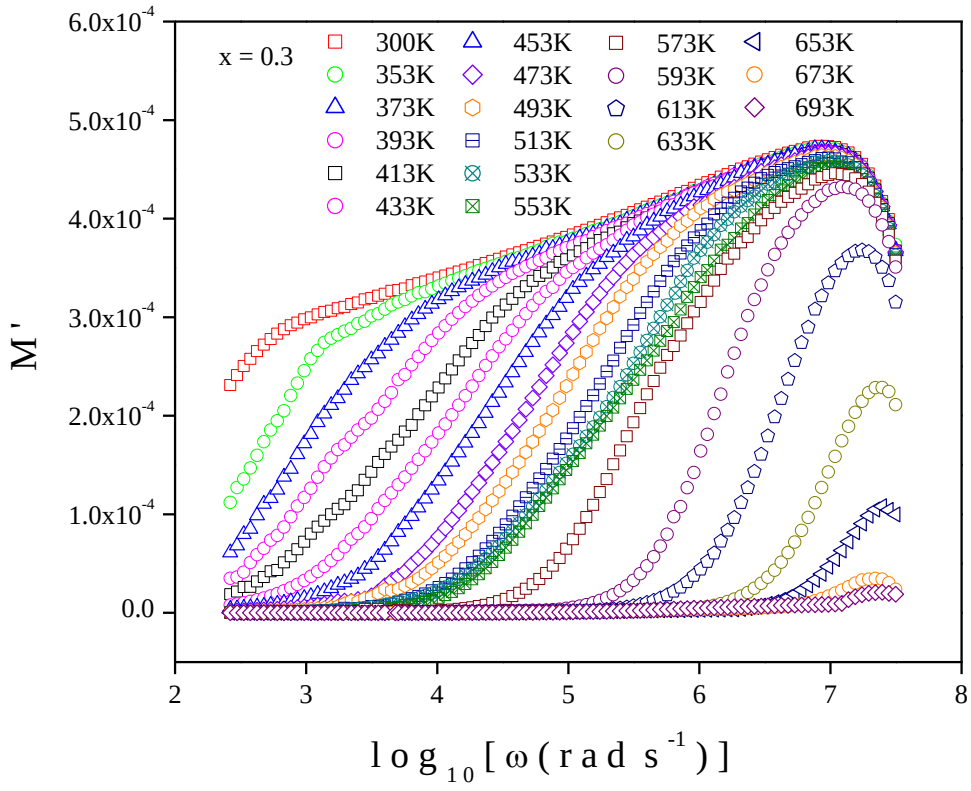

Fig. 3.16 (e) Spectra of M/ for x = 0.3

Graphs of the imaginary component of the electric modulus, $M^{//}$ against frequency are displayed in Fig. 3.17 (a) - (f). M″ corresponds to the loss of energy as heat or other irreversible processes during the polarization of the material. Characterization peaks in M″ occur at specific frequencies (ω_c) and are associated with relaxation times (τ_c) of dipoles or mobile ions in the material. The position and shift of these peaks with temperature or frequency can provide insight into ionic mobility and hopping mechanisms. As the temperature rises, as seen in Fig. 3.17, the $M^{//}$ peaks move towards higher frequencies, indicating a temperature-dependent relaxation process in the system. The flow of thermally activated charge carriers may shorten the duration of relaxation and increase its frequency. The conduction in these glasses below the peak relaxation frequency ω_c could be due to polaron hopping across long distances. The localized motion of charge carriers over small distances may be the cause of the conduction mechanism above ω_c [68-69]. The moving of the $M^{//}$ peak for an external force at elevated temperatures indicates that the system stabilizes rapidly.

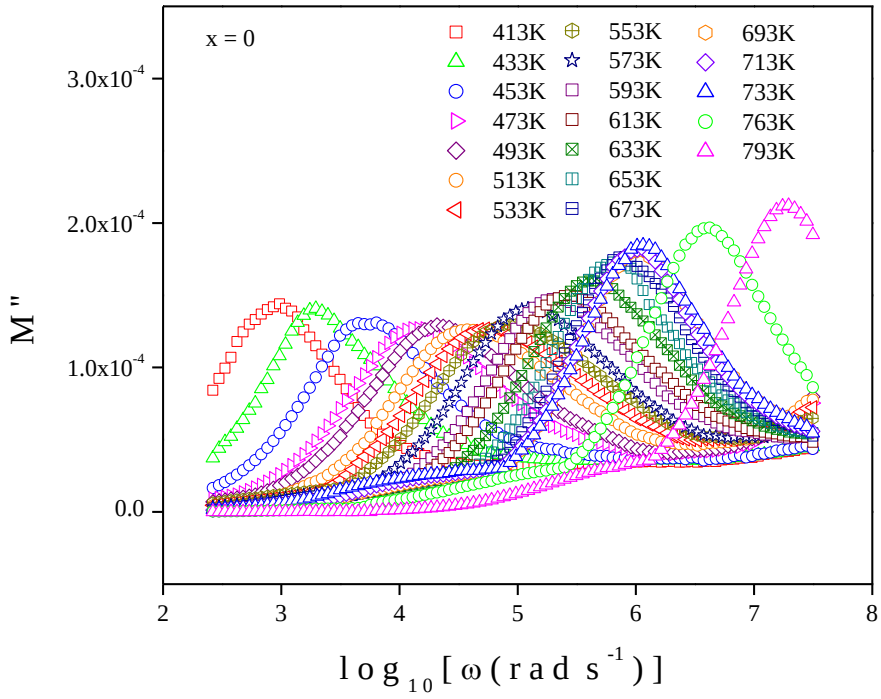

Fig. 3.17 (a) Spectra of $M^{//}$ for x = 0

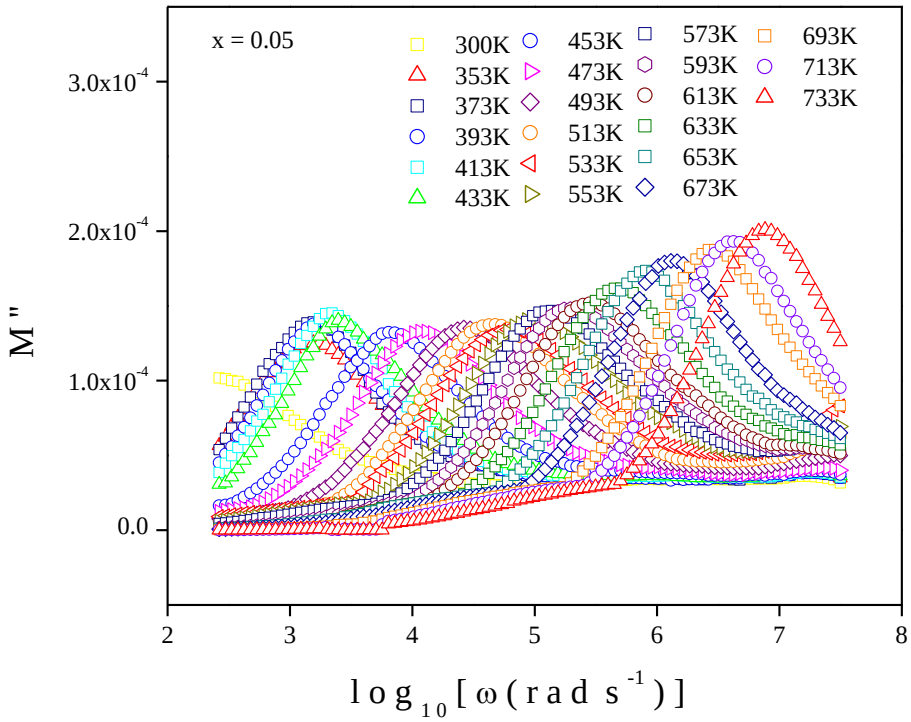

Fig. 3.17 (b) Spectra of $M^{//}$ for x = 0.05

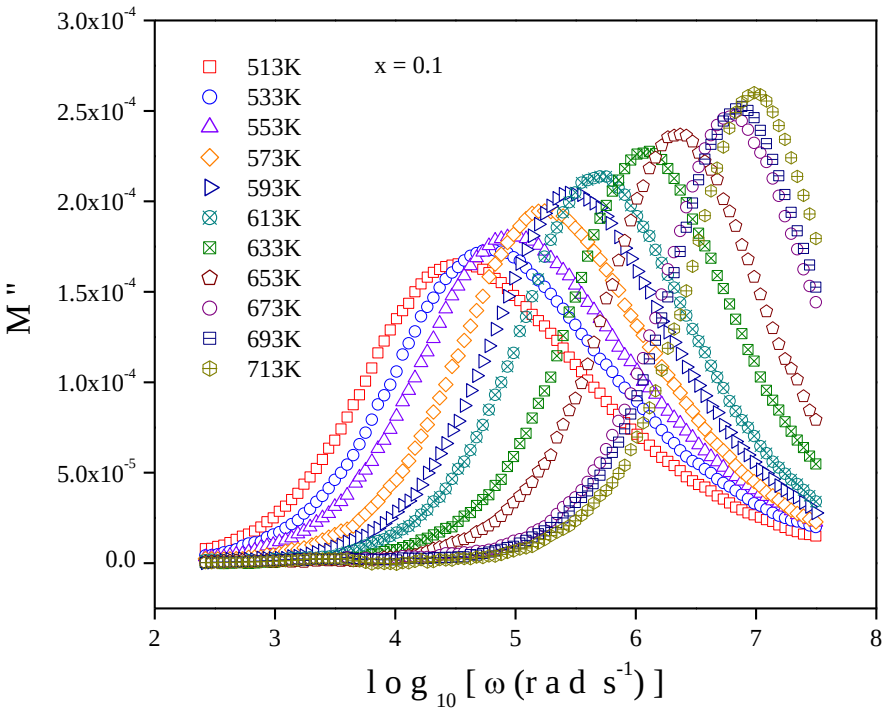

Fig. 3.17 (c) Spectra of $M^{//}$ for x = 0.1

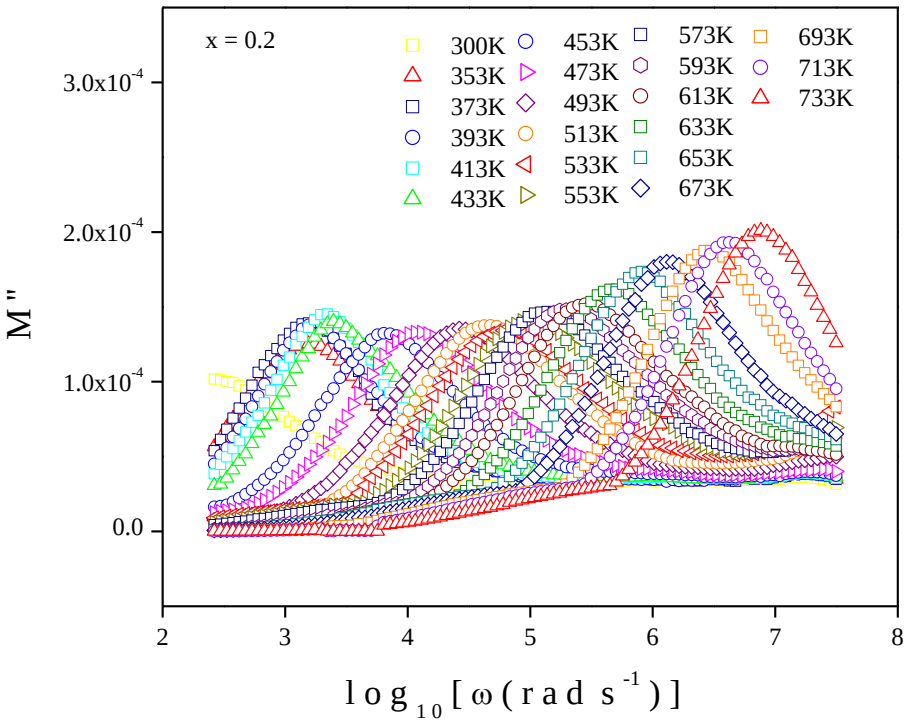

Fig. 3.17 (d) Spectra of $M^{//}$ for x = 0.2

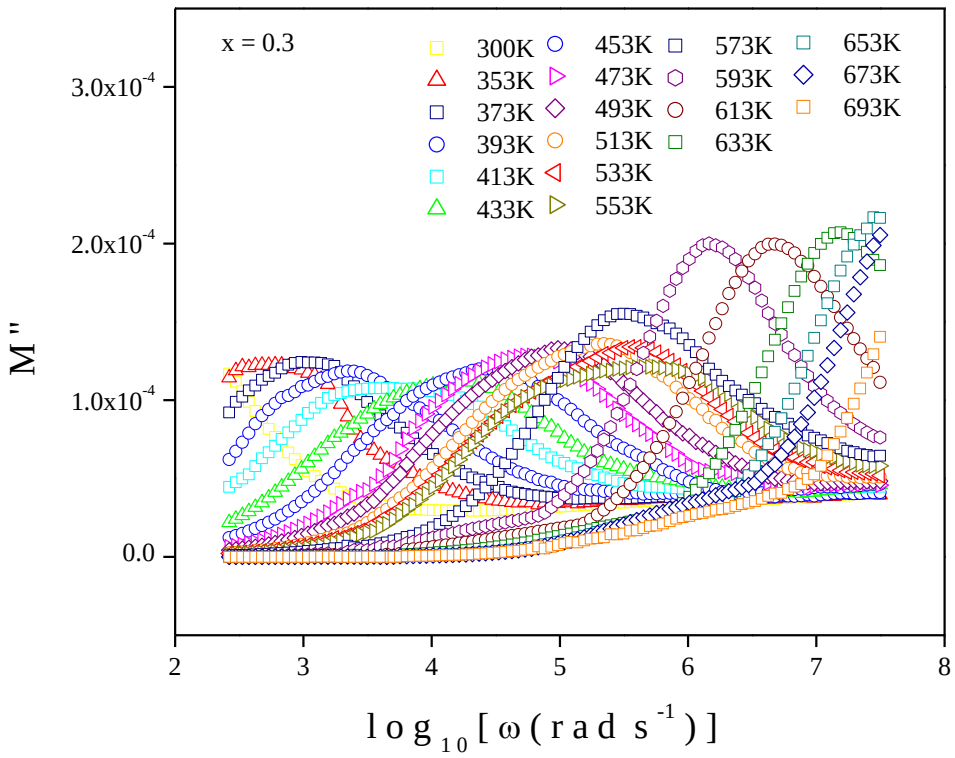

Fig. 3.17 (e) Spectra of $M^{//}$ for x = 0.3

M''_{max} position corresponds to the conductivity relaxation frequency ω_c which increases with temperature thus lowering the relaxation time τ_c. Conductivity relaxation frequency (ω_c) represents the transition from long-range order to short-range order mobility of charge carriers and conductivity relaxation time (τ_c) represents the characteristic time charge carriers (electrons, ions, or dipoles) take to reorient or return to equilibrium after an external electric field is removed. Average τ_c for all as-prepared samples have been plotted against composition in Fig. 3.18. The temperature dependence of the relaxation time often follows the Arrhenius equation given in Eq. 2.31 and thus activation energy due to relaxation time, E_τ has been estimated from the linear fits of the experimental data of τ_c. Both E_τ and τ_c decreases gradually with increasing AgI content after x = 0.2 as can be clearly seen from Fig. 3.18-3.19. A lower conductivity relaxation time indicates that ions can hop between available sites more efficiently which implies higher ionic conductivity.

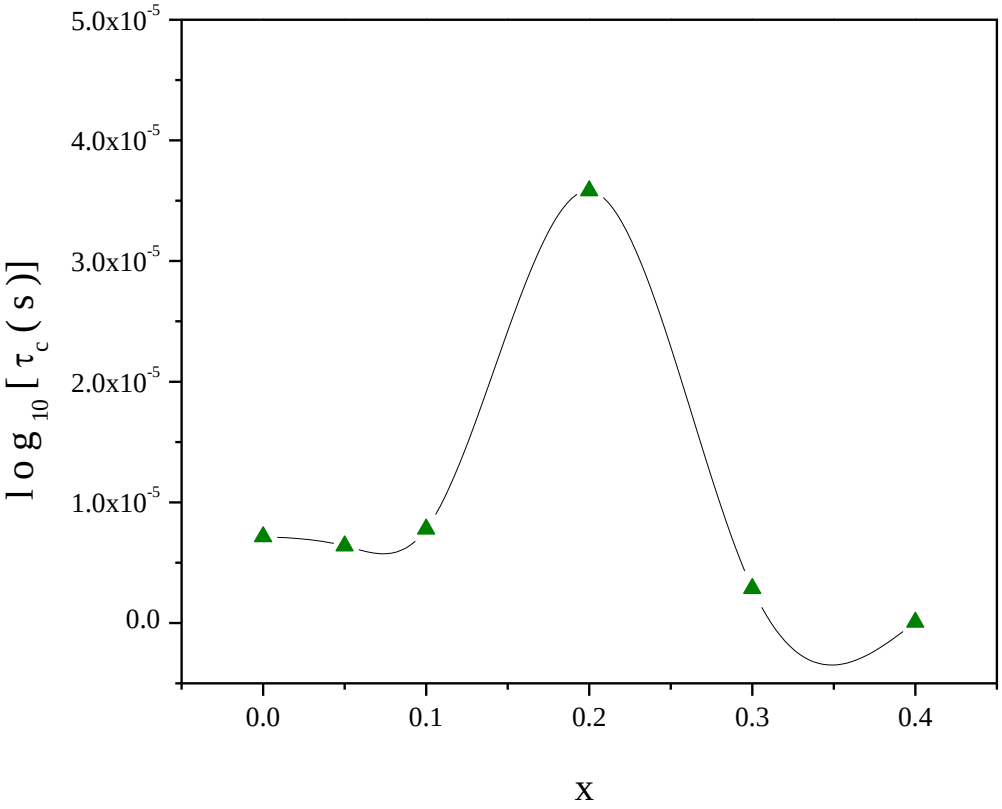

Fig. 3.18 Variation of average conductivity relaxation time (τ_c) with x

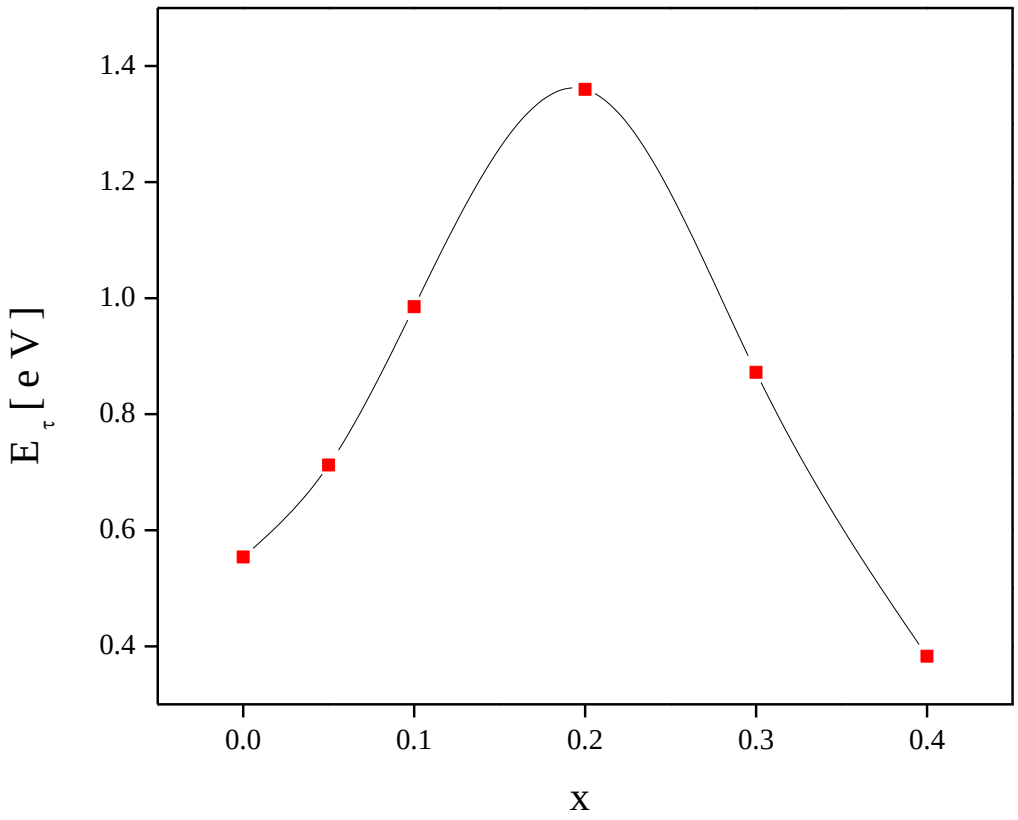

Fig. 3.19 Variation of activation energy (E_τ) with x

3.4 CONCLUSION

In this work, a novel AgI-doped glass nano-composite has been synthesized. As the dopant salt concentration rises, the samples take on a glassy appearance. PXRD and SEM examinations have been used to investigate the microstructure and the development of different nanophases in the glass-nanocomposites. The crystalline size of several nanophases has been determined and identified. The presence of different bands has been identified. As the dopant salt concentration rises, the samples' DC resistance gradually decreases and their electrical conductivity accordingly reaches its maximum. The mobility of the charge carriers is crucial to the conduction process, according to the carrier concentration study. It has been established that the current glassy systems' conductivity and dielectric characteristics are thermally triggered. As the amount of AgI increases, the dielectric constant steadily drops, indicating poor polarisation and increased conductivity. Higher conductivity phenomena are supported by a corresponding decrease in relaxation time and the accompanying activation energy. More bridging oxygen is anticipated to occur in the composition as the AgI content increases, and a strong covalent connection between Ag^{+} and O^{-2} may be the primary factor in silver ion transport over polaron hopping. It is possible to think of the double activation energy that corresponds to DC conductivity throughout a broad temperature range as the mark of the mixed conduction process in the current system. All ionic crystals of this type can be regarded as mixed conductors of varying degrees, regardless of whether they are primarily ion conducting or primarily electrically conducting. In solid-state electrochemical devices, this combined ionic–electronic conduction serves vital functional tasks.

References

[1] Kabi, S., & Ghosh, A. (2011). Dynamics of Ag+ ions and immobile salt effect in CdI2 doped silver phosphate glasses. Solid State Ionics, 187(1), 39-42.

[2] Shaw, A., & Ghosh, A. (2014). Dynamics of lithium ions in borotellurite mixed former glasses: correlation between the characteristic length scales of mobile ions and glass network structural units. The Journal of Chemical Physics, 141(16).

[3] Sanson, A., Rocca, F., Dalba, G., Fornasini, P., & Grisenti, R. (2007). Influence of temperature on the local structure around iodine in fast-ion-conducting AgI: Ag2MoO4 glasses. New Journal of Physics, 9(4), 88.

[4] Mustarelli, P., Tomasi, C., & Magistris, A. (2005). Fractal nanochannels as the basis of the ionic transport in AgI-based glasses. The Journal of Physical Chemistry B, 109(37), 17417-17421.

[5] Alrifai, B., Kassem, M., Toufaily, J., Bokova, M., & Bychkov, E. (2022). Pb2+ potentiometric chemical sensors based on lead and silver doped thioaresenate glasses. Solid State Sciences, 131, 106955.

[6] Shaw, A., & Ghosh, A. (2013). Correlation of microscopic length scales of ion dynamics with network structure in lithium-iodide–doped lithium metaphosphate glasses. Europhysics Letters, 100(6), 66003.

[7] El-Damrawi, G., Hassan, A. K., & Meikhail, M. S. (1996). Characterisation Studies of Quaternary Superionic AgX-Ag2O-MoO3-P2O5 Glasses (X= Cl, Br). Physics and chemistry of glasses, 37(3), 101-105.

[8] Barczyński, R. J., Król, P., & Murawski, L. (2010). Ac and dc conductivities in V2O5–P2O5 glasses containing alkaline ions. Journal of non-crystalline solids, 356(37-40), 1965-1967.

[9] Barde, R. V., & Waghuley, S. A. (2013). Preparation and electrical conductivity of novel vanadate borate glass system containing graphene oxide. Journal of non-crystalline solids, 376, 117-125.

[10] Paul, D. R. (2007). Handbook of Electronic and Photonic materials.

[11] Kumari, V., Kaswan, A., Patidar, D., Sharma, K., & Saxena, N. S. (2016). Electrical conduction mechanism in GeSeSb chalcogenide glasses. Bulletin of Materials Science, 39, 255-262.

[12] Fernandes, B. J., Ramesh, K., & Udayashankar, N. K. (2019). Crystallization kinetics of Si20Te80− xBix (0≤ x≤ 3) chalcogenide glasses. Materials Science and Engineering:

B, 246, 34-41.

[13] Pal, S. K., Kumar, A., & Mehta, N. (2019). Signature of rigidity percolation effect in dielectric behavior of germanium containing multi-component chalcogenide glasses (ChGs). Ceramics International, 45(13), 16279-16287.

[14] Ravagli, A., Naftaly, M., Craig, C., Weatherby, E., & Hewak, D. W. (2017). Dielectric and structural characterisation of chalcogenide glasses via terahertz time-domain spectroscopy. Optical Materials, 69, 339-343.

[15] Zhu, E., Liu, Y., Sun, X., Yin, G., Jiao, Q., Dai, S., & Lin, C. (2019). Correlation between thermo-mechanical properties and network structure in GexS100–x chalcogenide glasses. Journal of Non-Crystalline Solids: X, 1, 100015.

[16] Ariane K, Tamayo A, Chorfa A, Rubio F, Rubio J (2022). J Span Ceram Glass Soc 61:146.

[17] Alemi, A. A., Sedghi, H., Mirmohseni, A. R., & Golsanamlu, V. (2006). Synthesis and characterization of cadmium doped lead-borate glasses. Bulletin of Materials Science, 29, 55-58.

[18] Bhattacharya, S., & Ghosh, A. (2006). Electrical properties of ion conducting molybdate glasses. Journal of applied physics, 100(11).

[19] Karmakar, B., Rademann, K., & Stepanov, A. (Eds.). (2016). Glass nanocomposites: synthesis, properties and applications. William Andrew.

[20] Shukla AP, Shukla JK (2018. J Sci Adv Mater Devices 3:452.

[21] Venkatesan, A., Chandar, N. K., Arjunan, S., Marimuthu, K. N., Kumar, R. M., & Jayavel, R. (2013). Structural, morphological and optical properties of highly monodispersed PEG capped V2O5 nanoparticles synthesized through a non-aqueous route. Materials Letters, 91, 228-231.

[22] Shafeeq, K. M., Athira, V. P., Kishor, C. R., & Aneesh, P. M. (2020). Structural and optical properties of V 2 O 5 nanostructures grown by thermal decomposition technique. Applied Physics A, 126, 1-6.

[23] Youn, S., Jeong, S., & Kim, D. H. (2014). Effect of oxidation states of vanadium precursor solution in V2O5/TiO2 catalysts for low temperature NH3 selective catalytic reduction. Catalysis Today, 232, 185-191.

[24] Cheng, B., Xiao, Y., Wu, G., & Zhang, L. (2004). The vibrational properties of one-dimensional ZnO: Ce nanostructures. Applied physics letters, 84(3), 416-418.

[25] Kaneti, Y. V., Yue, J., Jiang, X., & Yu, A. (2013). Controllable synthesis of ZnO nanoflakes

with exposed (1010) for enhanced gas sensing performance. The Journal of Physical Chemistry C, 117(25), 13153-13162.

[26] Bhattacharya, S., & Ghosh, A. (2006). Formation of ZnO nanoparticles and α-AgI nanocrystals embedded in superionic glass nanocomposites. Applied physics letters, 88(13).

[27] Zak, A. K. (2012). Fabrication and characterization of zinc oxide and lead zirconate titanate nanostructures. University of Malaya (Malaysia).

[28] Lanje, A. S., Ningthoujam, R. S., Sharma, S. J., & Pode, R. B. (2011). Luminescence and electrical resistivity properties of cadmium oxide nanoparticles.

[29] S. Bhattacharya, R. Kundu, A. S. Das, D. Roy, IEEE CALCON, ISBN: 97893833303830 p-161 (2014).

[30] Jain, H., Issa, A., Anavekar, R. V., Böhmer, R., Kanert, O., & Küchler, R. (2009). Ionic-to-electronic conductivity transition in an oxide glass doped with gold. Applied Physics Letters, 95(14).

[31] N. F. Mott, Philos. Mag. 19, 853(1969).

[32] Carcia, P. F., & McCarron Iii, E. M. (1987). Synthesis and properties of thin film polymorphs of molybdenum trioxide. Thin Solid Films, 155(1), 53-63.

[33] Ghosh, A. (1990). Electrical transport properties of molybdenum tellurite glassy semiconductors. Philosophical Magazine B, 61(1), 87-96.

[34] Das, A. S., Roy, D., Mishra, G. C., Bar, A. K., & Bhattacharya, S. Development of nano-CdO doped glassy semiconductor.

[35] Greaves, G. N. (1973). Small polaron conduction in V2O5□ P2O5 glasses. Journal of Non-Crystalline Solids, 11(5), 427-446.

[36] Almond DP, West AR (1983) Mobile ion concentrations in solid electrolytes from an analysis of a.c. conductivity. Solid State Ion- ics 9–10:277.

[37] Bhattacharya, S. (2020). Metal oxide glass nanocomposites. In Metal Oxide Glass Nanocomposites (pp. 27-35). Elsevier.

[38] Almond, D. P., Duncan, G. K., & West, A. R. (1983). The determination of hopping rates and carrier concentrations in ionic conductors by a new analysis of ac conductivity. Solid State Ionics, 8(2), 159-164.

[39] Roling, B., Happe, A., Funke, K., & Ingram, M. D. (1997). Carrier concentrations and relaxation spectroscopy: new information from scaling properties of conductivity

spectra in ionically conducting glasses. Physical review letters, 78(11), 2160.

[40] Jonscher, A. K. (1999). Dielectric relaxation in solids. Journal of Physics D: Applied Physics, 32(14), R57.

[41] Hona, R. K., Guinn, M., Phuyal, U. S., Sanchez, S., & Dhaliwal, G. S. (2023). Alkali ionic conductivity in inorganic glassy electrolytes. Journal of Materials Science and Chemical Engineering, 11(07).

[42] Bosi, M., Fischer, J., & Maass, P. (2021). Network-forming units, energy landscapes, and conductivity activation energies in alkali borophosphate glasses: analytical approaches. The Journal of Physical Chemistry C, 125(11), 6260-6268.

[43] Martin, S.W. (1991). pp. 337-400. Springer.

[44] Schulz, A., Lunkenheimer, P., & Loidl, A. (2021). Lithium-salt-based deep eutectic solvents: Importance of glass formation and rotation-translation coupling for the ionic charge transport. The Journal of Chemical Physics, 155(4).

[45] Pietrzak, T. K., Wasiucionek, M., & Garbarczyk, J. E. (2021). Towards higher electric conductivity and wider phase stability range via nanostructured glass-ceramics processing. Nanomaterials, 11(5), 1321.

[46] Kurnosov, A., & Lubchenko, V. (2025). The mechanism of electrical conduction in glassy semiconductors. Proceedings of the National Academy of Sciences, 122(10), e2414650122.

[47] Boolchand, P., Georgiev, D. G., & Goodman, B. (2001). Discovery of the intermediate phase in chalcogenide glasses. Journal of Optoelectronics and Advanced Materials, 3(3), 703-720.

[48] Mott, N. F. (1968). Conduction in glasses containing transition metal ions. Journal of Non-Crystalline Solids, 1(1), 1-17.

[49] Murugaraj, R. (2007). Ac conductivity and its scaling behavior in borate and bismuthate glasses. Journal of materials science, 42(24), 10065-10073.

[50] Ghosh, A. (1990). Transport properties of vanadium germanate glassy semiconductors. Physical Review B, 42(9), 5665.

[51] Agrinskaya, N. V., Kozub, V. I., & Poloskin, D. S. (2010). Mixed conduction in doped semiconductor structures related to quasi-metallic conduction in the impurity band. Semiconductors, 44, 472-477.

[52] Angell, C. A. (1992). Mobile ions in amorphous solids. Annual review of physical

chemistry, 43(1), 693-717.

[53] Tatsumisago, M., Shinkuma, Y., Saito, T., & Minami, T. (1992). Formation of frozen α-AgI in superionic glass matrices at ambient temperature by rapid quenching. Solid State Ionics, 50(3-4), 273-279.

[54] Minami, T. (1985). Fast ion conducting glasses. Journal of Non-Crystalline Solids, 73(1-3), 273-284.

[55] Moynihan, C. T. (1973). Decay function for the electric field relaxation in vitreous ionic conductors. Phys. Chem. Glasses, 14, 122-125.

[56] Macedo, P. B., CT, M., & Bose, R. (1972). The role of ionic diffusion in polarisation in vitreous ionic conductors.

[57] Bhattacharya, S., & Ghosh, A. (2005). Relaxation of silver ions in fast ion conducting molybdate glasses. Solid State Ionics, 176(13-14), 1243-1247.

[58] Svare, I., Martin, S. W., & Borsa, F. (2000). Stretched exponentials with T-dependent exponents from fixed distributions of energy barriers for relaxation times in fast-ion conductors. Physical Review B, 61(1), 228.

[59] Sahoo, P. S., Panigrahi, A., Patri, S. K., & Choudhary, R. N. P. (2010). Impedance and modulus spectroscopy studies of Ba4SrSmTi3V7O30 ceramics. Materials Science-Poland, 28(4), 763.

[60] Bhattacharya, S., & Ghosh, A. (2005). Transport properties of AgI doped silver molybdate superionic glass-nanocomposites. Journal of Physics: Condensed Matter, 17(37), 5655.

[61] Mustarelli, P., Tomasi, C., Quartarone, E., Magistris, A., Cutroni, M., & Mandanici, A. (1998). Structure and cation dynamics in the system A g I: A g 2 MoO 4: A 109 Ag NMR study. Physical Review B, 58(14), 9054.

[62] Kamitsos, E. I., Kapoutsis, J. A., Chryssikos, G. D., Hutchinson, J. M., Pappin, A. J., Ingram, M. D., & Duffy, J. A. (1995). Infrared study of AgI containing superionic glasses. Physics and chemistry of glasses, 36(3), 141-149.

[63] Suzuki, T., Horibuchi, K., & Ohishi, Y. (2005). Structural and optical properties of ZnO–Al2O3–SiO2 system glass–ceramics containing Ni2+-doped nanocrystals. Journal of non-crystalline solids, 351(27-29), 2304-2309.

[64] Ma, J. G., Liu, Y. C., Xu, C. S., Liu, Y. X., Shao, C. L., Xu, H. Y., ... & Fan, X. W. (2005). Preparation and characterization of ZnO particles embedded in SiO2 matrix by reactive magnetron sputtering. Journal of applied physics, 97(10).

[65] Xiong, H. M., Zhao, X., & Chen, J. S. (2001). New polymer− inorganic nanocomposites: PEO− ZnO and PEO− ZnO− LiClO4 films. The Journal of Physical Chemistry B, 105(42), 10169-10174.

[66] Ahmad-Bitar, R., & Arafah, D. E. (1998). Processing effects on the structure of CdTe, CdS and SnO2 thin films. Solar energy materials and solar cells, 51(1), 83-93.

[67] Karmakar, B., Rademann, K., & Stepanov, A. (Eds.). (2016). Glass nanocomposites: synthesis, properties and applications. William Andrew.

[68] Bhattacharya, S., & Ghosh, A. (2008). Relaxation dynamics in superionic glass nanocomposites. Journal of the American Ceramic Society, 91(3), 753-759.

[69] Ojha, S., Roy, M., Chamuah, A., Bhattacharya, K., & Bhattacharya, S. (2020). AC conductivity and dielectric behavior of Cu-S-Te chalcogenide glassy system. Materials Letters, 258, 126792.

Chapter 4

Study of Mixed Former Effects on Electrical Transport Phenomena of AgI Doped $CdO - V_2O_5 - P_2O_5 - ZnO$ System

Outline

4.1 INTRODUCTION

According to the literature review, the inclusion of mixed formers [1-2] improves a glassy system's electrical conductivity. However, very little research has been done on how mixed formers affect silver ion mobility. It was exposed in our previously manufactured sample that silver ion conduction predominates in systems with high AgI concentrations. However, since P_2O_5 is the system's primary network former, the impact of mixed formers has not been investigated. Since V_2O_5 is present in very low concentrations, it is believed to behave as a network modifier solely, even if it may also act as a network former. On background of this, in this chapter we have re-synthesized the previously prepared sample but with a major alteration in the concentration of both V_2O_5 and P_2O_5 such that V_2O_5 may also take part in the formation of the glassy structure rather than behaving as a modifier only.

Studies have been conducted on the same system but with different ratios of the network formers, V_2O_5 and P_2O_5. The empirical formula of the system has been considered as 0.2 AgI – 0.8 (0.1CdO - y V_2O_5 - z P_2O_5 - 0.2 ZnO) and measurements have been done for different values of y and z. This chapter aims to discuss about the effect of the modifier oxides on the electrical transport of the silver ion conducting system. In view of this, values of y and z have been fixed in such a way that the ratio of the modifiers i.e. V_2O_5: P_2O_5 increase in a gradual manner. They are taken as 0.1 and 0.6, 0.2 and 0.5, 0.3 and 0.4 respectively. Thus, the systems formed, are having the compositions 0.2 AgI – 0.8 {0.1CdO – 0.1 V_2O_5 – 0.6 P_2O_5 – 0.2 ZnO}, 0.2 AgI – 0.8 {0.1CdO – 0.2 V_2O_5 – 0.5 P_2O_5 – 0.2 ZnO} and 0.2 AgI – 0.8 {0.1CdO – 0.3 V_2O_5 – 0.4 P_2O_5 – 0.2 ZnO} and the ratio of y and z is set to 0.17, 0.4, and 0.75 respectively. discusses the impact of mixed formers on the previously discussed AgI doped CdO - V_2O_5 – P_2O_5 – ZnO glassy system.

4.2 PREPARATION OF GLASSY SYSTEMS

A glassy system consisting of 0.2 AgI – 0.8 (0.1 CdO - y V_2O_5 - z P_2O_5 - 0.2 ZnO) has been prepared with different values of y and z using the traditional melt quenching method [3-7]. The samples were produced from enormously pure (Aldrich 99.9%) reagent grade chemicals for the various values of x, where x = y: z. The values of x have been calculated as 0.17, 0.4, and 0.75. Using an electromechanical analytical balance (Dhona 200D), all the required compounds were precisely weighed in agreement with their evaluated stoichiometric proportion, as discussed in section 2.3. The materials were then appropriately blended and

mixed in a thoroughly cleaned and rinsed mortar to form the powder. Once the powder had been prepared, it was placed within an crucible made up of alumina and kept inside an electric furnace. After that, the mixtures were melted in an electric furnace at temperatures that varied based on their composition, from 750°C to 1000°C. The melts were quenched between two metal plates after equilibrating for 30 minutes. This process produced glassy composites that were partially transparent and had a thickness of less than one millimeter.

Two-probe methods have been opted to conduct the electrical conductivity research on the samples. The samples were placed inside the sample holder which is connected with two spring-loaded, cleaned, and polished copper electrodes (manufactured by Joy-Crucible). The Hioki LCR tester (Model No. 3532–50) was then used to conduct a number of complex impedance measurements in the frequency range of 42 Hz to 5 MHz. The temperature range has been kept from 300 – 753K for the measurements and the observations have been recorded at regular intervals of 20ºC.

4.3 RESULTS AND ANALYSIS

4.3.1 Structural Characterization

The several methods of structural characterizations [8] that have been carried out on the as-prepared samples include determination of Density (ρ) and Molar Volume (V_M), X-ray Diffraction (XRD) and Fourier Transform Infrared (FT-IR) Spectroscopy.

4.3.1.1 Measurement of Density and Molar Volume

Following the Archimedes principle, explained in section 2.4.1, the density and molar volume of the as-prepared samples are measured. The calculation has been done as per Eq. 2.1 and 2.2. Acetone with ρ_b = 0.7845 gm/cm^3 has been used as the buoyant liquid. The weights of the as prepared samples were recorded on a mechanical balance (Dhona, Model: 200D) with precession of 0.0001 gm. Every measurement was performed at room temperature.

The calculated ρ and V_M values of this glassy system are given in Table 4.1. Fig. 4.1 displays the change in density and molar volume with the increase in the ratio of the mixed formers in the system.

Composition (x)	Density, ρ (g/ cc) (± 0.1)	Molar volume, V_M (cc/ mol) (± 0.1)
0.17	3.601	42.475
0.4	3.232	48.294
0.75	3.419	46.591

Table 4.1: ρ and V_M of the as-prepared systems for different values of x

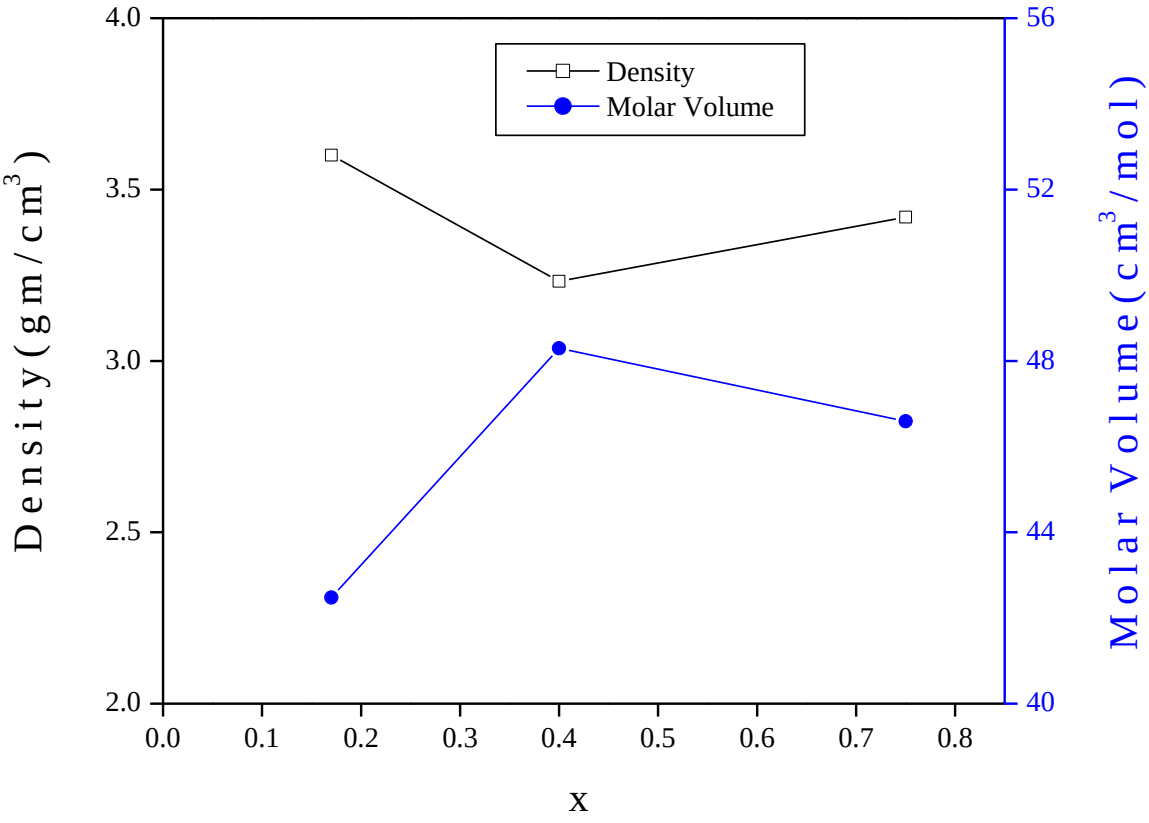

Fig. 4.1 Variation of density and molar volume at different values of x

4.3.1.2 X-ray Diffraction (XRD)

The X-ray diffraction study, explained in section 2.4.2, has been done on the different as-prepared samples to find out the nature of the samples. Fig. 4.2 displays the room temperature X-ray diffractogram patterns of all the as-prepared samples, highlighting different peaks for [h k l] values for different nanophases [9]. The sample with x = 0.17 has shown presence of various peaks indicating their polycrystalline nature [9] whereas with the slightest increase in the portion of V_2O_5 and the smallest decrease in the portion of P_2O_5, some intense peaks began to show up in the pattern. For the sample 2 with x = 0.4, partial crystallization has been observed. These peaks indicate the presence of crystallites: ZnP_4O_{11}, $AgZnPO_4$, $V_4(P_4O_{12})_3$, $Ag_4P_2O_7$, Ag_5Zn_8. The details of these peaks are listed in Table 1. It has been further observed that with the additional increase in the ratio of V_2O_5 to P_2O_5 i.e for x = 0.75, the peaks start disappearing and a broad hump has appeared instead signifying amorphous nature of the sample. The investigation clearly shows that the samples' development of a glassy structure was aided by the addition of V_2O_5.

From the diffraction result, the crystallite size (d), dislocation density (δ) and lattice strain (ε) can be calculated using Eq. 2.4, 2.5 and 2.6. The results of X-ray diffraction, different phases with their Miller indices formed are given in Table 4.2.

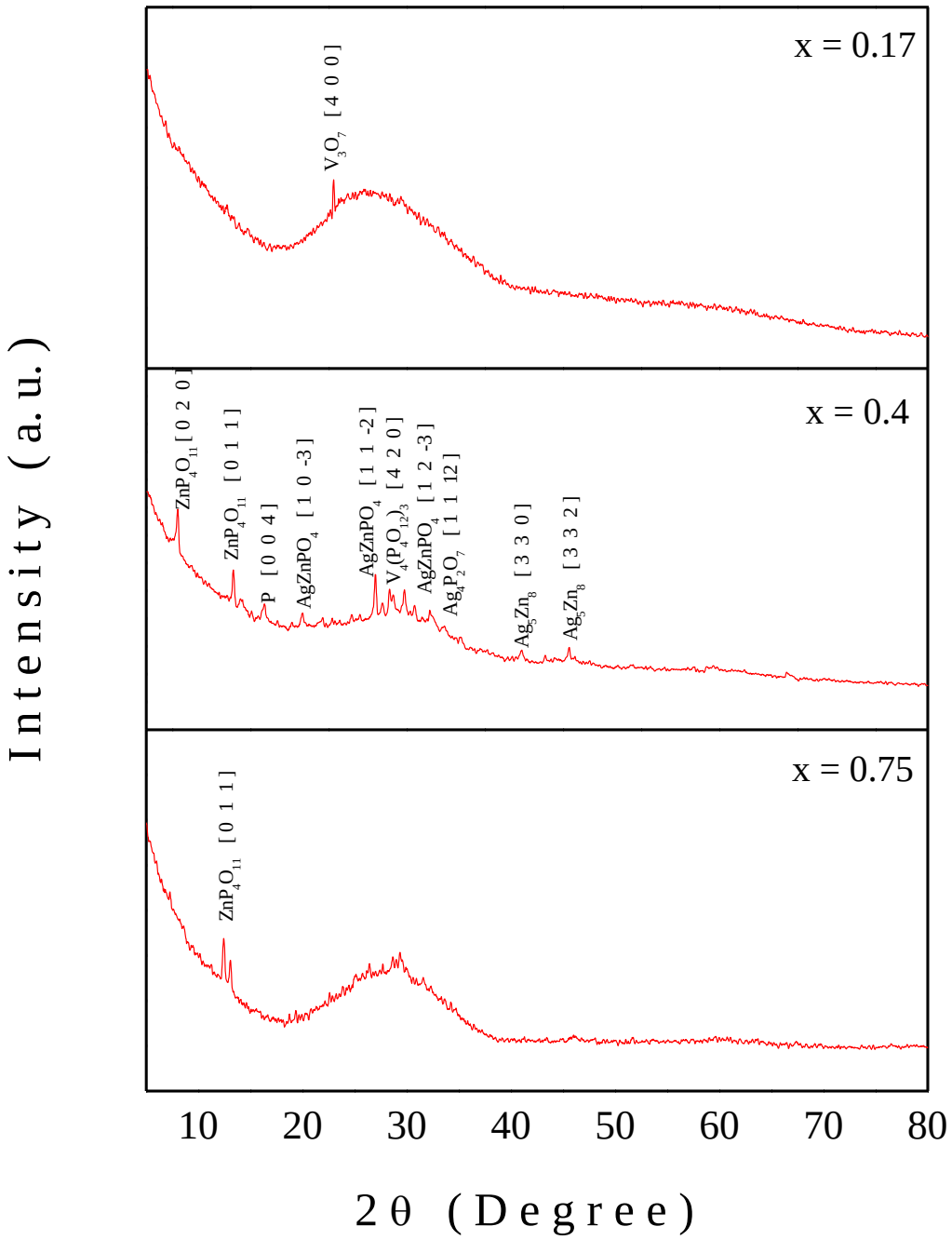

Fig. 4.2 X-ray diffractograms of the glass nanocomposites with different values of x

x	Nano-Phases	**Crystallite Size** (nm)	h k l	**Average Crystallite Size** (nm)	**Dislocation Density** (cm^{-2})	**Lattice** Strain
0.17	V_3O_7	14.24	4 0 0	14.24	0.004933264	0.010719758
0.4	ZnP_4O_{11}	0.32	0 2 0	0.29	9.875881729	1.559364297
	ZnP_4O_{11}	0.28	0 1 1		12.78675614	1.064922073
	P	0.24	0 0 4		17.91069607	1.033528184
	$AgZnPO_4$	0.27	1 0 -3		14.19572912	0.755264421
	$AgZnPO_4$	0.35	1 2 -2		8.092025115	0.422925544
	$V_4(P_4O_{12})_3$	0.19	4 2 0		27.41832504	0.741616664
	$AgZnPO_4$	0.35	1 2 -3		7.992912406	0.381631969
	$Ag_4P_2O_7$	0.19	1 1 12		26.89584177	0.644443185
	Ag_5Zn_8	0.32	3 3 0		9.995928046	0.31299233
	Ag_5Zn_8	0.40	3 3 2		6.200393347	0.223144046
0.75	ZnP_4O_{11}	0.91	0 1 1	0.91	1.209702816	0.33466035

Table 4.2: Crystallite Size, Dislocation Density and Lattice Strain of the system

4.3.2 Electrical Conductivity study

The effect of mixed formers on the electrical transport of the as-prepared sample are the main thrust area of our study. The electrical conductivity study has been carried out to study the

effect of dominant presence of V_2O_5 on the silver ion conducting system. In this section, the dynamics of the charge carriers have been examined with the help of electrical conductivity and dielectric relaxation process.

4.3.2.1 DC Conductivity Study

The Cole-Cole plots [10] of the as-prepared samples are shown in Fig. 4.3 (a) – (c). As can be seen, all of the curves are semicircular in shape, and the diameter of each curve can be used to estimate the corresponding DC conductivity [10]. It clearly illustrates two significant theories. The intercept of the semicircle on the Z' axis shifts towards the origin as temperature rises. A reduction in the semicircle's radius as temperature rises indicates the system's thermally activated conduction mechanism [10]. It also validates the fact that as the ratio of the mixed formers increase, the resistivity of the samples starts decreasing which in turn augments the conductivity of the samples. This shows that the presence of V_2O_5 in the environment of glassy system helps in better conductivity of the system. Also, the center of semicircle was found below Z' axis which indicates the non-Debye relaxation of ions [11-12].

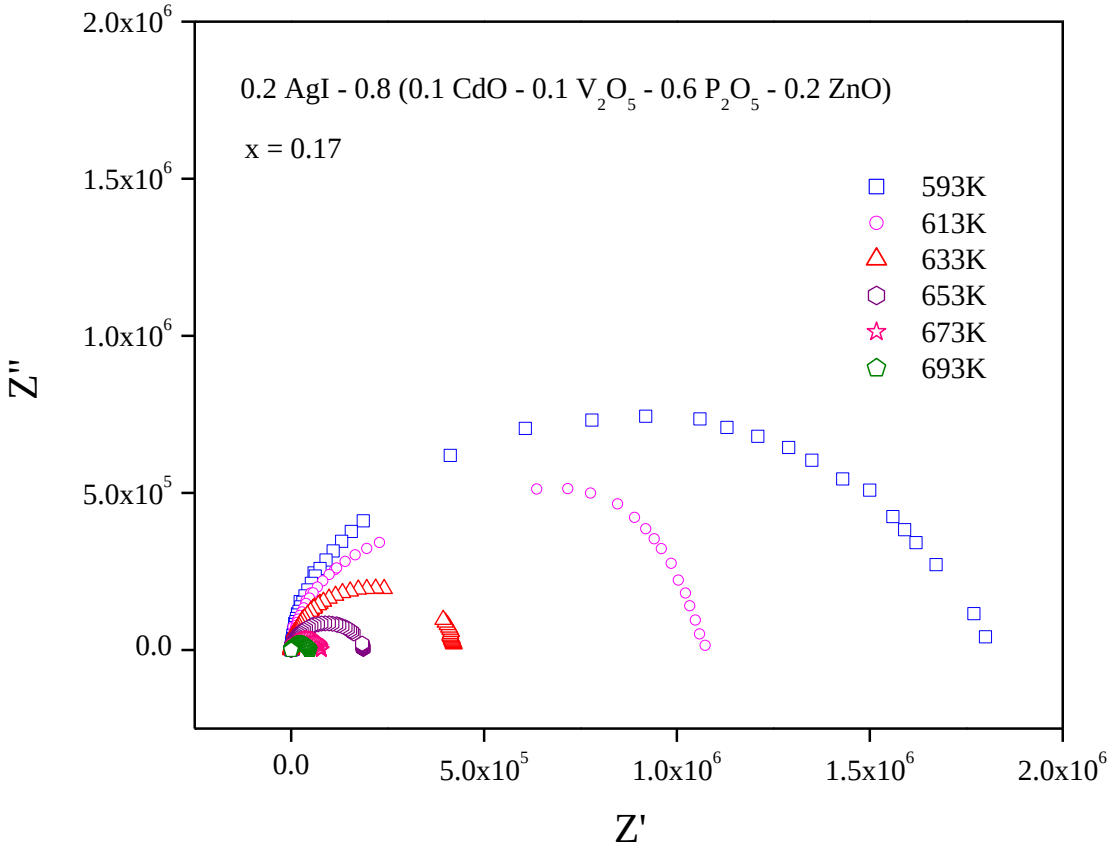

Fig. 4.3 (a) Complex impedance plot for x = 0.17 at various temperatures

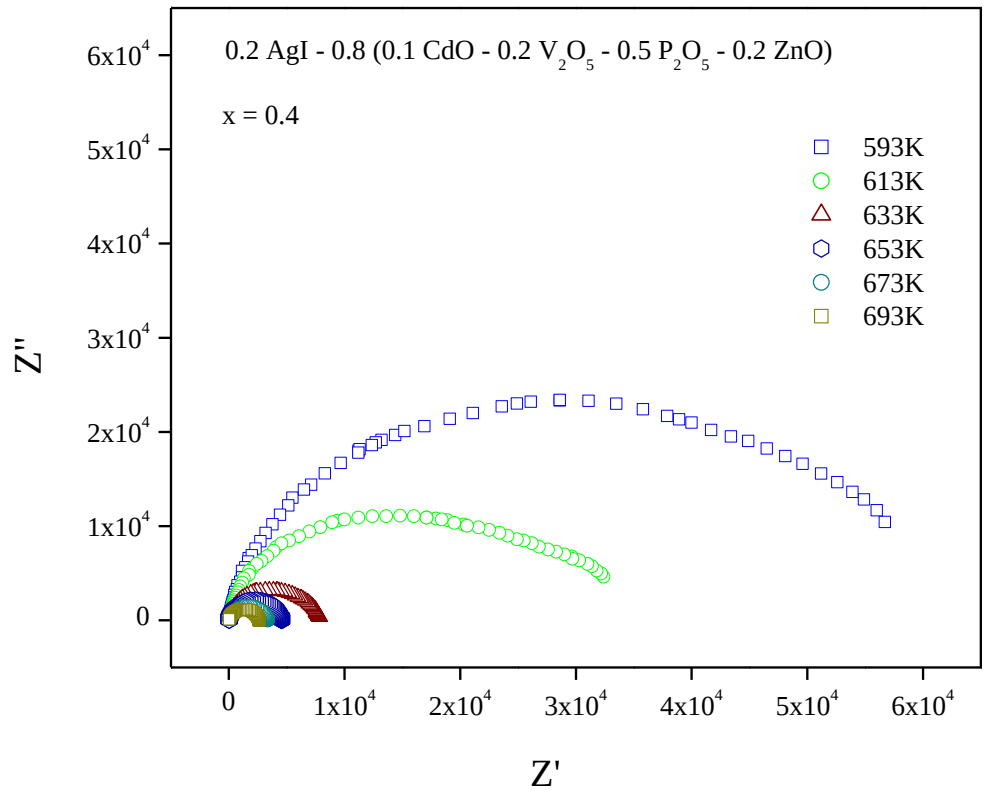

Fig. 4.3 (b) Complex impedance plot for x = 0.04 at various temperatures

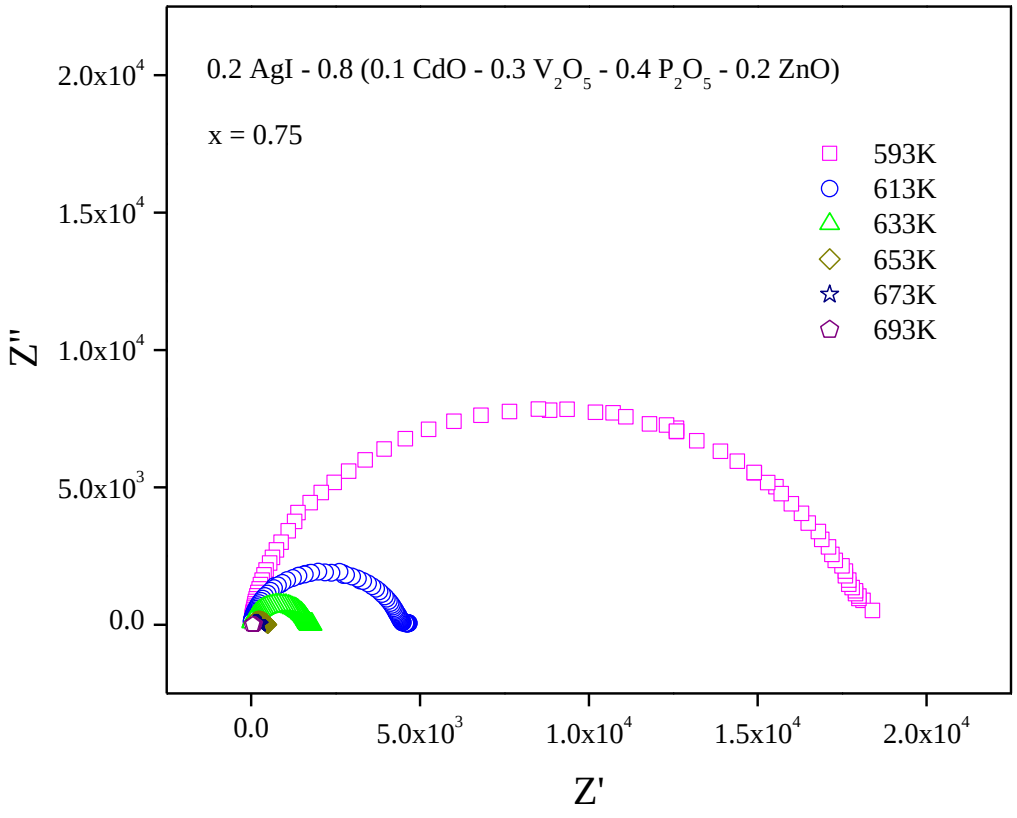

Fig. 4.3 (c) Complex impedance plot for x = 0.75 at various temperatures

DC conductivity [10,13] has been calculated by predicting DC resistivity from the measured diameter of the arcs in Fig. 4.3 (a) – (c). Estimated DC conductivity values in relation to reciprocal temperature are displayed in Fig. 4.4. A gradual increase in the conductivity with the rise in the temperature has been clearly noted. It conforms to the Arrhenius type of variation.

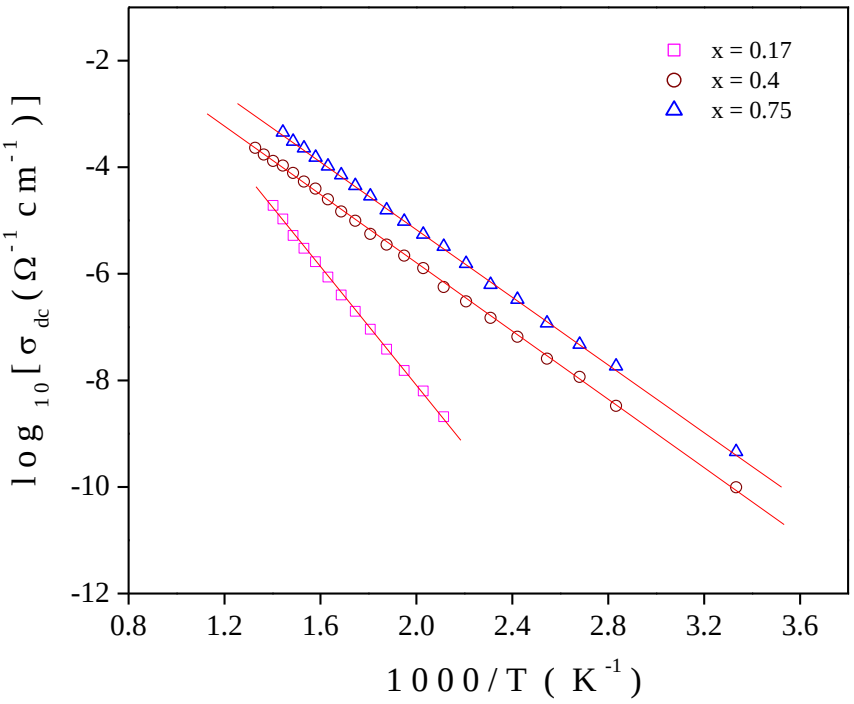

Fig. 4.4 Linear fit of temperature dependence plot of DC conductivity for all x

This escalation in the DC conductivity ought to be related to their structural properties which is completely composition-dependent. The activation energy corresponding to dc conductivity (E_{dc}) has been calculated by using the least-square straight-line fitting given in Eq. 2.8 and they are represented by solid lines in Fig. 4.4. The values of E_{dc} have been listed in Table 4.3. Fig. 4.5 clearly demonstrates that there is a fall in the values of activation energy as the ratio of the mixed formers escalate and accordingly there is a gradual rise in the values of dc conductivity. This study concludes that the effect of mixed formers boosts the conductivity in the samples under the dominant presence of V_2O_5.

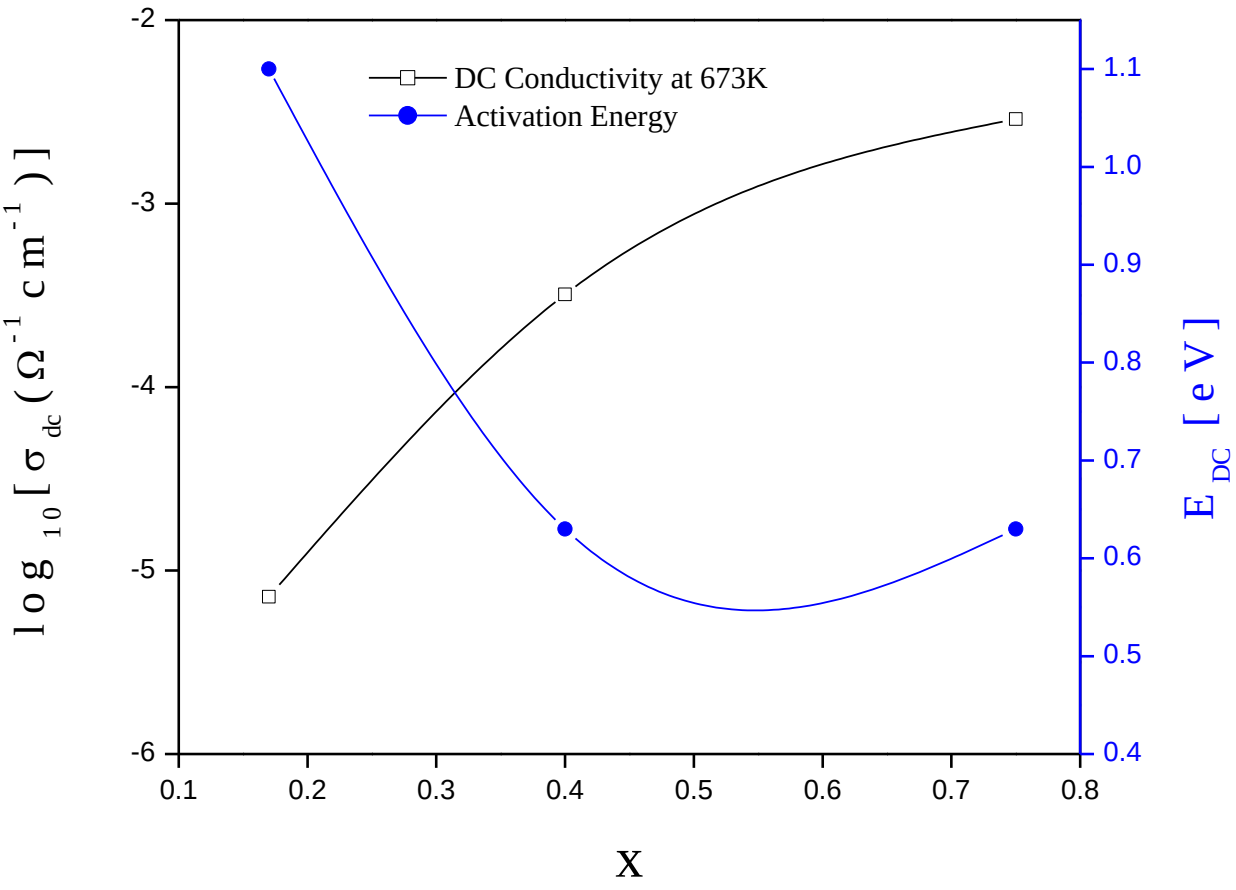

Fig. 4.5 Variation of DC conductivity at a fixed temperature 673K and activation energy corresponding to DC conductivity with respect to composition

Composition (x)	**n**	**Activation Energy due to DC Conductivity, E_{dc} (eV)**	**Activation Energy due to Hopping Frequency, E_h (eV)**
0.17	1.24	1.1	1.02
0.4	1.03	0.63	0.58
0.75	0.99	0.63	0.58

Table 4.3: Data of frequency exponent n, Activation energy corresponding to dc conductivity, hopping frequency corresponding to composition of as-prepared glasses

4.3.2.2 AC Conductivity Study

The AC conductivity spectra have been considered in the range of 42 Hz to 5 MHz at different temperatures for all the x. The plots, shown in Fig. 4.6 (a) - (c) has revealed that the ac conductivity rises with temperature at all frequencies. This explains why the prepared system is called thermally activated. The DC conductivity that may result from the polaron hopping phenomena [14-15] is correlated with the lower frequency area of the frequency independent AC conductivity. Fig. 4.6 illustrates that dispersion occurs at higher frequencies, primarily above crossover or hopping frequency [13,16]. As the temperature rises, the dispersion of AC conductivity spectra is observed to shift towards higher frequencies which implies that the hopping frequency and dc conductivity are thermally triggered. The total conductivity spectra are found to have a power law character [16], similar to that of ionic conductors. The plots have been fitted using the Almond West model [14], given by Eq. 2.16, in order to obtain the required information regarding the conductivity of the system.

Long-time dynamics in the low-frequency realm can be represented by random walks in terms of diffusive long-range charge carrier transport [13,16]. The motion becoming sub-diffusive as frequency rises is largely dependent on the short-time dynamics of charge carriers, namely their back-and-forth motion over restricted ranges [13,16]. Therefore, the high-frequency dispersive region (short-time dynamics) and the low-frequency plateau region (long-range transport) are separated by the crossover frequency [13,16]. In terms of determining the hopping rate of charge carriers, Almond and West [14] indicate that the crossover frequency has significance because it is the frequency at which charge carrier hopping begins.

Eq. 2.16 has been used to predict σ_{dc}, ω_H, and n based on the best fit of experimental data in Fig. 4.6 (a) – (c). Similar characteristics of the AC conductivity spectra have been seen in all of the systems produced and reviewed here. Therefore, it may be established that the hopping of polarons is the most likely explanation for the AC conduction of the as-prepared samples. The solid lines in Figure 4.6 (a) - (c) show the linear fitting of AC conductivity data. The calculated parameters σ_{dc}, ω_H and n are tabulated in Table 4.4 – 4.6.

x	T(K)	σdc ($W^{-1}cm^{-1}$)	ω_H (rad s^{-1})	n
0.17	473	4.10×10^{-11}	8.401	1.134
	493	1.90×10^{-10}	20.484	1.097
	513	9.30×10^{-09}	877.914	1.139
	533	3.56×10^{-08}	3255.212	1.165
	553	1.03×10^{-07}	10365.363	1.215
	573	2.04×10^{-07}	20445.434	1.229
	593	4.14×10^{-07}	42747.589	1.255
	613	8.20×10^{-07}	88367.396	1.284
	633	1.36×10^{-06}	140784.902	1.282
	653	3.73×10^{-06}	361305.66	1.305
	673	7.20×10^{-06}	636167.602	1.307
	693	0.00001	1203005.525	1.352
	713	0.00003	2289005.316	1.404

Table 4.4: Parameters obtained from Almond West fitting of x = 0.17

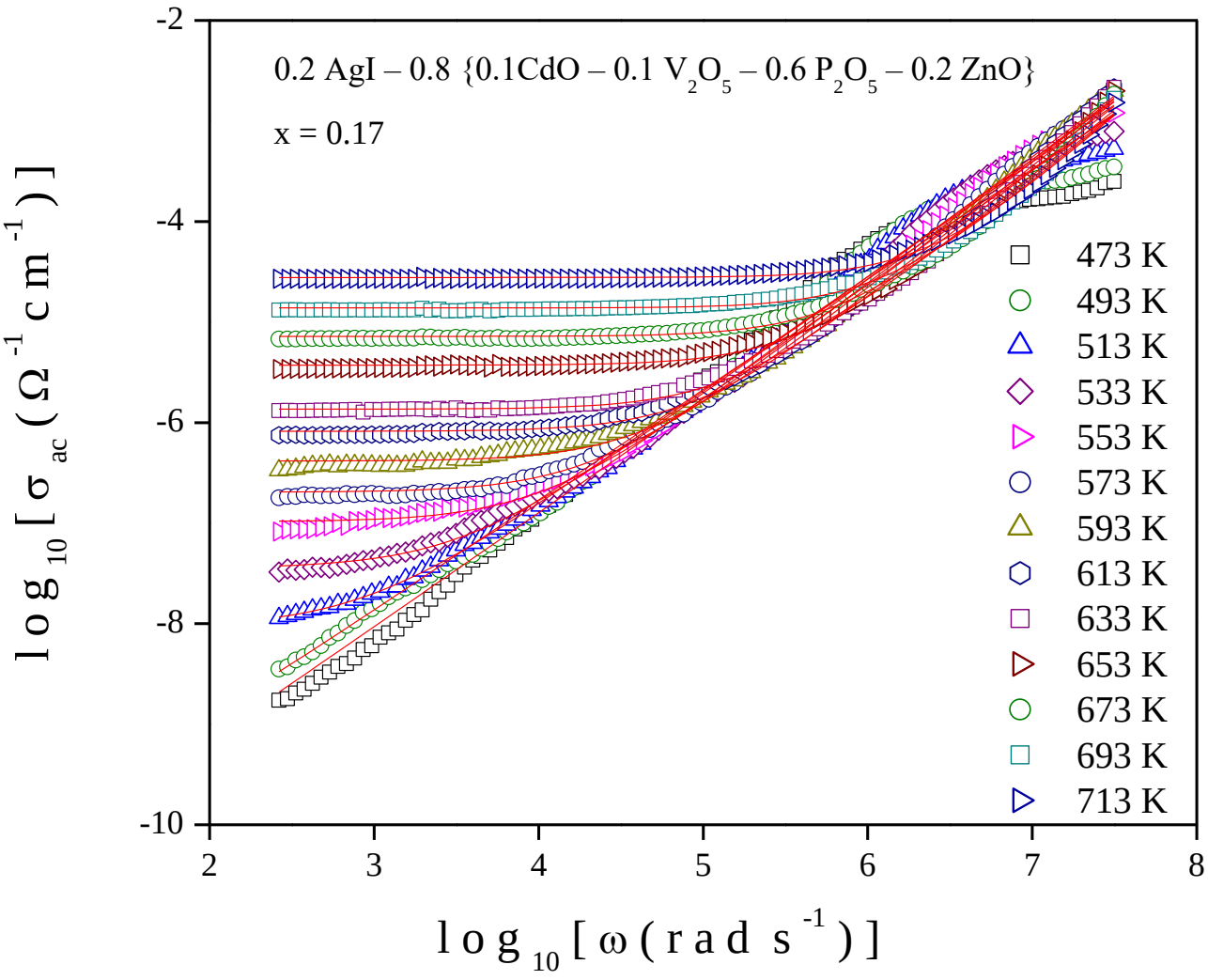

Fig. 4.6 (a) AC conductivity plot for x = 0.17 at various temperatures

x	T(K)	σdc ($W^{-1}cm^{-1}$)	ω_H (rad s^{-1})	n
0.4	300	2.49 x10^{-08}	1092.352	1.013
	353	6.05 x10^{-08}	2140.511	0.984
	373	1.08 x10^{-07}	3373.125	0.967
	393	1.65 x10^{-07}	4099.034	0.937
	413	2.76 x10^{-07}	5203.005	0.896
	433	5.03 x10^{-07}	8674.407	0.878
	453	8.82 x10^{-07}	11976.058	0.846
	473	1.07 x10^{-06}	11655.504	0.812
	493	1.37 x10^{-06}	12414.115	0.801
	513	1.47 x10^{-06}	10461.365	0.775
	533	1.19 x10^{-06}	9694.867	0.811
	553	1.01 x10^{-06}	12287.032	0.878
	573	8.21 x10^{-06}	115179.179	0.851
	593	0.00001	143564.912	0.855
	613	0.00006	1378412.397	0.984
	633	0.00011	2780421.356	0.975
	653	0.00026	8745586.454	1.331
	673	0.00032	10432195.34	1.351
	693	0.00044	12936363.94	1.417
	713	0.00048	13678113.17	1.415
	733	0.00053	14850228.59	1.478
	753	0.00052	14863926.11	1.461

Table 4.5: Parameters obtained from Almond West fitting of x = 0.4

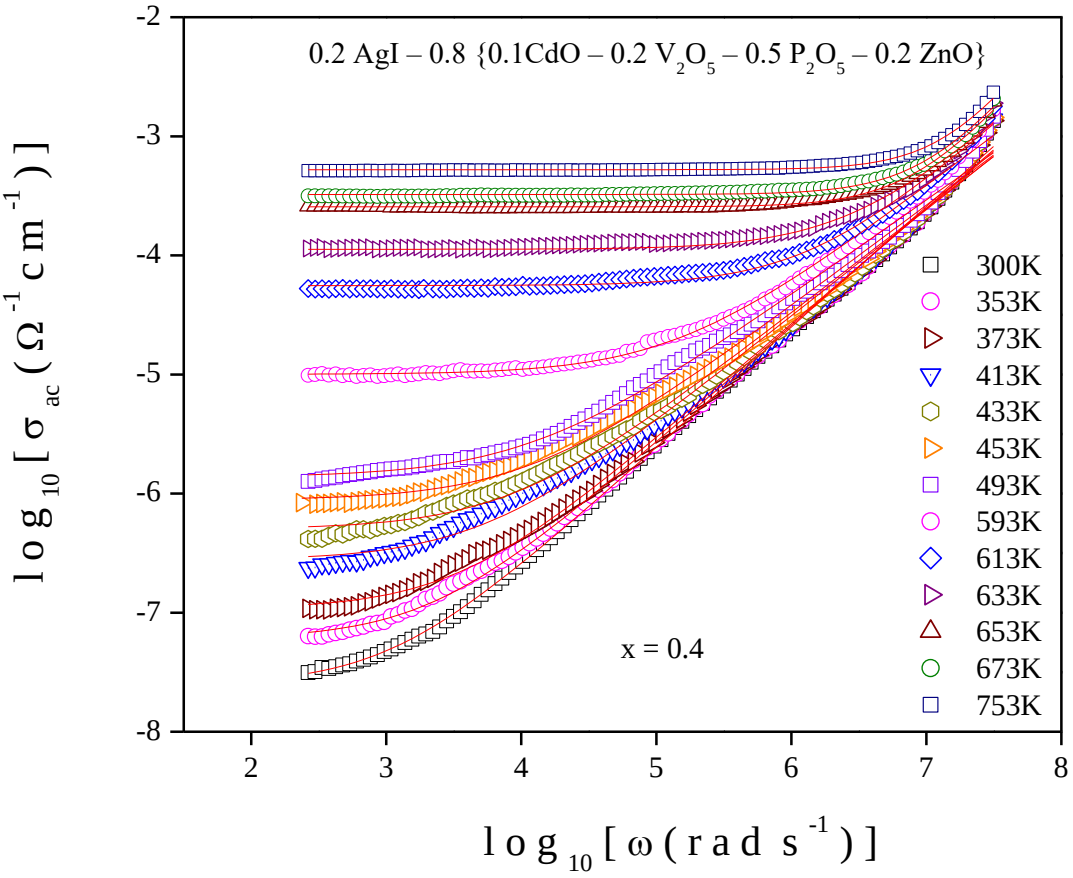

Fig. 4.6 (b) AC conductivity plot for x = 0.4 at various temperatures

x	T(K)	σdc ($W^{-1}cm^{-1}$)	ω_H (rad s^{-1})	n
0.75	300	1.66 x10^{-08}	1068.189	0.997
	353	3.79 x10^{-08}	1879.395	0.964
	373	4.33 x10^{-08}	1806.302	0.943
	393	6.30 x10^{-08}	2357.98	0.929
	413	9.39 x10^{-08}	3085.897	0.911
	433	1.36 x10^{-07}	3933.353	0.898
	453	2.57 x10^{-07}	7438.411	0.892
	473	4.93 x10^{-07}	13965.514	0.883
	493	1.09 x10^{-06}	31626.285	0.877
	513	2.50 x10^{-06}	76771.907	0.878
	533	4.46 x10^{-06}	156283.703	0.902
	553	9.77 x10^{-06}	486426.611	0.99
	573	0.00002	996688.481	1.088
	593	0.00005	2512586.097	1.117
	613	0.00015	6608043.094	1.097
	633	0.00049	14916476.96	1.192
	653	0.00138	20727124.56	1.14
	673	0.00289	27966258.22	1.355
	693	0.00802	69930976.93	0.835

Table 4.6: Parameters obtained from Almond West fitting of x = 0.75

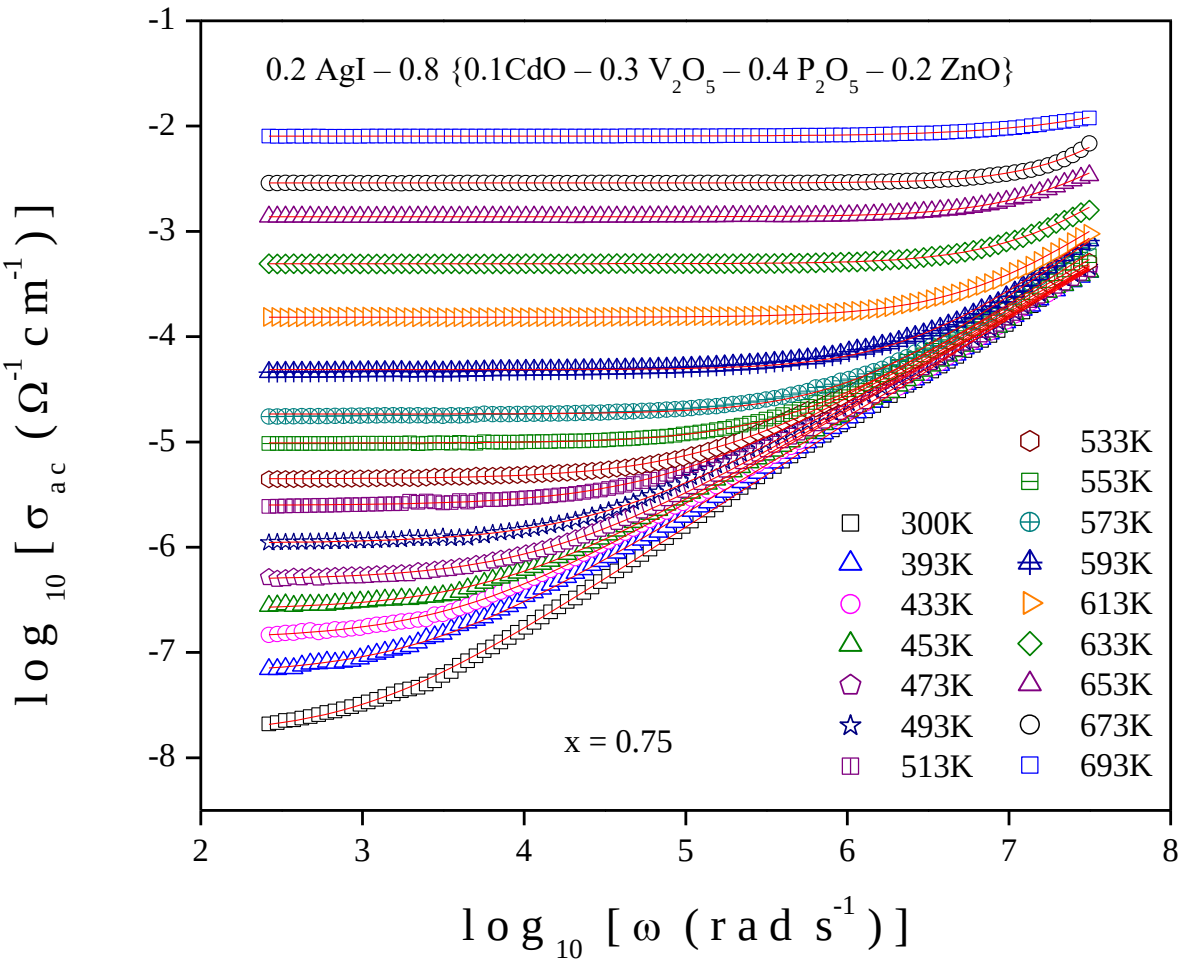

Fig. 4.6 (c) AC conductivity plot for x = 0.75 at various temperatures

The total conductivity spectra at 693K are displayed in Fig. 4.7 for all the samples. The conductivity is found to be augmented with frequency and with the proportion of V_2O_5. Plateau region of conductivity spectra in the Fig. 4.7 is found to shift upwards as we move from x = 0.17 to x = 0.75, implying elevation in conductivity.

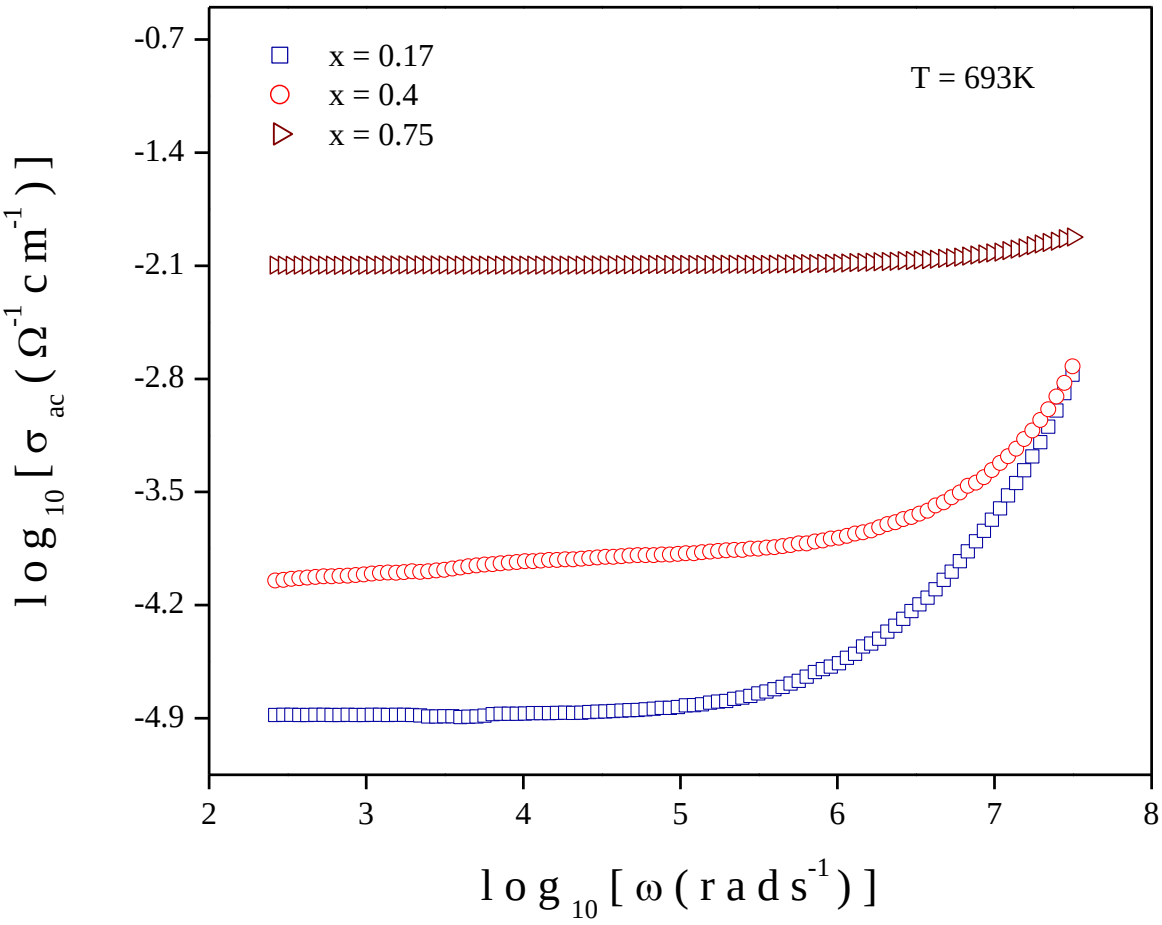

Fig. 4.7 AC conductivity spectra of all the sample at a fixed temperature 693K at various frequencies

Table 4.3 shows the values of relaxation time and validates the nature of variation of AC conductivity. It is distinct from the data that as the ratio of the mixed formers rises the relaxation time gets reduced. Reduction in relaxation time should lead to an increase in the rate of polaron hopping, which in turn increases the conductivity. This result points to the fact that the presence of mixed formers has a positive impact on the conductivity of the as-prepared glassy systems. For carrying out the comprehensive study on the conductivity of the samples, the variation of hopping frequency, ω_H with the temperature is displayed in the Fig.4.8. The pattern of the plots clearly suggests that it obeys Arrhenius nature. The activation energy (E_h) required for crossover or ion hopping frequency has been calculated by using the least-square straight-line fitting using Eq. 2.18 and they are represented by solid lines in Fig. 4.8.

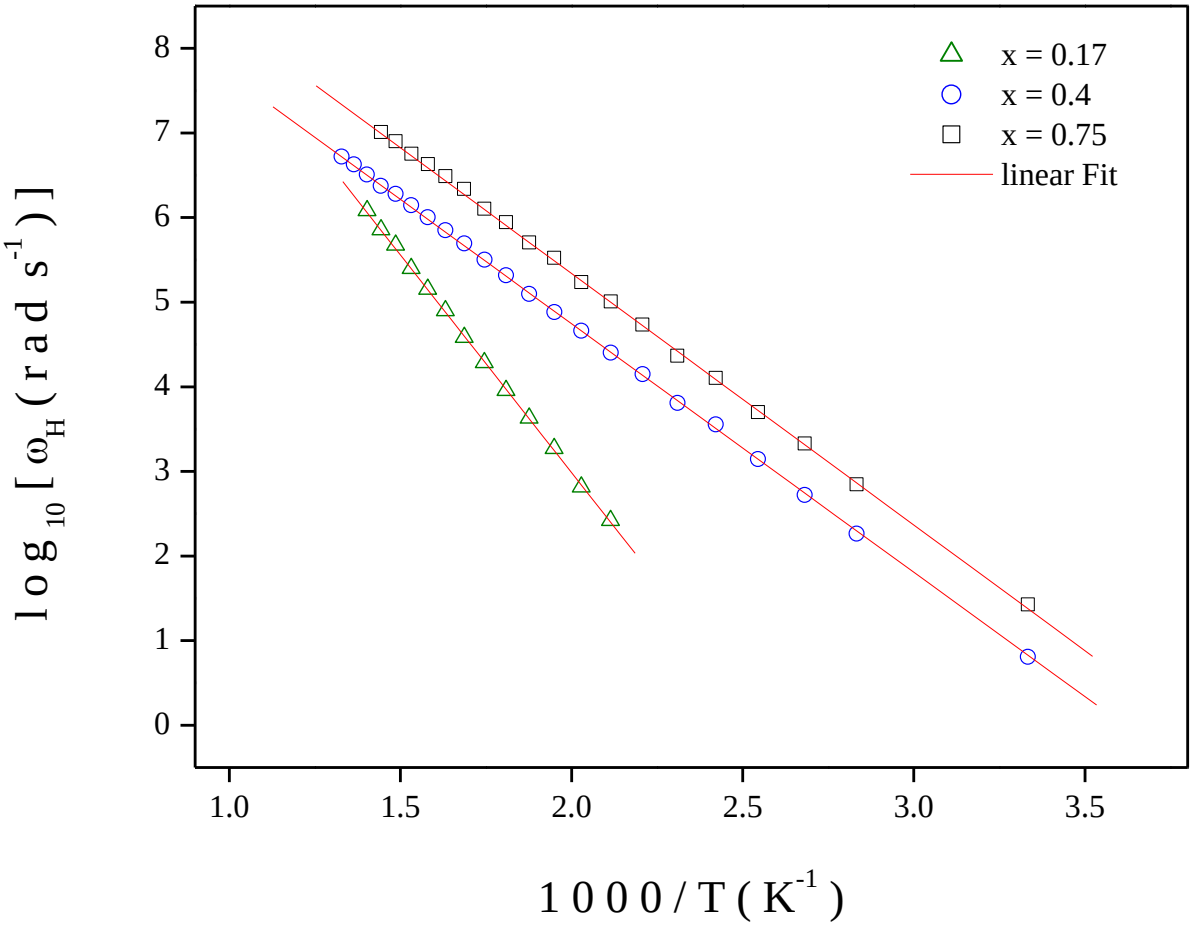

Fig. 4.8 Linear fit of hopping frequency of all the samples at various reciprocal temperatures

The values of the activation energy due to hopping frequency have been enlisted in Table 4.3 and the variations of E_H and ω_H with composition have been plotted in Fig.4.9. It can be clearly seen that ω_H escalates with x i.e. the ratio of the mixed formers (V_2O_5:P_2O_5) and E_h shows the reverse nature of ω_H. The reason behind this could be that, as the temperature elevates, according to Boltzmann statistics, thermal agitation causes the concentration of mobile Ag^+ ions to rise, which in turn generates an increasing number of trapping sites. Reduced values of E_h indorses elevation of the related hopping frequency and correspondingly the electrical conductivity increases [17]. The study concludes that the presence of mixed formers affects positively in the electrical conductivity of the as-prepared systems by reducing the activation energy and thus augmenting the hopping frequency.

The assessed values of the exponents (n), obtained from Eq. 2.16, have been listed in Table

4.3. The variation of n with the composition has been presented in Fig. 4.9. The distinct non-zero values of n correspond to the conductivity dispersion at higher frequencies. The larger the value of n, the more energy is contained in the amalgamated movement of polarons [18]. Higher values of n verify a single hop and imply a substantial drift of polarons, whereas smaller values of n indicate multiple hops [18].

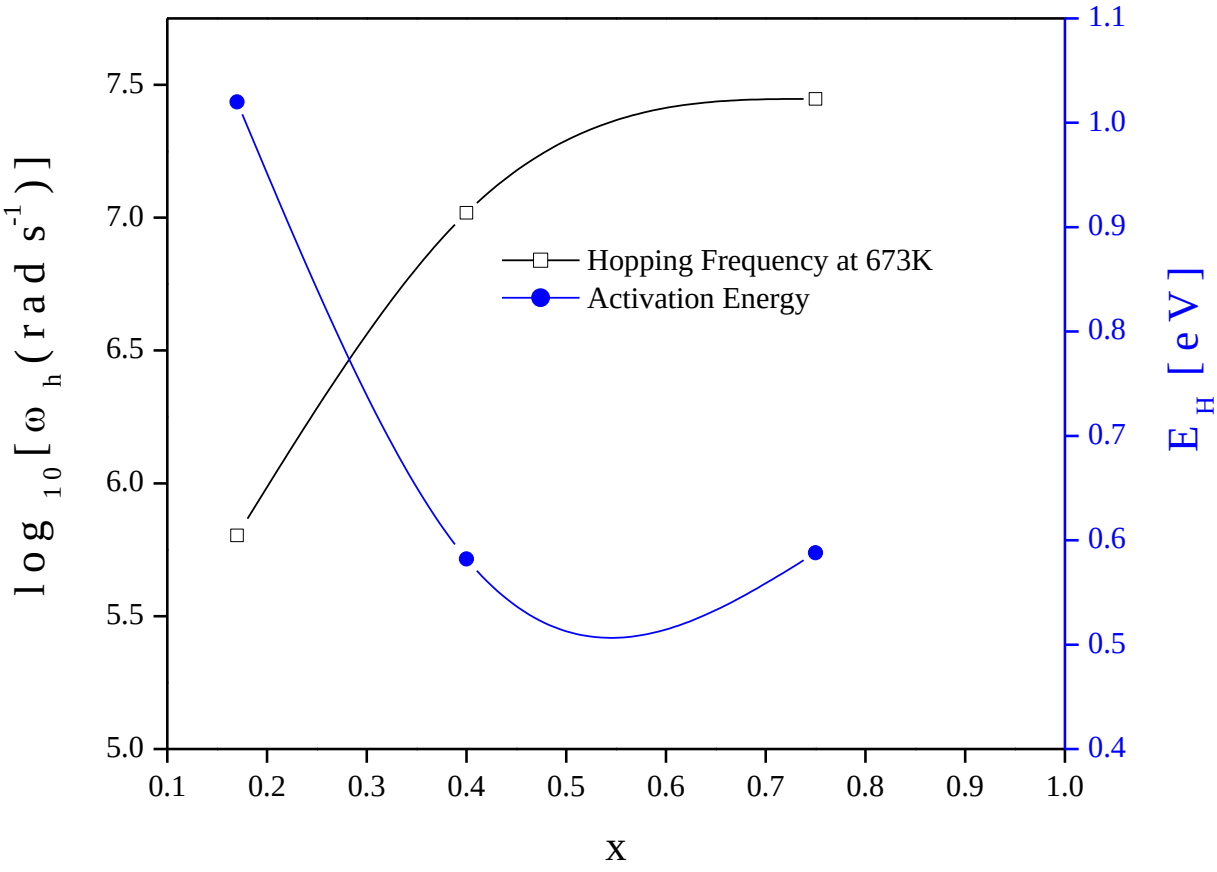

Fig. 4.9 Variation of hopping frequency at a fixed temperature 673K and activation energy corresponding to hopping frequency with respect to composition

From literature survey it has been observed that if the value of n lies within 0.7 to 1, it is an indication of the sudden polaron hopping between the randomly distributed localized charge states. The average values of n for all the samples are obtained in the range of 0.9 to 1.3 as can be seen from Table 4.3. A non-linear hopping motion is indicated by the values of n, which vary with temperature and should be dependent on composition [19]. The way that n fluctuates with temperature can be directly linked to the presence of a variety of relaxation mechanisms. The observed AC conductivity may be influenced by the magnitude of n and an ion diffusion

mechanism in the glassy matrix.

From Table 4.3 it can be pointed out that the value of n is smallest for the sample with highest value of x i.e. 0.2 AgI – 0.8 {0.1CdO – 0.3 V_2O_5 – 0.4 P_2O_5 – 0.2 ZnO}). This is an indication of a strong drift due to multiple polaron hopping and hence exhibits largest conductivity. Therefore, it can be established that with the enhancement in the ratio of mixed formers the conductivity of the as-prepared glass nano-composites also get amplified. It also indicates that the potential energy barriers between various sites should have been significantly altered with the increase in proportion of V_2O_5, which directly enhances the growth in the degree of polaron hopping [18].

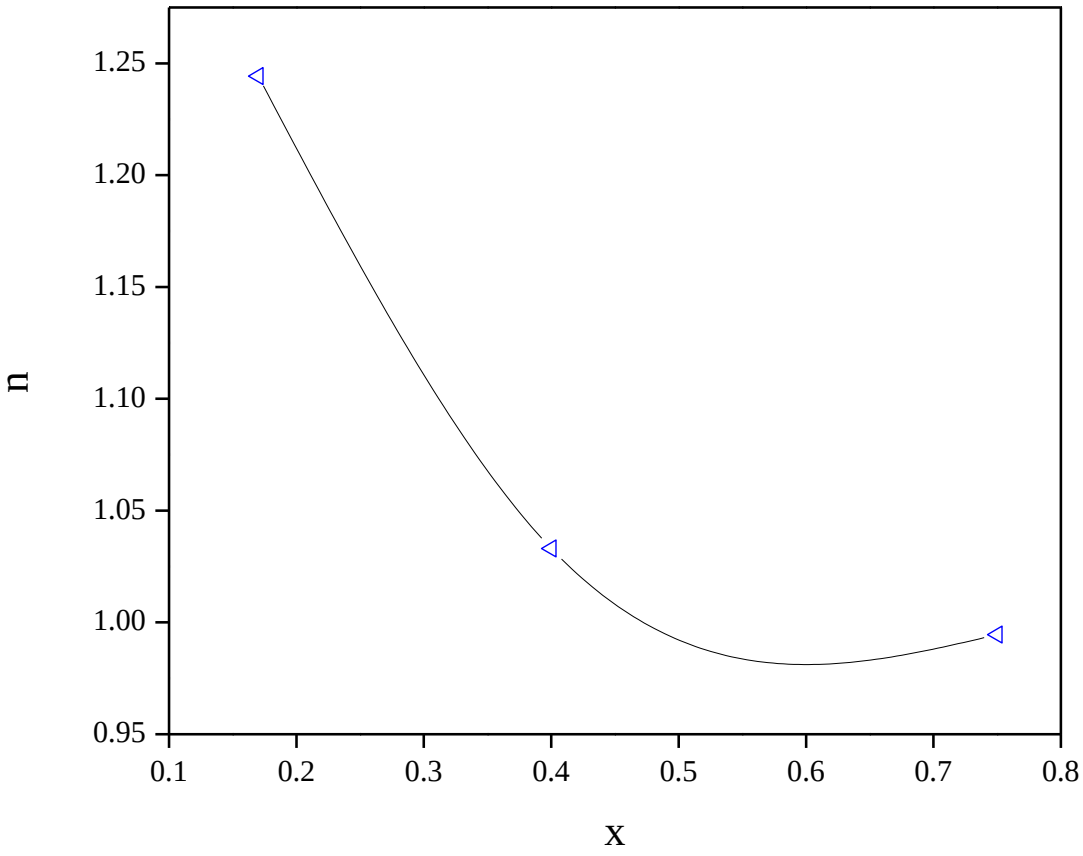

Fig. 4.10 Variation of frequency exponent (n) with respect to composition

4.3.3 Dielectric Property study

The dielectric constant ($\varepsilon^{/}$) and dielectric loss ($\varepsilon^{//}$) of the as prepared systems are studied at various temperatures (553K – 673K) in a wide frequency range of 42Hz - 5MHz. The rise in the proportion of V_2O_5 in the as-prepared glassy systems enhances their conductivity level which significantly lowers the activation energy required for polaron hopping and thus their

dielectric qualities are supposed to enhance [20-22]. This property permits them to be used in integrated circuits (ICs) device applications.

4.3.3.1 Study of electrical permittivity

In the frequency range of 42 Hz to 5 MHz, the dielectric constant $\varepsilon^{/}$ and dielectric loss $\varepsilon^{//}$ of the system has been investigated using Eqs. 2.24 – 2.25. The plots of $\varepsilon^{/}$ and $\varepsilon^{//}$ against angular frequency at various temperatures of the sample with x = 0.75 are shown in Fig. 4.11 (a) - (c) and Fig. 4.12 (a) - (c) respectively. As illustrated in figure, the current system's dielectric constant ($\varepsilon^{/}$) drops with growing frequency. This variation can be seen in the lower frequency zone. This spectra becomes frequency independent in the higher frequency region. At lower frequencies, the dielectric constant increases due to electrode polarization caused by the accumulation of space charges at the glass-electrode interface [23]. There is a noticeable high dispersion in both $\varepsilon^{/}$ and $\varepsilon^{//}$ at lower frequencies as the temperature rises. It is a main characteristic of systems with charged carriers [24]. The system's molecular dipoles find it increasingly challenging to track the rapid changes in the electric field as the frequency rises. As a result, the system's $\varepsilon^{/}$ and $\varepsilon^{//}$ begin to decrease as frequency increases, representing its frequency-independent nature.

Additionally, it can be observed from Fig. 4.11 and 4.12 that both $\varepsilon^{/}$ and $\varepsilon^{//}$ increase as temperature rises, which shows it's thermally activated nature. The primary cause of this is weakening of the intermolecular forces, which lowers bond energies and increases the polarization effect. This is a clear indication of higher conductivity. Thus, the dielectric study of the samples has also supported the fact that, with the increment in the portion of V_2O_5, the electrical conductivity also increases.

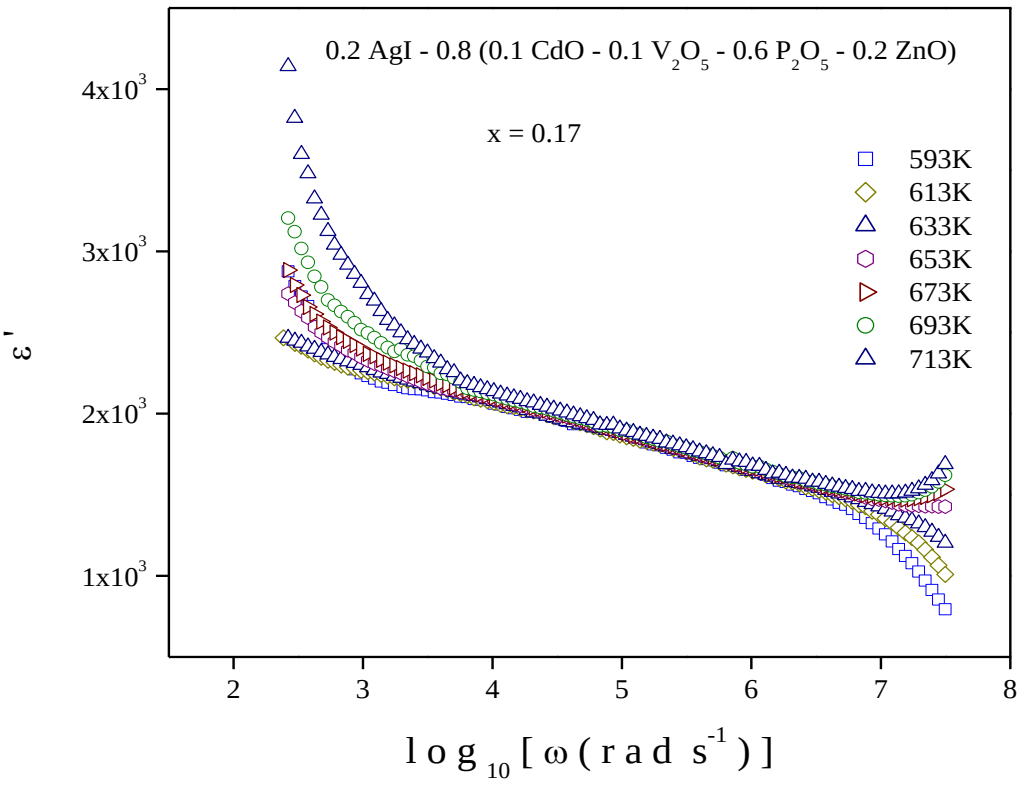

Fig. 4.11 (a) Spectra of dielectric constant ε' for x = 0.17

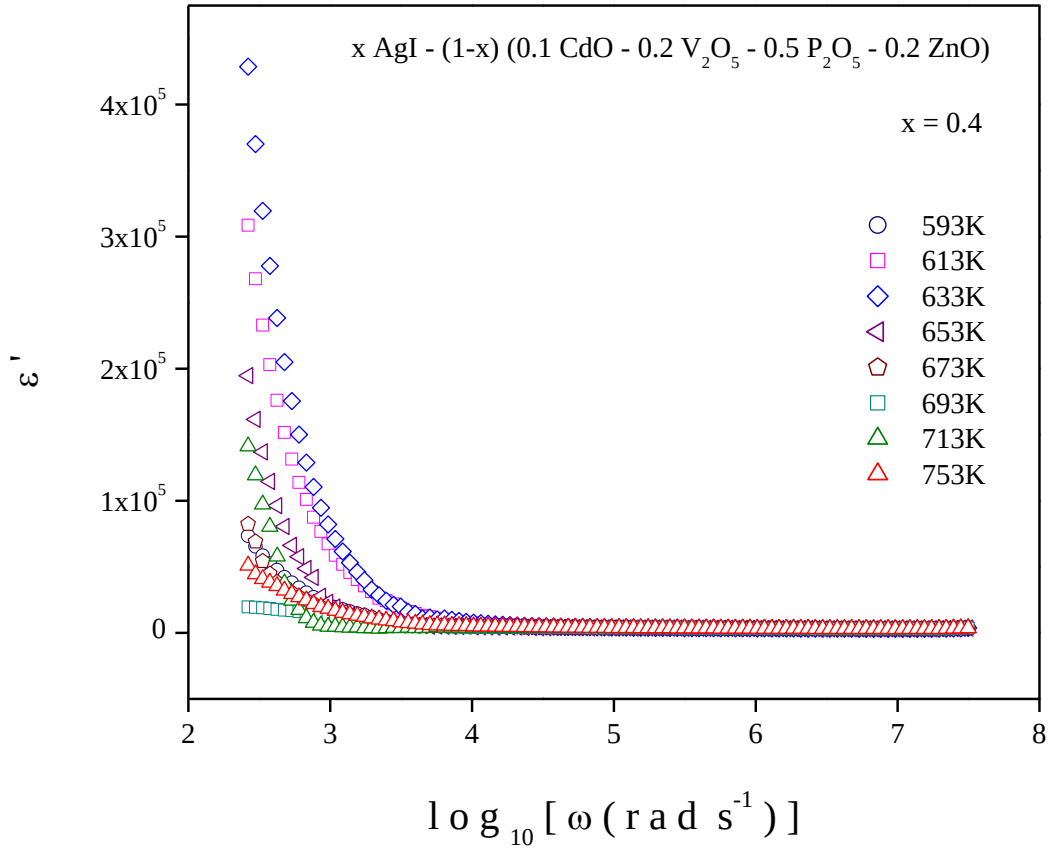

Fig. 4.11 (b) Spectra of dielectric constant ε' for x = 0.4

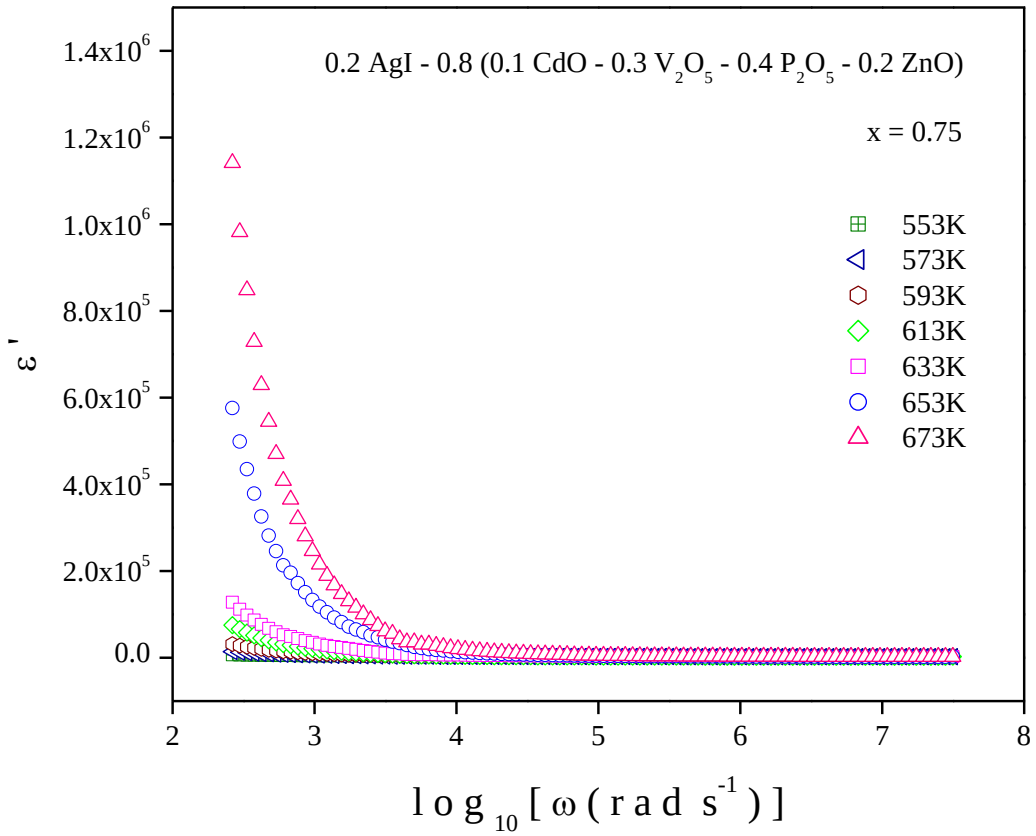

Fig. 4.11 (c) Spectra of dielectric constant $\varepsilon^{/}$ for x = 0.75

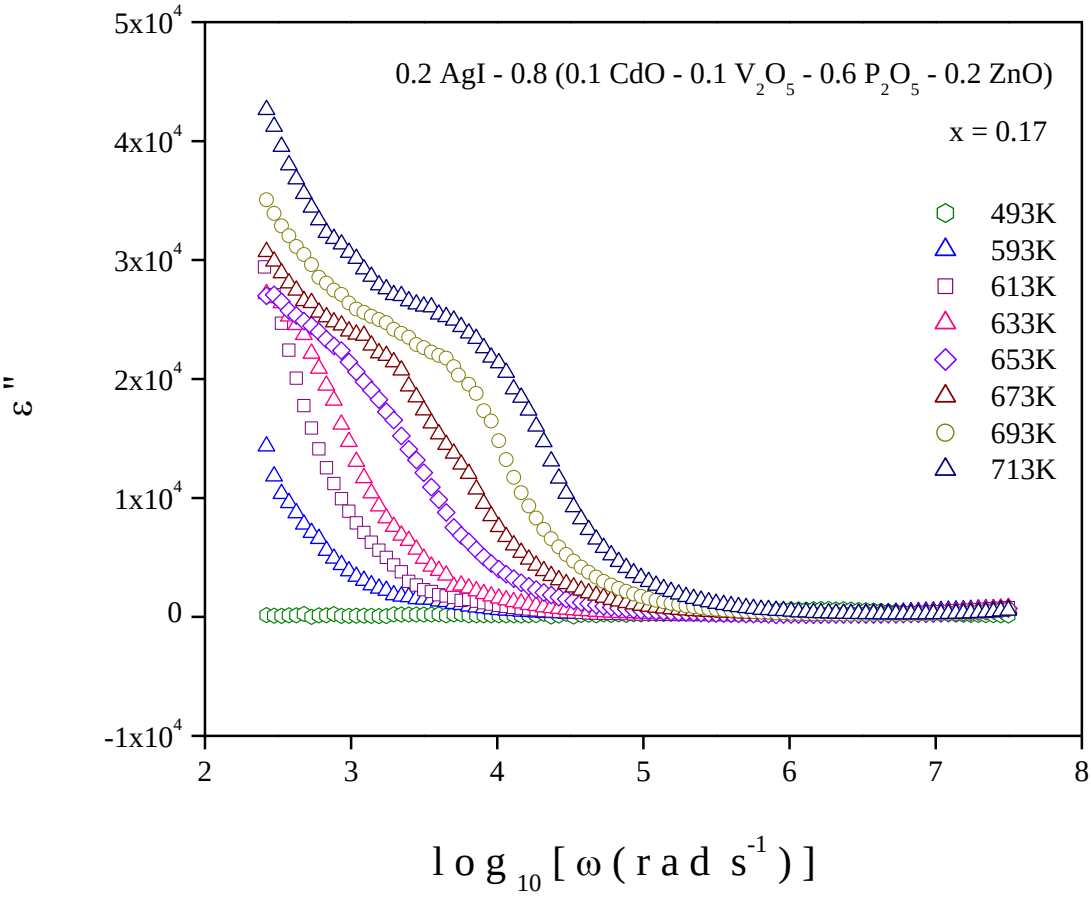

Fig. 4.12 (a) Spectra of dielectric loss $\varepsilon^{//}$ for x = 0.17

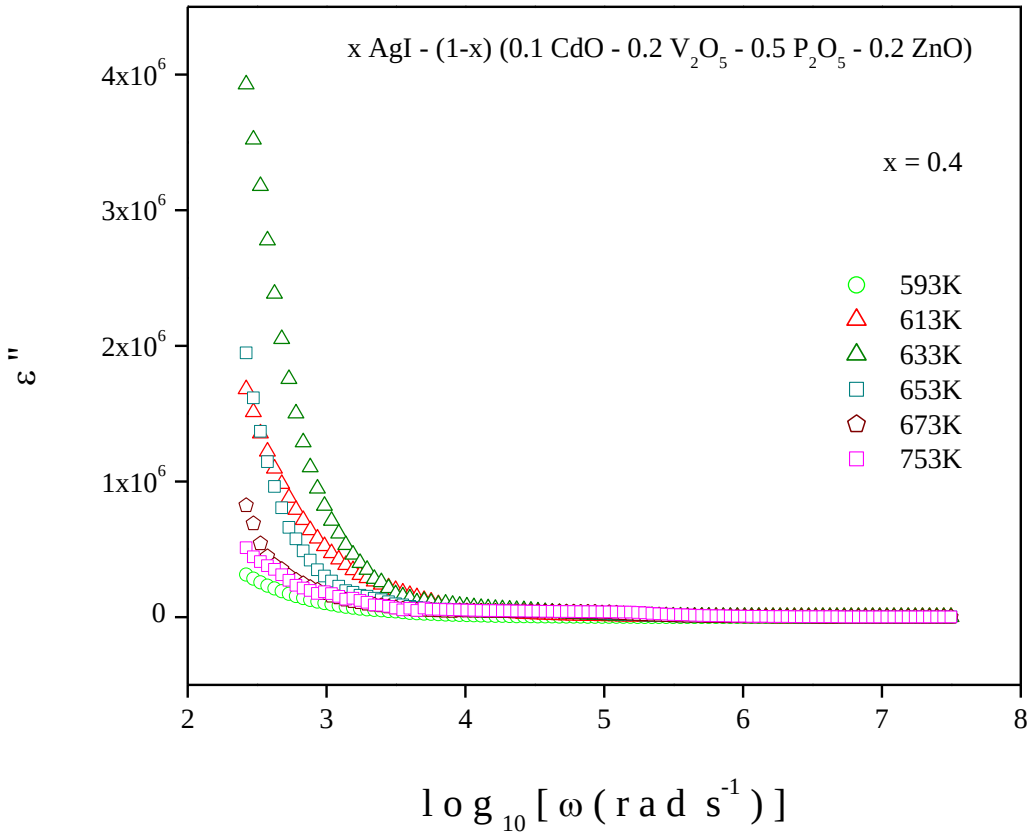

Fig. 4.12 (b) Spectra of dielectric loss $\varepsilon^{//}$ for x = 0.4

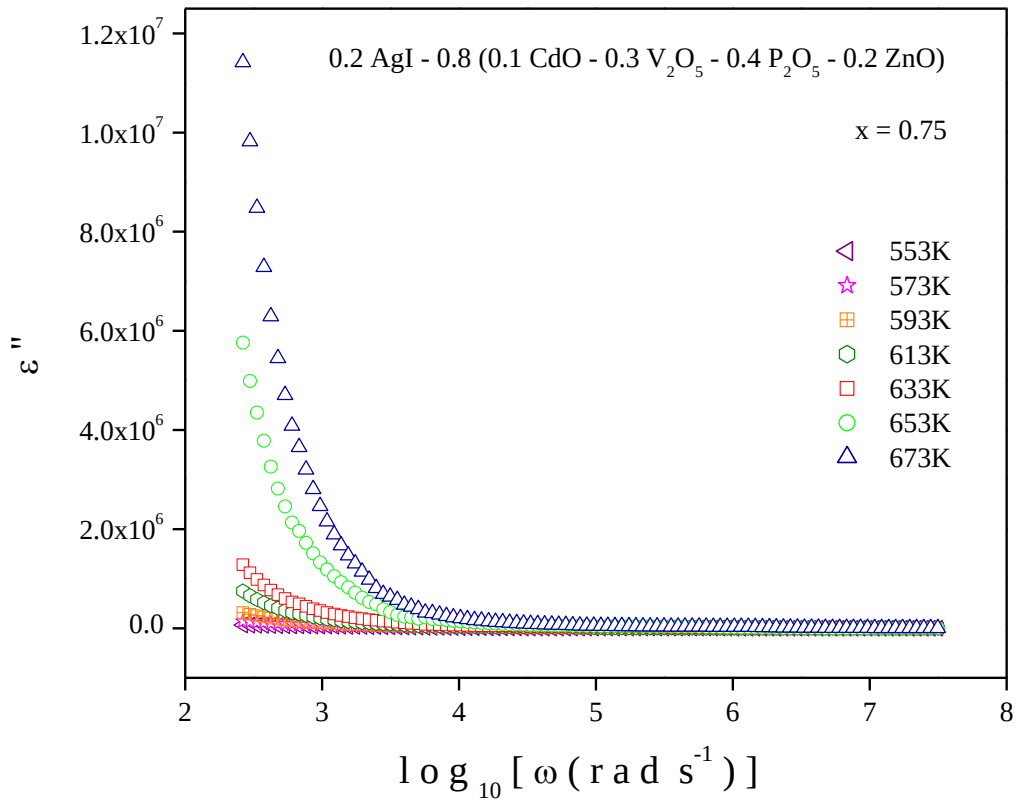

Fig. 4.12 (c) Spectra of dielectric loss $\varepsilon^{//}$ for x = 0.75

4.3.3.2 Study of Electric Modulus

Electric modulus formalism provides a more refined understanding of the contribution of conductivity effects by examining a system's complex electrical response by cancelling out the electrode polarization effect. Fig. 4.13 (a) - (c) and Fig. 4.14 (a) - (c) respectively depict the plots of the real and imaginary components of the fluctuations in electric modulus $M^{/}$ and $M^{//}$ with respect to frequency of all the samples. As there are no charge carrier restoring forces in the low frequency areas, electrode polarization is reduced [25]. As a result, $M^{/}$ approaches zero in the low frequency regions at all of the temperatures specified, as can be seen in Fig. 4.13 (a) - (c). But in the higher frequency region, the electrical relaxation of charge carriers causes dispersion in $M^{/}$ and $M^{//}$ and exhibits a maximum value, $(M_\infty) = (\varepsilon_\infty)^{-1}$ [25]. The gradual decrease in the values of $M^{/}$ on rising temperature could be observed in Fig. 4.13 (a) - (c) which may be an indication of short-range mobility of charge carriers in the conduction mechanism of the system [17].

The $M^{//}$ peaks in Fig. 4.14 (a) - (c) were observed to get shifted towards higher frequencies with the rise of temperature, implying thermally activated relaxation process. Peak relaxation frequency (ω_c) is correlated with $M^{//}$ peak positions in Fig. 4.14 (a) - (c). The approximation [11, 26-27] states that ω_c is the maximum frequency below which long-distance hopping by charge carriers or polron hopping is possible. At the frequencies above ω_c the conduction occurs due to the localized motion of carriers over small distances. Charge carriers are expected to be restricted to potential wells, where they are easily accessible, outside the ω_c area [11, 26-27]. This discussion leads to the conclusion that at ω_{max}, charge carriers' mobility shifts from long-range to short-range order.

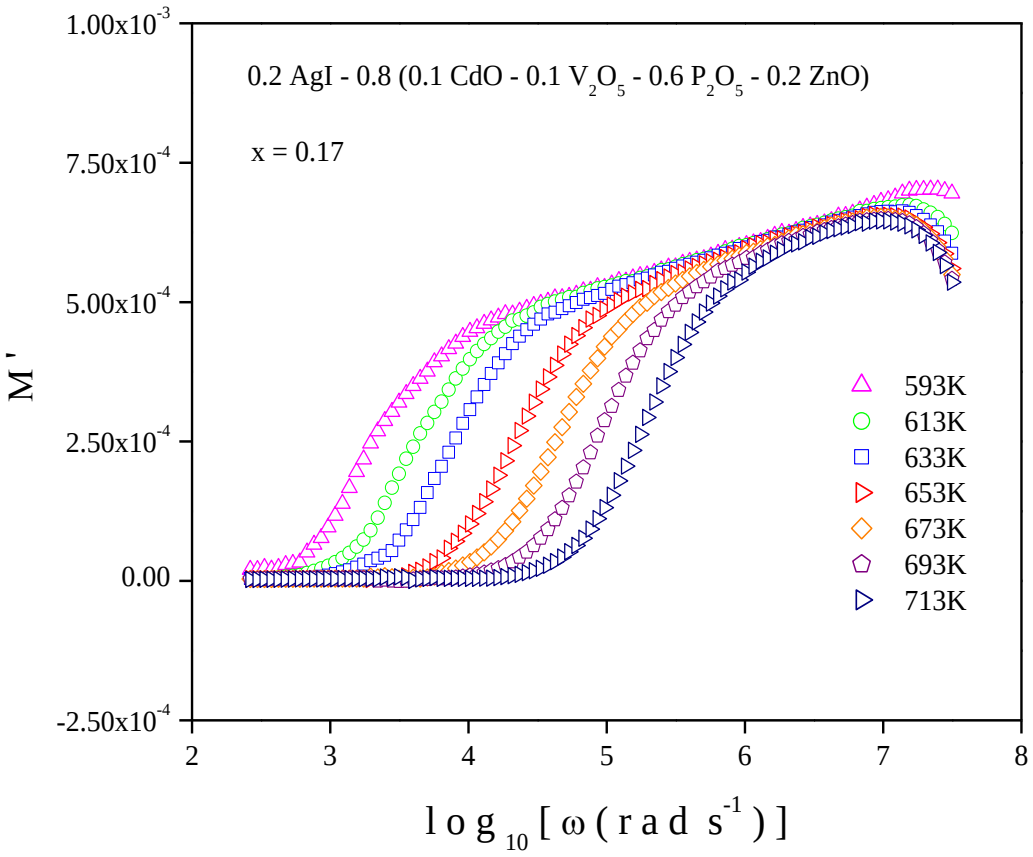

Fig. 4.13 (a) Real Modulus Spectra M/ for x = 0.17

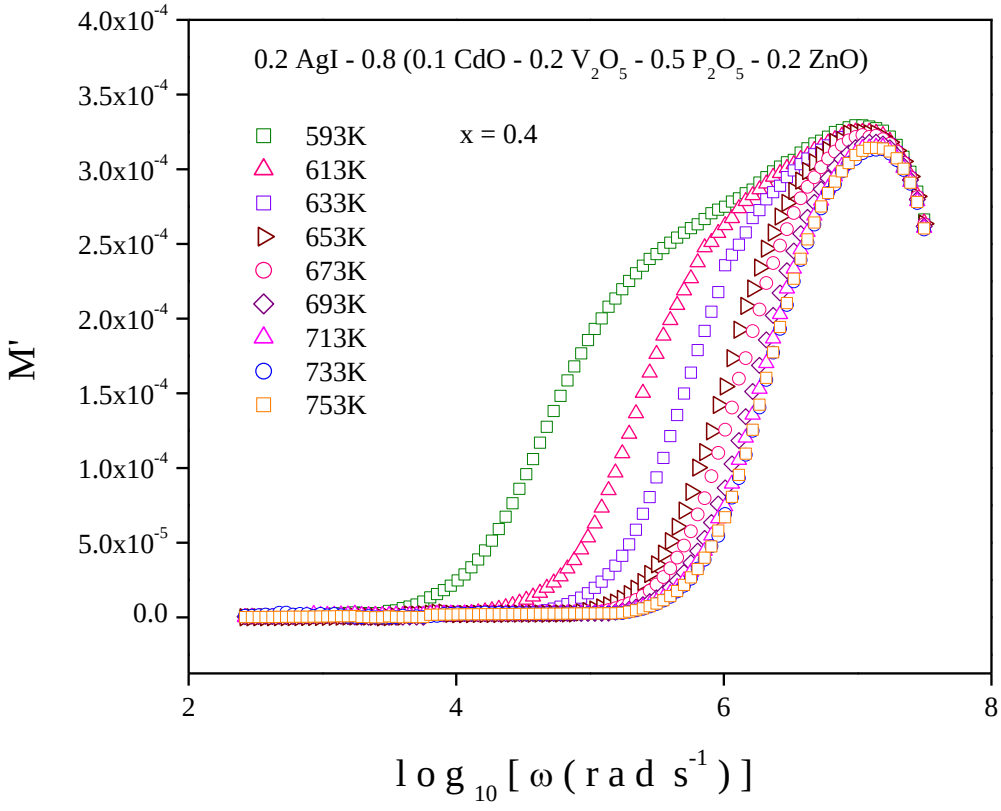

Fig. 4.13 (b) Real Modulus Spectra M/ for x = 0.4

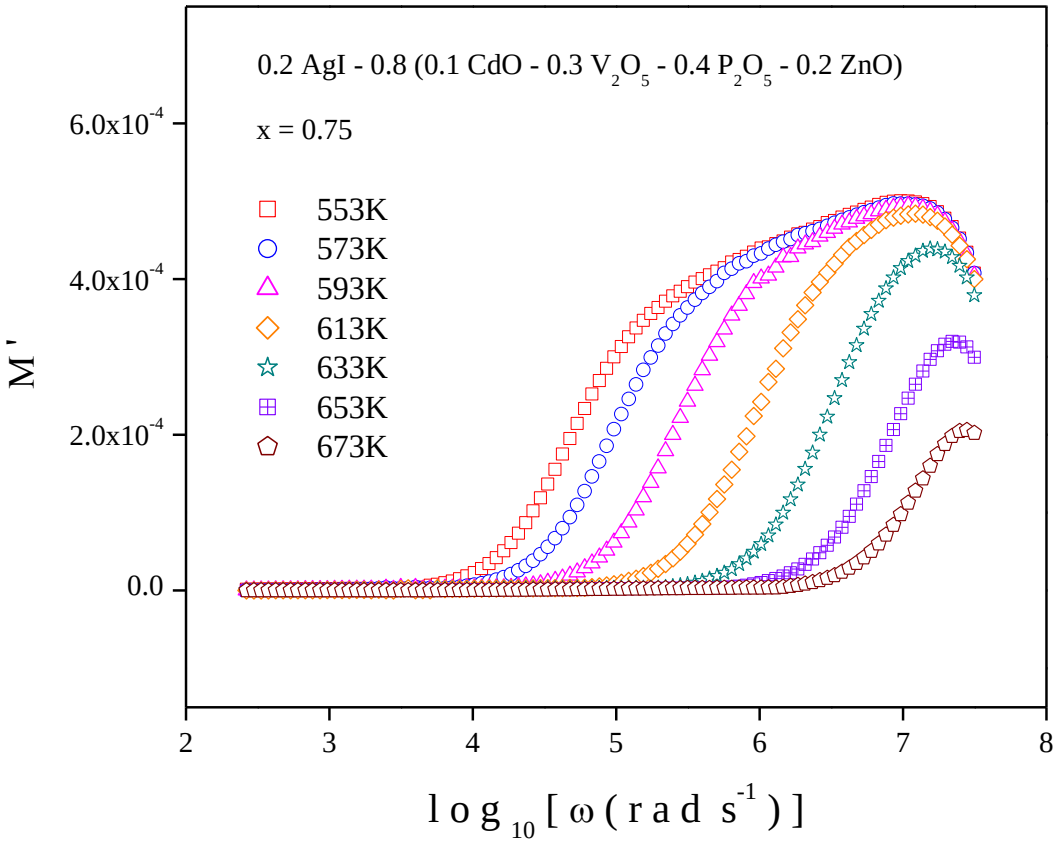

Fig. 4.13 (c) Real Modulus Spectra M/ for x = 0.75

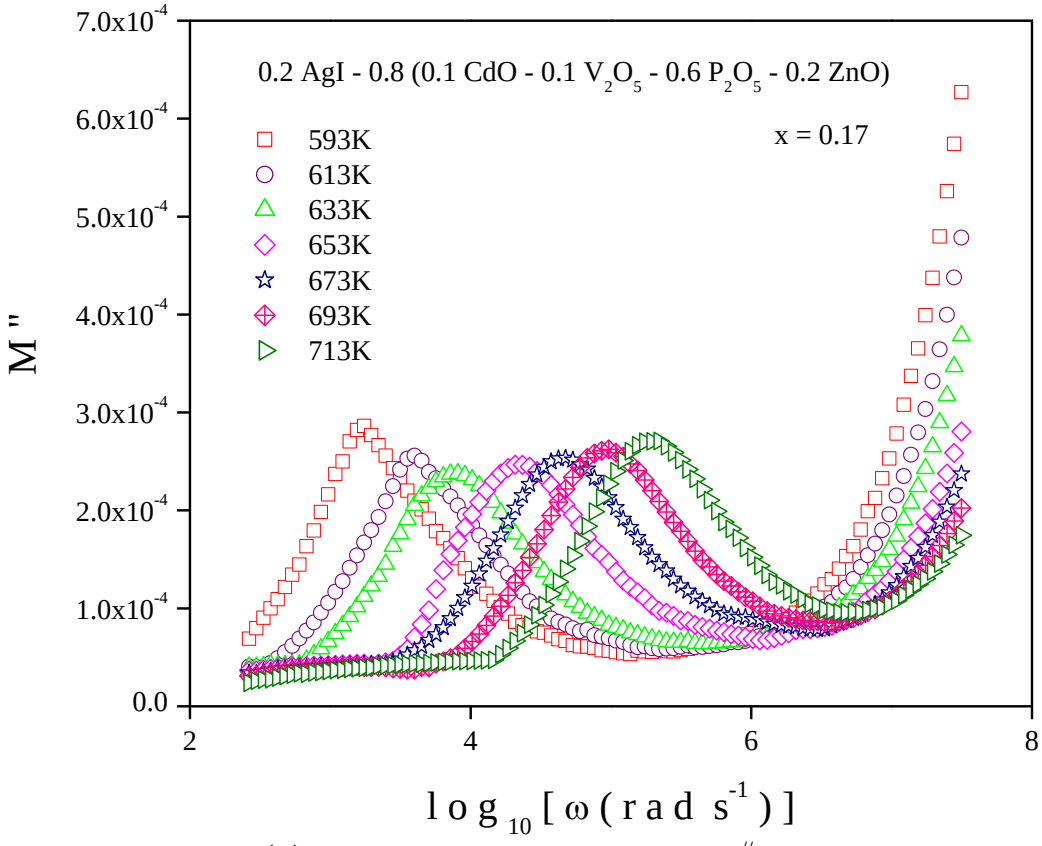

Fig. 4.14 (a) Imaginary Modulus Spectra M// for x = 0.17

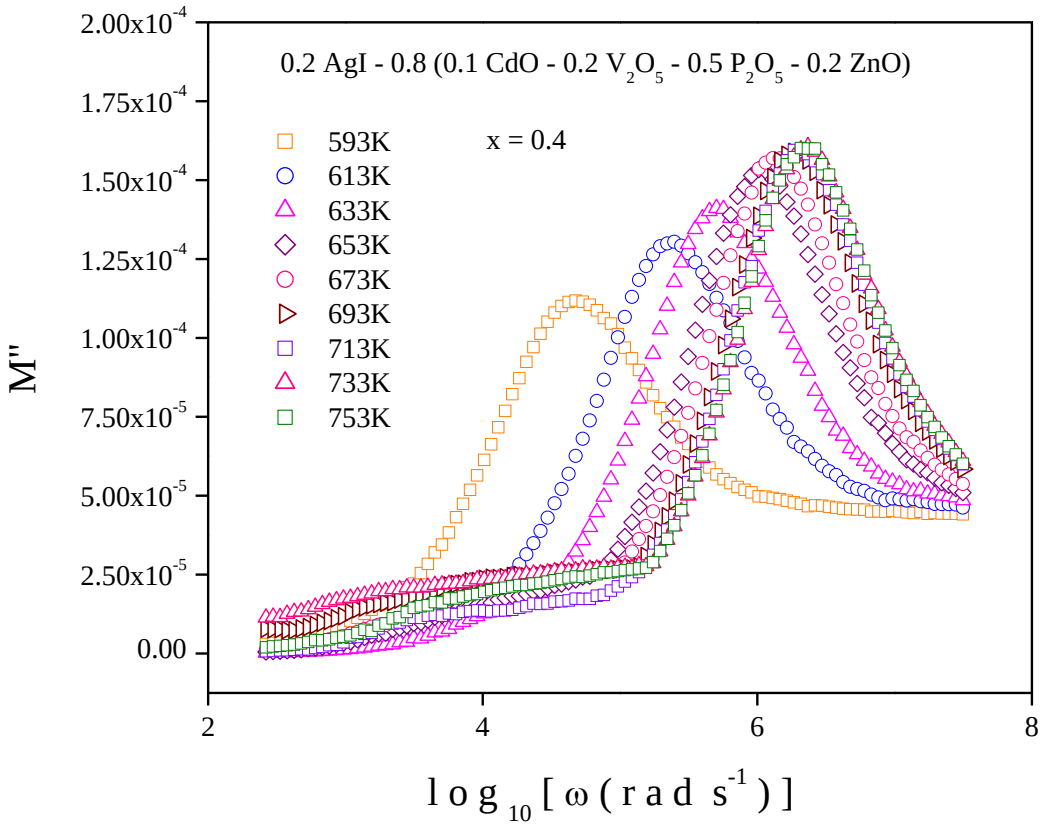

Fig. 4.14 (b) Imaginary Modulus Spectra $M^{//}$ for x = 0.4

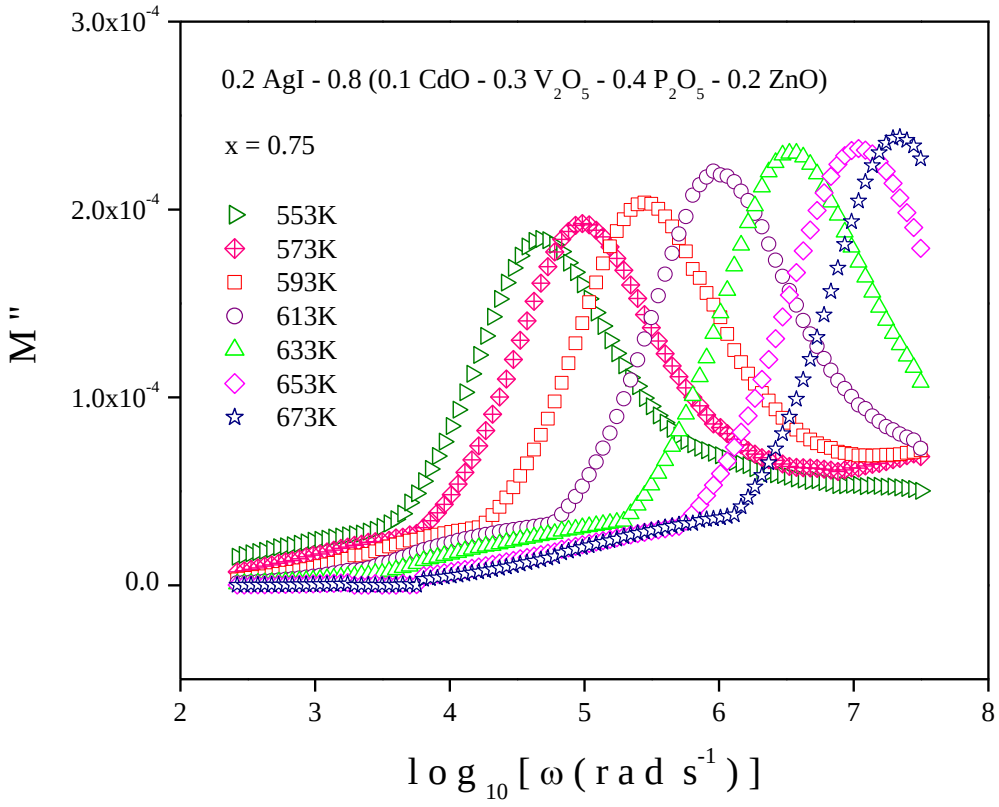

Fig. 4.14 (c) Imaginary Modulus Spectra $M^{//}$ for x = 0.75

The relaxation frequency of the thermally activated charge carriers may be increased by their movement which results in the reduction of the relaxation time. All the samples under study exhibit similar nature of electrical relaxation. Debye type relaxation is assumed for the current systems in order to examine the nature of the conduction process [11,22], which involves the crucial condition: $\omega_c\tau_c = 1$. The assessed value of relaxation time (τ_c) is projected in Table 4.7. Fig. 4.15 clearly displays thermally activated nature of the relaxation time (τ_c). With the increase in temperature, τ_c is found to diminish gradually, which confirms its semiconducting behavior.

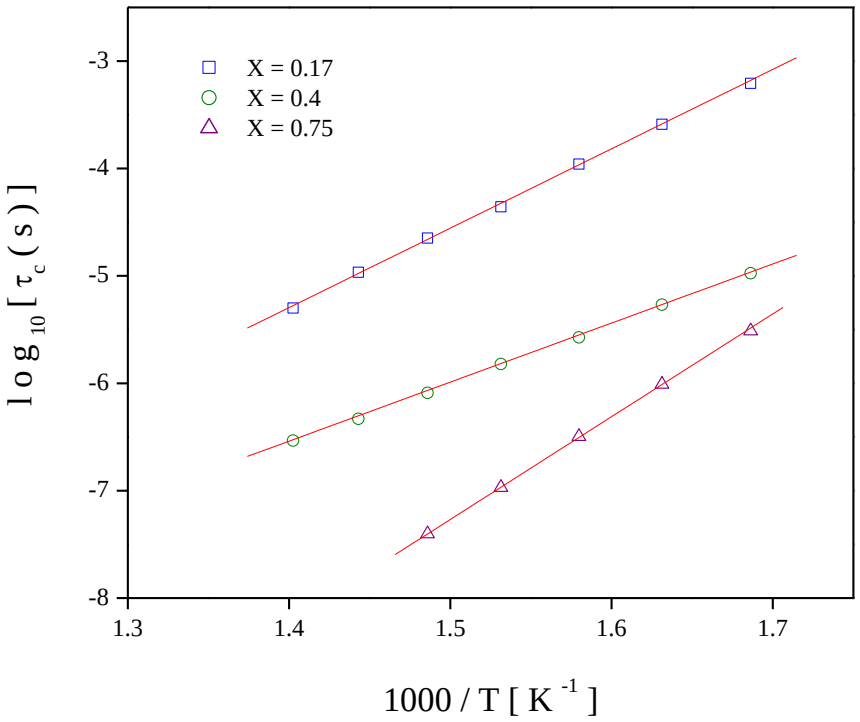

Fig. 4.15 Relaxation time (τ_c) spectra of all the samples at various reciprocal temperatures

It has been observed from the analysis that at a distinct temperature the sample with highest ratio of the mixed formers i.e. x = 0.75, show the highest relaxation frequency and thus possessing lowest relaxation time. Decrease in relaxation time clearly validates the fact of gradual rise in conductivity with the increasing value of the ratio of the mixed former. It concludes that the presence of V_2O_5 has a great positive effect in the electrical conduction of the glassy systems under preparation.

x	Activation Energy for Relaxation Time (E_τ) eV	Avg. Relaxation Time (τ_c), s
0.17	1.4639	1.55×10^{-4}
0.4	1.0888	4.36×10^{-6}
0.75	1.8944	9.85×10^{-7}

Table 4.7: Data of activation energy corresponding relaxation time and average relaxation time corresponding to composition of as-prepared glasses

Eq. 2.31 has been found to be the best linear fit for the experimental data presented in Fig. 4.15. Table 4.7 displays the estimated activation energy (E_τ), which is related to relaxation time, derived from the slopes of the best-fit solid straight lines. E_τ is found to increase and becomes maximum for x = 0.75. Higher activation energies and smaller relaxation times indicate increased conductivity in the system because of the higher rate of polaron hopping. Thus, it could be concluded that mixed formers have a great role to play in the conduction of the samples under consideration.

4.4 CONCLUSION

The glassy nature of the system as synthesised has been conclusively proven in this chapter through structural investigation, especially X-ray diffraction (XRD), which validates the samples' amorphous nature. The findings show that samples change from a crystalline to a glassy state as the percentage of mixed formers rises, emphasising the important role that glass-forming oxides play in altering the structural framework. Additionally, throughout a wide frequency and temperature range, the thermally activated nature of both electrical conductivity and dielectric characteristics has been confirmed, highlighting the impact of thermal energy on charge transport pathways in the oxide glassy system.

One important finding from the AC conductivity research is that, in the higher range, conductivity increases linearly with frequency. This is a typical behaviour of disordered systems where charge transport is dominated by ion or polaron hopping. Additional information is revealed by the Almond-West Formalism, which shows that the system's charge carriers move in a percolation-type manner in which polarons are transported over a network of interconnected sites. This result confirms that thermally induced hopping mechanisms, not long-range organised motion, are responsible for the conductivity in these glassy systems.

Additionally, the study shows that as the ratio of mixed formers grows, so does the activation

energy linked to both the hopping frequency and the relaxation. This implies that the structural dynamics of the glass matrix change with an increase in the secondary glass former (P_2O_5) in comparison to V_2O_5, which affects how easily charge carriers hop between accessible sites. The electrical and dielectric properties of the system are improved by increasing the V_2O_5:P_2O_5 ratio, according to the conductivity and dielectric investigations. The structural function of vanadium oxide, which contributes to electronic conductivity through different oxidation states (e.g., V^{5+}/V^{4+} redox couples) and adds new paths for charge transport, is probably the cause of this enhancement.

In addition to providing a better understanding of the basic charge transport mechanisms in oxide glassy systems, these findings also demonstrate the materials' potential for technological applications in energy storage systems, solid-state ionic devices, and sophisticated electronic components where ideal conductivity and dielectric behavior are required.

References

[1] Satyanarayana, N., Patcheammalle, R., Muralidharan, P., Venkateswarlu, M., & Rambabu, B. (2000). Preparation, characterization and impedance studies of the superionic conducting AgI–Ag2O–CrO3–V2O5 glassy system. Solid state ionics, 136, 1097-1100.

[2] Padmasree, K. P., Kanchan, D. K., Panchal, H. R., Awasthi, A. M., & Bharadwaj, S. (2005). Structural and transport properties of CdI2 doped silver ion conducting system. Solid state communications, 136(2), 102-107.

[3] Kumari, V., Kaswan, A., Patidar, D., Sharma, K., & Saxena, N. S. (2016). Electrical conduction mechanism in GeSeSb chalcogenide glasses. Bulletin of Materials Science, 39, 255-262.

[4] Fernandes, B. J., Ramesh, K., & Udayashankar, N. K. (2019). Crystallization kinetics of Si20Te80− xBix (0≤ x≤ 3) chalcogenide glasses. Materials Science and Engineering: B, 246, 34-41.

[5] Pal, S. K., Kumar, A., & Mehta, N. (2019). Signature of rigidity percolation effect in dielectric behavior of germanium containing multi-component chalcogenide glasses (ChGs). Ceramics International, 45(13), 16279-16287.

[6] Ravagli, A., Naftaly, M., Craig, C., Weatherby, E., & Hewak, D. W. (2017). Dielectric and structural characterisation of chalcogenide glasses via terahertz time-domain spectroscopy. Optical Materials, 69, 339-343.

[7] Zhu, E., Liu, Y., Sun, X., Yin, G., Jiao, Q., Dai, S., & Lin, C. (2019). Correlation between thermo-mechanical properties and network structure in GexS100–x chalcogenide glasses. Journal of Non-Crystalline Solids: X, 1, 100015.

[8] Alemi, A. A., Sedghi, H., Mirmohseni, A. R., & Golsanamlu, V. (2006). Synthesis and characterization of cadmium doped lead-borate glasses. Bulletin of Materials Science, 29, 55-58.

[9] Bhattacharya, S., & Ghosh, A. (2006). Electrical properties of ion conducting molybdate glasses. Journal of applied physics, 100(11).

[10] Almond, D. P., & West, A. R. (1983). Mobile ion concentrations in solid electrolytes from an analysis of ac conductivity. Solid State Ionics, 9, 277-282.

[11] Karmakar, B., Rademann, K., & Stepanov, A. (Eds.). (2016). Glass nanocomposites: synthesis, properties and applications.

[12] Kabi, S., & Ghosh, A. (2010). Polaron conduction in Lix [Ni1/3Mn1/3Co1/3] O2− δ (x= 1, 0.9 and δ=, 0.05) cathodes. Journal of Applied Physics, 107(10).

[13] Bhattacharya, S. (2020). Metal oxide glass nanocomposites. In Metal Oxide Glass Nanocomposites (pp. 27-35). Elsevier.

[14] Almond, D. P., Duncan, G. K., & West, A. R. (1983). The determination of hopping rates and carrier concentrations in ionic conductors by a new analysis of ac conductivity. Solid State Ionics, 8(2), 159-164.

[15] Roling, B., Happe, A., Funke, K., & Ingram, M. D. (1997). Carrier concentrations and relaxation spectroscopy: new information from scaling properties of conductivity spectra in ionically conducting glasses. Physical review letters, 78(11), 2160.

[16] Jonscher, A. K. (1999). Dielectric relaxation in solids. Journal of Physics D: Applied Physics, 32(14), R57.

[17] Ojha, S., Ali, M. S., Roy, M., & Bhattacharya, S. (2021). Hopping frequency and conductivity relaxation of promising chalcogenides: AC conductivity and dielectric relaxation approaches. Materials Research Express, 8(8), 085203.75.

[18] Bhattacharya, S. (2020). AC conductivity behaviour and charge carrier concentrations of some vanadate glassy system. Physics Letters A, 384(16), 126324.

[19] Kundu, R., Roy, D., & Bhattacharya, S. (2017). Microstructure, electrical conductivity and modulus spectra of CdI2 doped nanocomposite-electrolytes. Physica B: Condensed Matter, 507, 107-113.

[20] Qi, K., Cheng, B., Yu, J., & Ho, W. (2017). Review on the improvement of the photocatalytic and antibacterial activities of ZnO. Journal of Alloys and Compounds, 727, 792-820.

[21] Zang, Z. (2018). Efficiency enhancement of ZnO/Cu2O solar cells with well oriented and micrometer grain sized Cu2O films. Applied Physics Letters, 112(4).

[22] Mott, N. F., & Davis, E. A. (2012). Electronic processes in non-crystalline materials. OUP Oxford.

[23] Ahmad-Bitar, R., & Arafah, D. E. (1998). Processing effects on the structure of CdTe, CdS and SnO2 thin films. Solar energy materials and solar cells, 51(1), 83-93.

[24] Hunt, A. (1993). Non-Debye relaxation and the glass transition. Journal of non-crystalline solids, 160(3), 183-227.

[25] Dult, M., Kundu, R. S., Hooda, J., Murugavel, S., Punia, R., & Kishore, N. (2015). Temperature and frequency dependent conductivity and electric modulus formulation of manganese modified bismuth silicate glasses. Journal of Non-Crystalline Solids, 423, 1-8.

[26] Ojha, S., Roy, M., Chamuah, A., Bhattacharya, K., & Bhattacharya, S. (2020). AC conductivity

and dielectric behavior of Cu-S-Te chalcogenide glassy system. Materials Letters, 258, 126792.

[27] Bhattacharya, S., & Ghosh, A. (2008). Relaxation dynamics in superionic glass nanocomposites. Journal of the American Ceramic Society, 91(3), 753-759.

Chapter 5

Study Of Electrical Transport Phenomena in CdI_2 Doped $Ag_2O - V_2O_5 - P_2O_5 - ZnO$ System

Outline

The results presented in this chapter have been published in:

Ionics, 28, 2285–2292 (2022);

Materials Today: Proceedings, 66, Part 7, Pages 3373-3376 (2022).

5.1 INTRODUCTION

The electrical transport mechanisms in AgI-doped glassy systems were examined in the earlier chapters, and it was discovered that the presence of silver ions significantly improved the systems' electrical conductivities. Few studies on silver oxy-salt systems with dopant salts other than AgI such as PbI_2–Ag_2O–V_2O_5 [1], CuI–Ag_2MoO_4 [2], and CuI–Ag_2O–B_2O_3 [3] have also exposed new properties and the viability of high silver ion conductivity at room temperature. The advantages of doping cadmium iodide (CdI_2) in oxy-salt systems, especially in improving electrical conductivity, have been emphasized by the literature review [4–7]. It has been discovered that adding CdI_2 to these systems is essential for altering the ionic transport characteristics and enhancing charge carrier mobility.

This enhancement is ascribed to the structural changes and the development of novel pathways that promote ion migration, which is crucial for maximising the system's total conductivity. Building on this basis, the current work aims to learn more about how charge carriers behave in a system that contains both silver (Ag^+) and cadmium (Cd^+) ions. Given that silver ions are well-known for their exceptional ionic conductivity and great mobility, the coexistence of these two cations creates an intriguing dynamic. In order to better understand the basic processes behind ionic transport and investigate any potential synergistic effects that can result from their cohabitation, this study will methodically examine the interaction between Cd^+ and Ag^+ inside the host matrix. The advancement of high-performance ion-conducting materials, which have great potential for use in solid-state batteries, energy storage devices, and other electrochemical systems, depends on this kind of strategy.

5.2 PREPARATION OF GLASSY SYSTEMS

The extremely pure (Aldrich 99.9%) reagents were used to prepare the glassy system, $xCdI_2 - (1 - x)$ $(0.3\ Ag_2O - 0.3V_2O_5 - 0.3\ P_2O_5 - 0.1\ ZnO)$ with $x = 0.1$ and 0.2 via melt quenching method [8-12]. Every necessary chemical was meticulously weighed in accordance with its determined stoichiometric proportion, as discussed in section 2.3, in an electromechanical analytical balance (Dhona 200D). The powder was then created by thoroughly mixing the materials and pounding them in a mortar. Before being used, the mortar was thoroughly cleaned and rinsed. Following production, the powder was placed into an alumina crucible in an electric furnace. The mixtures were then melted at temperatures between 700 and 800 °C in an electric

furnace, depending on their composition. After 30 minutes of equilibration, the melts were quenched between two aluminum plates. Glassy composites that were around 1 mm thick and somewhat transparent were created using this technique. Using the two-probe technique, measurements were made on samples that were approximately 1 mm thick for the electrical conductivity analysis. Two polished, cleaned, and spring-loaded copper electrodes (manufactured by Joy-Crucible) were placed in contact with the sample inside the sample holder. The Hioki LCR tester (Model No. 3532-50) was then used to perform complex impedance measurements. in the frequency range of 42 Hz to 5 MHz.

5.3 RESULTS AND ANALYSIS

5.3.1 Structural Characterization

The several methods of structural characterizations [13] that have been carried out on the as-prepared samples include determination of Density (ρ) and Molar Volume (V_M), X-ray Diffraction (XRD) and Fourier Transform Infrared (FT-IR) Spectroscopy.

5.3.1.1 Measurement of Density and Molar Volume

The Archimedes principle, which is described in section 2.4.1, was used to measure the density (ρ) and molar volume (V_M) of the as-prepared glass nano-composite. Acetone with ρ_b = 0.7845 gm/cm^3 has been used as the buoyant liquid in the investigation, which was carried out using Eq. 2.1 and 2.2. A mechanical balance (Dhona, Model: 200D) was used to record the weights of the as-prepared samples (W_a and W_b) with a precession of 0.0001 gm. All of the measurements were taken at room temperature.

The calculated values of ρ and V_M of this oxide glassy system is recorded in Table 5.1 and Fig. 5.1 shows the variation of density and molar volume with the increase in concentration of CdI_2 in the system.

Composition (x)	Density, ρ (g/cc) (± 0.1)	Molar volume, V_M (cc/mol) (± 0.1)
0.1	4.069	54.824
0.2	4.351	53.318

Table 5.1: ρ and V_M of the as-prepared systems for different values of x

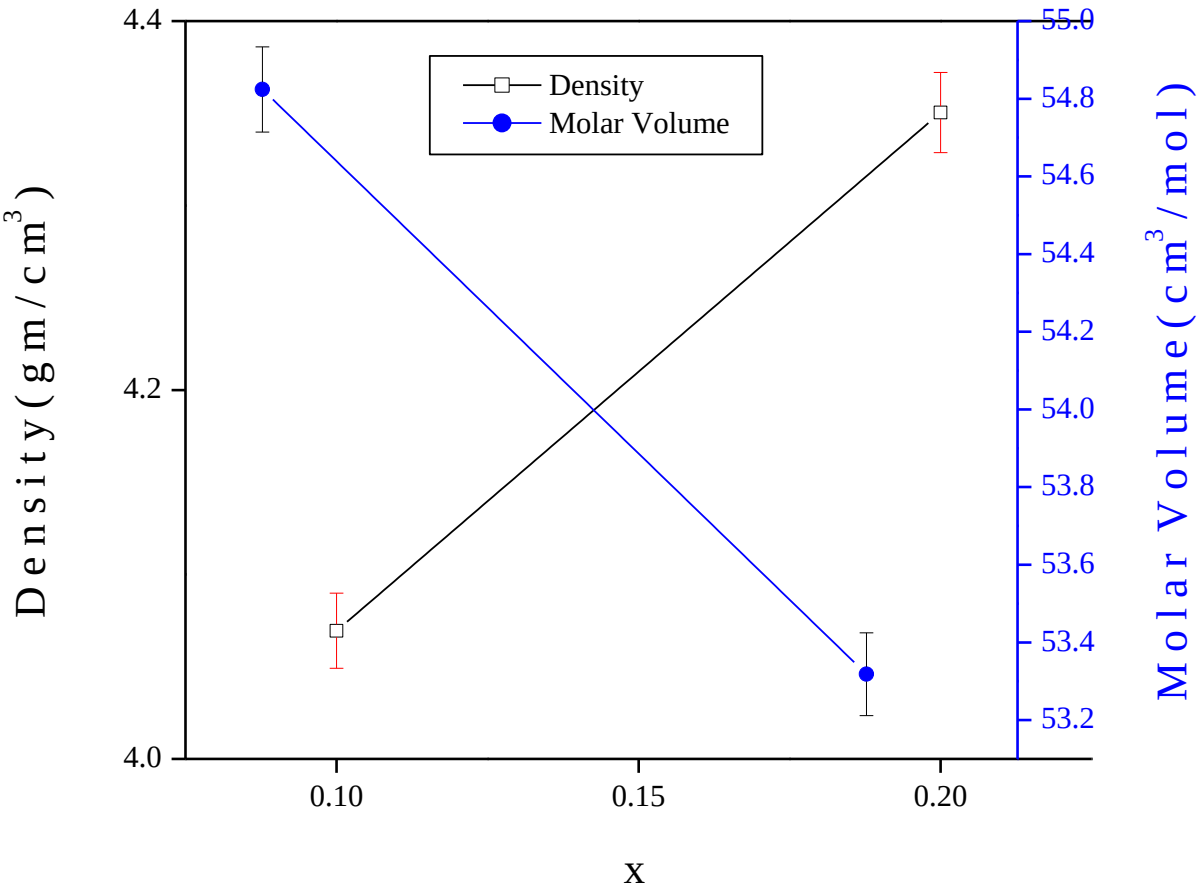

Fig. 5.1 Variation of density and molar volume for different values of x

It is evident from Fig. 5.1 that density rises with composition. As the composition's CdI_2 content gradually rises, a gradual increase in density may be an obvious indication of the current system's increasing compactness. This outcome would suggest that the current system's nature is less porous. However, as composition rises, the molar volume of the current system decreases, as seen in Fig. 5.1. The nature of the current glassy system, the quantity of

ions or molecules present, and the manner in which they can enter the glass network can all affect its density because it is a mixture of the constituent oxides.

5.3.1.2 X-ray Diffraction (XRD)

The prepared samples were subjected to the X-ray diffraction (XRD) analysis, which is outlined in section 2.4.2, in order to examine their structural properties. A key indication of the samples' amorphous nature is the large hump in the diffraction pattern, which suggests there is no long-range periodic atomic structure. This characteristic hump usually indicates the existence of a disordered or glassy phase, in which there is no clear crystalline order in the atomic arrangement. The lack of prominent and strong diffraction peaks indicates that long-range crystallinity is either completely suppressed or barely present. It is also possible, however, that some nanoscale crystalline phases exist inside the amorphous matrix but are not clearly visible in the XRD examination.

The orientation of these nanocrystalline domains may be the cause of this, as the generated crystallographic planes may not be orientated in a way that is favourable for X-ray diffraction to occur. As a result, their diffraction signatures may be under-represented or entirely absent in the patterns that are recorded [14–16]. The suppression of different diffraction peaks may also be caused by strain, defects, and the potential existence of extremely disordered interfacial regions between nano-phases. Because it can affect material properties like ionic conductivity, mechanical flexibility, and optical transparency, such an amorphous structure is particularly interesting for a variety of applications. As a result, these samples may be used in advanced technological applications such as solid electrolytes, optical materials, and energy storage devices.

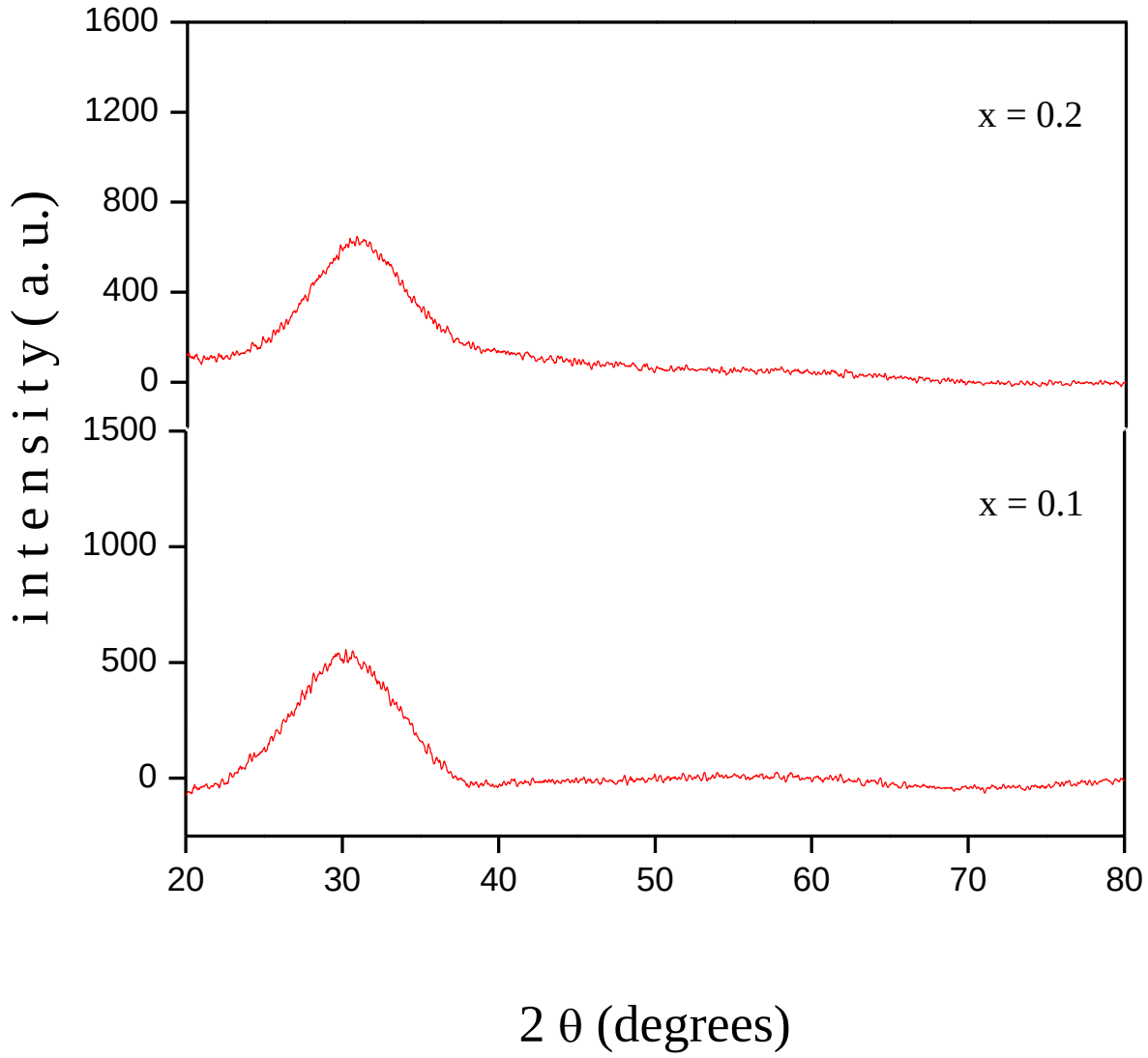

Fig. 5.2 X-ray diffractograms of the glass nano-composites with different values of x

5.3.2 Electrical Conductivity Study

Through DC and AC conductivity investigations, the impact of CdI2 on the electrical conductivity of the as-prepared samples has been methodically investigated. In order to enhance ion migration through the system, it is expected that the addition of CdI_2 will alter the structural framework or provide additional charge carriers. By examining the effects of CdI_2 on the dielectric response and impedance characteristics, these studies offer a greater understanding of charge carrier transport at different time scales.

5.3.2.1 DC Conductivity Study

Complex impedance plots [17] for all the samples, shown in the Fig. 5.4, have been used to calculate the dc electrical conductivity (σ_{dc}). Fig. 5.3 illustrates how the dc conductivity varies with temperature. All of the samples exhibit thermally activated nature in their dc conductivity. As the temperature rises, it is observed to rise as well. It exhibits variation of the Arrhenius type, as discussed in section 2.5.1. The complex impedance plots for all the as-prepared samples are shown in Fig. 5.3 (a) – (b). As can be seen, all of the curves are semicircular in shape, and the diameter of each curve can be used to estimate the corresponding DC conductivity [17]. Additionally, Fig. 5.3 makes it evident that there is no extra spur in any of the plots, indicating that the current system does not have a grain boundary impact [17]. The bulk resistivity is larger for x = 0.2 compared to x = 0.1, which is noteworthy. It may be because of intermolecular adjustment.

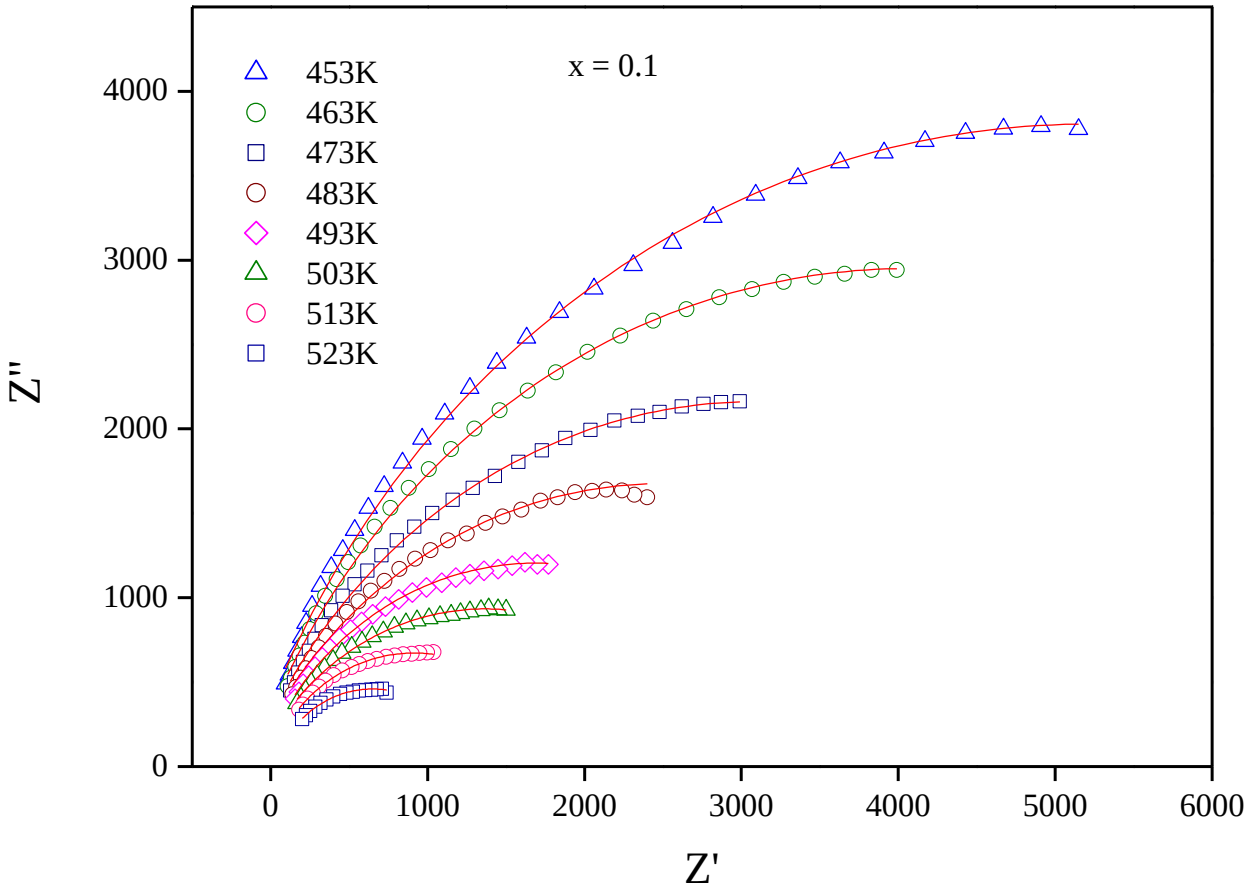

Fig. 5.3 (a) Complex impedance plot for x = 0.1 at various temperatures

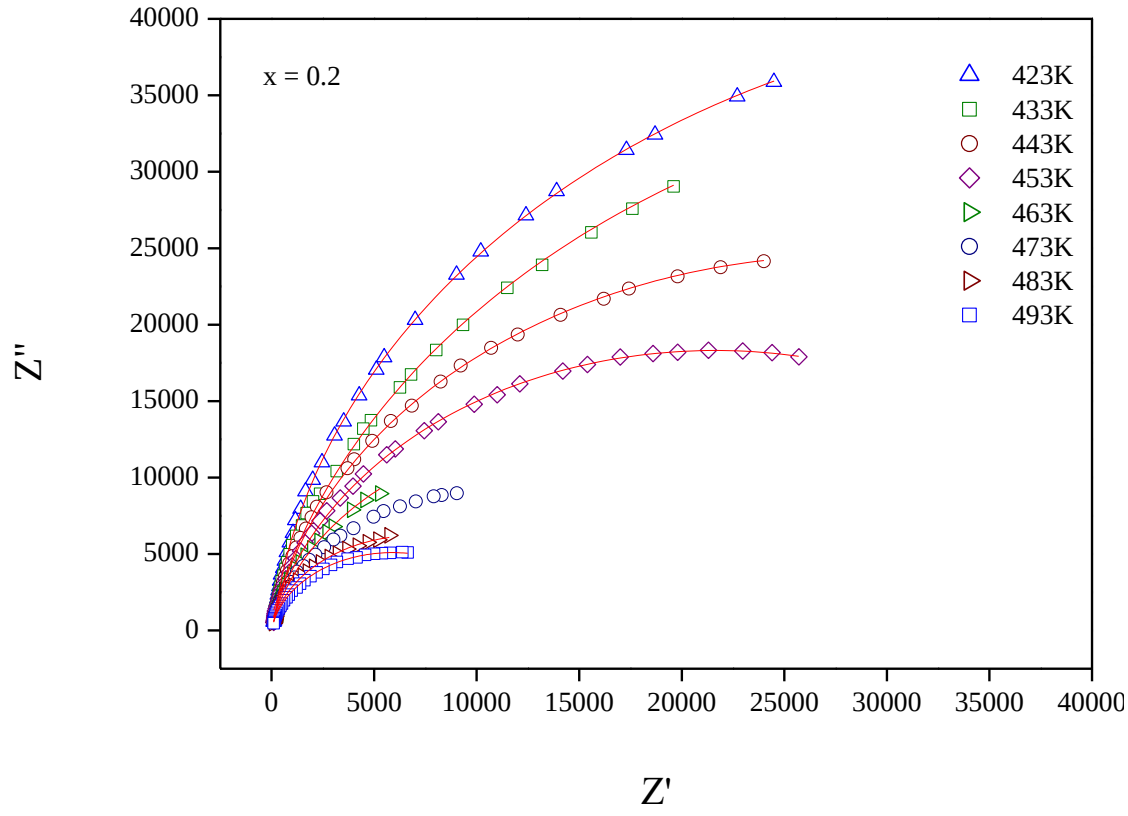

Fig. 5.3 (b) Complex impedance plot for x = 0.2 at various temperatures

DC conductivity [17] has been calculated from the measured values of DC resistivity estimated from Fig. 5.3 (a)–(b), DC conductivity [17] has been computed. As shown in Fig. 5.4, the DC conductivity of the produced sample is plotted against reciprocal temperature. It is evident that the DC conductivity of the present glassy system progressively rises as the dopant salt concentration does. The best way to fit this data and determine the activation energy (E_{dc}) from Fig. 5.4 is to use the Arrhenius relation, which is provided by Eq. 2.8. Table 5.2 shows that the activation energy required decreases as the salt concentration rises.

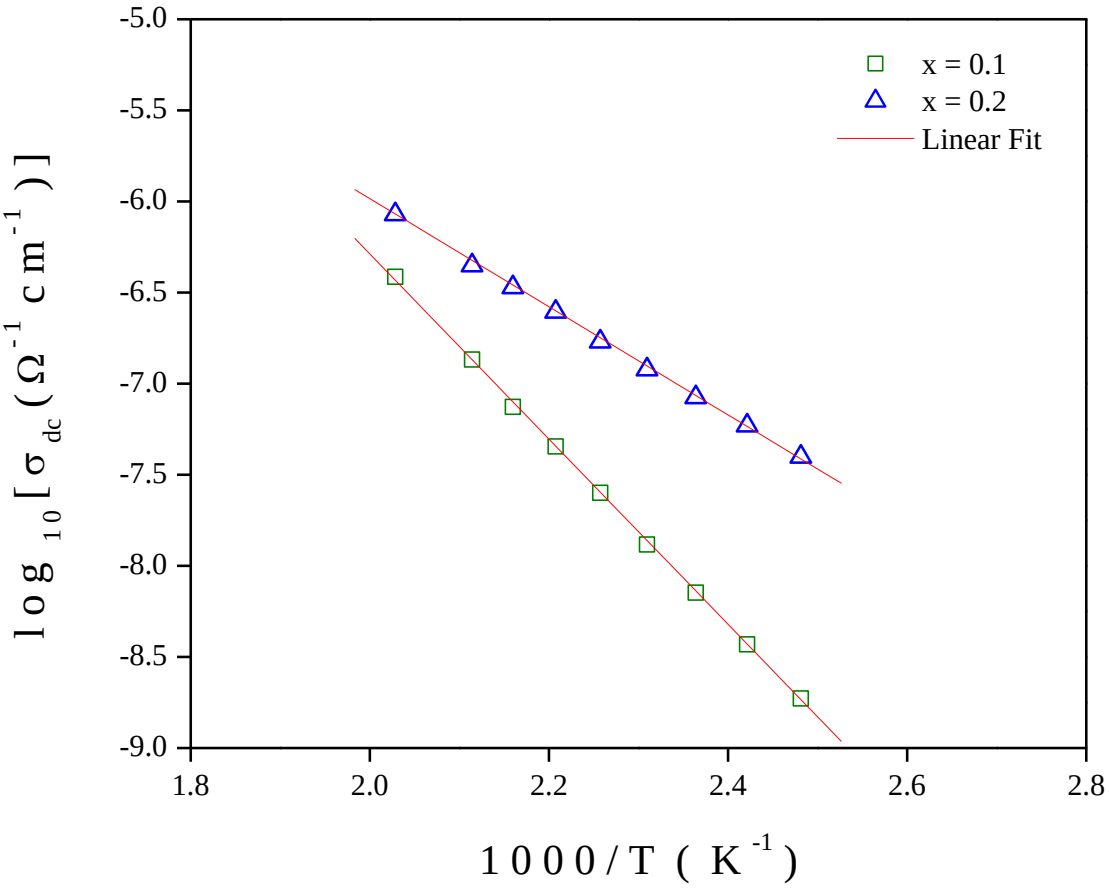

Fig. 5.4 DC conductivity plot for all x with reciprocal temperatures

Composition (x)	Activation Energy due to DC Conductivity, E_{dc} (eV)	Activation Energy due to Hopping Frequency, E_h (eV)
x = 0.1	1.01	2.27
x = 0.2	0.58	1.36

Table 5.2: Data of Activation energy corresponding to DC conductivity (E_{dc}) and Hopping frequency (E_h) corresponding to composition of as-prepared glasses

5.3.2.2 AC Conductivity Study

The AC conductivity spectra of the current glassy system has been studied in the frequency range (42 Hz to 5 MHz) at different temperatures for all the x and are shown in Fig. 5.5 (a) - (b). It is discovered that the nature of ac conductivity variation is identical to that of DC conductivity variation. It has been seen that the conductivity flattens out at low frequencies.

The DC conductivity is equivalent to this frequency-independent conductivity [15–16]. The diffusion of Ag^+ ions may be the cause of this kind of conductivity-independent behavior in the low-frequency range. Above hopping frequencies, the AC conductivity exhibits dispersion and has a power law behavior. This dispersion in the higher frequency range suggests that the Ag^+ ions are moving in a correlated and sub-diffusive manner. The literature [16,18] makes it clearly apparent that this correlated motion results from inter-ionic contact, which alters the power law exponent with ion concentration.

For the purpose of gathering enough information related to the electrical conduction in the system, AC conductivity spectra were fitted using the Almond West formalism, Eq. 2.16. The calculated parameters σ_{dc}, ω_H and n are tabulated in Table 5.3 – 5.4.

x	T(K)	σdc ($W^{-1}cm^{-1}$)	ω_H (rad s^{-1})	n
0.1	373	2.56 x10^{-09}	4.023	0.521
	383	7.42 x10^{-09}	0.107	0.48489
	393	1.11 x10^{-09}	0.094	0.46759
	403	3.51 x10^{-09}	0.103	0.41847
	413	1.65 x10^{-09}	0.019	0.43604
	423	4.70 x10^{-09}	0.478	0.47609
	433	1.81 x10^{-09}	0.105	0.50597
	443	1.11 x10^{-09}	5.146	0.52701
	453	3.62 x10^{-08}	51.157	0.54527
	463	7.03 x10^{-08}	225.772	0.57635
	473	1.65 x10^{-07}	1128.735	0.60777
	483	2.62 x10^{-07}	2172.538	0.62022
	493	5.39 x10^{-07}	4278.375	0.60379
	503	8.55 x10^{-07}	4033.724	0.55749
	513	1.26 x10^{-06}	4832.228	0.54622
	523	1.67 x10^{-06}	4317.95	0.5444

Table 5.3: Parameters obtained from Almond West fitting of x = 0.1

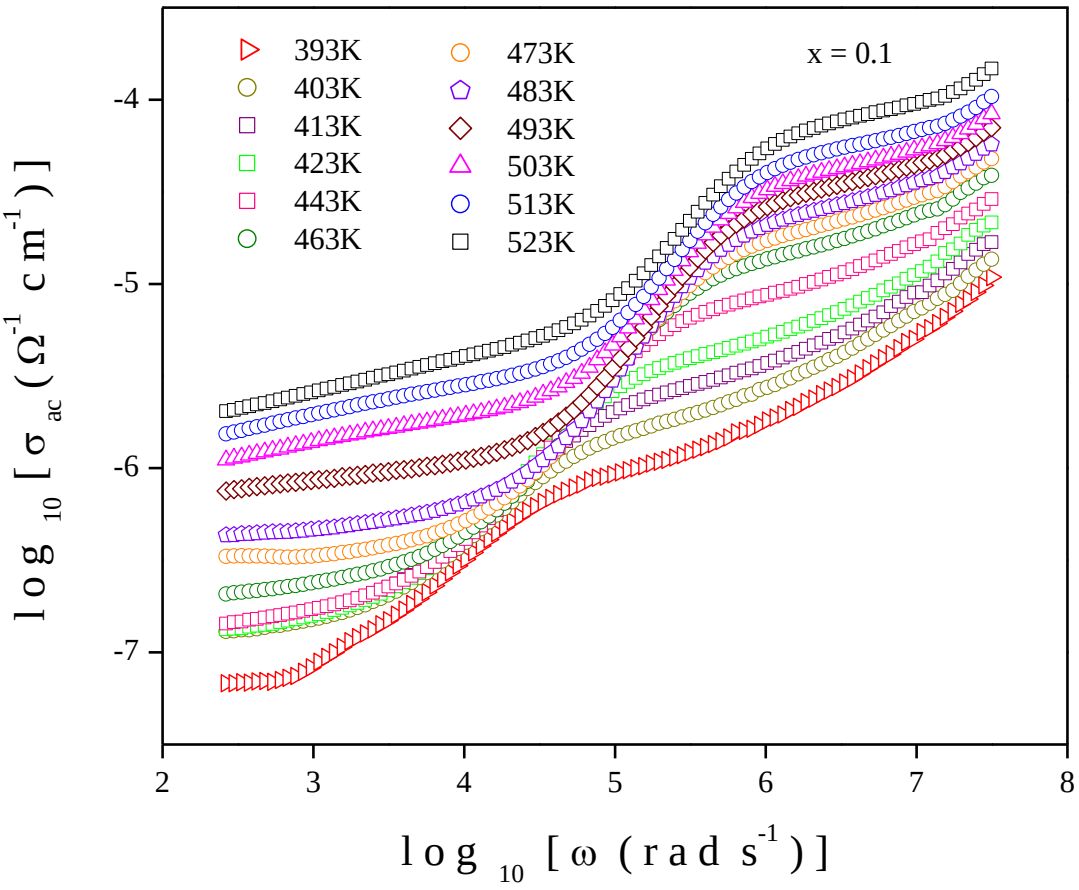

Fig. 5.5 (a) AC conductivity plot for x = 0.1 at various temperatures

x	T(K)	σdc ($W^{-1}cm^{-1}$)	ω_H (rad s^{-1})	n
0.2	403	7.44×10^{-08}	156913.917	0.85493
	413	1.07×10^{-07}	170450.3718	0.80898
	423	1.43×10^{-07}	192299.4458	0.77725
	433	1.93×10^{-07}	148486.8639	0.69146
	443	1.96×10^{-07}	64958.96986	0.58769
	453	2.59×10^{-07}	48705.69001	0.53221
	463	5.51×10^{-07}	137919.6267	0.49274
	473	6.84×10^{-07}	81052.03212	0.41689
	493	7.22×10^{-07}	34704.88254	0.40972

Table 5.4: Parameters obtained from Almond West fitting of x = 0.2

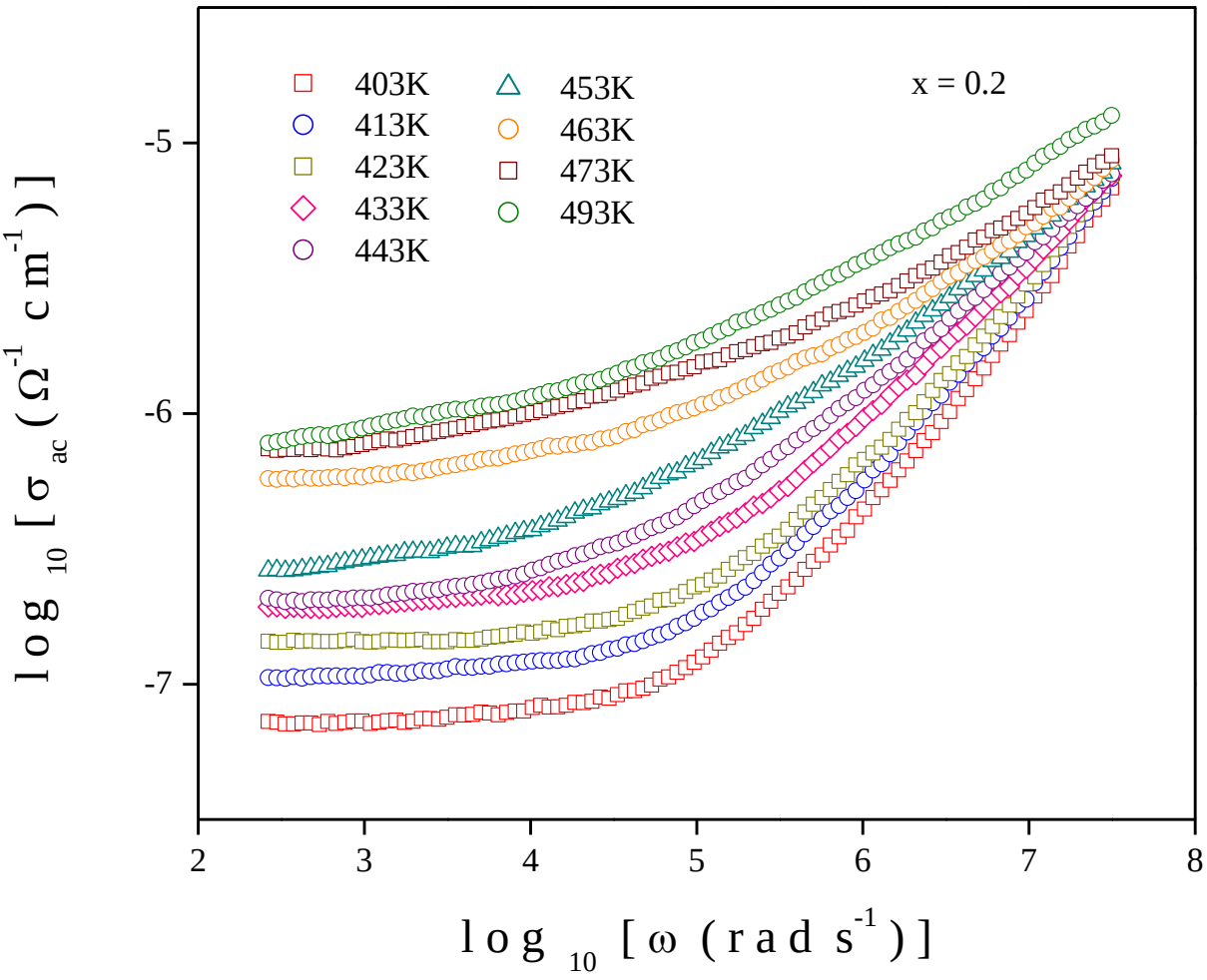

Fig. 5.5 (b) AC conductivity plot for x = 0.2 at various temperatures

The hopping frequency plays a vital role in the electrical conductivity as already discussed in previous chapters. Fig. 5.6 shows the variation of crossover or hopping frequency (ω_H) with temperature. It is clear that ω_H shows thermally activated nature. Table 5.2 displays the estimated activation energies (E_h) corresponding to crossover frequencies based on the best fits. The activation energy associated with ω_H is nearly identical to that of E_σ. This finding clearly shows that the current system's electrical conductivity is mostly regulated by the hopping frequency.

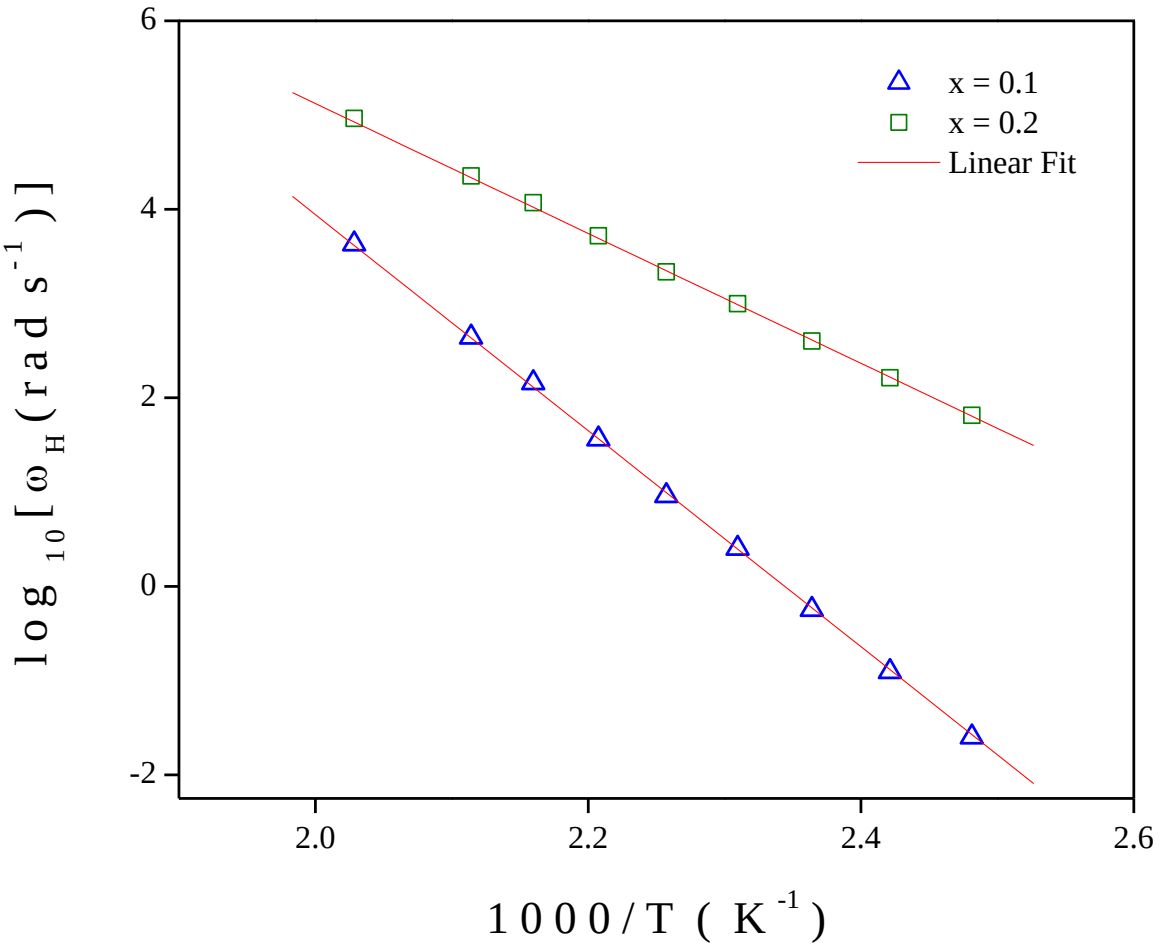

Fig. 5.6 Hopping or Crossover frequency plot for all x at various temperatures

Fig. 5.7 plots the anticipated values of the frequency exponent (n) against temperature. The values of n, range from 0.4 to 0.9 and vary with rising temperatures, indicating a composition-dependent non-linear hopping motion [15]. A variety of relaxation processes can be directly linked to the way that n varies with temperature. The magnitude of n and an ion diffusion mechanism in the glassy matrix may both influence the AC conductivity [15].

It can also be anticipated that the current values of dimensionality will be linked to the materials' growing grade of disorder. Higher values of the current system's frequency exponent (n) allow for the percolation motion of long-range Ag^{+} ion transport, which is of academic interest and technological significance from an application standpoint.

5.3.3 Dielectric Property study

The effect of CdI_2 doping on the electrical relaxation process of the system can be understood by studying dielectric properties of the samples. For the purpose of investigations on dielectric properties, study of electrical permittivity and electric modulus have been carried out here.

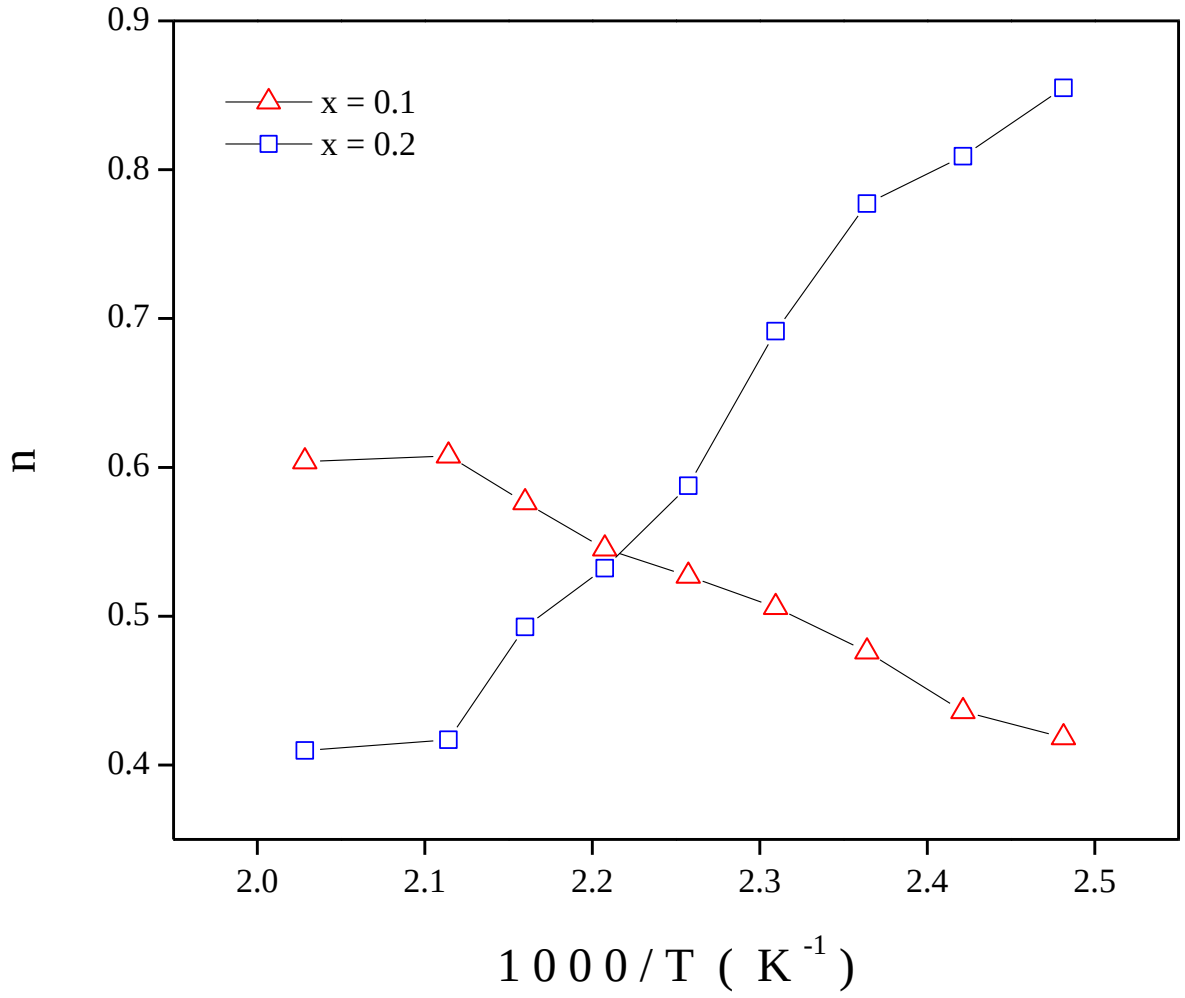

Fig. 5.7 Frequency exponent (n) with temperature

5.3.3.1 Study of electrical permittivity

The study of electrical permittivity has been done in the frequency range of 42 Hz to 5 MHz. It involves the exploration of variation in the dielectric constant ($\varepsilon^{/}$) and dielectric loss ($\varepsilon^{//}$). Fig. 5.8 (a) – (b) present the plots of $\varepsilon^{/}$ of the sample against frequency for all x at various temperatures. Likewise, Fig. 5.9 (a) – (b) present the plots of $\varepsilon^{//}$ of the sample against frequency for all x at various temperatures. Figures 5.8 and 5.9 show an exponential drop in both $\varepsilon^{/}$ and $\varepsilon^{//}$ as the frequency increases at varying temperatures. At lower frequencies, the

dielectric constant is higher because of electrode polarization caused by the buildup of space charges at the glass-electrode interface [19]. Since the system's molecular dipoles are unable to keep up with the electric field's rapid fluctuations, the effect of polarization diminishes as frequency rises. As a result, both $\varepsilon^{/}$ and $\varepsilon^{//}$ begin to drop and exhibit frequency independence as the system's frequency goes up.

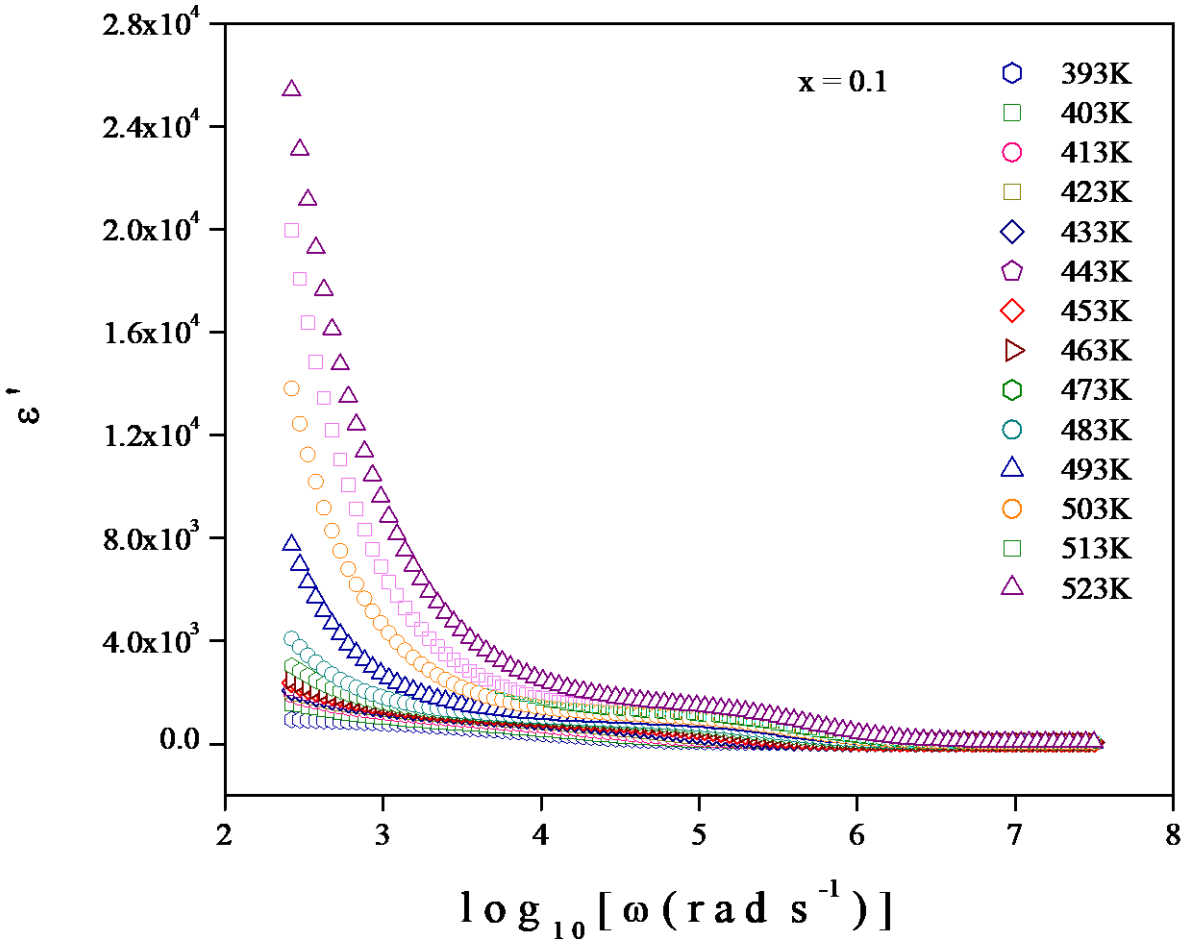

Fig. 5.8 (a) Spectra of dielectric constant $\varepsilon^{/}$ for x = 0.1

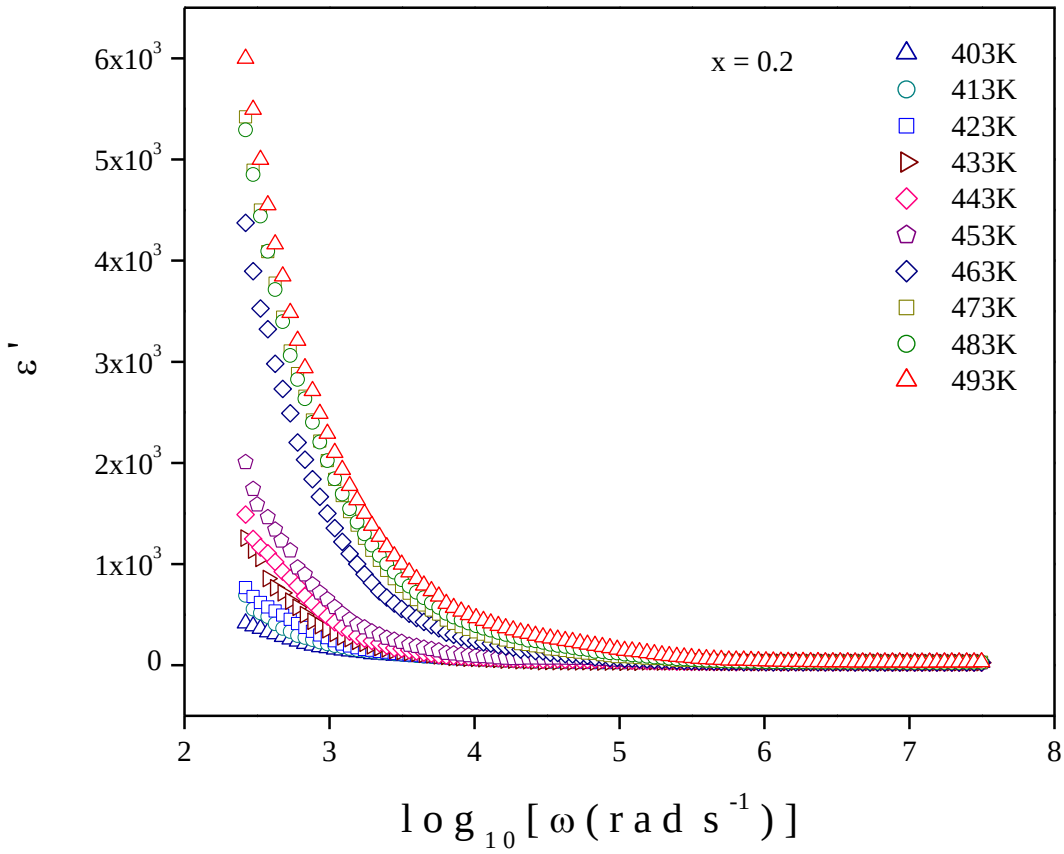

Fig. 5.8 (b) Spectra of dielectric constant $\varepsilon^{/}$ for x = 0.2

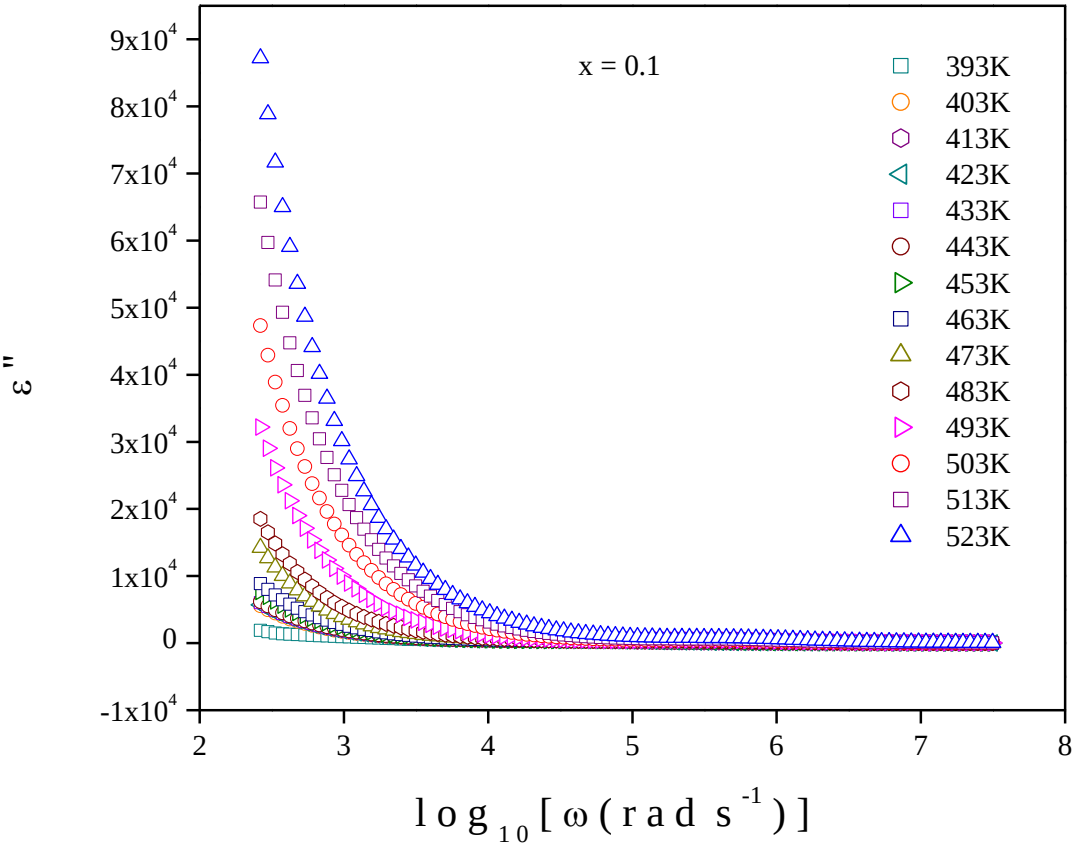

Fig. 5.9 (a) Spectra of dielectric loss $\varepsilon^{//}$ for x = 0.1

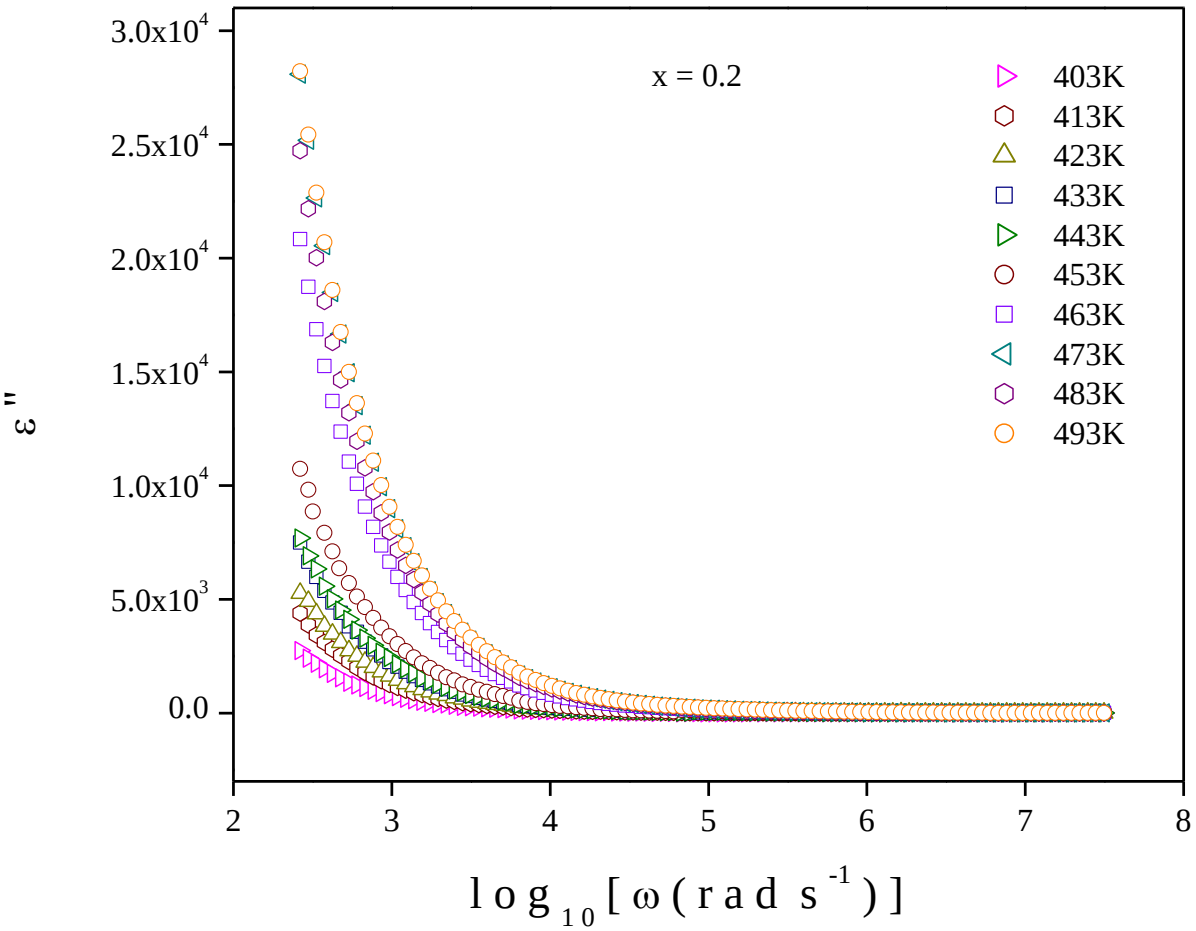

Fig. 5.9 (b) Spectra of dielectric loss $\varepsilon^{//}$ for x = 0.2

Both $\varepsilon^{/}$ and $\varepsilon^{//}$ increase with temperature rise, as shown in Figs. 5.8 and 5.9. This happens primarily because of the escalation in system's polarization effect due to a decrease in bond energies. It happens so as the intermolecular interactions weakens with rise in temperature. This also enhances orientational vibrations. It can also be noted that both $\varepsilon^{/}$ and $\varepsilon^{//}$ grow as x decreases in the current system's composition. This is a clear indication of higher conductivity which has already been confirmed from electrical conductivity studies.

5.3.3.2 Study of electric modulus

The real $M^{/}$ component of the electric modulus against frequency of the current glassy system are displayed in Fig. 5.10 (a) - (b). In the low frequency zone, $M^{/}$ approaches zero at all the temperatures shown in Fig. 5.10. This is mostly due to the suppression of electrode polarization caused by the lack of restoring forces of charge carriers (polarons) [20-21]. However, dispersion in $M^{/}$ has been discovered at higher frequencies, and due to the electrical relaxation of polaron, $M^{/}$ exhibits a maximum value, which is $(M) = (\varepsilon)^{-1}$ [20-21]. Fig. 5.10 shows a

progressive drop in $M^{/}$ as the temperature rises, which may indicate that the system's conduction mechanism involves the mobility of polaron in a limited range.

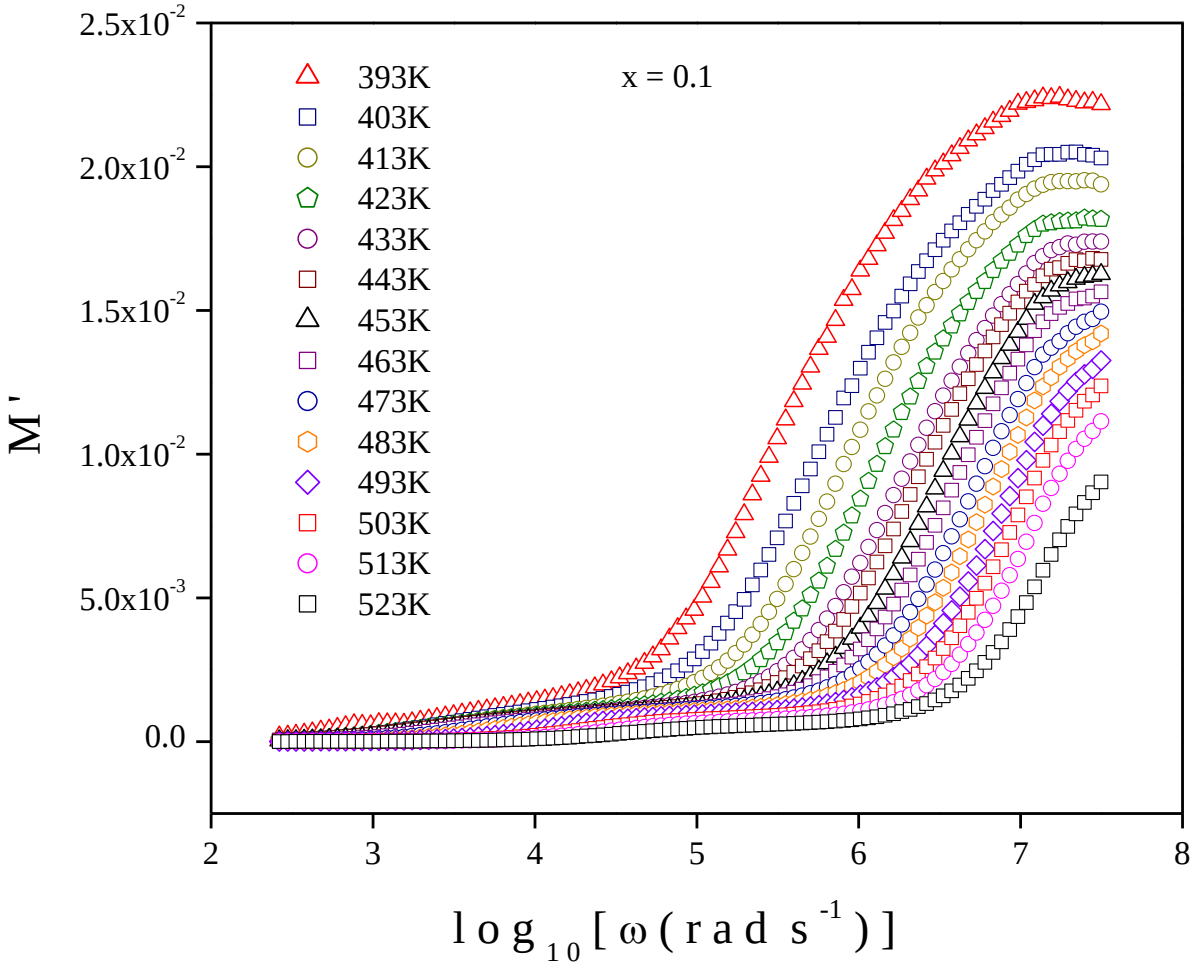

Fig. 5.10 (a) Spectra of $M^{/}$ for x = 0.1

Graphs of the imaginary $M^{//}$ component of the electric modulus against frequency are displayed in Fig. 5.11 (a) - (b). As the temperature rises, it can be seen that the $M^{//}$ peaks move towards higher frequencies, indicating a temperature-dependent relaxation process in the system. The flow of thermally activated charge carriers may shorten the duration of relaxation and increase its frequency. The conduction in these glasses below the peak relaxation frequency ω_c could be due to polaron hopping across long distances. The localized motion of charge carriers over small distances may be the cause of the conduction mechanism above ω_c [21-22]. The shifting of the $M^{//}$ peak indicates that the system stabilizes rapidly for an external force at a high temperature.

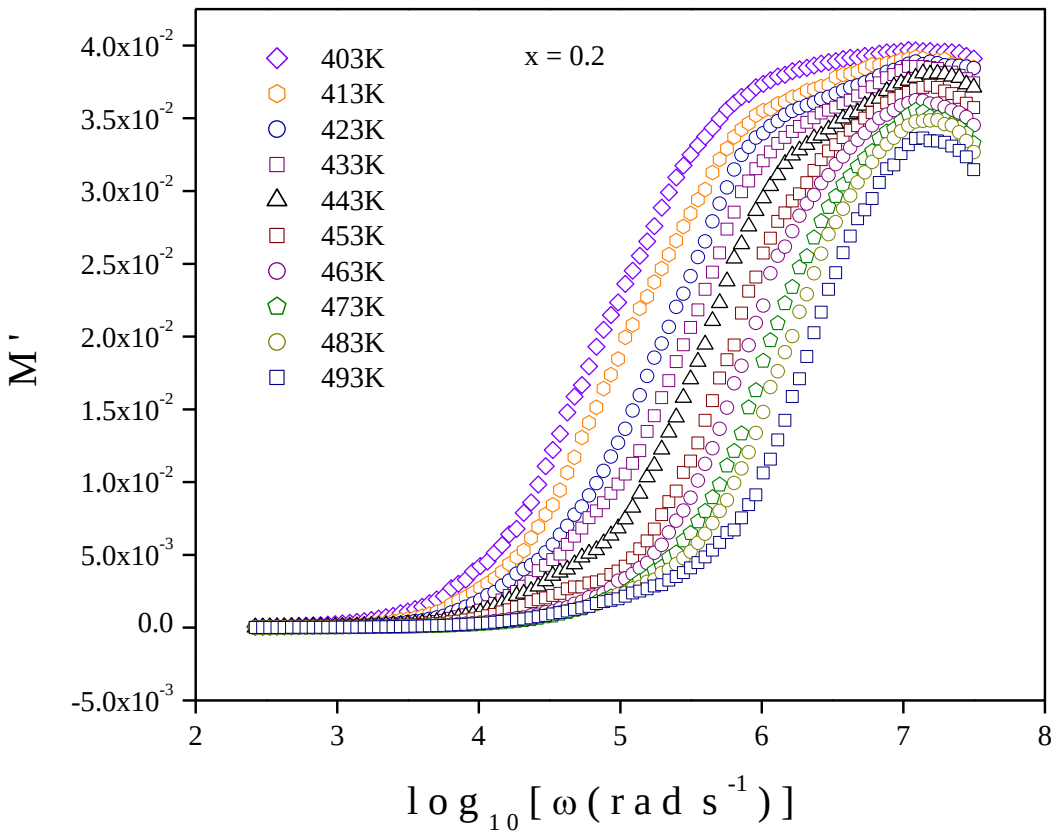

Fig. 5.10 (b) Spectra of M/ for x = 0.2

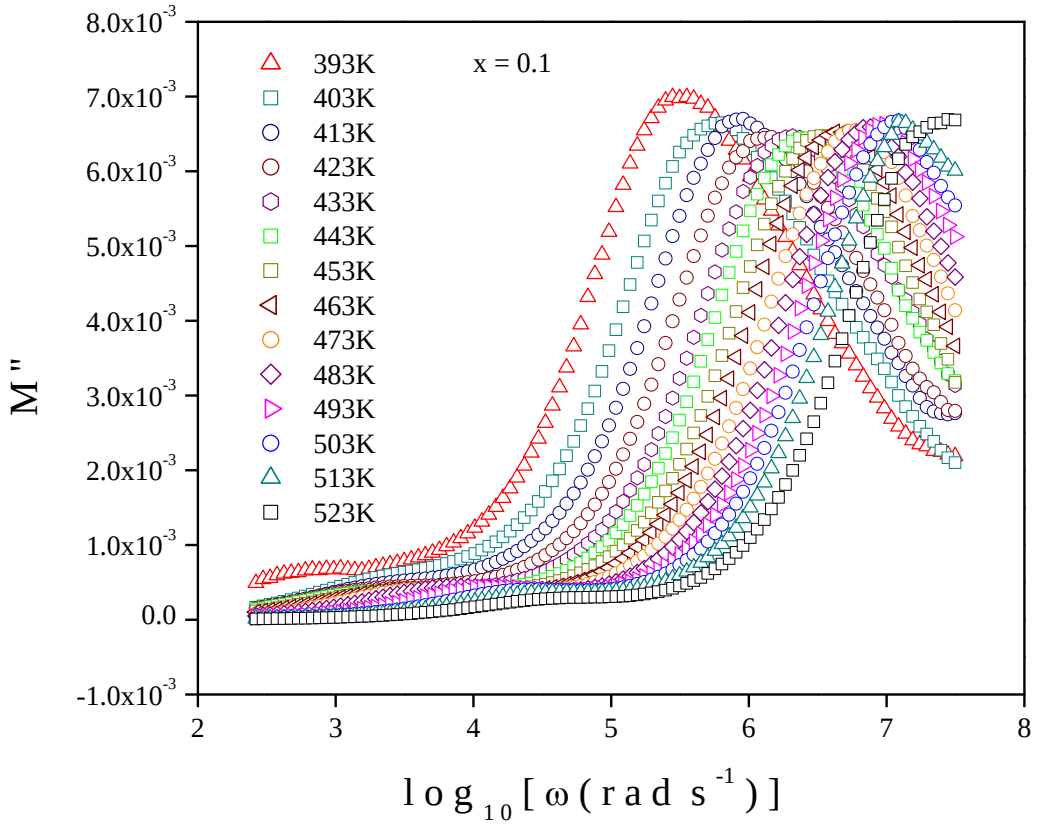

Fig. 5.11 (a) Spectra of M// for x = 0.1

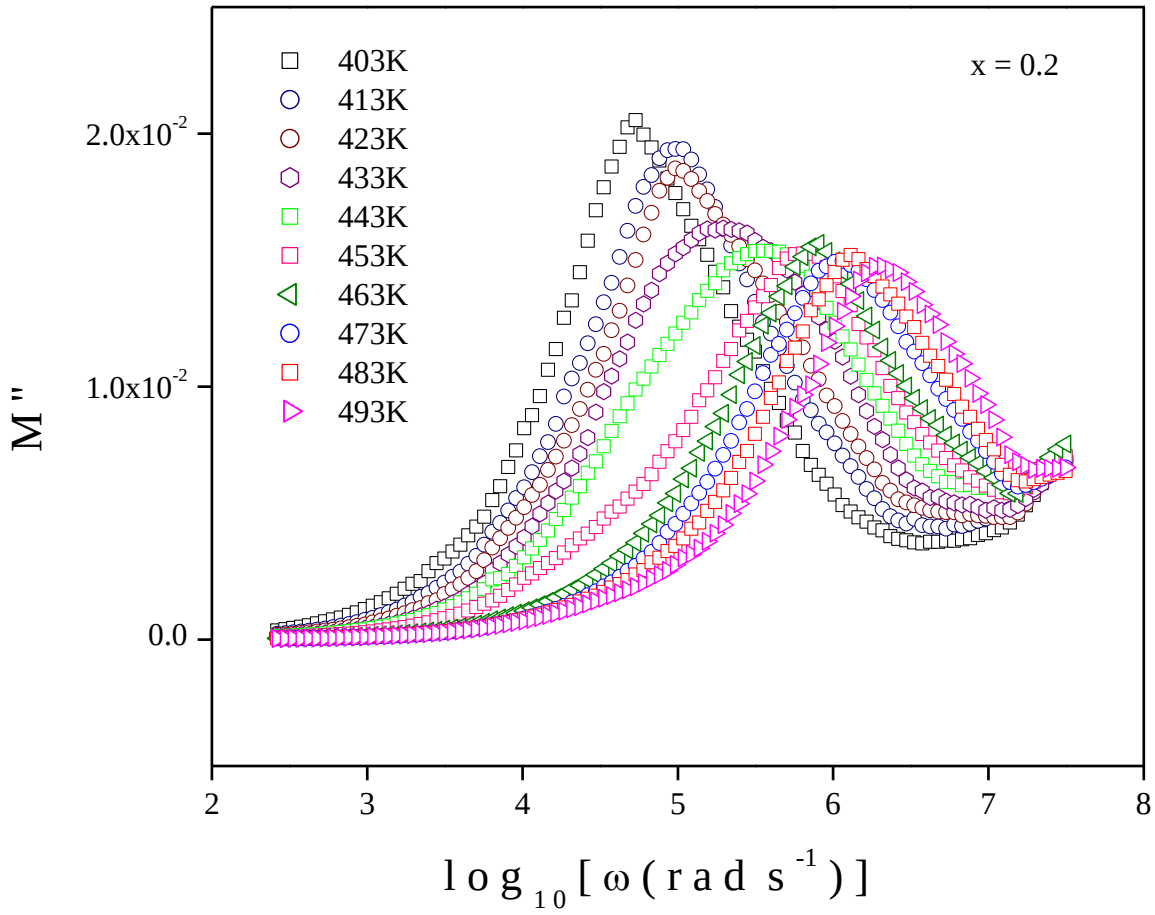

Fig. 5.11 (b) Spectra of $M^{//}$ for x = 0.2

5.4 CONCLUSION

The objective of this study has been accomplished since the conductivity behavior of oxy-salt glassy systems has been shown to be significantly improved by the addition of a new metal halide, CdI_2. The investigation's findings clearly show that a higher CdI_2 concentration increases Ag^+ ion mobility, which raises the system's total conductivity. According to the study, more Cd–Ag ionic exchanges take place when the CdI_2 level rises, which promotes the migration of Ag^+ ions and raises DC conductivity. The structural changes brought about by CdI_2 doping are responsible for this improved ionic mobility. These changes most likely reduce bonding contacts or open up new channels that previously impeded Ag^+ transport. It is additionally speculated that the noticed dispersion in high-frequency AC conductivity reflects the irregular, correlated, and sub-diffusive migration of Ag^+ ions. Inter-ionic interactions inside the matrix may cause such correlated ion motion, which would affect the power law exponent as a function of ion concentration. Because it sheds light on the ion transport pathways in

disordered materials, this phenomenon is highly interesting to academics. Furthermore, from the standpoint of application, comprehending and managing these conductivity improvements is essential for the creation of sophisticated electrochemical devices, such as superionic conductors, solid-state batteries, and sensors. The results of this study significantly enhance the potential of oxy-salt glassy systems in technological applications by opening the door for material composition optimization to obtain superior ionic conduction.

References

[1] Kumar, R. S., & Hariharan, K. (1997). Ion transport studies in PbI2–Ag2O–V2O5 glassy system. Solid State Ionics, 104(3-4), 227-236.

[2] Viswanathan, A., & Suthanthiraraj, S. A. (1993). Impedance and modulus spectroscopic studies on the fast ion conducting system CuI□ Ag2MoO4. Solid State Ionics, 62(1-2), 79-83.

[3] Chandrasekhar, V. G., & Suthanthiraraj, S. A. (1993). Preparation and transport studies of the new superionic system (CuI) x·[(Ag2O) 3·(B2O3)] 100− x (35⩽ x⩽ 75). Solid State Ionics, 62(1-2), 61-67.

[4] Kabi, S., & Ghosh, A. (2012). Microstructure and optical properties of CdI2 doped silver vanadate glass-nanocomposites. Materials Research Bulletin, 47(11), 3195-3200.

[5] Rao, P. N., Ramesh Kumar, E., & Appa Rao, B. (2018). Structural and transport studies of CdI 2-doped silver borotellurite fast ion-conducting system. Journal of Solid State Electrochemistry, 22, 3863-3871.

[6] Ghosh, A., Dutta, D., Kabi, S., & Ghosh, A. (2009). Electrical relaxation in CdI2 doped silver vanadate superionic glasses. Journal of Applied Physics, 105(6).

[7] Padmasree, K. P., & Kanchan, D. K. (2005). Dielectric studies on CdI2 doped Ag2O–V2O5–B2O3 system. Materials chemistry and physics, 91(2-3), 551-557.

[8] Kumari, V., Kaswan, A., Patidar, D., Sharma, K., & Saxena, N. S. (2016). Electrical conduction mechanism in GeSeSb chalcogenide glasses. Bulletin of Materials Science, 39, 255-262.

[9] Fernandes, B. J., Ramesh, K., & Udayashankar, N. K. (2019). Crystallization kinetics of Si20Te80− xBix (0≤ x≤ 3) chalcogenide glasses. Materials Science and Engineering: B, 246, 34-41.

[10] Pal, S. K., Kumar, A., & Mehta, N. (2019). Signature of rigidity percolation effect in dielectric behavior of germanium containing multi-component chalcogenide glasses (ChGs). Ceramics International, 45(13), 16279-16287.

[11] Ravagli, A., Naftaly, M., Craig, C., Weatherby, E., & Hewak, D. W. (2017). Dielectric and structural characterisation of chalcogenide glasses via terahertz time-domain spectroscopy. Optical Materials, 69, 339-343.

[12] Zhu, E., Liu, Y., Sun, X., Yin, G., Jiao, Q., Dai, S., & Lin, C. (2019). Correlation

between thermo-mechanical properties and network structure in GexS100–x chalcogenide glasses. Journal of Non-Crystalline Solids: X, 1, 100015.

[13] Barczyński, R. J., Król, P., & Murawski, L. (2010). Ac and dc conductivities in V2O5–P2O5 glasses containing alkaline ions. Journal of non-crystalline solids, 356(37-40), 1965-1967.

[14] Bhattacharya, S., & Ghosh, A. (2006). Electrical properties of ion conducting molybdate glasses. Journal of applied physics, 100(11).

[15] Kundu, R., Roy, D., & Bhattacharya, S. (2017). Microstructure, electrical conductivity and modulus spectra of CdI2 doped nanocomposite-electrolytes. Physica B: Condensed Matter, 507, 107-113.

[16] Kundu, R., Roy, D., & Bhattacharya, S. (2015). Electrical transport of mixed phased glassy nanocomposites. Transactions of the Indian Ceramic Society, 74(1), 35-40.

[17] Almond, D. P., & West, A. R. (1983). Mobile ion concentrations in solid electrolytes from an analysis of ac conductivity. Solid State Ionics, 9, 277-282.

[18] Deb, B., & Ghosh, A. (2010). Dielectric and conductivity relaxation in AgI doped silver selenite superionic glasses. Journal of Applied Physics, 108(7).

[19] Ahmad-Bitar, R., & Arafah, D. E. (1998). Processing effects on the structure of CdTe, CdS and SnO2 thin films. Solar energy materials and solar cells, 51(1), 83-93.

[20] Karmakar, B., Rademann, K., & Stepanov, A. (Eds.). (2016). Glass nanocomposites: synthesis, properties and applications. William Andrew.

[21] Bhattacharya, S., & Ghosh, A. (2008). Relaxation dynamics in superionic glass nanocomposites. Journal of the American Ceramic Society, 91(3), 753-759.

[22] Ojha, S., Roy, M., Chamuah, A., Bhattacharya, K., & Bhattacharya, S. (2020). AC conductivity and dielectric behavior of Cu-S-Te chalcogenide glassy system. Materials Letters, 258, 126792.

Chapter 6

Study of Effects of Different Formers on Electrical Transport Phenomena of CdI_2 Doped $Ag_2O - P_2O_5 - ZnO$ System

Outline

6.1 INTRODUCTION

The work on the CdI_2-doped silver oxy-salt system in the previous chapter showed that the material can efficiently accommodate CdI_2, demonstrating its stability as a host. Even still, the system only shows a moderate level of electrical conductivity, indicating that more changes are necessary to improve its functionality. A comprehensive review of the literature has shown that, in glassy systems like the one being studied, conductivity tends to increase as the AgO/PO_5 ratio rises while the CdI_2 content stays constant [1]. This suggests that improving ionic transport may require modifying the glass composition.

Furthermore, research has demonstrated that the electrical characteristics of CdI_2-doped silver oxy-salt systems could be markedly improved by the incorporation of TeO_2. The favorable characteristics of tellurite-based glasses [2–7], such as their high thermal expansion coefficient, low glass transition temperature, and decreased hygroscopicity, all of which enhance ionic mobility and structural stability, make them particularly desirable. Additionally, it has been shown that adding MoO_3 improves the electrical conductivity of glassy systems doped with CdI_2. By adding non-bridging oxygen ions, molybdenum oxide is known to alter the glass network, improving ionic conduction and charge carrier mobility [8–13].

Based on these findings, additional research has been aimed to carry out on the previously prepared glassy system incorporating TeO_2, and MoO_3 in the replacement of V_2O_5 along with a gradual increase in Ag_2O to P_2O_5 ratio. The study intends to a promising approach for further improvement of the electrical properties of CdI_2-doped silver oxy-salt systems, making them more suitable for applications in solid-state ionic devices and energy storage technologies.

6.2 PREPARATION OF GLASSY SYSTEMS

The glassy systems $0.3CdI_2 – 0.7\ (0.3\ Ag_2O – 0.3MoO_3 – 0.3\ P_2O_5 – 0.1\ ZnO)$ and $0.3CdI_2 – 0.7\ (0.3\ Ag_2O – 0.3TeO_2 – 0.3\ P_2O_5 – 0.1\ ZnO)$ are made using the melt quenching process [14-18] with exceptionally pure (Aldrich 99.9%) reagent grade chemicals. Using an electromechanical analytical balance (Dhona 200D), each required chemical was carefully weighed according to its predetermined stoichiometric proportion, as discussed in section 2.3. The materials were then thoroughly mixed and pounded in a mortar to produce the

powder. The mortar was carefully cleaned and rinsed before use. The produced powder was then melted at temperatures between 700 and 800°C in an electric furnace, depending on their composition.

After 30 minutes of equilibration, the melts were quenched between two aluminum plates. Glassy composites that were around 1 mm thick and somewhat transparent were created using this technique. For the electrical conductivity analysis, samples that were roughly 1 mm thick were measured by means of the two-probe approach. Two copper electrodes (manufactured by Joy-Crucible) that had been polished, cleaned, and spring-loaded were in contact with the sample while it was inside the sample container. Then, complex impedance measurements in the frequency range of 42 Hz to 5 MHz were carried out using the Hioki LCR tester (Model No. 3532-50). At regular intervals of 10 K, measurements were taken in the temperature range of 300–593 K.

6.3 RESULTS AND ANALYSIS

6.3.1 Structural Characterization

As already discussed in section 2.4.2, investigation of the structural characterization of the as-prepared samples are primarily necessary to gather knowledge about its certain spectrographic and microscopic measurements [19]. The various techniques include the study of Density (ρ) and Molar Volume (V_M), XRD, SEM and FT-IR on the samples under consideration.

6.3.1.1 Measurement of Density and Molar Volume

The density and molar volume of the as-prepared samples are measured using the Archimedes principle, which is described in section 2.4.1. Considering Eq. 2.1 and 2.2, the density and molar volume of the produced glass nano-composites have been calculated. Acetone with density (ρ_b) 0.7845 gm/cm^3 has been utilized as the buoyant liquid. The weights of the as prepared samples were recorded on an electromechanical balance (Dhona, Model: 200D) with precession of 0.0001 gm. Every measurement was performed at room

temperature.

Fig 6.1 (a) and (b) shows the variation of density (ρ) and molar volume (V_M) with the increase in the value of x (where, x = y: z) for the as-prepared samples $0.3CdI_2 – 0.7$ (y Ag_2O – $0.3TeO_2$ – z P_2O_5 – 0.1 ZnO) and $0.3CdI_2 – 0.7$ (y Ag_2O – $0.3MoO_3$ – z P_2O_5 – 0.1 ZnO) respectively. In both instances, the density value increases while the molar volume value decreases in tandem. The increase in density of the samples indicates the increase in compactness and less porous nature of the as-prepared glassy systems with the rise in the concentration ratio of Ag_2O to P_2O_5. The decrease in volume may indicate the enhancement in the amount of non-bridging oxygen in the system. Thus, it can be inferred that with the augmentation in the concentration of Ag_2O to P_2O_5 the system produces more and more NBOs and thus leads to more and more disordered structure. The measured values of ρ and V_M are recorded in Table 6.1.

As-prepared glassy systems	**Composition**	**Density, ρ (g/ cc) (± 0.1)**	**Molar volume, V_M (cc/ mol) (± 0.1)**
$0.3CdI_2 – 0.7$ (y Ag_2O – 0.3 TeO_2 – z P_2O_5 – 0.1 ZnO)	x = 0.2 {y = 0.1, z = 0.5}	3.9515	56.3175
	x = 1 {y = 0.3, z = 0.3}	6.3761	39.2451
$0.3CdI_2 – 0.7$ (y Ag_2O – 0.3 MoO_3 – z P_2O_5 – 0.1 ZnO)	x = 0.2 {y = 0.1, z = 0.5}	4.5629	48.0506
	x = 1 {y = 0.3, z = 0.3}	5.7126	43.2276

Table 6.1: ρ and V_M of the as-prepared systems for different values of y and z

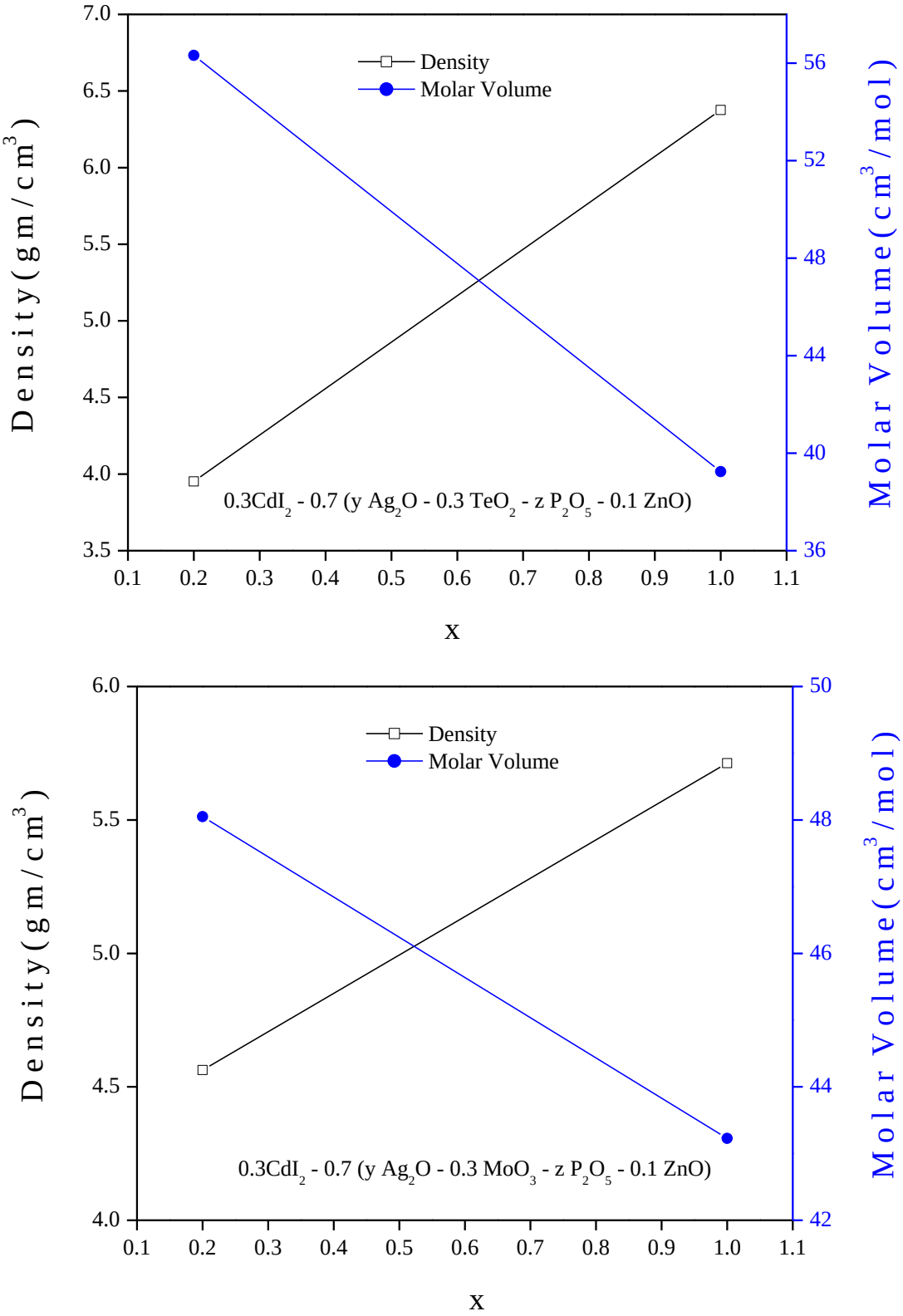

Fig. 6.1 Variation of density and molar volume of (a) $0.3CdI_2 - 0.7$ (y $Ag_2O - 0.3TeO_2 -$ z $P_2O_5 - 0.1$ ZnO) and (b) $0.3CdI_2 - 0.7$ (y $Ag_2O - 0.3MoO_3 -$ z $P_2O_5 - 0.1$ ZnO) for different values of y and z

6.3.1.2 X-ray Diffraction (XRD)

The as-prepared samples were undergone to the X-ray diffraction (XRD) analysis, which is detailed in section 2.4.2, in order to examine their structural properties. The observed broad hump in the diffraction pattern is a significant indication of the amorphous nature of the samples, signifying a lack of long-range periodic atomic arrangement. This characteristic hump typically suggests the existence of a disordered or glassy phase, where the atomic arrangement does not exhibit well-defined crystalline order. The fact that there are no clear, strong diffraction peaks indicates that long-range crystallinity is either completely or very partially suppressed. It is also possible, nevertheless, that some nanoscale crystalline phases exist inside the amorphous matrix but are not clearly visible in the XRD examination. An under-representation or even the lack of their diffraction signals in the recorded patterns may result from the orientation of these nanocrystalline domains, where the formed crystallographic planes may not be favorably orientated for X-ray diffraction to occur. The suppression of different diffraction peaks may also be caused by strain, defects, and the potential existence of extremely disordered interfacial regions between nano-phases. The ability of such an amorphous structure to affect material properties like ionic conductivity, mechanical flexibility, and optical transparency makes these samples potentially appropriate for use in cutting-edge technological applications, such as solid electrolytes, optical materials, and energy storage devices. The XRD spectra of the as-prepared samples are given in Fig. 6.2 (a) and (b).

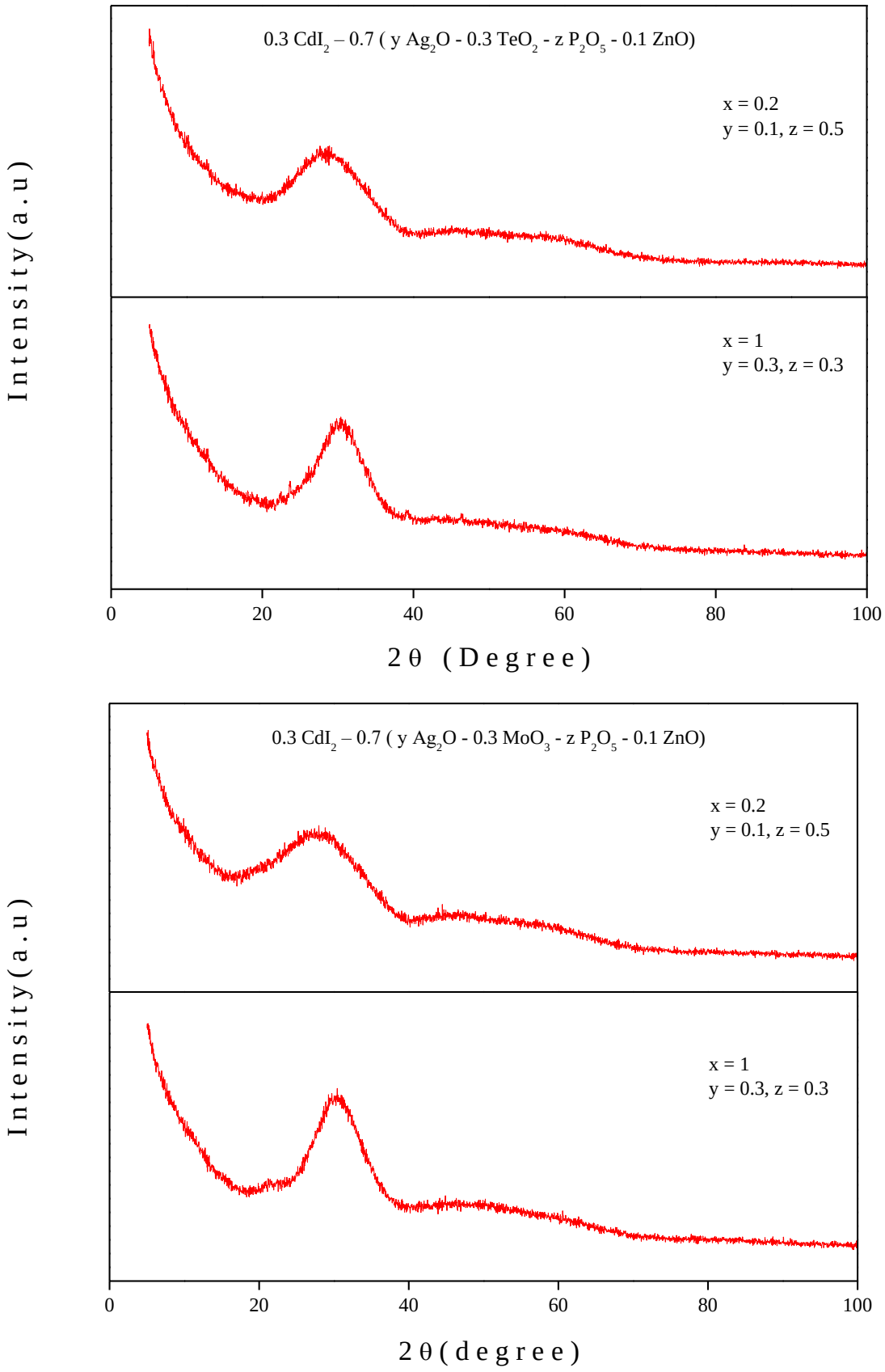

Fig. 6.2 XRD of (a) $0.3CdI_2 – 0.7 (y\ Ag_2O – 0.3TeO_2 – z\ P_2O_5 – 0.1\ ZnO)$ and (b) $0.3CdI_2 – 0.7 (y\ Ag_2O – 0.3MoO_3 – z\ P_2O_5 – 0.1\ ZnO)$ for different values of y and z

6.3.1.3 Fourier Transform Infrared Spectroscopy (FT-IR)

As mentioned in section 2.4.3, the FT-IR transmittance spectra of the current glassy system in the mid-infrared region (spectral range 4000 cm^{-1} – 400 cm^{-1}) are shown in Fig. 6.3. Vibrational bands associated with the system's basic chemical bonds were not detectable because they were below the 400 cm^{-1} wave number.

Analysis of the FT-IR spectroscopy of the as-prepared sample $0.3CdI_2 – 0.7$ (y Ag_2O – 0.3 TeO_2 – z P_2O_5 – 0.1 ZnO) gives the idea about the presence of the possible bands as follows. Peaks at 3430 cm^{-1} and 3510 cm^{-1} can be designated as stretching vibrations of O-H bond [20-21], indicating that they are hygroscopic in nature. The bending Vibration of H-O-H bands has appeared at 1644 cm^{-1} and 1619 cm^{-1}. The H-O-H bending vibration typically appears when the two hydrogen atoms move closer together while the oxygen remains relatively stationary. It helps to identify water content in samples [20-21]. Asymmetric Stretching of P-O-P bands have appeared at 1075 cm^{-1} and 1087 cm^{-1}. It appears due to asymmetric stretching of the P-O-P bridge. It often appears in polyphosphates and condensed phosphate structures. Symmetric stretching vibrations of P-O-P bands have appeared at 897 cm^{-1} and 917 cm^{-1}. Generally, it is observed in linear and cyclic phosphates. In the glassy systems like this, metal-oxygen vibrations may arise from the interaction between metal cations and oxygen anions. These bands are more prominent in heavy metal oxides and transition metal complexes. These bands correspond to stretching, bending, and lattice vibrations of metal-oxygen bonds in oxides, minerals, and metal complexes. In our systems, it is expected that possible metal-oxygen vibrations have appeared at 540 cm^{-1}, 544 cm^{-1} and at 718 cm^{-1}.

The sample with MoO_3 as network modifier also shows presence of these bands but it can be seen that the wavenumbers have been shifted slightly. The presence of stretching vibrations of O-H bond could be identified at 3437 cm^{-1} and 3486 cm^{-1}. Peaks at 1628 cm^{-1} and 1623 cm^{-1} correspond to the bending vibration of H-O-H bands. Asymmetric Stretching of P-O-P bands appear at 1043 cm^{-1} and 1149 cm^{-1}. Symmetric stretching vibrations of P-O-P bands have appeared at 910 cm^{-1} and 911 cm^{-1}. Possible metal-oxygen vibrations have appeared at 703 cm^{-1}, 552 cm^{-1} and at 744 cm^{-1}. The FT-IR spectra of the as-prepared systems are shown in Fig. 6.3.

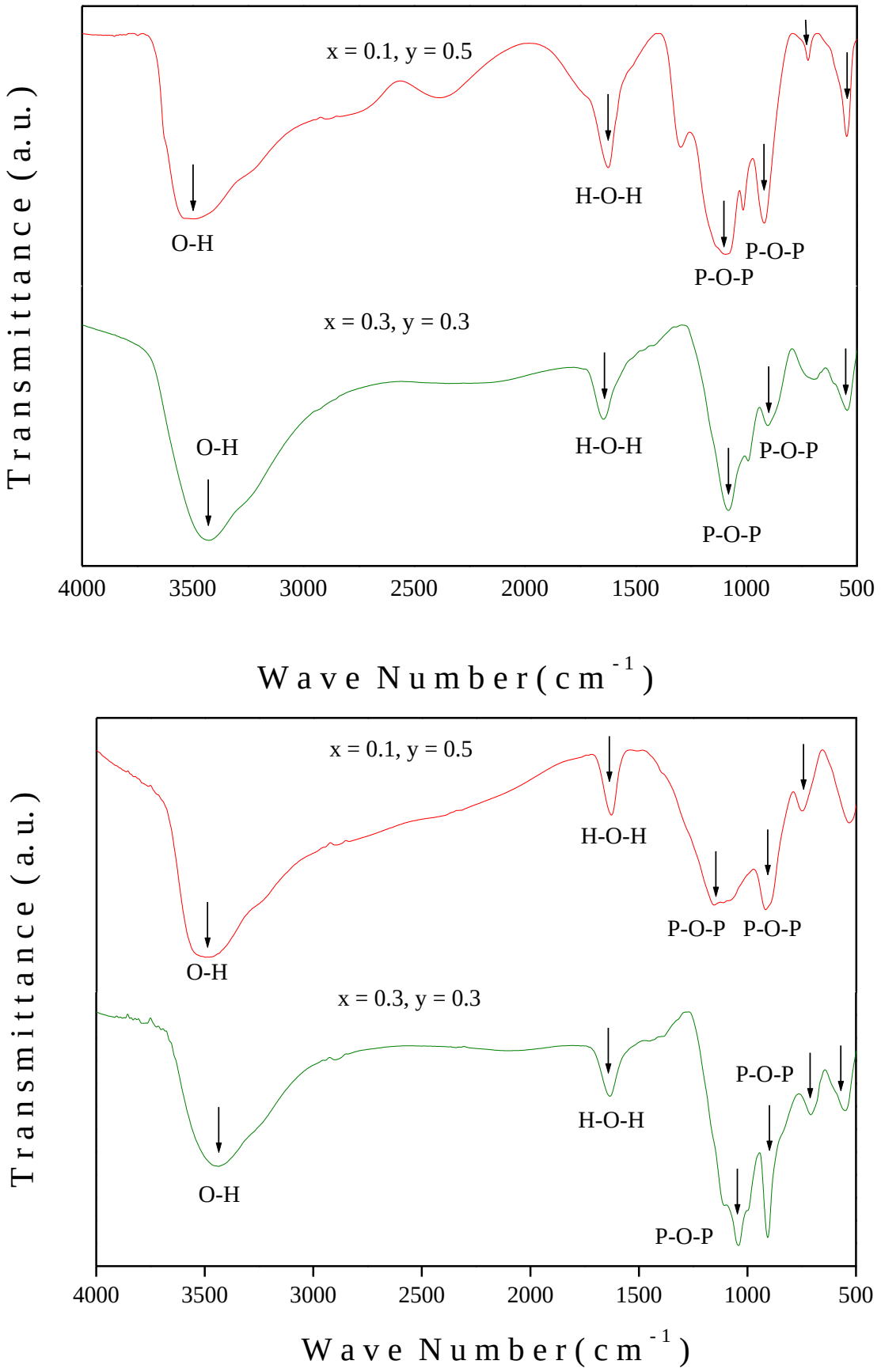

Fig. 6.3 FT-IR spectra of (a) $0.3CdI_2 - 0.7\ (y\ Ag_2O - 0.3TeO_2 - z\ P_2O_5 - 0.1\ ZnO)$ and (b) $0.3CdI_2 - 0.7\ (y\ Ag_2O - 0.3MoO_3 - z\ P_2O_5 - 0.1\ ZnO)$ for different values of y and z

6.3.2 Electrical Conductivity Study

The effect of variation in the concentration of the compositions on the electrical conductivity of the as-prepared samples has been systematically explored through electrical conductivity and relaxation studies. The presence of TeO_2 is expected to augment the conductivity of the as-prepared oxide glassy system [22-23] whereas MoO_3, along with other glass-forming oxides, like P_2O_5 is supposed to transform the glass structure [24]. It is anticipated that the addition of CdI_2 in such system will change the structural framework or provide more charge carriers, which will facilitate ion migration through the system. These investigations is expected to provide a profound knowledge about the charge carrier transport analyzing the impact of CdI_2 in the environment of different modifier oxides.

6.3.2.1 DC Conductivity Study

Fig. 6.4 displays the complex impedance graphs [25] of all the as-prepared samples at different temperatures. The plots' flawless semicircular shape suggests that there are no influences from grain boundaries. The radius of the semicircular arcs progressively shrinks as the temperature rises, indicating that all of the samples are thermally activated in nature. A progressive reduction in radius suggests a corresponding increase in conductivity. After evaluating the corresponding dc electrical conductivity (σ_{dc}) [25-26], it is necessary to examine whether the temperature dependence of dc conductivity exhibits Arrhenius-type variation or not and all of our systems have been found to follow Arrhenius-type variation, as given by Eq. 2.8. From the plots of Fig. 6.5, it is evident that in the system containing transition metal-oxide MoO_3 dc conductivity (σ_{dc}) rises as Ag_2O concentration grows to P_2O_5. On the other hand, as the concentration of Ag_2O increases, the conductivity of the TeO_2-containing system gradually decreases. The activation energy (E_{dc}) has been calculated from the gradients of the linearly fitted data of dc conductivity. Values of E_{dc} have been recorded in Table 6.2.

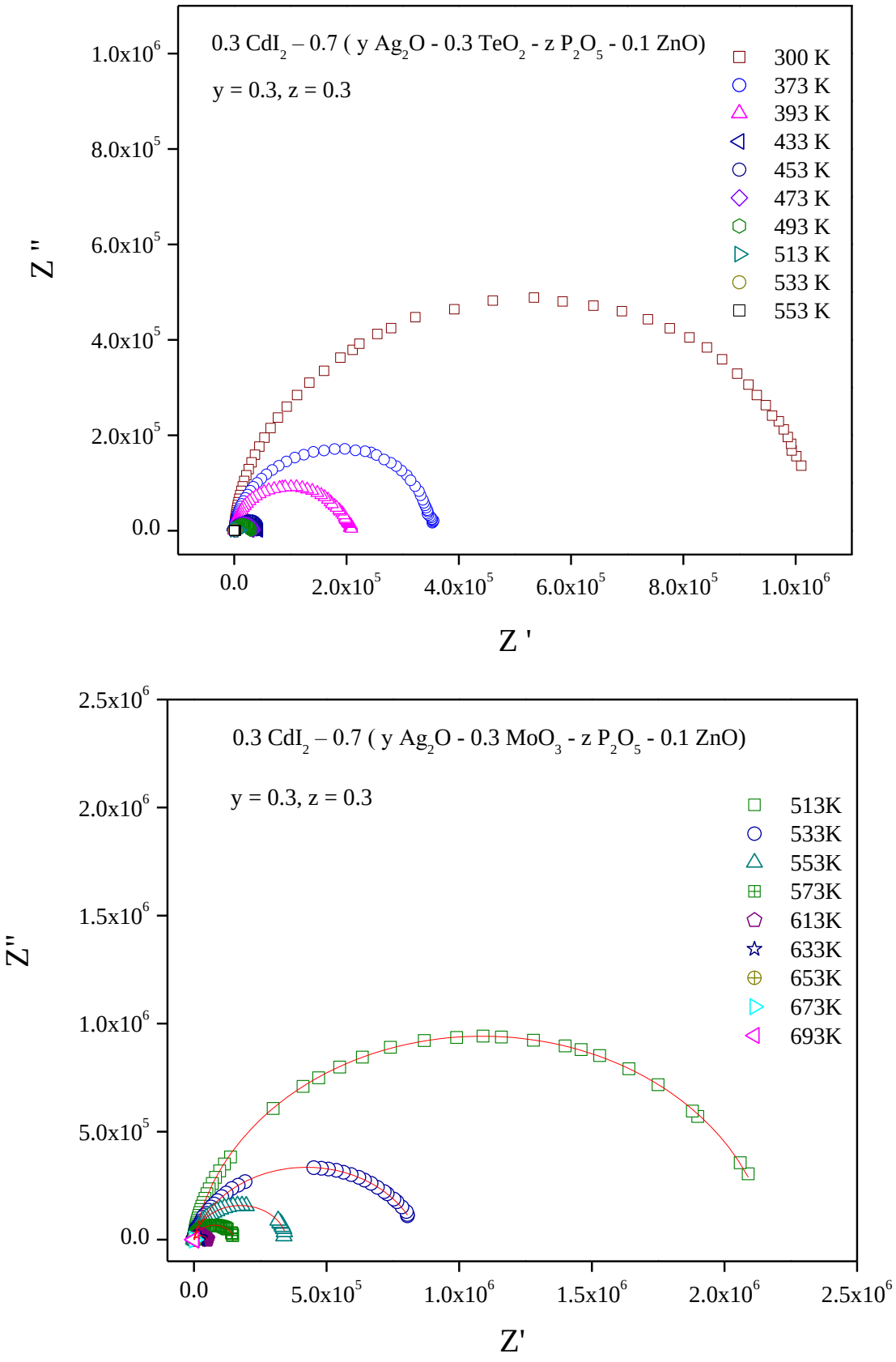

Fig. 6.4 Complex impedance plot of (a) $0.3CdI_2 – 0.7 (y\ Ag_2O – 0.3TeO_2 – z\ P_2O_5 – 0.1$ ZnO) and (b) $0.3CdI_2 – 0.7 (y\ Ag_2O – 0.3MoO_3 – z\ P_2O_5 – 0.1\ ZnO)$ for y = 0.3, z = 0.3

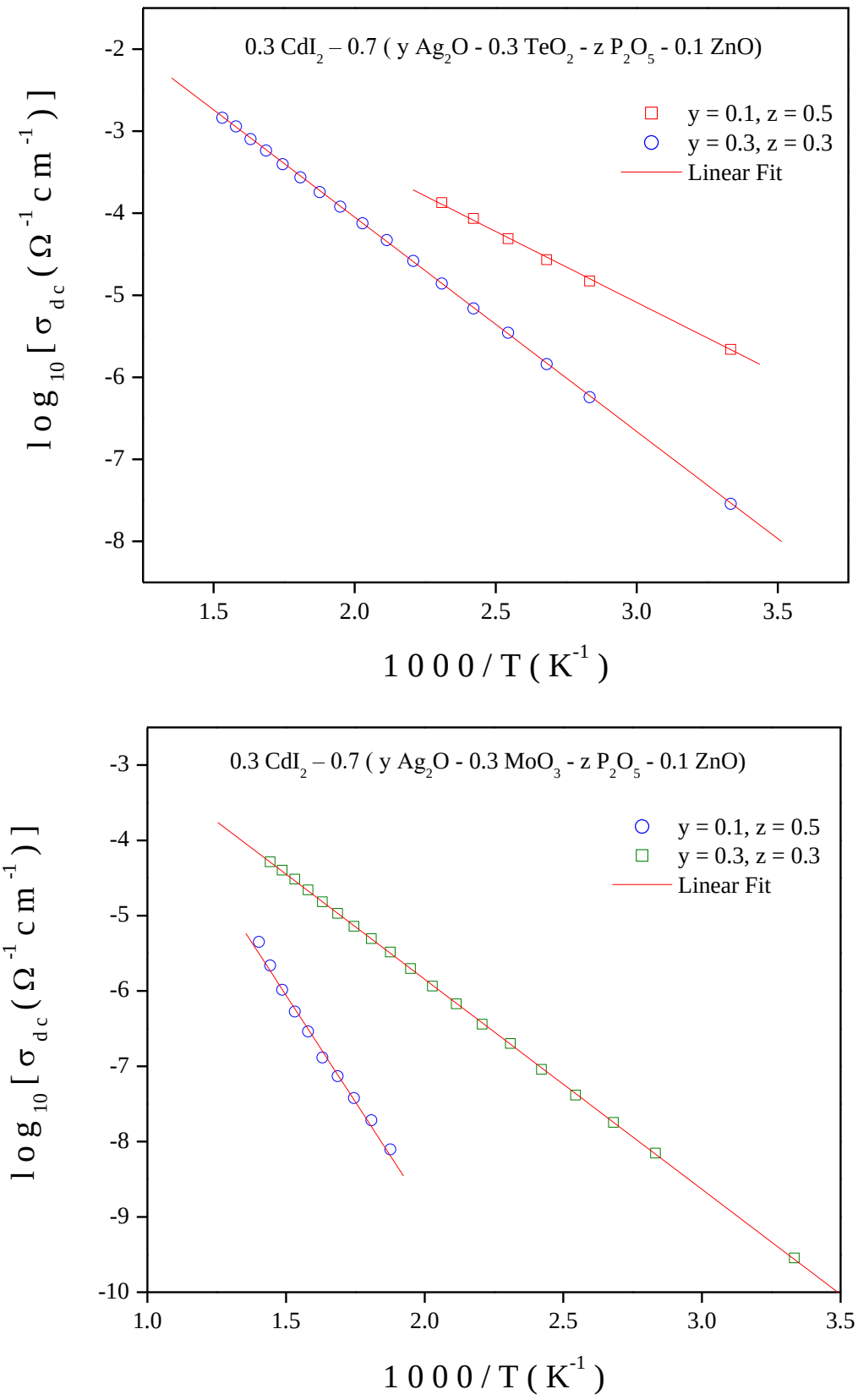

Fig. 6.5 Temperature dependence of DC conductivity plot of (a) $0.3CdI_2 – 0.7 (y\ Ag_2O – 0.3TeO_2 – z\ P_2O_5 – 0.1\ ZnO)$ and (b) $0.3CdI_2 – 0.7 (y\ Ag_2O – 0.3MoO_3 – z\ P_2O_5 – 0.1\ ZnO)$ for different values of y and z

As-prepared glassy systems	Composition (x)	Activation Energy due to DC Conductivity, E_{dc} (eV)	Activation Energy due to Hopping Frequency, E_h (eV)
$0.3CdI_2 – 0.7 (y\ Ag_2O – 0.3\ TeO_2 – z\ P_2O_5 – 0.1\ ZnO)$	x = 0.2 {y = 0.1, z = 0.5}	0.34	0.32
	x = 1 {y = 0.3, z = 0.3}	0.52	0.40
$0.3CdI_2 – 0.7 (y\ Ag_2O – 0.3\ MoO_3 – z\ P_2O_5 – 0.1\ ZnO)$	x = 0.2 {y = 0.1, z = 0.5}	1.12	1.03
	x = 1 {y = 0.3, z = 0.3}	0.55	0.47

Table 6.2: E_{dc} and E_h of the as-prepared systems with different values of x

6.3.2.2 AC Conductivity Study

The AC conductivity spectra of the present glassy systems with respect to frequency (42 Hz to 5 MHz) for all x are displayed in Fig. 6.6 and Fig. 6.7 at various temperatures. It is discovered that the nature of ac conductivity variation is identical to that of DC conductivity fluctuation. It has been seen that the conductivity flattens out at low frequencies. The DC conductivity is equivalent to this frequency-independent conductivity [27-28]. The diffusion of Ag^+ ions may be the cause of this kind of conductivity which shows the frequency independent behavior in the low-frequency range. The AC conductivity displays dispersion and power law behaviour beyond crossover or hopping frequencies. This dispersion in the spectrum of higher frequencies indicates that the Ag^+ ions are moving in a correlated and sub-diffusive manner rather than random motion. The literature [28-29] makes it readily apparent that the inter-ionic interaction that causes this correlated motion changes the power law exponent as ion concentration increases.

Since conductivity is shown to increase with temperature, the AC conductivity spectra demonstrate a thermally activated nature. To gather knowledge about the conductivity, at a particular temperature, AC conductivity spectra have been plotted for all the samples in Fig. 6.8 and it reveals that TeO_2-doped system exhibits reduction in conductivity and MoO_3-doped system exhibits the opposite nature with the increase in the ratio of Ag_2O to P_2O_5. For the purpose of gathering enough information related to the electrical conduction in the system, AC conductivity spectra were fitted using the Almond West formalism, Eq. 2.16. The calculated

parameters σ_{dc}, ω_H and n are tabulated in Table 6.3 and 6.4.

The hopping frequency plays a vital role in the electrical conductivity as already discussed in previous chapters. The variation of hopping frequency with temperature has been shown in Fig. 6.9 and it has been found to rise with temperature as well like conductivity spectra. The TeO_2-doped system's hopping frequency gradually decreases as the Ag_2O:P_2O_5 concentration rises. The opposite effect has been observed when MoO_3 is present. The temperature dependence of hopping frequency has to be found to follow Arrhenius relation, as given in Eq. 2.17. Thus, activation energy due to hopping frequency (E_h) has been calculated from the slopes of the linearly fitted data. Activation energy has been found to increase for the TeO_2-doped system and decrease for the MoO_3-doped system. The variation of hopping frequency and activation energy with rise in the concentration of Ag_2O:P_2O_5 has been shown in Fig. 6.10 and the calculated activation energy due to hopping frequency has been given in Table 6.2.

x	T(K)	σdc ($W^{-1}cm^{-1}$)	ω_H (rad s^{-1})	n
0.2	300	3.43 x10^{-06}	99406.504	0.846
	353	2.00 x10^{-05}	729007.081	0.915
	373	3.00 x10^{-05}	1300281.529	0.931
	393	5.00 x10^{-05}	2087686.176	0.934
	413	9.00 x10^{-05}	4666366.93	1.019
	433	1.40 x10^{-04}	6646047.239	1.033
1	300	4.28 x10^{-07}	54400.364	0.995
	353	8.94 x10^{-07}	100860.717	0.98
	373	1.13 x10^{-06}	131467.096	0.992
	393	2.25 x10^{-06}	279768.31	1.013
	413	6.74 x10^{-06}	846636.657	1.032
	433	9.89 x10^{-06}	1339788.684	1.08
	453	1.00 x10^{-05}	1306057.666	1.049
	473	1.00 x10^{-05}	1497214.388	1.04
	493	1.00 x10^{-05}	1623921.71	1.044
	513	4.00 x10^{-05}	4178766.957	1.036
	533	1.00 x10^{-04}	10804692.52	1.168
	553	1.40 x10^{-04}	13206200.35	1.165
	573	6.70 x10^{-04}	31626371.06	1.298
	593	0.00151	40830937.11	1.373
	613	0.0029	44665088.36	1.925
	633	0.00349	51924045.1	1.561
	653	0.00378	45851784.89	2.168

Table 6.3: Parameters obtained from Almond West fitting of $0.3CdI_2 – 0.7$ (y Ag_2O – 0.3 TeO_2 – z P_2O_5 – 0.1 ZnO) for different values of x

x	T(K)	σdc ($W^{-1}cm^{-1}$)	ω_H (rad s^{-1})	n
0.2	533	3.97 x10^{-09}	556.185	1.202
	553	1.44 x10^{-08}	1546.610	1.188
	573	3.48 x10^{-08}	3309.369	1.166
	593	6.49 x10^{-08}	5514.599	1.151
	613	1.35 x10^{-07}	10918.223	1.141
	633	2.57 x10^{-07}	19708.496	1.133
	653	4.42 x10^{-07}	31339.288	1.119
	673	7.46 x10^{-07}	51958.512	1.114
	693	2.06 x10^{-06}	151324.781	1.157
	713	4.70 x10^{-06}	327552.151	1.165
1	300	8.38 x10^{-09}	612.212	1.077
	353	3.23 x10^{-08}	2369.642	1.093
	373	3.45 x10^{-08}	2522.837	1.092
	393	3.19 x10^{-08}	2285.001	1.091
	413	3.82 x10^{-08}	2541.484	1.082
	433	4.07 x10^{-08}	2588.309	1.077
	453	6.27 x10^{-08}	3550.101	1.063
	473	1.03 x10^{-07}	5389.484	1.058
	493	1.84 x10^{-07}	9174.077	1.061
	513	4.30 x10^{-07}	19283.153	1.046
	533	9.17 x10^{-07}	37899.805	1.045
	553	2.64 x10^{-06}	129156.647	1.107
	573	5.38 x10^{-06}	250517.646	1.126
	593	0.00001	487211.381	1.147
	613	0.00002	859637.198	1.219
	633	0.00004	1470314.42	1.198
	653	0.00018	2804178.974	0.982
	673	0.00081	11010143.79	1.198
	693	0.00143	15639118.23	1.123

Table 6.4: Parameters obtained from Almond West fitting of AC conductivity plots of $0.3CdI_2 – 0.7\ (y\ Ag_2O – 0.3MoO_3 – z\ P_2O_5 – 0.1\ ZnO)$ for different values of x

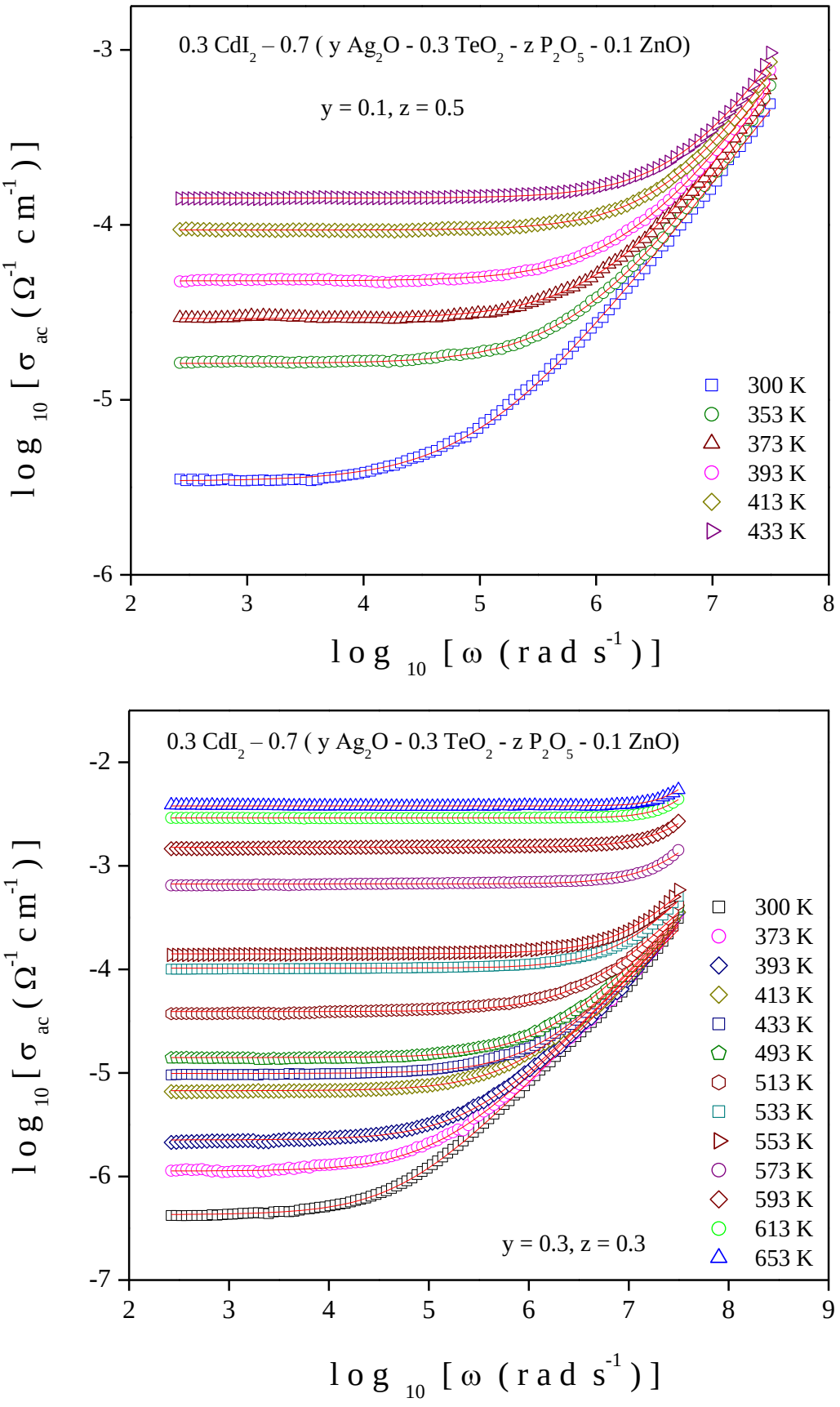

Fig. 6.6 AC conductivity spectra of $0.3CdI_2 – 0.7 (y\ Ag_2O – 0.3TeO_2 – z\ P_2O_5 – 0.1\ ZnO)$ at various temperatures for different values of y and z

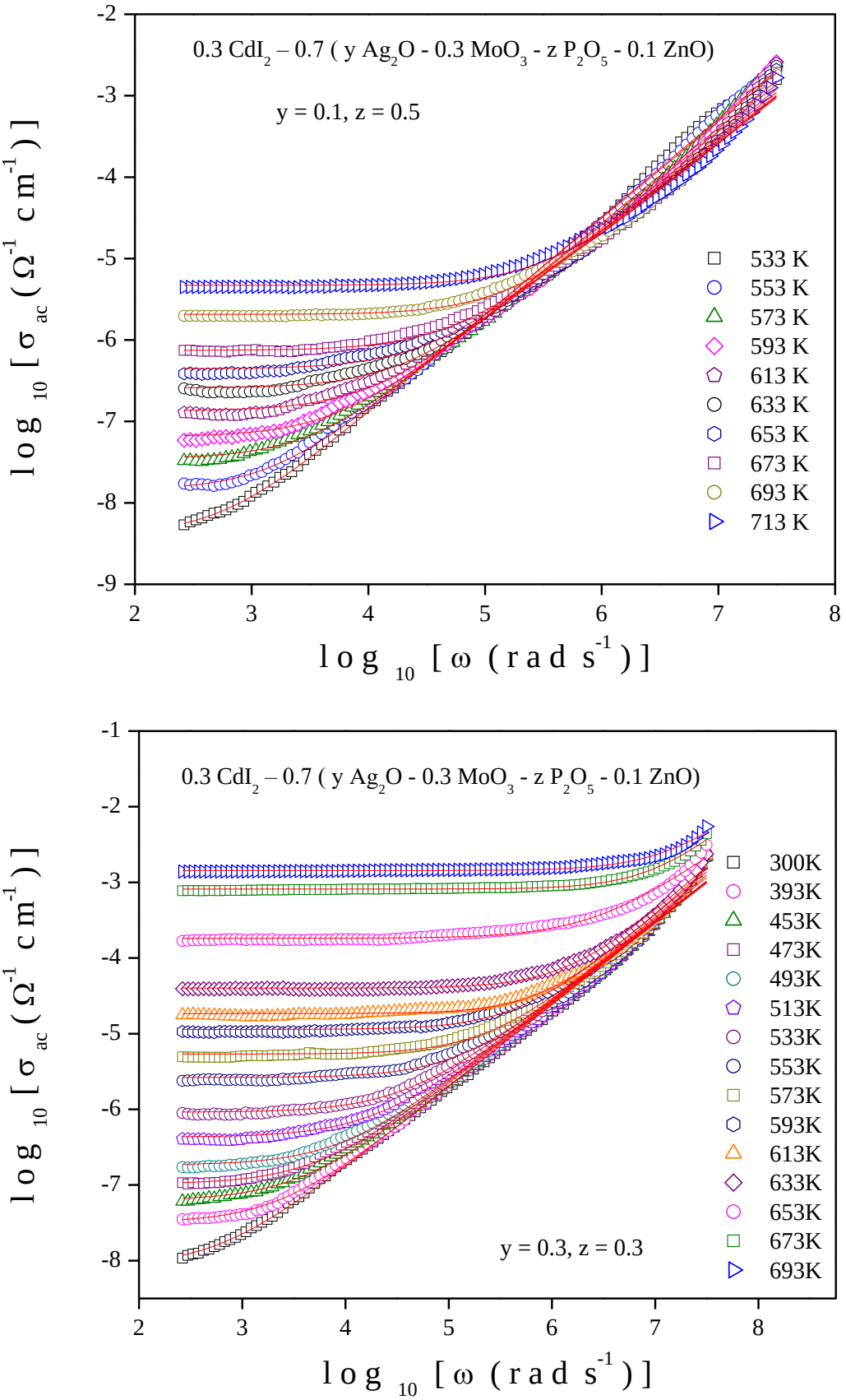

Fig. 6.7 AC conductivity spectra of $0.3CdI_2 – 0.7$ (y $Ag_2O – 0.3MoO_3 – z\ P_2O_5 – 0.1$ ZnO) at various temperatures for different values of y and z

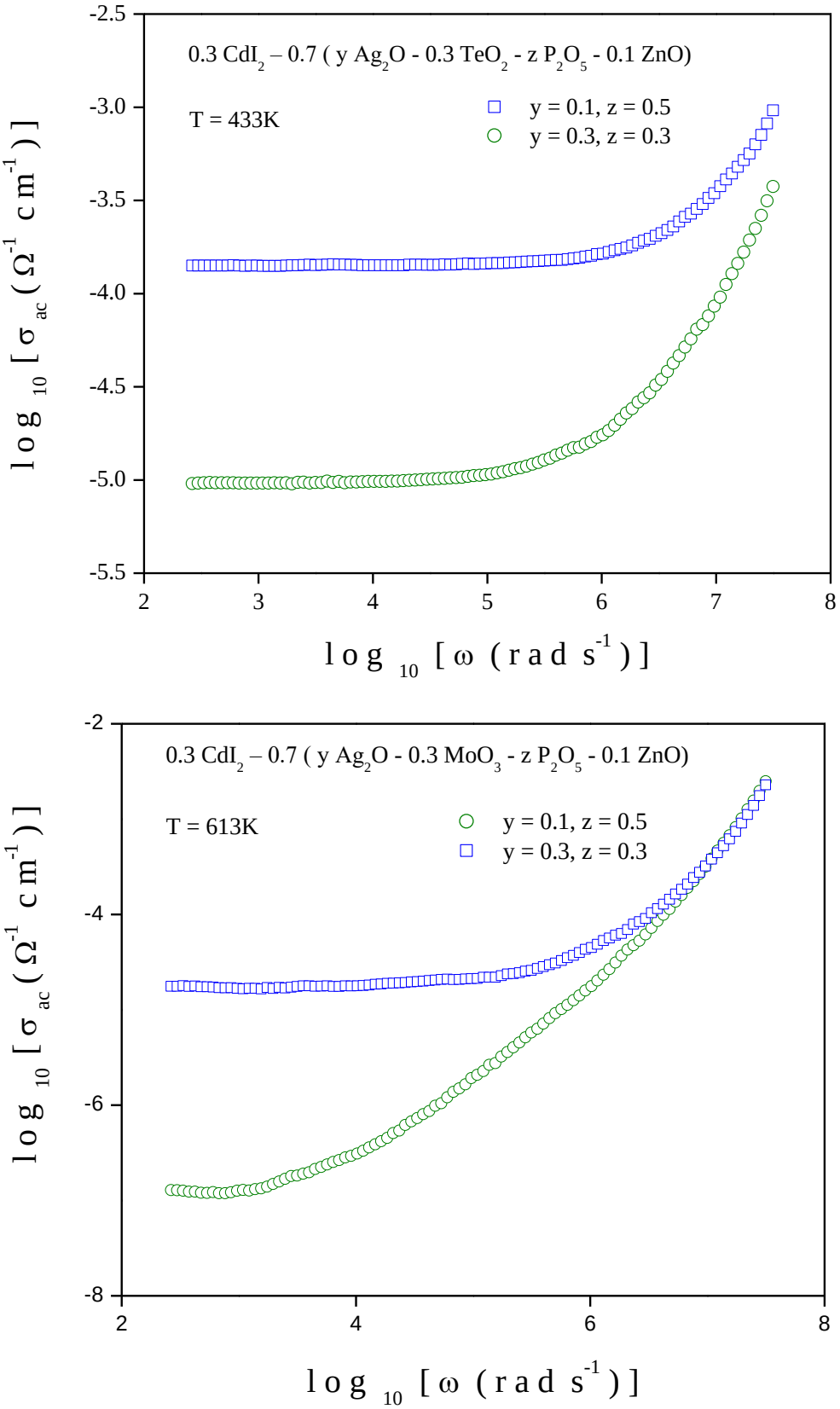

Fig. 6.8 AC conductivity spectra of (a) $0.3CdI_2 – 0.7 (y\ Ag_2O – 0.3TeO_2 – z\ P_2O_5 – 0.1$ ZnO) and (b) $0.3CdI_2 – 0.7 (y\ Ag_2O – 0.3MoO_3 – z\ P_2O_5 – 0.1\ ZnO)$ at a fixed temperature for different values of y and z

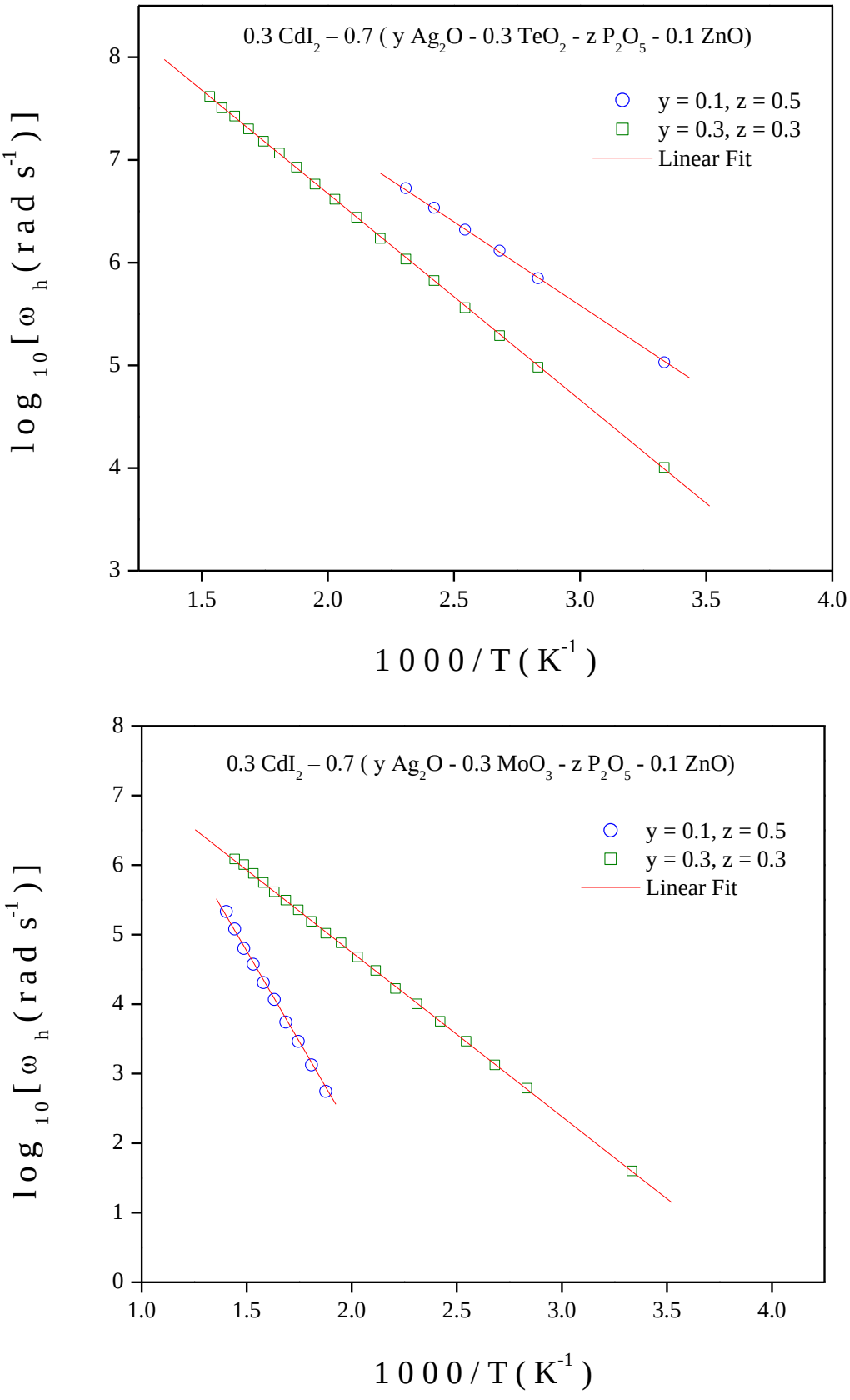

Fig. 6.9 Temperature dependence of hopping frequency plot of (a) $0.3CdI_2 – 0.7 (y\ Ag_2O – 0.3TeO_2 – z\ P_2O_5 – 0.1\ ZnO)$ and (b) $0.3CdI_2 – 0.7 (y\ Ag_2O – 0.3MoO_3 – z\ P_2O_5 – 0.1\ ZnO)$ for different values of y and z

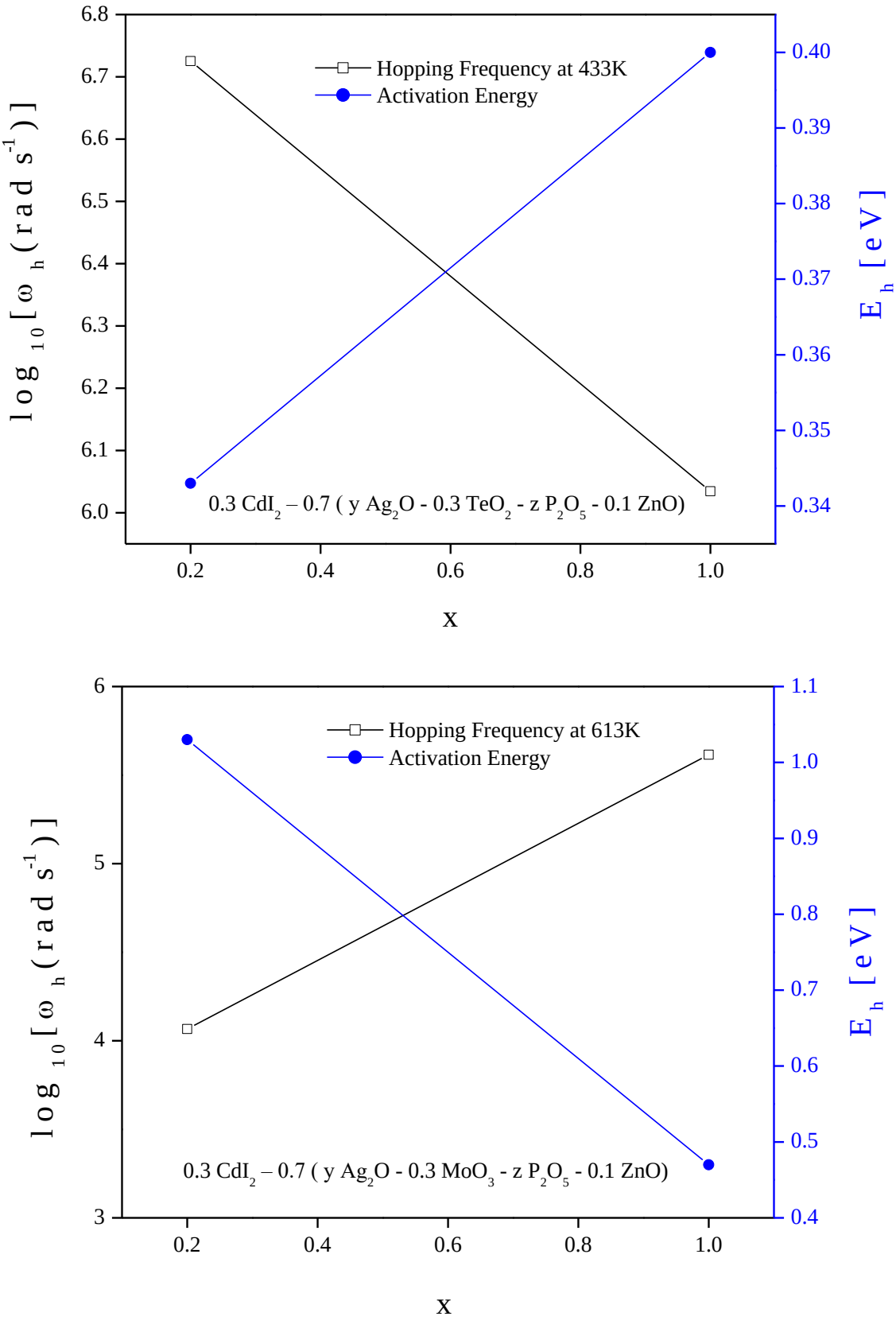

Fig. 6.10 Variation of hopping frequency and activation energy due to hopping frequency of (a) $0.3CdI_2 – 0.7 (y\ Ag_2O – 0.3TeO_2 – z\ P_2O_5 – 0.1\ ZnO)$ and (b) $0.3CdI_2 – 0.7 (y\ Ag_2O – 0.3MoO_3 – z\ P_2O_5 – 0.1\ ZnO)$ for different values of y and z

6.3.3 Dielectric Property study

The dielectric relaxation study, as discussed in section 2.5.3, has been carried out to gather knowledge about the impact of rise in the ratio of $Ag_2O:P_2O_5$ in the CdI_2 doped silver oxy-salt system. The relationship between temperature and frequency in dielectric constant ($\varepsilon^{/}$) and dielectric loss ($\varepsilon^{//}$) [30] of the as prepared systems are studied at various temperatures in a wide frequency range of 42Hz - 5MHz to study ion dynamics in the as-prepared systems. The electric modulus spectra have been studied to examine the temperature dependent relaxation process [31] of the charge carriers.

6.3.3.1 Study of electrical permittivity

The study of electrical permittivity involves the exploration of variation in the dielectric constant ($\varepsilon^{/}$) and dielectric loss ($\varepsilon^{//}$). The dielectric parameters have been calculated using Eq. 2.24 and 2.25. Fig. 6.11 displays the dielectric constant change with respect to frequency at different temperatures for both as-prepared systems. When all other parameters and the concentration of the formers and modifier oxides are held constant, it is evident that the TeO_2-containing system has a higher dominating dielectric constant value than the MoO_3-doped system. A high ε' value indicates the material's high polarizability and can store a significant amount of electrical energy [32]. The variation in dielectric loss with frequency at various temperatures for both as-prepared systems is shown in Fig. 6.12. The dielectric loss has been found more in the TeO_2-containing system. It is expected as the as-prepared material loses significant energy during polarization. Both $\varepsilon^{/}$ and $\varepsilon^{//}$ begin to drop and exhibit frequency independence as the system's frequency goes up. Both $\varepsilon^{/}$ and $\varepsilon^{//}$ increase with temperature rise, as shown in Figs. 6.11 and 6.12. This happens primarily because of the escalation in system's polarization effect due to a decrease in bond energies. It happens so as the intermolecular interactions weakens with rise in temperature. This also enhances orientational vibrations. It can also be noted that both $\varepsilon^{/}$ and $\varepsilon^{//}$ grow as x decreases in the current system's composition. This is a clear indication of higher conductivity which has already been confirmed from electrical conductivity studies.

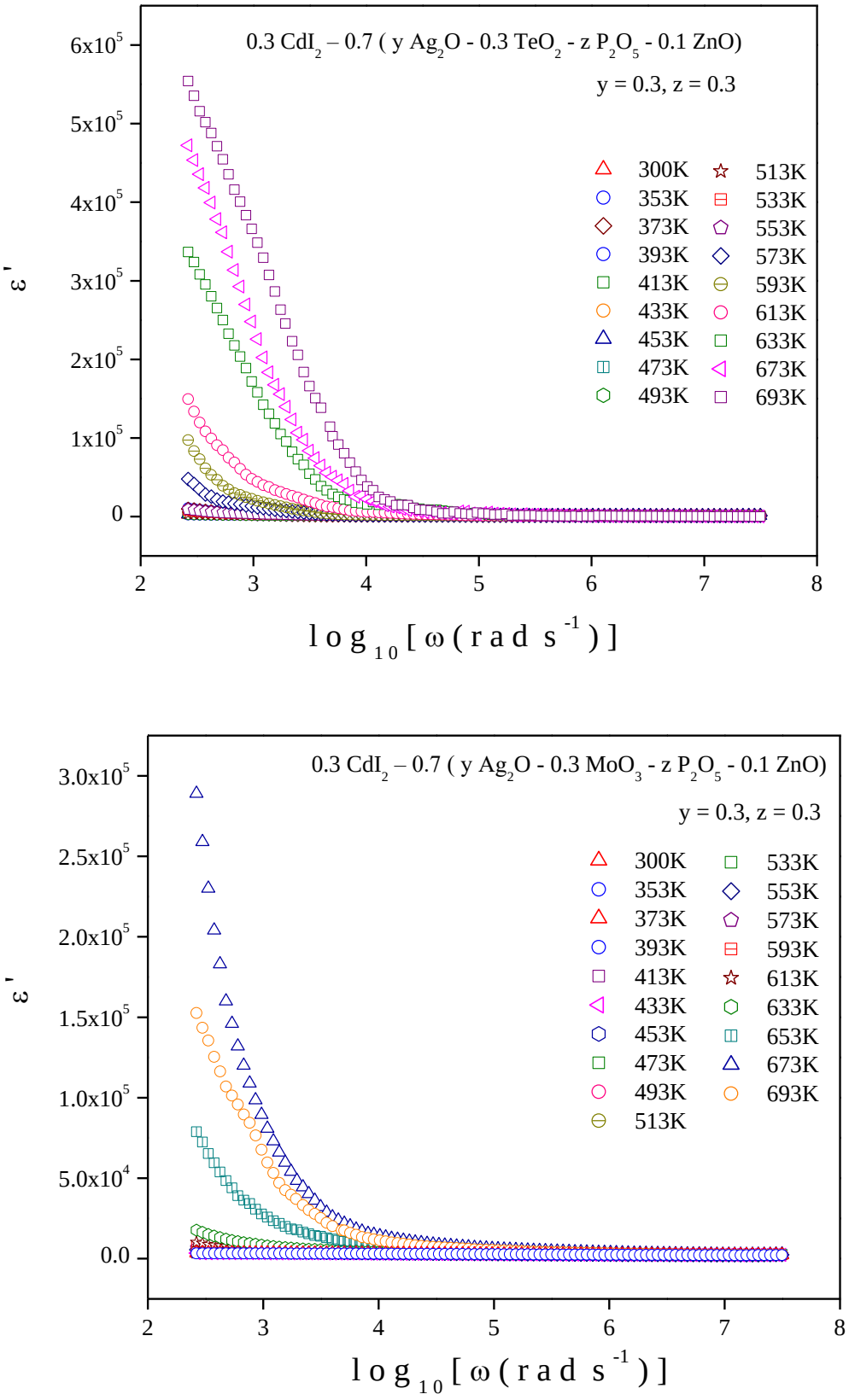

Fig. 6.11 Spectra of dielectric constant of (a) $0.3CdI_2 – 0.7 (y\ Ag_2O – 0.3TeO_2 – z\ P_2O_5 – 0.1\ ZnO)$ and (b) $0.3CdI_2 – 0.7 (y\ Ag_2O – 0.3MoO_3 – z\ P_2O_5 – 0.1\ ZnO)$ for fixed values of y and z

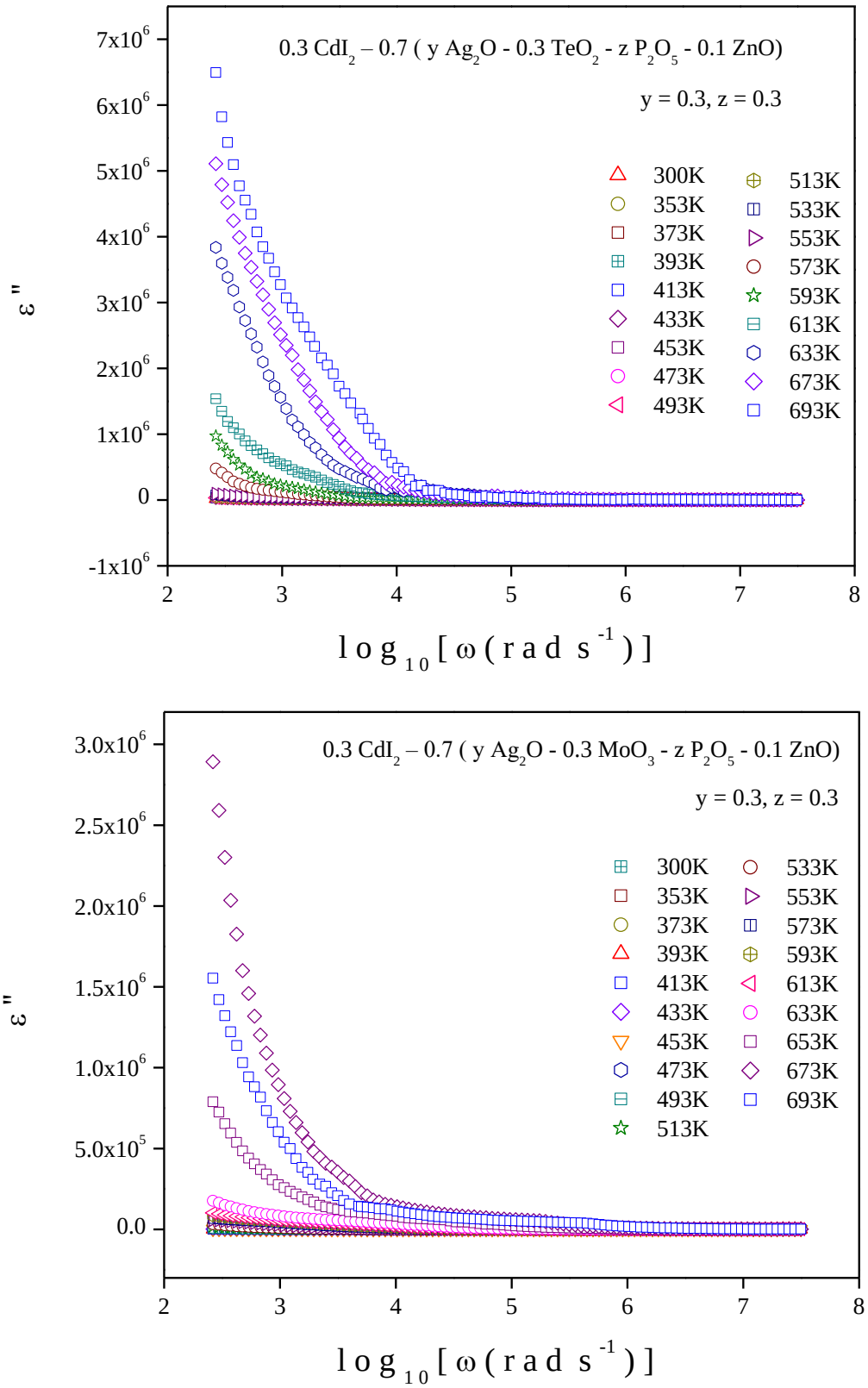

Fig. 6.12 Spectra of dielectric loss of (a) $0.3CdI_2 – 0.7 (y\ Ag_2O – 0.3TeO_2 – z\ P_2O_5 – 0.1$ ZnO) and (b) $0.3CdI_2 – 0.7 (y\ Ag_2O – 0.3MoO_3 – z\ P_2O_5 – 0.1\ ZnO)$ for fixed values of y and z

6.3.3.2 Study of electric modulus

The electric modulus of the current systems has been determined using Eq. 2.28. The spectra of real part of electric modulus, $M^{/}$ against frequency of the current glassy systems is displayed in Fig. 6.13. In the low frequency zone, $M^{/}$ approaches zero as long-range charge movement dominates (high permittivity) at all the temperatures. This is mostly due to the suppression of electrode polarization caused by the lack of restoring forces of charge carriers (polarons) [33-34]. However, dispersion in $M^{/}$ has been discovered at higher frequencies, and due to the electrical relaxation of polaron, $M^{/}$ exhibits a maximum value, which is $(M) = (\varepsilon)^{-1}$ [33-34]. Fig. 6.13 shows a progressive drop in $M^{/}$ as the temperature rises, which may indicate that the system's conduction mechanism involves the mobility of polaron in a limited range.

Graphs of the imaginary $M^{//}$ component of the electric modulus against frequency are displayed in Fig. 6.14. As the temperature rises, it can be seen that the $M^{//}$ peaks move towards higher frequencies, indicating a temperature-dependent relaxation process in the system. The flow of thermally activated charge carriers may shorten the duration of relaxation and increase its frequency. The conduction in these glasses below the peak relaxation frequency ω_c could be due to polaron hopping across long distances. The localized motion of charge carriers over small distances may be the cause of the conduction mechanism above ω_c [34-35]. At high temperatures, the shifting of the $M^{//}$ peak indicates that the system stabilizes rapidly in response to an external stimulus.

Relaxation time (τ_c) corresponding to relaxation frequency has been calculated and it has been found to decrease with the elevation in temperature. Charge carriers of MoO_3–doped system requires much more relaxation time than the charge carriers present in TeO_2–doped system at a specific temperature. A lower τ_c indicates that ions can hop between available sites more efficiently and implies higher ionic conductivity. Thus, it can be established that TeO_2–doped system shows higher electrical conductivity than the MoO_3–doped system at a given temperature. The temperature dependent spectra of relaxation time (τ_c) has been found to follow Arrhenius nature, as discussed in section 2.5.3.2 and thus activation energy due to relaxation time (E_τ) has been calculated from the gradients of the linearly fitted experimental data of τ_c applying Eq. 2.31. The calculated value of activation energy (E_τ) [36-37] has been found more for TeO_2–doped system indicating charge carries require more energy to move. The average values of τ_c and E_τ have been recorded in Table 6.5.

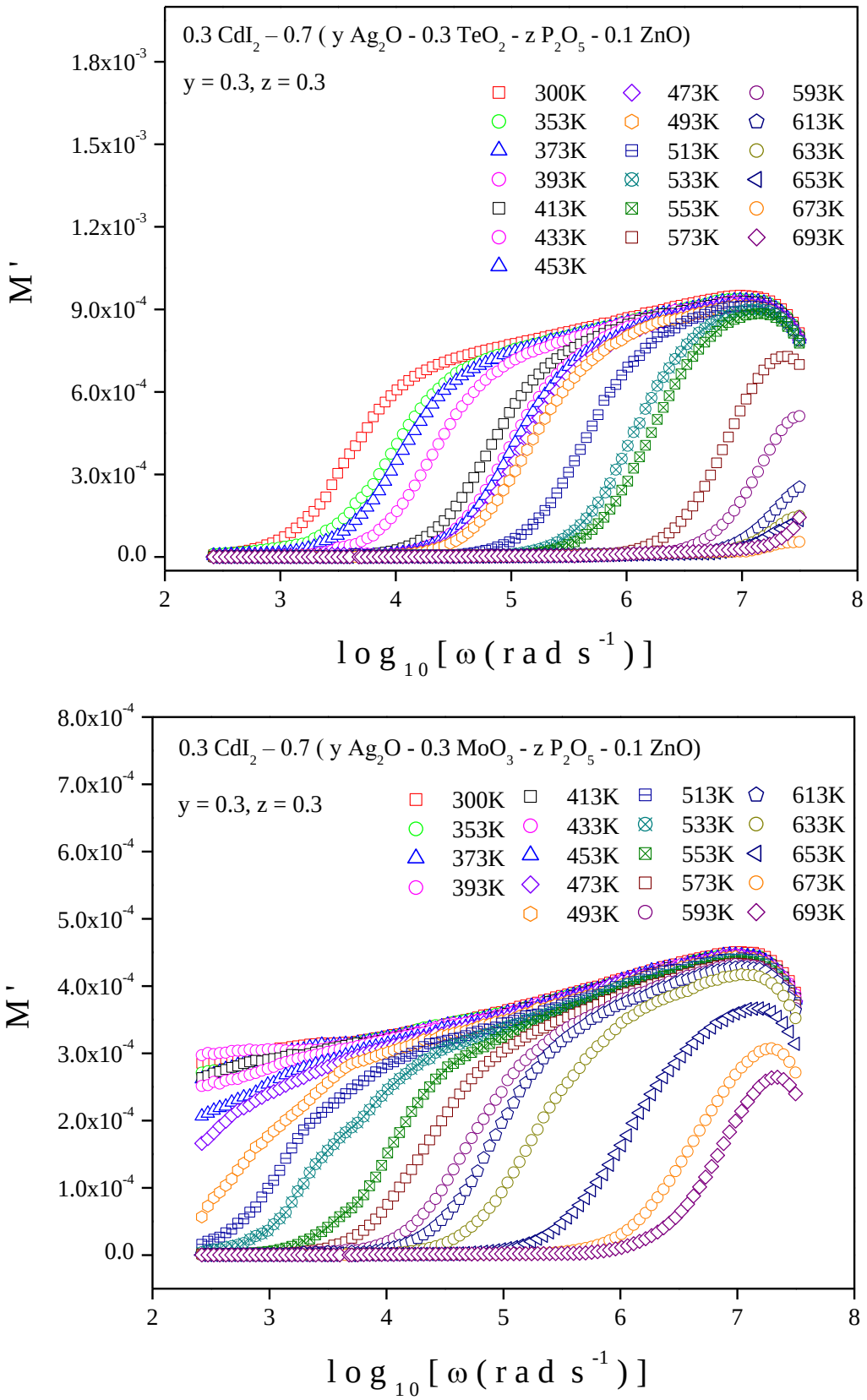

Fig. 6.13 Spectra of real part of electric modulus of (a) $0.3CdI_2 – 0.7 (y\ Ag_2O – 0.3TeO_2 – z\ P_2O_5 – 0.1\ ZnO)$ and (b) $0.3CdI_2 – 0.7 (y\ Ag_2O – 0.3MoO_3 – z\ P_2O_5 – 0.1\ ZnO)$ for fixed values of y and z

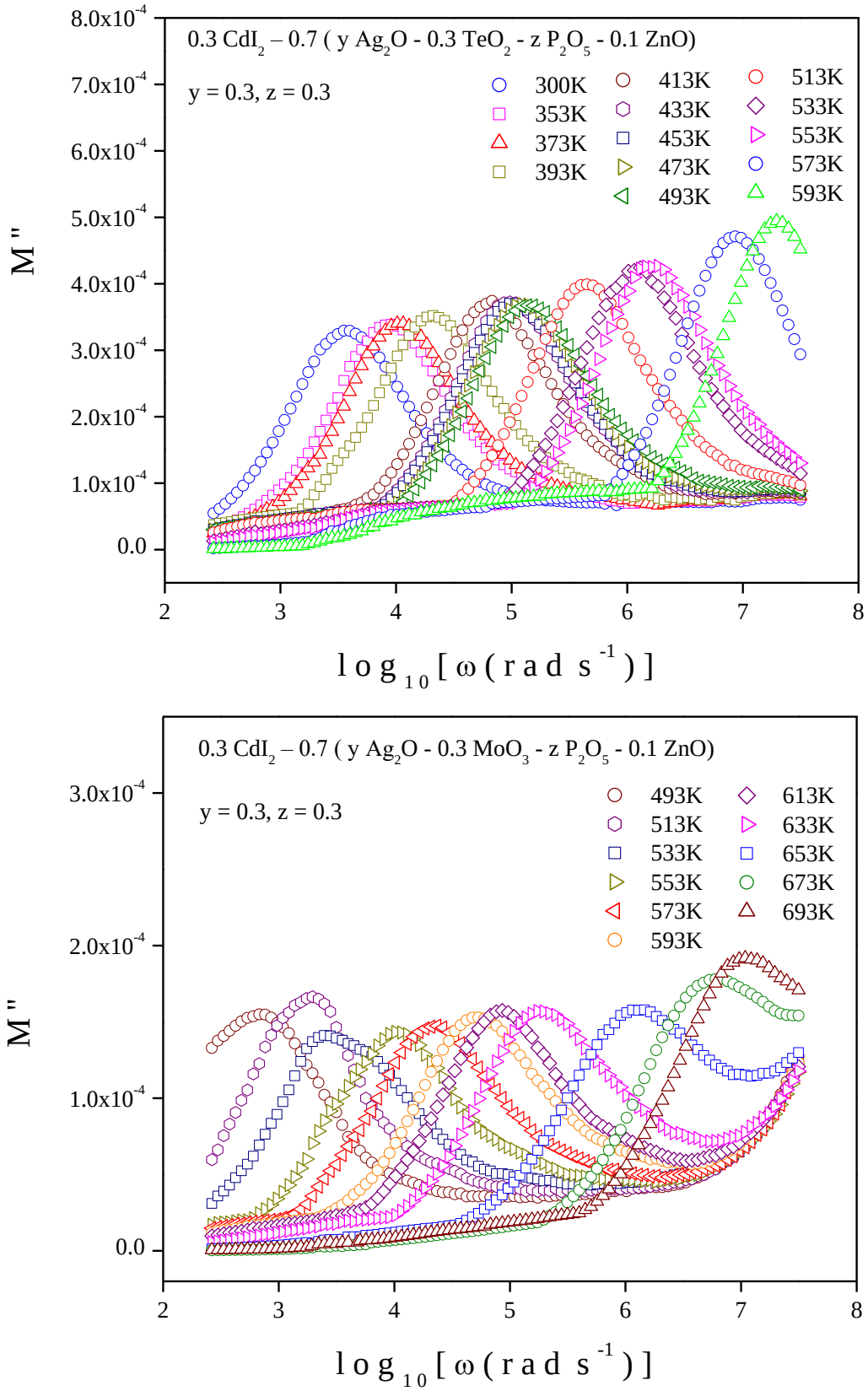

Fig. 6.14 Spectra of imaginary part of electric modulus of (a) $0.3CdI_2 – 0.7 (y\ Ag_2O – 0.3TeO_2 – z\ P_2O_5 – 0.1\ ZnO)$ and (b) $0.3CdI_2 – 0.7 (y\ Ag_2O – 0.3MoO_3 – z\ P_2O_5 – 0.1\ ZnO)$ for fixed values of y and z

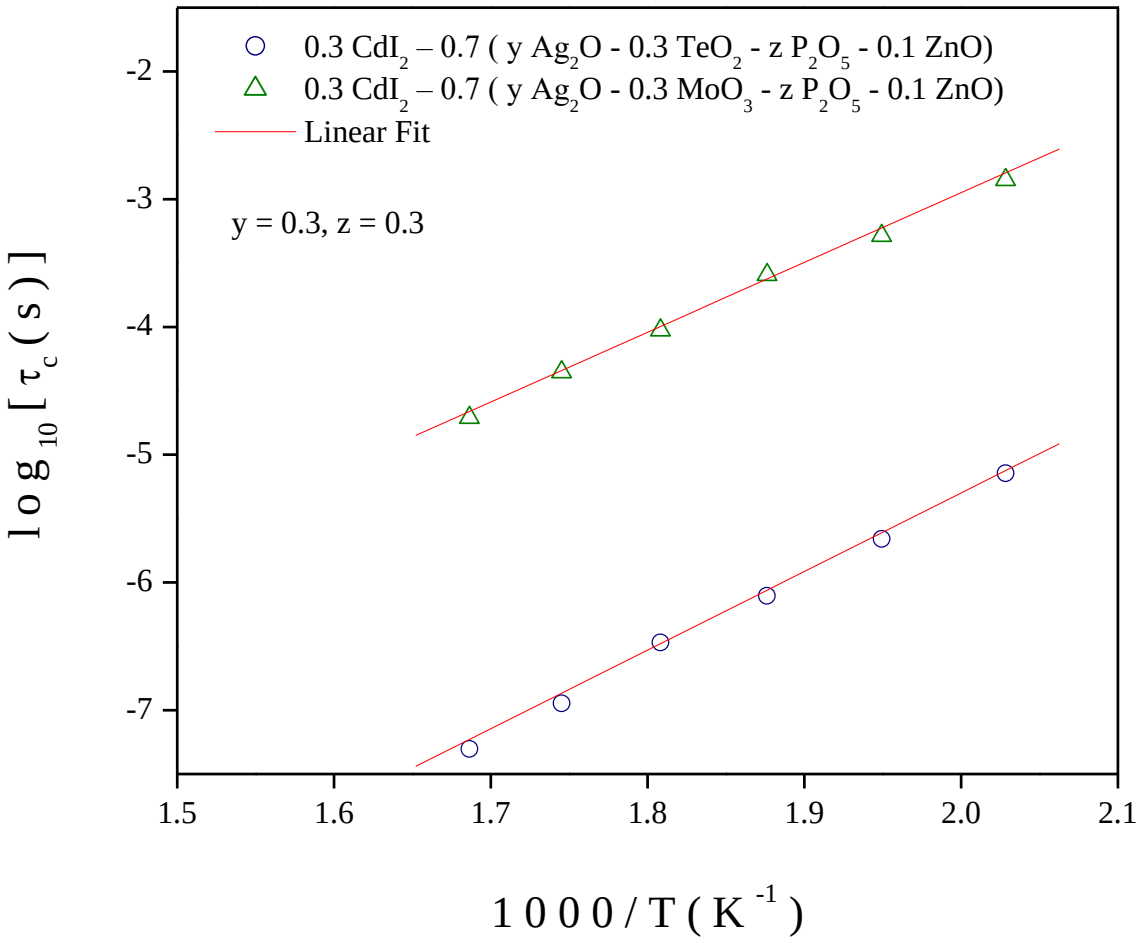

Fig. 6.15 Spectra of relaxation time of the as-prepared samples for fixed values of y and z

As-prepared glassy systems	Composition (x)	Avg. Relaxation Time, τ_c (s)	Activation Energy for Relaxation Time, E□, (eV)
$0.3CdI_2 - 0.7\ (y\ Ag_2O - 0.3\ TeO_2 - z\ P_2O_5 - 0.1\ ZnO)$	x = 1 {y = 0.3, z = 0.3}	1.82×10^{-6}	1.22
$0.3CdI_2 - 0.7\ (y\ Ag_2O - 0.3\ MoO_3 - z\ P_2O_5 - 0.1\ ZnO)$	x = 1 {y = 0.3, z = 0.3}	4.12×10^{-4}	1.08

Table 6.5: Data of activation energy corresponding to relaxation time and average relaxation time corresponding to composition of as-prepared glasses

6.4 CONCLUSION

Both systems acquire a glassy nature when prepared utilizing the melt-quench approach, according to the investigation conducted on the as-prepared samples. Due to a number of structural and compositional variables, the MoO_3-doped system shows a noticeable rise in electrical conductivity when the Ag_2O:P_2O_5 ratio rises. Ag_2O functions as a network modifier in glassy systems, introducing non-bridging oxygen (NBO) sites and disrupting the rigid phosphate (P_2O_5) network. These NBOs provide advantageous ionic migration channels, especially for Ag^+ ions, the system's principal charge carriers. An increase in the proportion of Ag_2O to P_2O_5 causes the glass network to become more open and disordered, which promotes improved ion transport. The inclusion of MoO_3 improves conductivity by altering the glass structure and opening up new channels for the flow of charge carriers. Polaronic hopping conduction, which facilitates charge transfer within the system, is made possible by the fact that molybdenum ions can exist in a variety of oxidation states, including Mo^{6+} and Mo^{4+}. Furthermore, MoO_3 is essential for improving ionic mobility by altering the glass matrix and increasing the density of mobile Ag^+ ions. When Ag_2O content and MoO_3 doping are combined, the network becomes more conductive and the mobility of silver ions is improved because of structural changes and a higher concentration of charge carriers.

On the other hand, as the Ag_2O:P_2O_5 ratio increases in a TeO_2-doped system, a decrease in electrical conductivity is observed, which can be attributed to several structural and compositional factors. In contrast to phosphate networks, tellurium dioxide (TeO_2) is known to form a very stable and partially covalent glass network. By producing TeO_4 and TeO_3 structural units, TeO_2 adds to glass stiffness in contrast to P_2O_5, which offers a more open and flexible structure for ion movement. These units create a network that is denser and less disturbed, which may reduce the number of pathways available for the conduction of Ag ions. By decreasing the amount of available non-bridging oxygens that serve as conduction sites, the dominance of tellurite-based structural units further limits ion mobility when the Ag_2O:PO_5 ratio rises. Furthermore, a rise in Ag_2O content may cause the glass network to become overly modified, which would hinder the development of continuous routes that are essential for effective charge transport. This further contributes to the observed decrease in electrical conductivity by raising the activation energy needed for Ag^+ ion movement. Moreover, increased interactions between silver ions and tellurium-based structural units may potentially be the cause of the decreased conductivity in TeO_2-doped systems at higher

$Ag_2O:P_2O_5$ ratios, which would partially immobilize charge carriers.

However, the TeO_2-doped system exhibits more conductivity than the other system at a particular temperature. This deduction has been also validated from the dielectric relaxation studies. Charge carriers of MoO_3–doped system requires much more relaxation time than the charge carriers present in TeO_2–doped system at a specific temperature. The lower relaxation time indicates that ions can hop between available sites more efficiently and implies higher ionic conductivity of the TeO_2-doped system. However, this system has higher dielectric constants and dielectric losses compared to MoO_3–doped system, suggesting that they may find application in fields where electrical energy storage is crucial. The as-prepared systems' thermally activated nature is illustrated by the conductivity and dielectric spectra.

The study's findings unequivocally demonstrate that the Cd–Ag ion exchange is primarily responsible for conductivity, which raises DC conductivity. It is anticipated that the dispersion in the higher frequency AC conductivity will represent the sub-diffusive, correlated, and non-random mobility of Ag^+ ions. Inter-ionic interaction, which results in a notable shift in the power law exponent with ion concentration, could be the reason of this correlated motion. This phenomenon has both academic and technological significance from the perspective of application.

References

[1] Kabi, S., & Ghosh, A. (2011). Dynamics of Ag+ ions and immobile salt effect in CdI2 doped silver phosphate glasses. *Solid State Ionics*, *187*(1), 39-42.

[2] Rao, P. N., Ramesh Kumar, E., & Appa Rao, B. (2018). Structural and transport studies of CdI 2-doped silver borotellurite fast ion-conducting system. *Journal of Solid State Electrochemistry*, *22*, 3863-3871.

[3] Sujatha, B., Narayana Reddy, C., & Chakradhar, R. P. S. (2010). Dielectric relaxation and ion transport in silver–boro-tellurite glasses. *Philosophical magazine*, *90*(19), 2635-2650.

[4] Tron, A., Nosenko, A., Park, Y. D., & Mun, J. (2017). Synthesis of the solid electrolyte Li2O–LiF–P2O5 and its application for lithium-ion batteries. *Solid State Ionics*, *308*, 40-45.

[5] Lefterova, E. D., Angelov, P. V., & Dimitriev, Y. B. (2000). Glasses from the system AgI–Ag_2O–TeO_2. B_2O_3. *Physics and chemistry of glasses*, *41*(6), 362-364.

[6] Ma, H., Ma, E., & Xu, J. (2003). A new Mg65Cu7. 5Ni7. 5Zn5Ag5Y10 bulk metallic glass with strong glass-forming ability. *Journal of materials research*, *18*(10), 2288-2291.

[7] Kumar, E. R., Rao, P. N., Veeraiah, N., & Rao, B. A. (2019). Effect of modifier on battery studies of silver-based FIC glasses. *Ionics*, *25*, 215-219.

[8] Šubčík, Jiří, Ladislav Koudelka, Petr Mošner, Lionel Montagne, Gregory Tricot, Laurent Delevoye, and Ivan Gregora. "Glass-forming ability and structure of ZnO–MoO3–P2O5 glasses." *Journal of non-crystalline solids* 356, no. 44-49 (2010): 2509-2516.

[9] Chowdari, B. V. R., Gopalakrishnan, R., Tang, S. H., & Kuok, M. H. (1988). Characterization of Ag2O: MoO3: P2O5 glasses. *Solid State Ionics*, *28*, 704-709.

[10] Chowdari, B. V. R., Tan, K. L., & Chia, W. T. (1992). Structural and physical characterization of Li2O: P2O5: MO3 (M= Cr2, Mo, W) ion conducting glasses. *MRS Online Proceedings Library (OPL)*, *293*, 325.

[11] Bih, L., El Omari, M., Réau, J. M., Haddad, M., Boudlich, D., Yacoubi, A., & Nadiri, A. (2000). Electronic and ionic conductivity of glasses inside the Li2O–MoO3–P2O5 system. *Solid State Ionics*, *132*(1-2), 71-85.

[12] Bih, L., El Omari, M., Réau, J. M., Haddad, M., Boudlich, D., Yacoubi, A., & Nadiri, A. (2000). Electronic and ionic conductivity of glasses inside the Li2O–MoO3–P2O5

system. *Solid State Ionics*, *132*(1-2), 71-85.

[13] Bih, L., Nadiri, A., & Aride, J. (2002). Thermal Study of A 2 O–(MoO 3) 2–P 2 O 5 (A= Li, Na) Glasses. *Journal of thermal analysis and calorimetry*, *68*, 965-972.

[14] Kumari, V., Kaswan, A., Patidar, D., Sharma, K., & Saxena, N. S. (2016). Electrical conduction mechanism in GeSeSb chalcogenide glasses. *Bulletin of Materials Science*, *39*, 255-262.

[15] Fernandes, B. J., Ramesh, K., & Udayashankar, N. K. (2019). Crystallization kinetics of Si20Te80− xBix (0≤ x≤ 3) chalcogenide glasses. *Materials Science and Engineering: B*, *246*, 34-41.

[16] Pal, S. K., Kumar, A., & Mehta, N. (2019). Signature of rigidity percolation effect in dielectric behavior of germanium containing multi-component chalcogenide glasses (ChGs). *Ceramics International*, *45*(13), 16279-16287.

[17] Ravagli, A., Naftaly, M., Craig, C., Weatherby, E., & Hewak, D. W. (2017). Dielectric and structural characterisation of chalcogenide glasses via terahertz time-domain spectroscopy. *Optical Materials*, *69*, 339-343.

[18] Zhu, E., Liu, Y., Sun, X., Yin, G., Jiao, Q., Dai, S., & Lin, C. (2019). Correlation between thermo-mechanical properties and network structure in GexS100–x chalcogenide glasses. *Journal of Non-Crystalline Solids: X*, *1*, 100015.

[19] Alemi, A. A., Sedghi, H., Mirmohseni, A. R., & Golsanamlu, V. (2006). Synthesis and characterization of cadmium doped lead-borate glasses. *Bulletin of Materials Science*, *29*, 55-58.

[20] Chauhan, P. S., Parekh, M., Sahoo, S., Kumar, S., Mahapatra, A. D., Sharma, P., ... & Misra, A. (2024). Influence of electrolyte on the photo-charging capability of a ZnO–FTO supercapacitor. *Journal of Materials Chemistry A*, *12*(34), 22725-22736.

[21] Venkatesan, A., Chandar, N. K., Arjunan, S., Marimuthu, K. N., Kumar, R. M., & Jayavel, R. (2013). Structural, morphological and optical properties of highly monodispersed PEG capped V2O5 nanoparticles synthesized through a non-aqueous route. *Materials Letters*, *91*, 228-231.

[22] Yamamoto, H., Nasu, H., Matsuoka, J., & Kamiya, K. (1994). X-ray absorption fine structure (XAFS) study on the coordination of Te in PbO-TiO2- TeO2 glasses with high third-order optical non-linearity. *Journal of non-crystalline solids*, *170*(1), 87-96.

[23] Nanba, T., Osaka, A., Takada, J., Miura, Y., Inoue, H., Akasaka, Y., ... & Yasui, I. (1992). Network structure of AlF3BaF2CaF2 glass. *Journal of non-crystalline solids*, *140*, 269-274.

[24] El-Damrawi, G., Hassan, A. K., & Meikhail, M. S. (1996). Characterisation Studies of Quaternary Superionic AgX-Ag2O-MoO3-P2O5 Glasses (X= Cl, Br). *Physics and chemistry of glasses*, *37*(3), 101-105.

[25] Almond, D. P., & West, A. R. (1983). Mobile ion concentrations in solid electrolytes from an analysis of ac conductivity. *Solid State Ionics*, *9*, 277-282.

[26] Bhattacharya, S. (2020). Metal oxide glass nanocomposites. In *Metal Oxide Glass Nanocomposites* (pp. 27-35). Elsevier.

[27] Kundu, R., Roy, D., & Bhattacharya, S. (2017). Microstructure, electrical conductivity and modulus spectra of CdI2 doped nanocomposite-electrolytes. *Physica B: Condensed Matter*, *507*, 107-113.

[28] Kundu, R., Roy, D., & Bhattacharya, S. (2015). Electrical transport of mixed phased glassy nanocomposites. *Transactions of the Indian Ceramic Society*, *74*(1), 35-40.

[29] Deb, B., & Ghosh, A. (2010). Dielectric and conductivity relaxation in AgI doped silver selenite superionic glasses. *Journal of Applied Physics*, *108*(7).

[30] Camargo, P. H. C., Satyanarayana, K. G., & Wypych, F. (2009). Nanocomposites: synthesis, structure, properties and new application opportunities. *Materials Research*, *12*, 1-39.

[31] Dult, M., Kundu, R. S., Hooda, J., Murugavel, S., Punia, R., & Kishore, N. (2015). Temperature and frequency dependent conductivity and electric modulus formulation of manganese modified bismuth silicate glasses. *Journal of Non-Crystalline Solids*, *423*, 1-8.

[32] Ahmad-Bitar, R., & Arafah, D. E. (1998). Processing effects on the structure of CdTe, CdS and SnO2 thin films. *Solar energy materials and solar cells*, *51*(1), 83-93.

[33] Karmakar, B., Rademann, K., & Stepanov, A. (Eds.). (2016). *Glass nanocomposites: synthesis, properties and applications*. William Andrew.

[34] Bhattacharya, S., & Ghosh, A. (2008). Relaxation dynamics in superionic glass nanocomposites. *Journal of the American Ceramic Society*, *91*(3), 753-759.

[35] Ojha, S., Roy, M., Chamuah, A., Bhattacharya, K., & Bhattacharya, S. (2020). AC conductivity and dielectric behavior of Cu-S-Te chalcogenide glassy

system. *Materials Letters*, *258*, 126792.

[36] Karmakar, B., Rademann, K., & Stepanov, A. (Eds.). (2016). *Glass nanocomposites: synthesis, properties and applications*. William Andrew.

[37] Bhattacharya, S., & Ghosh, A. (2008). Relaxation dynamics in superionic glass nanocomposites. *Journal of the American Ceramic Society*, *91*(3), 753-759.

Chapter 7

Conclusion and Future Scopes

Outline

7.1 CONCLUDING REMARKS

The development of a new generation of composites with their interesting electrical transport characteristics and a broad variety of applications have been the key area of investigation in our work. Restriction on studies on a wide composition range and exploration of their electrical properties have been a major limitation in this area of research. In our work some novel glassy systems with new combination of network formers and modifiers have been developed and exploration of their molecular structure and electrical transport phenomena have been done. According to the results of the literature review, glassy systems that conduct silver ions have been shown to have high conductivity. In parallel, the mixed former effect also improves conductivity; however, there hasn't been much research on how mixed network formers affect Ag^+ mobility. Our study has made a contribution to this field of study. All of the constructed systems have undergone structural characterization and electrical relaxation experiments utilizing a variety of methods to gather knowledge about the electrical transport properties of the as-prepared oxide glassy systems.

The correlation between electrical conduction parameters (Resistivity, Conductivity etc.) and some physical parameters (structure, size of particles etc.) of our prepared novel glassy systems have been established. AgI doped systems have been reported to exhibit some degree of crystallinity, while CdI_2 doped systems are entirely amorphous. It might imply that the presence of crystal structures may improve the charge carrier mobility in the AgI-doped systems which ought to have increased electrical conductivity. DC conductivity spectra has validated the assumptions made from structural characterization. Systems doped with AgI have demonstrated superior conductivity compared to those doped with CdI_2. The conductivity is somewhat enhanced by the addition of certain modifier oxides, such as TeO_2 or MoO_3. Hoping frequency spectrum analysis also shows that AgI-doped systems exhibit a higher hopping frequency than CdI_2-doped systems. In systems where hopping is the predominant transport mechanism, it signifies a faster flow of charge carriers between localised sites, which directly results in better conductivity. In addition to ionic conduction, glassy systems containing V_2O_5 exhibit electronic conduction. The study points towards the fact that larger V_2O_5 concentrations introduce an electronic contribution when present in the glassy system. Ionic conduction takes precedence over electrical conductivity as the concentration steadily drops. As far the dielectric relaxation study is concerned, AgI-doped systems have shown a higher dielectric constant

range relative to CdI_2-doped systems. It put forward that in situations where greater energy storage capacity is needed, AgI-doped systems may be employed.

7.2 APPLICATIONS

Research on metal nanoparticle-based nano-composites dispersed in glass matrices is extensive due to their unique mechanical, electrical, optical, and linear and nonlinear properties [1-8]. As a result, their use has increased dramatically in a variety of applications, such as microelectronics [9], waveguides [10], solar cells [11], biosensors [12-13], data storage systems [14-15], aeroplanes [16], and more. Different types of metal ions have been integrated into glass using a variety of methods, such as low energy ion beam mixing [17], direct metal-ion implantation [18], sol-gel [19], ion-exchange [20–21], vacuum deposition [22–23], and others. Here some key applications areas have been discussed.

7.2.1 Optoelectronics and Photonics: Oxide glass nano-composites can be used in optical fibers for improved signal transmission. It could be employed in display technologies such as OLEDs and LCDs and can be utilized in laser materials and optical sensors.

7.2.2 Energy Storage and Conversion: Glass nano-composites are employed in solid-state batteries for improved ionic conductivity. They are used as electrolytes and electrodes in fuel cells and incorporated in solar cells to enhance light absorption and efficiency. Compared to traditional batteries like lead-acid, Ni–Cd, Ni–MH, and Ag–Zn, the voltage of lithium rechargeable batteries is higher (the standard voltage being 3.6 V), a greater energy density or specific energy (125 W h/kg L), and an extended cycle life (>1,000 cycles). Large-scale Li-ion batteries also hold tremendous promise for stationary energy storage systems and electric cars [24].

7.2.3 Biomedical Applications: They could be used in bioactive glass for bone regeneration and dental applications. They are employed in drug delivery systems due to controlled degradation properties. They could be integrated into biosensors for medical diagnostics.

7.2.4 Electronic Applications: They are used in thin-film transistors and microelectronic

devices. They are employed as dielectric materials in capacitors and integrated into flexible and transparent electronics. Glassy nanocomposite materials can be used as gas sensors, memory devices, Schottky diodes, or photovoltaic devices, depending on the type that is produced. These electronic gadgets will soon be made from glassy nanocomposite materials, which could make for an interesting field of research [25-27].

7.2.5 Structural and Coating Applications: They are used in scratch-resistant coatings for glasses and screens. They could be applied in anti-corrosion and protective coatings for metals. They are utilized in heat-resistant glass-ceramics.

7.2.6 Applications in Semiconductor Industry: Applications such as noise reduction, tuning, filtering, decoupling, bypassing, termination, and frequency determination, as well as digital electronics assemblies, particularly cell phones, camcorders, computers, and defence devices, can benefit from the use of discrete capacitors made of nano-composite materials [28].

7.3 FUTURE PROSPECTS

Ionic and semiconducting glassy nano-composites have a theoretical and experimental foundation that is still in its early stages, which means that there is limited material production and potential for novel uses. Certain glass nano-composites can be produced using the conventional methodology as long as the right reduction environment and melting conditions are maintained. The experiment's findings, which are presented in this thesis, open up the possibility of the subsequent research.

1. Development of some more new oxide glassy systems with different combination of metal halide and network formers would be a vast area of pending job.

2. To take advantage of their prospective uses in optoelectronic and photovoltaic systems, the optical characteristics of synthesised nano-composites will be thoroughly investigated. In the near future, necessary experiments such as photoluminescence (PL), current-voltage, capacitance-voltage, and ultraviolet spectroscopy (Uv-Vis) under light and dark circumstances [26] for as-prepared glassy systems will be processed.

3. We used the melt-quenching procedure to prepare the samples for this study. We will use additional methods, such as chemical beam deposition (CBD) and electron beam deposition (EBD), to create glass nano-composites on a similar pattern. These techniques can be used to make a microfilm of these glass nano-composites, which is crucial for some application-focused investigations [25-26].
4. It is a credible working assumption that a fairly straightforward adaptable model can be used to describe ion transport in disordered materials. To stimulate additional investigation into the principles of ion dynamics in these materials, new theoretical models considering the recent developing concerns could be addressed.

5. Determination of the potential industrial area and scholarly usage of these as-prepared semiconducting glass nano-composites is a pending job.

6. If a comprehensive study of the mechanical and optical behaviour of these glass nano-composites could be carried out, their probable usage in a range of applications might be determined.

References

[1] Brooks, I., Lin, P., Palumbo, G., Hibbard, G. D., & Erb, U. (2008). Analysis of hardness–tensile strength relationships for electroformed nanocrystalline materials. Materials Science and Engineering: A, 491(1-2), 412-419.

[2] Laila, S., Suraya, A. K., & Yahya, A. K. (2014). Effect of glass network modification on elastic and structural properties of mixed electronicionic 35V2O5-(65-x) TeO2-(x) Li2O glass system. Chalcogenide Lett, 11(2), 91-104.

[3] Pelton, M., & Bryant, G. W. (2013). Introduction to metal-nanoparticle plasmonics. John Wiley & Sons.

[4] Jeon, I. Y., & Baek, J. B. (2010). Nanocomposites derived from polymers and inorganic nanoparticles. Materials, 3(6), 3654-3674.

[5] Irimpan, L., Nampoori, V. P. N., & Radhakrishnan, P. (2008). Enhanced luminescence and nonlinear optical properties of nanocomposites of ZnO–Cu. Journal of Materials Research, 23(11), 2836-2845.

[6] Stalmashonak, A., Seifert, G., & Abdolvand, A. (2013). Ultra-short pulsed laser engineered metal-glass nanocomposites (pp. 5-15). New York, NY, USA: Springer.

[7] Melesse, A. L. (1995). Synthesis and properties of copper doped glass nanocomposites. Technische Universiteit Eindhoven.

[8] Faraji, N., Yunus, W. M. M., Kharazmi, A., Saion, E., Shahmiri, M., & Tamchek, N. (2012). Synthesis, characterization and nonlinear optical properties of silver/PVA nanocomposites. Journal of the European Optical Society-Rapid publications, 7, 12040.

[9] Jyoti Rozra, Ph. D. Thesis on "Study of Structural, Optical, Electrical and Mechanical Properties of Silver-Glass Nanocomposites", Kurukshetra University, India, (2013).

[10] Karmakar, B., Som, T., Singh, S. P., & Nath, M. (2010). Nanometal-glass hybrid nanocomposites: synthesis, properties and applications. Transactions of the Indian Ceramic Society, 69(3), 171-186.

[11] Dinca, I., Ban, C., Stefan, A., & Pelin, G. (2012). Nanocomposites as advanced materials for aerospace industry. Incas Bulletin, 4(4), 73.

[12] Karmakar, B., Rademann, K., & Stepanov, A. (Eds.). (2016). Glass nanocomposites: synthesis, properties and applications. William Andrew.

[13] Manocha, L. M., Valand, J., Patel, N., Warrier, A., & Manocha, S. (2006). Nanocomposites for structural applications.

[14] Sanchez, C., Julián, B., Belleville, P., & Popall, M. (2005). Applications of hybrid organic–inorganic nanocomposites. Journal of materials chemistry, 15(35-36), 3559-3592.

[15] Petrov, M. (2013). Glass-metal nanocomposites for photonics applications (Doctoral dissertation, Itä-Suomen yliopisto).

[16] El-Sheikhy, R., Akira, K., & Al-Shamrani, M. (2009). Application of Natural Nano Silicate Powder in Advanced Smart Nanocomposite Coating. Transactions of JWRI, 38(2), 49-52.

[17] Vishwam, T. (2015). SS Sastry, BR Venkateswara Rao &. Indian J Phys, 89, 73-80.

[18] Bhattacharya, S., Bar, A. K., Roy, D., Graca, M. P. F., & Valente, M. A. (2010). Fractal dimensionality of ion conduction in glass-nanocomposites. Materials Physics and Mechanics, 10(1-2), 56-61.

[19] Sancho-Parramon, J., Janicki, V., Dubček, P., Karlušić, M., Gracin, D., Jakšić, M., ... & Juraić, K. (2010). Optical and structural properties of silver nanoparticles in glass matrix formed by thermal annealing of field assisted film dissolution. Optical materials, 32(4), 510-514.

[20] Dubiel, M., Haug, J., Kruth, H., Hofmeister, H., & Seifert, W. (2009, November). Temperature dependence of EXAFS cumulants of Ag nanoparticles in glass. In Journal of Physics: Conference Series (Vol. 190, No. 1, p. 012123). IOP Publishing.

[21] Khan, A., Khan, A. A. P., Rahman, M. M., Asiri, A. M., Alfaifi, S. Y., & Taib, L. A. (2018). Toward facile preparation and design of mulberry-shaped poly (2-methylaniline)-Ce2 (WO4) 3@ CNT nanocomposite and its application for electrochemical Cd2+ ion detection for environment remediation. Polymer-Plastics Technology and Engineering, 57(4), 335-345.

[22] Rozra, J., Saini, I., Aggarwal, S., & Sharma, A. (2013). Spectroscopic analysis of Ag nanoparticles embedded in glass. Adv. Mater. Lett, 4, 598-604.

[23] de Kwaadsteniet, M., Botes, M., & Cloete, T. E. (2011). Nano: brief reports and reviews.

[24] Merhari, L. (Ed.). (2009). Hybrid nanocomposites for nanotechnology (pp. 795-825). New York, NY, USA: Springer US.

[25] Sultana, J., Das, A., Das, A., Saha, N. R., Karmakar, A., & Chattopadhyay, S. (2016). Characterization of nano-powder grown ultra-thin film p-CuO/n-Si hetero-junctions by employing vapour-liquid-solid method for photovoltaic applications. Thin Solid Films, 612, 331-336.

[26] Sultana, J., Paul, S., Karmakar, A., Yi, R., Dalapati, G. K., & Chattopadhyay, S. (2017). Chemical bath deposited (CBD) CuO thin films on n-silicon substrate for electronic and optical applications: Impact of growth time. Applied surface science, 418, 380-387.

[27] Sarkar, K., Palit, M., Guhathakurata, S., Chattopadhyay, S., & Banerji, P. (2017). Single InxGa1−xAs nanowire/p-Si hetero-junction based nano-rectifier diode. Nanotechnology, 28(38), 385202.

[28] Xu, J., Bhattacharya, S., Moon, K. S., Lu, J., Englert, B., & Wong, C. P. (2006, May). Large-area processable high k nanocomposite-based embedded capacitors. In 56th Electronic Components and Technology Conference 2006 (pp. 13-pp). IEEE.